



UCL

**Cone photoreceptor neuroprotection in inherited
retinal degenerations**

A thesis submitted for the degree of
Doctor of Philosophy
2011

Edward J.K. Lee

Department of Genetics,
University College London Institute of Ophthalmology

Declaration:

I, Edward Lee confirm that the work presented is my own. Where information has been derived from other sources, I confirm that this has been indicated.

Abstract:

High resolution and colour vision is derived from cone photoreceptors within the retina of the eye. These highly specialised neuronal cells convert energy from incident light into changes in cellular membrane potential. Action potentials are then relayed and processed within the inner retina and the cerebral cortex. Loss of function in the cone photoreceptors is the direct cause of visual loss for millions of patients. Yet for many of the most common causes of blindness cone photoreceptor dysfunction occurs late on in the disease and is secondary to inherited and/or environmental influences that primarily affect other cell types. Cone photoreceptors are then secondarily affected and it is once their function is lost that the patient becomes visually disabled.

The aim of this thesis was to evaluate therapies targeting the molecular steps of cone photoreceptor death rather than the underlying pathology. If effective at slowing cone photoreceptor degeneration and preserving function, such therapies could be applicable to large numbers of patients with a variety of underlying defects. There will however be continued stimuli for cell death as the primary defect has not been corrected and so it is important to determine the magnitude and duration of any treatment effect. The experiments of this thesis were performed in an animal model of inherited retinal degeneration derived to allow repeated *in vivo* assessments of cone photoreceptor function and survival. Gene therapy and intra-ocular injections were used to evaluate proteins with contrasting modes of action.

Contents:

Chapter 1 Introduction	16
1.1 Overview	16
1.2 The mammalian eye.....	17
1.2.1 The neuroretina	18
The retinal pigment epithelium	22
1.2.2 Phototransduction.....	24
1.2.3 The visual cycle.....	27
1.3 Inherited retinal degenerations	29
1.3.1 Classifications and Genotype-Phenotype Correlations	29
1.3.2 Retinitis Pigmentosa.....	32
1.3.3 Gene mutations in RP.....	36
1.4 Photoreceptor cell death in inherited retinal degenerations.....	39
1.4.1 Secondary loss of cone photoreceptors	40
1.4.2 Molecular mechanisms of photoreceptor cell death.....	45
1.5 Therapeutic approaches for retinal diseases	49
1.5.1 Gene replacement therapies	49
1.5.2 Gene silencing	50
1.5.3 Neuroprotection.....	52
1.5.4 Cell replacement therapies	59
1.6 Sustained delivery of therapeutic proteins to the retina	60
1.6.1 Direct gene transfer	61
1.6.2 Vitreous implants	62
1.7 Rodent models of RP	63
1.8 Thesis aims	67

Chapter 2 Materials & methods.....	68
2.1 Buffers & media and solutions	69
2.2 Molecular biology.....	71
2.2.1 mRNA extraction	71
2.2.2 Generation of cDNA	71
2.2.3 Plasmid preparation.....	72
2.2.4 Electrophoresis, gel extraction & ligation of DNA.....	74
2.2.5 Amplification of DNA in bacteria.....	75
2.2.6 Restriction enzyme digests.....	76
2.2.7 DNA precipitation	77
2.2.8 DNA Sequencing.....	77
2.3 Cell culture	77
2.4 rAAV production.....	78
2.4.1 rAAV 2/2 production	80
2.4.2 rAAV 2/8 production	81
2.4.3 Vector genomic titres	85
2.4.4 Polyacrylamide gel electrophoresis (PAGE) and protein stain.....	89
2.4.5 Transmission electron microscopy.....	90
2.5 PCR.....	90
2.5.1 Primer design and manufacture.....	90
2.5.2 Standard PCR	91
2.5.3 Real-time PCR.....	91
2.6 Testing of plasmid and vector transgene expression in vitro	92
2.6.1 Cell culture transfection with plasmids.....	92
2.6.2 Cell culture infection and superinfection with AAV2/2	93
2.7 In vivo procedures	93
2.7.1 Anaesthesia and recovery.....	93

2.7.2 Electroretinogram.....	95
2.7.3 Sub-retinal and intra-vitreous Injections.....	98
2.7.4 Confocal scanning laser ophthalmoscopy.....	99
2.7.5 Optical coherence tomography.....	103
2.8 Immunohistochemistry.....	104
2.8.1 Tissue preparation.....	104
2.8.2 Antibody staining.....	104
2.8.3 Histology.....	106
2.9 Protein Detection.....	107
2.9.1 Evaluation of Protein Concentration.....	107
2.9.2 ELISA.....	107
2.9.3 Western Blotting.....	108
Chapter 3 A novel model for the <i>in-vivo</i> study of rod-cone degeneration.....	109
3.1 Introduction.....	109
3.2 Colony Generation and Maintenance.....	112
3.3 Cone-specific GFP expression.....	113
3.4 In-vivo imaging of cone photoreceptors.....	119
3.5 Characterisation of the cone degeneration in the Rho ^{-/-} Opn.gfp mouse.....	124
3.5.1 Loss of cone function.....	124
3.5.2 Cone photoreceptor survival.....	128
3.5.3 Non-functional cones.....	130
3.6 The <i>Opn.gfp</i> mouse.....	134
3.7 Discussion.....	138
3.7.1 Cone photoreceptor degeneration.....	138
3.7.2 Ventral-dorsal gradient.....	140
3.7.3 A valuable model to evaluate cone-related outcome measures.....	142

Chapter 4 GDNF as a potential therapy for retinitis pigmentosa.....	144
4.1 Introduction	144
4.1.1 GDNF pathways in the retina.....	145
4.1.2 Anti-apoptotic effects in the retina.....	146
4.1.3 Aims	152
4.2 GDNF receptor expression	153
4.2.1 Primer design and testing	154
4.2.2 GFR α 1 and GFR α 2 expression in the <i>Rho</i> ^{-/-} <i>Opn.gfp</i> mouse over time.....	155
4.3 Intra-vitreous delivery of recombinant protein.	155
4.3.1 Validation of assay	156
4.3.2 Pharmacokinetics	157
4.3.3 Evaluation of single bolus	160
4.3.4 Evaluation of repeated bolus	165
4.3.5 Conclusions	169
Chapter 5 Inner-retinal GDNF gene therapy	171
5.1 Introduction	171
5.2 Gene Therapy to express GDNF in the inner retina	172
5.2.1 The cmv.gdnf plasmid and in vitro testing.....	172
5.2.2 AAV 2/2 production and <i>in vitro</i> testing.....	174
5.2.3 <i>In vivo</i> quantification of Gdnf after intra-vitreous rAAV2/2.....	176
5.3 In vivo examination of the effect of inner retinal GDNF production on cone photoreceptor loss.	177
5.3.1 The effect of intra-vitreous injection and inner retinal cell transduction on cone photoreceptor mediated retinal function.	178
5.3.2 Inner retinal GDNF expression and cone photoreceptor degeneration.....	182
5.4 Discussion.....	185

Chapter 6 Outer-retinal GDNF gene therapy.....	187
6.1 Introduction	187
6.2 AAV2/8 mediated delivery of GDNF to the outer retina	188
6.2.1 Viral vector production and testing.....	188
6.2.2 The effect of rAAV2/8.CMV.GDNF (batch#1) on cone degeneration.....	191
6.2.3 Sub-retinal injection in degenerating retina	194
6.2.4 Sub-retinal injection in wild-type retina.....	198
6.2.5 Titration series of rAAV2/8.CMV.GDNF (batch#1)	201
6.2.6 Modified Vector Purification Protocol: Phase Separation	204
6.2.7 The effect of AAV2/8 CMV.GDNF on cone degeneration	212
6.3 Discussion.....	215
Chapter 7 Inhibition of apoptosis	219
7.1 Introduction	219
7.1.1 Apoptosis pathways and the caspase enzymes.....	219
7.1.2 Bcl-2 regulatory proteins.....	221
7.1.3 Inhibitor of apoptosis (IAP) proteins and their regulation	221
7.1.4 Physiological roles of XIAP.....	225
7.1.5 Over-expression of XIAP	226
7.1.6 XIAP mediated resistance to photoreceptor apoptosis.....	226
7.2 Aims.....	228
7.3 The cone arrestin promoter.....	229
7.4 Testing of CMV.XIAP in vitro.....	233
7.4.1 Species-specific primers.....	233
7.4.2 <i>In vitro</i> testing of plasmid expression	234
7.5 Confirmation of transgene expression in vivo.....	239
7.6 XIAP expression and degeneration of cone function	240
7.7 XAF1 expression	243
7.8 Discussion.....	246

7.8.1 rAAV2/8.CMV.XIAP in the <i>Rho</i> ^{-/-} <i>Opn.gfp</i> mouse.....	246
7.8.2 The ARR4 promoter.....	248
Chapter 8 Rhodopsin gene replacement.....	250
8.1 Introduction	250
8.1.1 Strategies for adRP.....	251
8.1.2 The challenges of rhodopsin gene replacement	253
8.1.3 Aims	254
8.2 rAAV-mediated rhodopsin expression <i>in vivo</i>	254
8.3 Assessment of the effect of rhodopsin expression on rod function.....	259
8.4 Timing of rhodopsin expression	262
8.5 Combination with GDNF	265
8.6 Optimisation of expression.....	267
8.6.1 Intron insertion	267
8.6.2 Kozak consensus sequence optimisation.....	268
8.6.3 Codon optimisation	270
8.6.4 Evaluation of optimised plasmid.....	271
8.7 Discussion.....	274
Chapter 9 Discussion.....	277
9.1 Neuroprotection	277
9.2 Transducing the outer retina.....	279
9.3 Dosing and gene therapy	281
9.4 Efficiency of expression	284
9.5 Future work.....	286
Chapter 10 Acknowledgements.....	289
Chapter 11 Supplementary Data	290
11.1 Model characterisation.....	290
11.2 Plasmid maps	292

11.2.1	CMV.GDNF plasmid	293
11.2.2	Null plasmid	293
11.2.3	CBA.RFP.....	294
11.2.4	CMV.XIAP	294
11.2.5	bRHO.hRHO	295
11.3	rAAV2/8.CMV. <i>Gdnf</i>	296
11.3.1	Virus titre.....	296
11.3.2	Protein concentration in samples from rAAV2/8 CMV.GDNF treated eyes.....	297
11.4	Control Virus	298
11.4.1	Titre of control virus	298
11.4.2	Confirmation of absence of transgene expression with control virus	298
11.5	Rhodopsin constructs	301
11.6	Optimised bRHO.hRHO plasmid	302
11.7	Quantitative real-time PCR.....	306
11.8	Wild Type ERG	308
Chapter 12 Abbreviations.....		309
Chapter 13 References		313

Figures

Figure 1-1 Cross section of the eye	17
Figure 1-2 Cross section of retina from a transgenic mouse with green fluorescent protein (GFP) expressed in cone photoreceptors.....	21
Figure 1-3 Field emission scanning electron microscope image of human retina showing rod and cone outer segments.	21
Figure 1-4 RPE cells in relation to principal retinal cell types	23
Figure 1-5 Scanning electron micrograph of the RPE monolayer	23
Figure 1-6 Activation of the phototransduction cascade.....	26
Figure 1-7 The steps of the visual cycle.....	28
Figure 1-8 The number of mapped and identified retinal disease genes from 1980 to 2010...	31
Figure 1-9 Collage of fundus photographs showing typical features of retinitis pigmentosa.	34
Figure 1-10 Estimated prevalence of retinitis pigmentosa sub-types	35
Figure 1-11 Classical pathways of cellular death.....	47
Figure 1-12 Therapeutic strategies for inherited retinal degenerations.....	51
Figure 1-13 Summary of principal advantages and issues to be resolved regarding neuroprotection.....	52
Figure 1-14 Duration of a neuro-protective effect.	55
Figure 2-1 <i>In vitro</i> rAAV2/2 vector production.....	79
Figure 2-2 ERG recording apparatus	96
Figure 2-3 Example of photopic flash ERG traces	97
Figure 2-4 The a and b waves demonstrated on a typical ERG waveform.....	98
Figure 2-5 Schematic diagram of a confocal scanning laser system.....	100
Figure 2-6 The Heidelberg Spectralis adapted for use with animal models.	100
Figure 2-7 <i>In vivo</i> infra-red imaging of the murine retina.	102
Figure 3-1 GFP expression in cone photoreceptors.. ..	114
Figure 3-2 GFP and PNA in the <i>Rho^{-/-}Opn.gfp</i> mouse at 6 weeks of age.....	117

Figure 3-3 Composite image along the superior-inferior axis of the eye of a 6 week old <i>Rho-/-Opn.gfp</i> mouse.	118
Figure 3-4 Autofluorescence images of the retina of a <i>Rho-/-Opn.gfp</i> mouse	119
Figure 3-5 <i>In vivo</i> imaging of cone photoreceptors	121
Figure 3-6 The retinal vasculature and branching pattern in flatmounted retinas	122
Figure 3-7 Histopathological correlation of the SLO image.....	123
Figure 3-8 Degeneration in cone function in the <i>Rho-/-Opn.gfp</i> mouse.....	125
Figure 3-9 The effect of GFP expression on cone function..	127
Figure 3-10 Cone counts over time	129
Figure 3-11 Example cone degeneration images from <i>Rho-/-Opn.gfp</i> and <i>Opn.gfp</i> mice.....	129
Figure 3-12 Cone transducin in the <i>Rho-/-Opn.gfp</i> mouse.	132
Figure 3-13 Cone arrestin expression in the <i>Rho-/-Opn.gfp</i> mouse.....	133
Figure 3-14 Changes in cone morphology over time in the <i>Rho-/- Opn.gfp mouse</i>	134
Figure 3-15 Comparison of cone function in the <i>Opn.gfp</i> , wild type and rhodopsin knockout (KO) mouse.....	136
Figure 3-16 ERGs in one year old <i>Opn.gfp</i> mice.....	137
Figure 3-17 Cryosections from an 8 month old <i>Opn.gfp</i> mouse.....	137
Figure 4-1 Validation of primers for murine GDNF receptors.	154
Figure 4-2 Detection of GFR α 1 and GFR α 2 mRNA.	155
Figure 4-3 ELISA detection of human and murine recombinant GDNF protein.....	157
Figure 4-4 Standard curve from ELISA experiment to determine concentration of GDNF in wild type mouse eyes.	158
Figure 4-5 The decrease in GDNF levels following intravitreal injection.....	159
Figure 4-6 Application of an exponential best fit line to the GDNF level results.	160
Figure 4-7 The effect of single intravitreal rGDNF or PBS injections in the <i>Rho-/-Opn.gfp</i> mouse.	163
Figure 4-8 The effect of repeated GDNF bolus injections on cone function.	167
Figure 4-9 Central cone density for GDNF and PBS treated eyes of 3 animals at p77.....	168

Figure 5-1 The pd10 plasmid following ligation with the CMV promoter and murine <i>Gdnf</i> transgene.....	173
Figure 5-2 In vitro testing of the CMV.GDNF plasmid and rAAV2/2.....	175
Figure 5-3 Measurement of AAV2/2 CMV.GDNF titre by dot-blot analysis.	176
Figure 5-4 GDNF protein assays in AAV2/2 CMV.GDNF treated and untreated fellow eyes of 4 <i>Rho</i> ^{-/-} <i>Opn.gfp</i> mice.....	177
Figure 5-5 The effect of AAV2/2 CBA.RFP on cone function in the rhodopsin knockout cone-GFP mouse.	180
Figure 5-6 RFP expression in AV2/2 CBA.RFP treated eyes of the rhodopsin knockout cone-GFP mouse..	181
Figure 5-7 Cone function over time in treated and untreated eyes of the rhodopsin knockout cone-GFP mouse.	183
Figure 5-8 <i>In vivo</i> cone photoreceptor quantification in the rhodopsin knockout cone-GFP mouse..	185
Figure 6-1 ELISA identifying GDNF after rAAV2/8 CMV.GDNF injection.....	190
Figure 6-2 Assessment of cone function following treatment with rAAV2/8.CMV.GDNF (batch#1).....	192
Figure 6-3 Retinal morphology in the eyes of <i>Rho</i> ^{-/-} <i>Opn.gfp</i> treated with AAV2/8.CMV.GDNF (batch#1).....	193
Figure 6-4 GDNF and null plasmids.....	195
Figure 6-5 Comparison of cone function in control vector or PBS treated and untreated eyes.	197
Figure 6-6 The effect of sub-retinal injections on rod and cone function in the wild type mouse.	200
Figure 6-7 Dilution series of rAAV2/8 CMV.GDNF (batch#1)..	202
Figure 6-8 Comparison of the effects of titre matched rAAV.CMV.GDNF and control vector preparations on cone function.	203
Figure 6-9 Two-phase separation.....	206
Figure 6-10 Genomic titres of the CMV.GDNF vector made with and without two phase separation..	207
Figure 6-11 SDS-PAGE separation and protein staining of vector samples.....	208

Figure 6-12 Transmission electron micrographs of rAAV2/8 purified with and without two-phase separation..	210
Figure 6-13 Genome packaging in vectors sample purified with and without phase separation.	211
Figure 6-14 Cone function in rAAV2/8 CMV.GDNF treated and untreated eyes (n=4).	212
Figure 6-15 Central cone counts in GDNF and untreated eyes.	213
Figure 6-16 <i>In vivo</i> imaging of cone photoreceptors in GDNF treated and untreated eyes of degenerating retina..	214
Figure 7-1 The Intrinsic and Extrinsic pathways of Apoptosis.	220
Figure 7-2 The structural and regulatory domains of XIAP.	224
Figure 7-3 Collage of SLO images from ARR4-GFP injected eye.	231
Figure 7-4 Immunohistochemistry of retina treated with rAAV2/8.ARR4.hrGFP.	232
Figure 7-5 Determination of primer efficacy and specificity.	234
Figure 7-6 Testing for hXIAP in transfected BHK cells.	236
Figure 7-7 PEI transfected 3T3 cells expressing GFP	237
Figure 7-8 PCR detection of XIAP expression	238
Figure 7-9 Confirmation of hXIAP transgene expression	239
Figure 7-10 The effect of rAAV2/8 on cone function in the <i>Rho</i> ^{-/-} <i>Opn.gfp</i> mouse.	241
Figure 7-11 Percentage change in cone function with rAAV2/8 treatment.	242
Figure 7-12 XAF1 expression levels in CMV.XIAP treated and untreated eyes of the <i>Rho</i> ^{-/-} <i>Opn.gfp</i> mouse	245
Figure 8-1 Rhodopsin protein in AAV2/8 treated rhodopsin knockout mice	256
Figure 8-2 Comparison of rhodopsin and transducin expression in treated rhodopsin knockout and untreated wild type retina.	258
Figure 8-3 Rod and cone function in the rhodopsin knockout mouse treated with rAAV2/8.bRHO.hrRHO	260
Figure 8-4 Rod function in young wild type mice	261
Figure 8-5 Timing of neuronal cell development in murine retina.	262
Figure 8-6 Rhodopsin gene replacement in the neonatal rhodopsin knockout mouse.	264
Figure 8-7 Combination treatment with rhodopsin and GDNF in the <i>Rho</i> ^{-/-} <i>Opn.gfp</i> mouse.	266
Figure 8-8 The pd10 rhodopsin plasmid optimised for protein expression.	268

Figure 8-9 Graphical representation of relative nucleotide abundances at locations either side of the AUG translation initiation site in mammalian mRNAs.	270
Figure 8-10 ERG function in rAAV2/8 bRHO.hRHO ^{Optimised} treated eyes.	273
Figure 9-1 Exogenous and endogenous modifiers are used to control gene expression.....	283
Figure 11-1 Degeneration of the outer retina in the <i>Rho</i> ^{-/-} <i>Opn.gfp</i> mouse.	290
Figure 11-2 The rhodopsin knockout phenotype: rod function as assessed with the scotopic ERG in 6 week old mice.	291
Figure 11-3 The rhodopsin knockout phenotype: cone function as assessed with the photopic and flicker ERG.....	292
Figure 11-4 Genomic titre of the rAAV2/8.CMV. <i>Gdnf</i> vector.....	296
Figure 11-5 Total protein concentration in the eyes of six mice that had been treated with rAAV2/8.CMV.GDNF.....	297
Figure 11-6 Dot-blot titre of rAAV2/8.CMV.HA (no ATG) virus.....	298
Figure 11-7 Western blots to validate HA plasmid and control virus.....	300
Figure 11-8 The titre of the rhodopsin construct (un-optimised).....	301
Figure 11-9 Rhodopsin construct nucleotide sequence before and after optimisation.....	302
Figure 11-10 Frequency of optimal codons pre and post optimisation.....	303
Figure 11-11 The distribution of codon usage frequency along the length of the gene sequence.	303
Figure 11-12 Distribution of guanine (G) and cytosine (C) in transgene DNA.....	304
Figure 11-13 Protein alignment following optimisation	304
Figure 11-14 Protein stain of the bRHO.hRHO (optimised #1) vector	305
Figure 11-15 Examples of β -actin quantitative real-time PCR reaction traces.....	306
Figure 11-16 Examples of XAF1 quantitative real-time PCR reaction traces.	307
Figure 11-17 Cone function in one year old wild type mice.....	308

Tables

Table 1-1 Mapped and identified genes for the major sub-types of RP.....	36
Table 1-2 Markers of apoptosis.....	48
Table 1-3 Summary of relevant murine models of retinal degeneration.....	65
Table 1-4 Commonly used rhodopsin transgenic rat models of RP.....	66
Table 2-1 Buffers, Media & Solutions	70
Table 2-2 KOD polymerase PCR reaction.....	73
Table 2-3 Growth media used for cell culture.....	78
Table 2-4 Transfection mix for AAV2/2.....	80
Table 2-5 rAAV2/8 calcium chloride transfection mix	82
Table 2-6: Proteinase K digest of rAAV.....	87
Table 2-7: DotBlot Labelling protocol.....	88
Table 2-8 Lipofectin Transfection mix	92
Table 2-9 PEI Transfection mix	93
Table 2-10 Primary Antibodies	105
Table 2-11 Antibodies used for Western Blotting	108
Table 7-1 Species specific XIAP PCR primers.....	233

Chapter 1 Introduction

1.1 Overview

Retinal diseases severely impair vision for millions of people. For many of the most common disorders, including rod-cone dystrophies and age-related macular degeneration (AMD), the cone photoreceptors continue to function until the late stages of the disease. However, in time the cone photoreceptors become secondarily affected resulting in the loss of the high acuity central visual field, and colour vision, on which normal functional lives are so dependent.

The recent trials of gene-replacement therapy for a form of Leber's congenital amaurosis have demonstrated that selected monogenic disorders can be treated safely and effectively by targeting the underlying genetic mutation.¹⁻⁶ However genetic heterogeneity, early onset structural changes, gain of function mutations, dominant negative mutations, and poorly characterised aetiology all present significant challenges for similar treatments to be used for the majority of retinal disorders.

In contrast 'proof of concept' experiments have been performed with neuroprotective factors to show that targeting the process of photoreceptor death may provide a treatment of widespread use regardless of the underlying disease. Even a limited slowing of photoreceptor degeneration could give millions of people valuable years of extra sight. CNTF, a cytokine with neuroprotective effects, is currently in phase II clinical trials,⁷ though studies in animal models have identified dose-related toxic effects on photoreceptors.^{8;9} Other means of neuroprotection are also under investigation but important questions remain, particularly as to whether any effect is sustained over time and whether rescuing cone photoreceptors, with their importance for normal quality of life, is feasible in the presence of established rod photoreceptor degeneration.

1.2 The mammalian eye

The mammalian eye consists of three major anatomical layers, which are shown in Figure 1-1. The outermost layer consists of relatively tough tissues, namely the opaque fibrocollagenous sclera and the transparent cornea. The middle layer in contrast consists of highly vascular tissues, known collectively as the uvea. In the posterior segment of the eye the uveal tissue constitutes the choroid, which is the major blood supply to this portion of the eye and is also known as the choriocapillaris. Anterior to the choroid is the ciliary body and then iris. It is within the ciliary body that the aqueous fluid filling the anterior portion of the eye is continuously produced, and that the muscles are found which act to alter the shape and hence refractive strength of the intraocular lens. The iris too contains within it smooth muscle tissues and is the pigmented sphincter that determines the pupillary aperture of the eye.

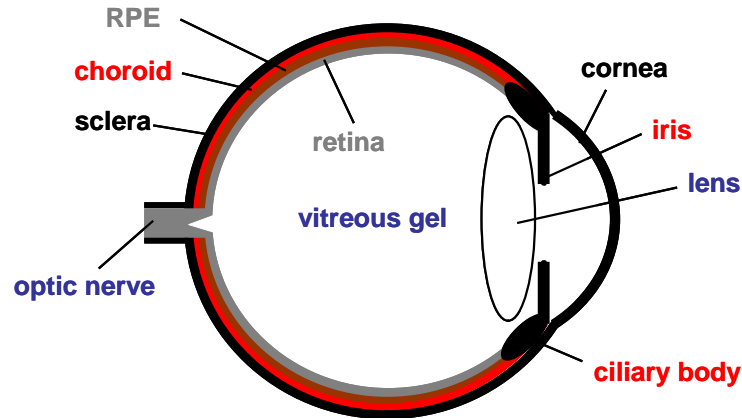


Figure 1-1 Cross section of the eye. The eye consists of 3 principal layers: 1: sclera and cornea (labels in black); 2: choroid, iris and ciliary body (labels in red); 3: retina and retinal pigment epithelium (RPE) (labels in grey). The vitreous gel, neighbouring the innermost border of the neuroretina, is approximately 98% water and translucent in the adult eye.

The inner most layer consists of the retinal pigment epithelium (RPE) and neuroretina, with the latter bordering the vitreous cavity. It is within the neuroretina that incident light is absorbed, having been focussed by the cornea and lens. The process through which photons stimulate a change in membrane potential is known as phototransduction and this occurs in specialised neuronal cells known as photoreceptors. Photoreceptor derived changes in membrane potential are processed within inner retinal layers, and in turn lead to action potentials within ganglion cells, the axons of which leave the eye within the optic nerve to synapse in sub-cortical visual centres of the brain.

1.2.1 The neuroretina

The mammalian retina is a highly specialised multilayered tissue, as shown in Figure 1-2, consisting of 6 major neuronal cell types. The photo-sensitive cells, the sensory neurons of the visual system, are the rod and cone photoreceptors whose nuclei reside in the outer nuclear layer (ONL). Extending in from the ONL the photoreceptors have cellular processes that synapse in the inner plexiform layer (IPL). Extending out from the ONL, into the sub-retinal space, these cells have inner and outer segments.¹⁰ The outer segments of cone photoreceptors are conical in shape, whilst those of rods are long, thin and cylindrical (Figures 1-3 and 1-4). In both cases the inner segments are rich in mitochondria and the cellular apparatus necessary for protein synthesis, whilst the outer segments are densely packed with membranes in which the light-sensitive photopigments are located. In cones the outer segment membranes are formed by repeated invaginations of the cellular membrane, where as in rods there are discrete intracellular membrane discs. The protein rich outer segment membranes are continually renewed, with old membranes discarded for degradation by the neighbouring retinal pigment epithelial (RPE cells).

Cone photoreceptors sub-serve high resolution and colour vision in high ambient light conditions (referred to as photopic conditions). They have much lower light sensitivity than rod photoreceptors, but produce faster responses and adapt to light more efficiently. This means that under natural light conditions cones do

not become saturated, and provide greater temporal resolution vision than is derived from rods. In humans there are three types of cone photoreceptor with distinct opsin proteins bound to a common chromophore (11-*cis*-retinal) giving the different absorption spectra for colour vision. Peak sensitivities are at approximately 420nm, 530 nm and 560 nm for S- (short/blue), M- (middle/green) and L- (long/red) cone photopigments respectively. M- and L-cone opsins have about 96% amino acid sequence homology with each other and about 42% sequence homology with S-cone and the rod opsin protein.¹¹ Humans and selected non-human primates have a specialised region at the posterior pole of the eye known as the fovea which consists of densely packed cones, devoid of rod photoreceptors or overlying blood vessels; it is this portion of the retina that is used for fixation and for highest acuity vision.

In mice there are only two types of cone opsin (M- and S-). Most cones in mice express both these opsins, but the degree of M-opsin expression varies across the retina, being greatest in the superior retina and least in the inferior retina.¹² Furthermore, in the mouse cones are evenly distributed across the retinal surface without any specialised fovea.^{13;14} As in Figure 1-2 cone photoreceptor nuclei in the mouse eye form a single row at the outermost edge of the ONL.

Rod photoreceptor cells, in both humans and rodents, are widely distributed across the retina and far outweigh the number of cones (making up 97% of the total photoreceptor population in mice¹³ and 95% in humans).¹⁵ In the rodent it is the rod nuclei that form the bulk of the ONL, though in humans this varies with position in the retina.¹⁵ Rods are extremely sensitive to light and able to detect single photons. Peripheral vision in scotopic (i.e. low light level) conditions is primarily mediated through rod photoreceptors, but their ability to adapt to bright light is limited. The peak sensitivity of the rod pigment is approximately 496 nm.

In the outer plexiform layer of the retina the photoreceptive rods and cones synapse with the second order neurons of the visual system, the horizontal and bipolar cells whose nuclei are found in the inner nuclear layer. The synapses between these cells and amacrine cells allow intra-retinal processing of the inputs

to the visual system.¹⁶ Within the inner plexiform layer cells of the INL synapse with cells of the innermost layer, the ganglion cell layer. It is the axons of the ganglion cells that pass into the optic nerve to form the afferent connection from the retina to the brain.

In addition to the neuronal cells of the retina there are permanent populations of glial cells. Mueller glia, the processes of which transverse the retina, provide physical as well as physiological support to the other cells of the retina. Through a network of adherens junctions the inner foot processes of glia cells form the inner limiting membrane of the retina which separates the retina from the vitreous cavity. The outer foot processes of the Mueller glia are aligned with the photoreceptor inner segments, and likewise through inter-cellular junctions, form an outerlimiting membrane that is of structural importance to the photoreceptors. Of note in the context of cone neuroprotection, Mueller glia respond to a variety of stimuli by releasing trophic factors that act directly to support photoreceptor survival and function.¹⁷ Other factors and cytokines released by Mueller glia influence vascular permeability and retinal homeostasis. They have also recently been found to have a role in intra-retinal visual pigment recycling for cones under bright daytime light conditions.¹⁸ Other glial cells found in the retina include astrocytes and microglia. Astrocytes too are heavily involved in retinal haemostasis, in part through interactions with intra-retinal blood vessels. The retinal microglia, derived from circulating monocytes, are central to immune responses and tissue repair; they are activated early on in retinal degenerations and are seen to migrate to the ONL, though the extent to which they perpetuate the processes of neuronal death, as opposed to being merely reactive, is less clear.¹⁹

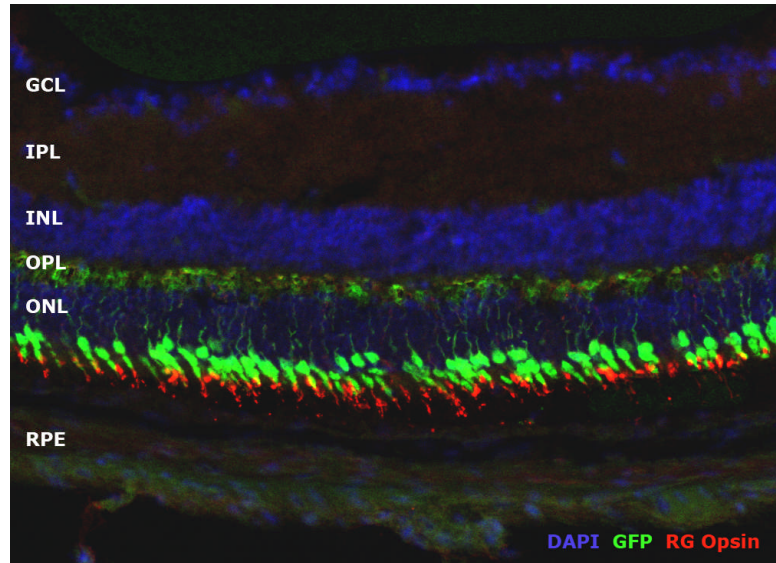


Figure 1-2 Cross section of retina from a transgenic mouse with green fluorescent protein (GFP) expressed in cone photoreceptors. The section has been stained with an antibody for RG opsin, which is found in cone photoreceptor outer segments. DAPI has been used to stain nuclei. The principal layers of the retina are evident: outer nuclear layer (ONL), outer plexiform layer (OPL), inner nuclear layer (INL), inner plexiform layer (IPL) and ganglion cell layer (GCL). The ganglion cell layer is the innermost, and neighbours the vitreous cavity.

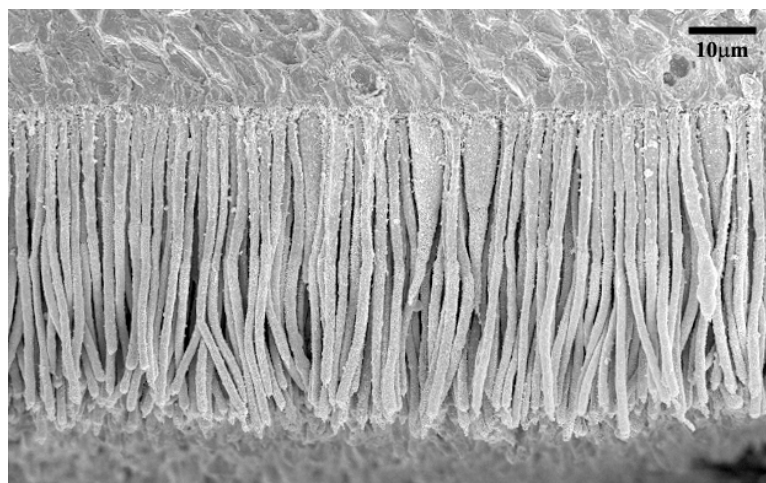


Figure 1-3 Field emission scanning electron microscope image of human retina showing rod and cone outer segments. Image courtesy of Dr P Munro, Imaging Dept, UCL Institute of Ophthalmology

The retinal pigment epithelium

The RPE, on the outermost border of the neuroretina, consists of a single layer of polarised and pigmented cuboidal epithelial cells (Figure 1-4 and Figure 1-5). The melanin pigment within these cells reduces scattering of light within the retina, and thus contributes to the high degree of spatial discrimination and acuity that the visual system can achieve. The cells are also closely adherent to one another through intervening tight, gap and adherens junctions and thus create a physiological barrier between the choriocapillaris on one side and the neuroretina on the other. By controlling the passage of water, ions and selected molecules the RPE cell layer actively maintains the chemical environment and homeostasis of the outer retina. Furthermore the apical surface of these cells consists of microvilli that interdigitate between the photoreceptors of the outer neuroretina. Through these close approximations the RPE cells assist in cellular functions and produce neurotrophic factors required for photoreceptor cell viability. The RPE cells also phagocytose outer segments membranes that are discarded by photoreceptors in the process of continual renewal; degradation of these within the RPE cells generates lipofuscin pigments as a by-product, accumulation of which has been identified as an important pathological step in several inherited retinal degenerations.

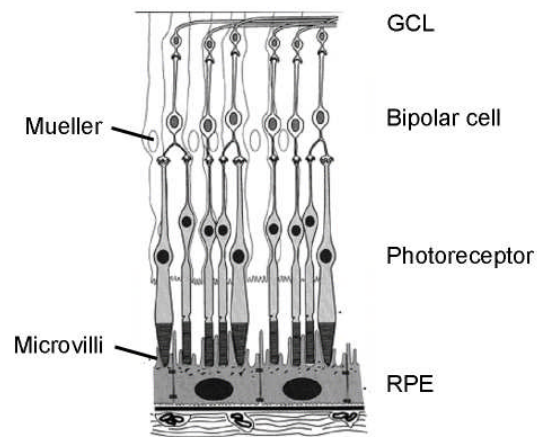


Figure 1-4 RPE cells in relation to principal retinal cell types. RPE microvilli are seen to interdigitate between photoreceptor outer segments. Adapted from Deubner, Journal American College of Nutrition, 2000.

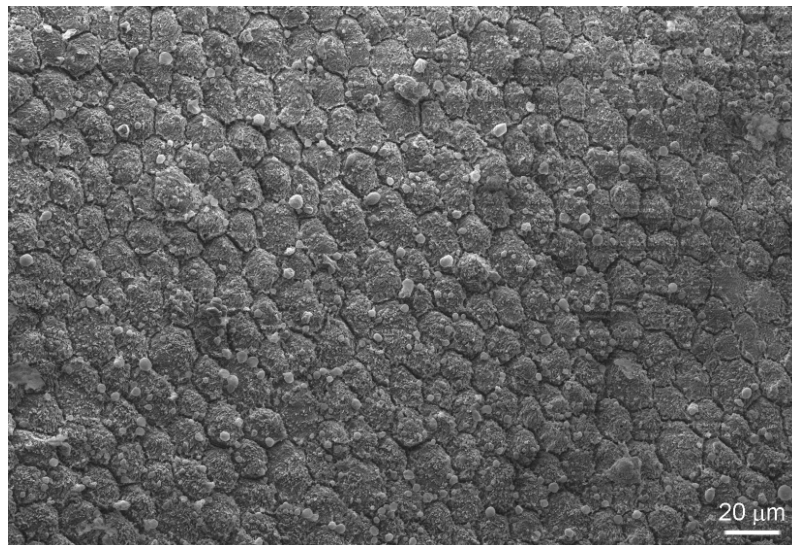


Figure 1-5 Scanning electron micrograph of the RPE monolayer. The RPE cells are closely adherent to one another to form a continuous layer which regulates the passage of water and metabolites to and from the retina. This image is taken from a macaque eye that had undergone experimental surgery; the small spheres on the surface of some RPE cells are residual heavy liquid following the surgery, and not a normal feature of the RPE monolayer.

1.2.2 Phototransduction

The process through which light stimulates a change in membrane potential is known as phototransduction. Central to this is the light sensitive molecule, known as a chromophore, 11-*cis*-retinal. On absorption of a photon the 11-*cis*-retinal molecule undergoes a conformation change (a *cis*- to *trans*- isomerisation resulting in straightening of the molecule) such that it becomes all-*trans*-retinal. In mammalian photoreceptors the chromophore is bound through a covalent Schiff-base linkage to a lysine residue in the seventh helix of an opsin molecule. The opsin molecules all have seven transmembrane helices and the 11-*cis*-retinal nests in between these. Variations in the opsin molecule sequence determine the peak absorption spectrum of the complex.

The steps through which photo-isomerisation of the rod chromophore-opsin complex leads to a change in membrane potential are shown in Figure 1-6. Of note, prior to activation of the phototransduction process the cGMP-gated (CNG) channel is open permitting a constant influx of cations; this is known as the 'dark current'. Activation of the phototransduction process results in closure of these channels and membrane hyperpolarisation. This in turn leads to decreased release of neurotransmitter at the OPL synapse.

In contrast to most neuronal cells where activation leads to an all or nothing depolarisation, the hyperpolarisation and change in neurotransmitter release in stimulated photoreceptors cells is graded and proportional to stimulus strength. In part this is due to the phototransduction cascade activation being tightly regulated by negative feedback mechanisms. In addition to the calcium dependent feedback mechanisms shown and discussed in Figure 1-6, the cascade is also terminated by phosphorylation of activated rhodopsin by rhodopsin kinase and the subsequent binding of phosphorylated rhodopsin by arrestin. Also the bound GTP promoting activation of the transducin α -subunit is hydrolysed resulting in the phosphodiesterase complex returning to its inhibited state. Although the phototransduction process in cones is very similar to that shown in Figure 1-6 for rods a number of the proteins involved are cell-type specific. These differences are likely to account for the differences in response kinetics

between rods and cones (cones are approximately 100 times less sensitive than rods but their response kinetics are faster). The protein differences are also important when considering disease mechanisms and the cells primarily affected by a mutation. For example the cGMP-gated channel subunits in rods are CNGA1 and CNGB1, whereas in cones the analogous subunits are CNGA3 and CNGB3. Cones also have specific transducin and cGMP-PDE proteins, and alternatives to the arrestin and recoverin molecules seen in rods (known as X-arrestin and visinin in cones respectively).^{20;21}

The number of different proteins involved in these high-energy pathways is a factor in why there are so many disease-causing mutations involving phototransduction proteins. In addition of course, the capacity for repair or regeneration in these neuronal cells is limited. Indeed, by definition the IRD-causing mutations that affect the phototransduction cascade lead not only to loss of function, but also to photoreceptor death.

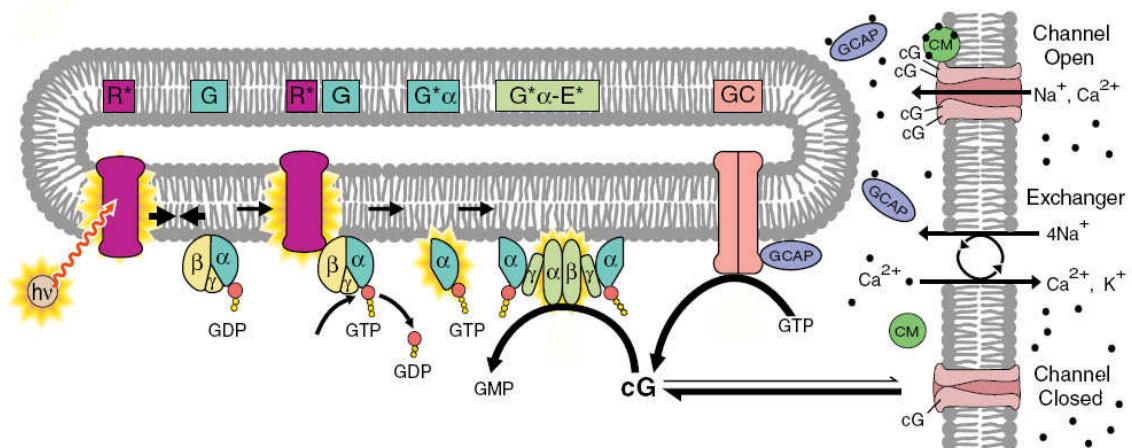


Figure 1-6 Activation of the phototransduction cascade. *11-cis*-retinal-rhodopsin, bound to disc membrane in the rod outer segment, is activated by an incident photon ($h\nu$). The activated rhodopsin (R^+) in turn binds the heterotrimeric G-protein, transducin (G), catalysing the exchange of GDP for GTP and resulting in the formation of an activated α -subunit ($G^+\alpha$) bound to GTP. Two activated G protein α -subunits in turn bind and activate photoreceptor cell specific phosphodiesterase (PDE6) ($G^+\alpha$ - E^+), leading to hydrolysis of cGMP (cG). The activation step involves the removal of inhibitory γ -subunits from the active site of this enzyme. The consequent decrease in cytoplasmic cGMP levels leads to closure of a cGMP gated cation channel and cessation of the resting influx of sodium and calcium ions. The cell therefore hyperpolarises. Feedback mechanisms are simultaneously activated in part through cytoplasmic calcium levels. As a sodium/calcium exchanger continues to function the cytoplasmic calcium levels decline and calcium is released from both the guanylyl cyclase activating protein (GCAP) and membrane bound calmodulin (CM); calcium free GCAP then binds and activates guanylate cyclase (GC), leading to regeneration of cGMP. Calcium-free calmodulin dissociates from the cGMP gated cation channels altering their affinity for cGMP. Calcium ions also inhibit the phosphorylation of rhodopsin via the protein recoverin or S-modulin. Adapted from Lamb and Pugh.²²

1.2.3 The visual cycle

Chromophore pigment is recycled in an enzyme cascade known as the visual cycle, the key steps of which are shown in Figure 1-7. *All-trans*-retinol, obtained either following phototransduction in photoreceptors or de novo from the blood vessels is isomerised within the RPE to 11-*cis*-retinol. Cone photopigment recycling is also performed in Mueller cells, which like the RPE cells, are in close proximity.²³

In addition to the steps and enzymes shown in Figure 1-7, two others are of note because of their pathological significance:

1. RPE-retinal G-protein coupled receptor (RGR).

All-trans-retinol (vitamin A) is also delivered to the RPE cells from the systemic circulation bound to serum retinol binding-protein. *All-trans*-retinol binds to the RPE-retinal G-protein coupled receptor (RGR); like rhodopsin this protein is a seven transmembrane domain receptor and mutations within its gene (RGR) are a cause of RP.

2. Cellular retinaldehyde binding-protein (CRalBP)

Once *all-trans* retinal esters have been isomerised to 11-*cis*-retinol the latter is bound to cellular retinaldehyde binding-protein (CRalBP) prior to binding by 11-*cis* retinol dehydrogenase 5. Mutations in the CRalBP gene (*RLBP1*) are also found in RP.

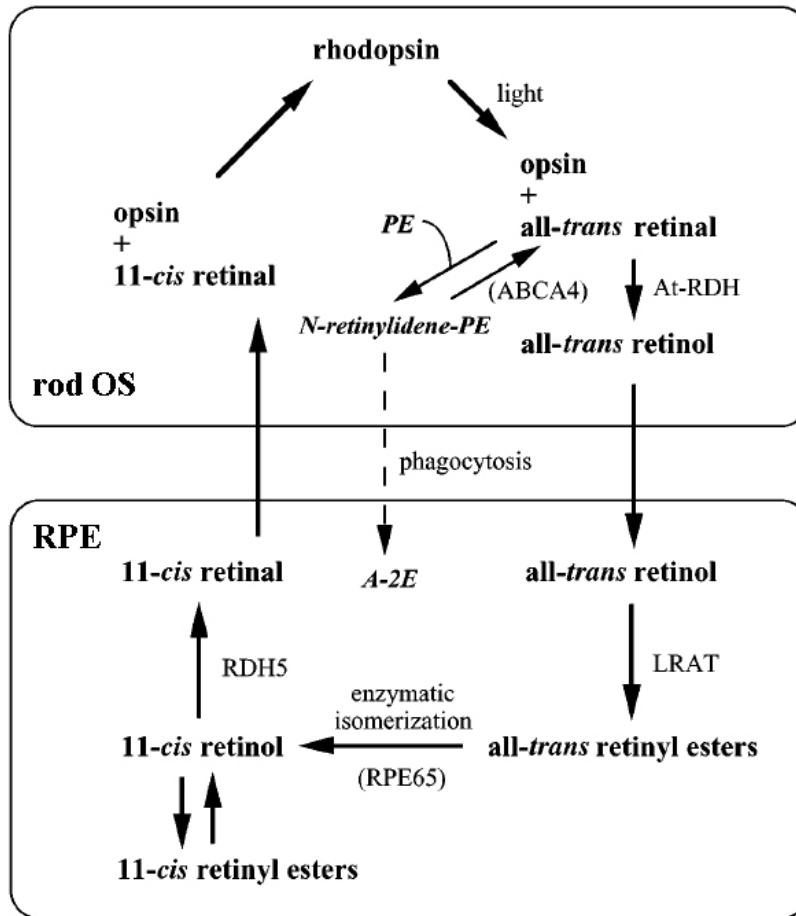


Figure 1-7 The steps of the visual cycle. The activation of rhodopsin by light occurs through the isomerisation of the bound chromophore, 11-*cis*-retinal, to all-*trans*-retinal. This is then released from rhodopsin and reacts with the membrane lipid phosphatidylethanolamine (PE) before being transported back to the cytoplasm by ABCA4. After modification to all-*trans*-retinol by retinol dehydrogenase (At-RDH) it is transported to the RPE and trans-isomerised to 11-*cis*-retinal through the actions of LRAT, RPE65 and RDH5. The reaction of all-*trans* retinal with PE also generates the precursors of lipofuscin fluorophores (e.g., N-retinylidene-PE) which are taken up by the RPE through phagocytosis to form lipofuscin fluorophores (e.g., A-2E). Abbreviations: At-RDH, all-*trans* retinol dehydrogenase; LRAT, lecithin-retinol acyltransferase; RPE65, retinal pigment epithelium-specific protein, 65-kDa; RDH5, 11-*cis*-retinol dehydrogenase 5; PE, phosphatidylethanolamine; A-2E, N-retinylidene-N-retinylethanolamine. Adapted from Pacione et al.²⁴

1.3 Inherited retinal degenerations

In the developed world inherited retinal degenerations (IRDs) are an important cause of blindness in children and those of a working age, and at present no curative treatments exist. Retinitis pigmentosa, the most prevalent form of IRD, affects between 1/7000 and 1/3000 of the population, typically causing blindness in the 4th or 5th decade of life.²⁵⁻²⁷ Other IRDs include X-linked retinoschisis, Best's disease, Stargardt's disease and the progressive cone and cone-rod dystrophies. Recently age-related macular degeneration (AMD) has been shown to have an underlying genetic basis, but involving several genes (reviewed by Zanke *et al.*)²⁸

1.3.1 Classifications and Genotype-Phenotype Correlations

The classification of IRDs has historically been on the basis of clinical characteristics and patterns of inheritance. However, since the 1980s there has been a rapid increase in the understanding of the molecular basis for these diseases with over 200 retinal disease loci, and 160 disease-causing genes identified to date (Figure 1-8).²⁹ Complexity arises however as the effect of a specific mutation can vary markedly between individuals. In part this can be due to the effect of other genes as is well illustrated with the *Rdh8* and *Abca4* double-knockout mouse.³⁰ Absence of both of these genes, which are involved in all-*trans*-retinal clearance from photoreceptors results in a fast retinal degeneration whereas absence of either in isolation does not; the resultant retinal degeneration can therefore be described as a digenic disorder. However, the degeneration is not seen in all double-knockout animals and it has been found that in part incidence is determined by which of two different alleles of *Rpe65* are also carried. An allele variant with leucine (Leu) instead of methionine (Met) at position 450 leads to greater all-*trans*-retinal clearance (A2E) accumulation.³¹ A2E is a by-product of all-*trans-retinal* metabolism and its accumulation is toxic to RPE cells.^{32;33} A greater incidence of retinal degeneration is therefore seen in mice that carry the Leu⁴⁵⁰ variant of *Rpe65* in addition to the *Rdh8* and *Abca4* double-knockout.

In patients, digenic forms of retinitis pigmentosa are not common but are seen with a protein-truncating or null-sequence change in *ROM1* in conjunction with a single mis-sense mutation in *RDS*.^{34:35} Both these genes encode structural proteins required for the formation and maintenance of rod outer segment discs. *RDS* mutations in particular are associated with variable phenotypes. Different mutations within this same gene cause phenotypes including autosomal dominant retinitis pigmentosa (adRP), fundus flavimaculatus, retinitis punctata albescens, central areolar choroidal atrophy, diffuse choriocapillaris atrophy, cone-rod dystrophy, age-related macular degeneration-like maculopathy, choroidal neovascularisation, pattern dystrophy, butterfly-shaped pigment dystrophy and adult-onset foveomacular dystrophy.³⁶ In addition for some of the mutations marked diversity is seen within families, where genetic diversity between individuals will be limited. Although difficult to prove this is likely to be due to environmental interactions as well as the influence of additional modifier genes. The complexity of the underlying genetics means that in practice a careful phenotypic description is as important as ever to help guide where to look for mutations and how to interpret them.

Determination of the phenotype of patients with inherited retinal degenerations is greatly aided by the use of the electroretinogram (ERG). In this procedure the summed electrical responses of the retina to a stimulus are recorded with an electrode in contact with the cornea. By varying the stimulus or background light characteristics it is possible to specifically examine rod or cone photoreceptor mediated responses. To examine rod-pathway responses the patient can be dark-adapted and then dim light flashes are presented under scotopic (dark-adapted) conditions. Conversely, to examine cone-pathway responses the patient can be light-adapted to achieve bleaching of the rod photoreceptors, and then whilst still exposed to bright background light (photopic) conditions bright flashes are presented to the subject. Further cone-specificity can be achieved using high frequency stimuli, as is the case in photopic flicker ERG protocols. The initial response recorded under photopic or scotopic conditions is a negative reflection (known as the a-wave) which is as a direct result of cyclic nucleotide gated cation channels closing in photoreceptor outer segments. Subsequently there is a larger positive displacement reflecting post-

photoreceptor neuronal activity within the retina.³⁷ By determining the extent of functional impairment in specific photoreceptor populations the ERG can be used as an objective means of detecting progression and allows detailed phenotypic descriptions to be made. Furthermore, with limited adaptations similar protocols can be used both in experimental animal models and in humans facilitating research and genotype-phenotype correlations.

The combination of detailed history taking, clinical examination and clinical testing, coupled with molecular genetics gives a powerful tool to diagnose patients and give appropriate prognoses and genetic counselling. Only by knowing which variant of a disease or syndrome the patient is suffering from can health services move towards individualised care. Furthermore, the associated understanding of the disease pathology and mechanisms has driven research into potential therapies.

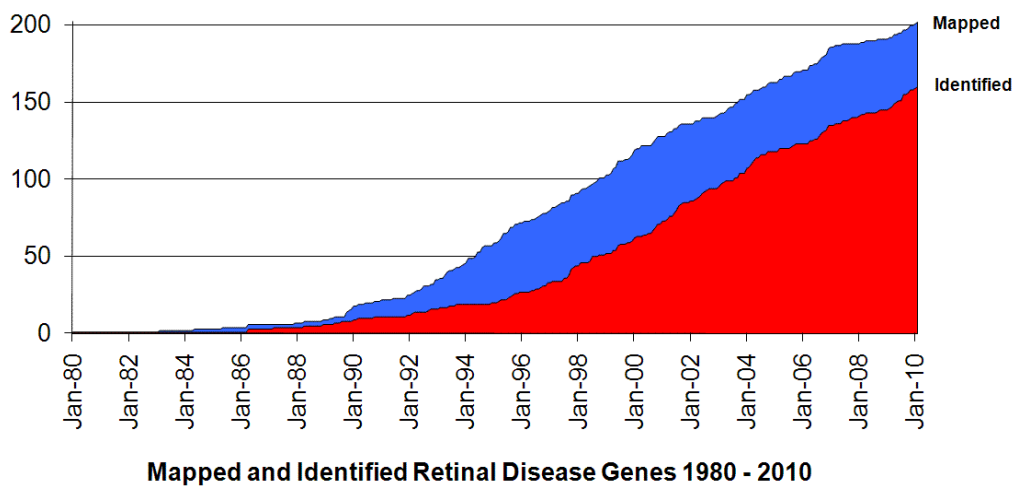


Figure 1-8 The number of mapped and identified retinal disease genes from 1980 to 2010. Graph from the Retinal Information Network provided by the University of Texas-Houston Health Science Centre (www.sph.uth.tmc.edu/RetNet)

1.3.2 Retinitis Pigmentosa

The term 'retinitis pigmentosa' (RP) is used to describe a heterogeneous group of inherited disorders in which there are shared clinical features and hence a common phenotype. The underlying biological pathways and disease mechanisms giving rise to that phenotype are however highly variable. Typically patients with RP have a progressive rod-cone dystrophy and so the early symptoms are related to rod dysfunction in the peripheral visual field. This may not be noticed until advanced or tested for, but the peripheral rod photoreceptor loss results in nyctalopia (poor night vision) and reduced sensitivity in the peripheral visual field (tunnel vision) that will in time render the patient ineligible for driving. The loss of photoreceptors is associated with disruption of cells in the retinal pigment epithelium and the release of pigment granules and so one of the characteristic clinical signs is the development of peripheral sub-retinal pigment deposits.³⁸ These are shown in Figure 1-9 and are most marked alongside blood vessels forming perivascular clusters known as bone-spicules due to their morphological appearance.³⁹ The rod photoreceptor loss is progressive from the retinal periphery towards the macula, and so an abnormal retinal reflex may sometimes be seen as ring at the advancing edge of the area of pigmentation. In time there follows a secondary loss of cone photoreceptors and it is this that has the greatest impact on the patients. Patients with early RP, as with those with congenital stationary night blindness in which there is only rod photoreceptor loss, commonly continue to work and live mobile and independent lives. In the early stages they can continue to hold a full driving licence. However in RP patients the cone photoreceptors become secondarily affected in time leading to a deterioration in central visual acuity and colour vision. It is this loss of cone-based vision that is of greatest functional significance to patients and ultimately leads to patients being registered as blind.

Although most case of RP are characterised by the typical rod-cone loss, there are multiple variants, including those where the loss of cone photoreceptors is simultaneous to that of rods.^{40;41} These are referred to as cone-rod degenerations and have symptoms of cone loss from early on in the disease.

The clinical signs seen in RP in addition to bone-spicule formation also relate to photoreceptor loss. Retinal blood vessels are subject to autoregulation, so as photoreceptors loss progresses and oxygen demand diminishes the retinal arteries are seen to become attenuated. The reduced blood flow also gives the optic disc an altered appearance, described as 'waxy' in colour. This is in contrast to the pale disc of arteriolar occlusions as in RP the inner retina is preserved⁴² and so there is not the axonal loss seen in other causes of reduced nerve head perfusion. In advanced RP the macula itself may be seen to be abnormal with atrophic or cellophane features. Cystoid macular oedema may occur as a further complication. Loss of retinal thickness can also lead to a relative unmasking of the large choroidal vessels that can not ordinarily be seen.³⁹

The timecourse of disease progression in RP is very variable, again reflecting that it is now known to be a heterogeneous group of conditions with a large variety of underlying genetic mutations and additional influences. In general though, symptoms or signs of the disease typically present during the 2nd or 3rd decade of life, with legal blindness following in the 4th to 5th decades once cone photoreceptor function is also affected. X-linked, autosomal recessive and autosomal dominant cases generally have their age of onset at successively greater ages, though there is considerable overlap. Leber's congenital amaurosis is a severe congenital form and syndromic cases usually present in infancy.

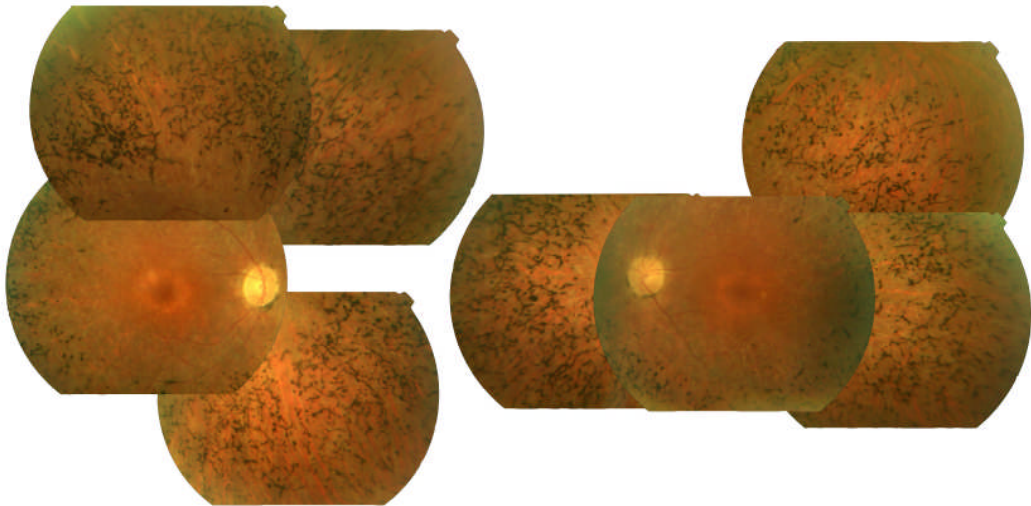


Figure 1-9 Collage of fundus photographs showing typical features of retinitis pigmentosa. In the retinal periphery there is evidence of bone spicule formation. Retinal blood vessels are attenuated and the optic disc has a waxy pallor appearance.

Prior to the onset of genetic tests patients were described on the basis of the phenotype and pattern of inheritance. These distinctions are still used both clinically and to sub-classify the large variety of identified mutations as in Table 1-1.²⁹ The major sub-classifications and figures for their approximate prevalence are shown in Figure 1-10. Autosomal dominant RP (AdRP), autosomal recessive, and x-linked RP encompass approximately 30%, 20% and 15% of non-syndromic cases respectively. Alternatively these may be described in terms of total RP cases, in which case the prevalences are 20%, 13% and 8%. Approximately 5% of the non-syndromic cases are early-onset forms of RP that are termed recessive Leber congenital amaurosis (LCA). The remaining 30% of non-syndromic cases are of sporadic or unknown inheritance and these will include undiagnosed recessive mutations as well as de-novo dominant mutations. In addition to the non-syndromic cases of RP there are also the syndromic forms which involve other organs in addition to the eye. For example, in Usher syndrome the development of RP is preceded by congenital hearing impairment. In Bardet-Biedl syndrome ophthalmic features are accompanied by polydactyly, obesity, renal abnormalities, and mental retardation. Multiple other, and relatively rare, systemic associations also exist.²⁹ Prevalence estimates vary with the population studied and due to variations in how diagnostic criteria and

definitions are applied.²⁷ The percentages given in Figure 1-10 are therefore approximations.²⁶

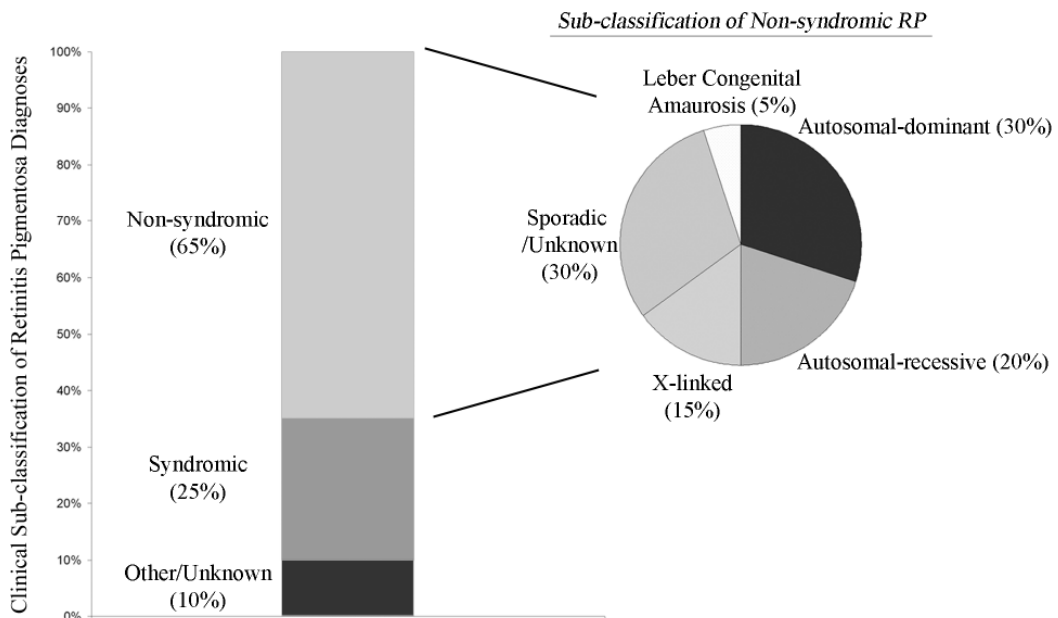


Figure 1-10 Estimated prevalence of retinitis pigmentosa sub-types. Clinically cases of RP are described in terms of a syndromic or non-syndromic phenotype if this can be determined. The non-syndromic cases are then described in terms of inheritance. Autosomal-dominant RP (AdRP) represents the most prevalent single sub-type, representing approximately 30% of all non-syndromic cases (and 20% of all RP cases). The most common single cause of syndromic RP is Usher syndrome. Estimates of prevalence are adapted from Daiger et al.²⁶

1.3.3 Gene mutations in RP

The progress in molecular genetics and diagnostic services available means that in practice the responsible mutation can be identified in about 50-60% of adRP patients and 30% of those with recessive RP.⁴³ In all over 45 different genes have been identified as causing RP, and further loci have been linked though the responsible genes have yet to be identified (Table 1-1).²⁹

RP sub-type	Mapped and identified genes
Autosomal dominant	<i>CA4, CRX, FSCN2, GUCA1B, IMPDH1, KLHL7, NR2E3, NRL, PRPF3, PRPF8, PRPF31, PRPH2, RDH12, RHO, ROM1, RP1, RP9, SEMA4A, SNRNP200, TOPORS</i>
Autosomal recessive	<i>ABCA4, C2ORF71, CERKL, CNGA1, CNGB1, CRB1, EYS, IDH3B, LRAT, MERTK, NR2E3, NRL, PDE6A, PDE6B, PRCD, PROM1, RBP3, RGR, RHO, RLBP1, RP1, RPE65, SAG, SPATA7, TULP1, USH2A</i>
X-linked	<i>RP2, RPGR</i>

Table 1-1 Mapped and identified genes for the major sub-types of RP. Source RetNet online database, accessed September 2010.²⁹

The majority of genes in which mutations causing RP are found are directly involved in phototransduction. Other genes mutated in RP are for proteins involved in the visual cycle, photoreceptor structure and additional cellular functions. The fact that there are so many different disease causing mutations in photoreceptor related genes may reflect the complexity of these cells, their high energy requirements and that damaged cells are not replaced in the mature retina.^{44;45}

Phototransduction proteins

The gene for rhodopsin (*RHO*) was the first to be associated with RP^{46;47} and mutations in this gene remain the most common single cause of RP, accounting

for approximately 25% of autosomal dominant cases⁴⁸ as well as autosomal recessive and sporadic cases.⁴⁹⁻⁵¹ A large variety of disease-causing mutations are found within the gene; to date more than 120 point mutations alone have been identified,²⁹ about 60% of which localise to the transmembrane domain of the protein and 35% to the extracellular loops; only rarely are mutations affecting the intracellular loops pathogenic.⁵² Rhodopsin mutations are commonly described in terms of classes based on their behaviour in tissue culture experiments.^{53;54} Class II mutations are the most common and are thought to result in defective folding such that there is abnormal protein aggregation. Such proteins are then usually marked for degradation within the cell. Class I mutations cause abnormal trafficking of the mutant rhodopsin protein within the cell.

Mutations in the genes for the α catalytic unit and β subunits of PDE6 (*PDE6A* and *PDE6B* respectively), the α subunit of the rod cyclic nucleotide gated channel (*CNGA1*), and arrestin (*SAG*) have also been identified as causes of RP (reviewed by Phelan and Bok).³⁸ Mutations in these phototransduction-related genes are also important causes of other inherited retinal degenerations in addition to RP, including congenital stationary night blindness and cone dystrophies.

Visual cycle proteins

The second most common group of genes mutated in RP are those encoding proteins involved in the visual cycle. The genes encoding RPE65 (*RPE65*), CRalBP (*RLBP1*), RGR (*RGR*) and ABCR (*ABCA4*) are all known to be mutated in cases of RP.³⁸ Of these the *ABCA4* gene is of note because of the wide variety of phenotypes that can be caused by mutations in the gene.⁵⁵ The first phenotype to be associated with *ABCA4* mutations was that of Stargardt macular dystrophy and fundus flavimaculatus. Since then mutations in the gene have also been identified as the most common cause of autosomal recessive cone-rod dystrophy,⁵⁶ in addition to being a cause of autosomal recessive RP.^{57;58} Mutations in the *ABCA4* gene were also initially described as a cause of AMD, but repeated studies since have not validated that claim, and have instead highlighted the

challenges of ascribing pathological significance to changes in such a large gene (50 exons) in which sequence changes are so common in the general population (reviewed by Lotery and Trump).⁵⁹

Structural proteins

Peripherin/RDS and ROM1 are proteins with four transmembrane domains that are of integral structural importance for rod outer segment discs, though they may also have additional functions. The proteins are encoded by the genes *RDS* and *ROM1* respectively. Mutations in *RDS* alone cause RP^{60;61} and mutations in the combination of *RDS* and *ROM1* are a cause of digenic RP.^{34;35} However there is also evidence that *ROM1* mutations in isolation are causative of RP.⁶²⁻⁶⁴

Transcription factors

Mutations of the photoreceptor cell transcription factors *NRL* (*NRL*) and *CRX* (*CRX*) interfere with photoreceptor development and later in life cause retinal degeneration. *NR2E3* mutations are best known as a cause of enhanced S cone syndrome, in which there is photoreceptor death but a relative increase in the number and function of short-wavelength cones.⁶⁵ They are also however causative of RP.⁶⁶

Mutations in syndromic RP

In contrast to the non-syndromic RP mutations affecting photoreceptor or RPE-specific proteins, the causative mutations in syndromic RP typically affect proteins of systemic importance. For example in Bardet-Biedel syndrome (BBS) causative mutations affect proteins related to the primary cilium, a microtubule-based organelle that protrudes from the surface of almost all human cell types and which is of importance in extracellular signalling pathways.⁶⁷ Patients with mutations in such proteins are characterised by obesity, renal dysfunction, retinal degeneration, cognitive impairment, and polydactyly. Likewise in Refsum's disease mutations in *PEX1* affect cellular degradation pathways in a variety of

cell types,⁶⁸ in Usher syndrome a myosin mutation (*MYO7A*) leads to impaired organelle motility within cells,⁶⁹ and in Stickler syndrome the function of collagen proteins are compromised throughout the body leading to joint, hearing and cleft abnormalities in addition to retinopathy.^{29;70}

1.4 Photoreceptor cell death in inherited retinal degenerations

In most cases of RP the disease-causing allele is expressed exclusively in rod photoreceptors, and not in cone photoreceptors. Examples include mutations in rhodopsin,^{46;47;71} or rod-specific cyclic GMP.^{72;73} Early stages of the disease are therefore characterised by rod dysfunction and subsequently by rod photoreceptor cell loss. However, a common feature of the disease is that the mutation-dependent rod photoreceptor death is then followed by a secondary degeneration of the previously healthy cone photoreceptors.⁷⁴ This secondary loss of cone photoreceptors occurs regardless of the underlying mutation and furthermore it is this loss of cone photoreceptors that leads to the greatest reduction in quality of life.

Another common feature, regardless of the underlying mutation, is that the photoreceptor death progresses in a controlled manner without significant inflammation or disruption to the inner retina. Common molecular pathways of cell death are employed, again despite the large variety of causal mutations.

Studies to elucidate these mutual mechanisms leading to secondary cone photoreceptor degeneration, and orderly photoreceptor cell death have furthered understanding of the disease. They have also permitted identification of potential therapeutic targets which are of relevance to large numbers of RP patients, regardless of their precise genotype.

1.4.1 Secondary loss of cone photoreceptors

To date, there is no known form of retinal degeneration in humans or mice where rod photoreceptor death is not followed by cone photoreceptor death.⁷⁵ In contrast there are well described progressive cone dystrophies (PCDs) in which the functional deficit is confined to the photopic system, at least until late stages of the disease. These include patients affected by mutations in the *GUCAIA* gene, which encodes the phototransduction protein guanylate cyclase activating protein-1 (GCAP1), and patients with *CNGA3* and *CNGB3* mutations, which encode the α - and β - subunits of cone cGMP-gated cation channels. *CNGA3* and *CNGB3* mutations are more commonly associated with achromatopsia (a stationary cone dysfunction) but are also seen in PCDs (reviewed by Michaelides et al.).⁵⁶ There is good circumstantial evidence therefore of a cone dependency on rod photoreceptor survival which is not reciprocal.

Studies in murine models in particular have helped identify multiple molecular mechanisms and pathways that contribute to the dependency of cones on rods for survival. Although mice do not have a fovea the relative numbers of rods and cones in the peripheral retina is similar to that in humans, and there are many similarities in the nature of rod-cone degenerations in humans and mice.^{13;15} Ultimately however, the challenge is to detect how such mechanisms cause a slow and progressive degeneration in human cones for years after the rods have almost completely degenerated, and to identify therapeutic targets. Even a partial slowing of this secondary cone loss could yield valuable years of extra sight for millions of people.

Rod-derived paracrine effects

Transplantation studies in the *rd1* mouse demonstrated limited morphological rescue of degenerating cone photoreceptors following the injection of rod photoreceptors into the sub-retinal space.⁷⁶ This suggested that the rods themselves released a diffusible factor causative of the preservation seen. Indeed co-culture experiments were supportive of this hypothesis⁷⁷ and subsequently Leveillard et al. isolated a protein produced by rods that promoted short-term

cone survival in vitro and in vivo in the rd mouse.⁷⁸ The protein was called Rod derived cone viability factor (RdCVF) and is encoded by the *Nxn11* (*Txn16*) gene.⁷⁹ The principal limitation of such studies in the rd mouse is however, that the speed of degeneration is such that the rods are degenerating before the mouse photoreceptor layer is fully developed.⁸⁰ Developmental factors are therefore still likely to be of influence and the course of degeneration contrasts with that in most patients.

In further experiments RdCVF has been evaluated in the P23H rat.⁸¹ This is a better model of rod-cone degeneration, in which a mutated mouse rhodopsin gene (P23H) is expressed under the control of the rhodopsin promoter.⁸² The mutation is clinically relevant (causing 12% of autosomal dominant RP in the United States)⁷¹ and produces a rod-cone degeneration in the heterozygous rats. The authors demonstrated that repeated injections into the subretinal space did produce morphological and functional preservation of cones, compared to PBS-treated and control eyes, at a single late timepoint. The absolute values of cone numbers preserved and improvement in ERG function were small compared to normal values in non-degenerate retina. This was despite the injections being administered at timepoints when rod loss was almost complete and endogenous levels of RdCVF in the degenerate retina were presumably minimal. It will be interesting to see if greater efficacy, supporting a major role for this protein, is achieved with more sustained expression (eg with a viral vector). However, at present the data is more suggestive of a supportive role for this protein as opposed to being the dominant rod-cone influence. This function is further supported by the work of Punzo *et al.* which found that in multiple murine models of RP the cones survive prolonged periods after the rods after almost completely degenerated.⁷⁵ This is similar to observations in humans and indicates that some cones do survive prolonged periods even when the number of surviving rods, and so presumably concentration of rod-derived trophic factors, is minimal.⁸³

Toxins and microglia

The death of rods may be associated with the release of toxic factors, and mobilisation of microglia, that could themselves damage cones.⁸⁴ Kedzierski *et al.* studied a hemizygous-transgenic rds mouse in which the rds transgene had been integrated into the x-chromosome.⁸⁵ The authors noted that in contrast to the random mosaic pattern of photoreceptor degeneration that could be expected, the degeneration was noted to occur in patches involving both cells that were expressing the transgene and others that were not. This could be explained by the spread of some disease causing factor from genetically damaged cells to the neighbouring genetically healthy cells. Such a factor could travel through the extracellular space or through connecting gap junctions; the latter method is referred to as the ‘bystander effect’ and is reviewed by H.Ripps.⁸⁶ Gupta *et al.* proposed a related theory in which rod death activates mobile microglia which in turn also destroy cones.⁸⁴

Where as a diffusible factor or inflammatory reaction would be expected to cause a fairly uniform effect across the retinal surface, in practice sharp demarcation lines are commonly seen between diseased and normal retina. This is evident for example, on the borders of sectorial defects or at the edge of the retained central island of preserved cone function in patients with advanced RP.⁸⁷⁻⁸⁹ In addition, in many patients the cone cell death occurs slowly over many years or decades after the rods have almost entirely disappeared. Detailed studies in a variety of animal models have characterised the timings further and found that cone cell death only commences after the major phase of rod death is largely complete.⁷⁵ Toxic factors and microglia may play a role, but were they the dominant initiator of cone cell death one would expect to see a closer temporal relationship between the peak of rod photoreceptor and commencement of cone photoreceptor death.

Loss of structural support

In the mouse retina, and in peripheral areas of the human retina, the ONL is predominantly made up of rod photoreceptors. It had been suggested that a lack of surrounding rods could lead to a lack of physical support for the cone

photoreceptors, and subsequently to their loss of function and death. This seems plausible for the murine retina, where for example in the rhodopsin knockout the outer nuclear layer diminishes from 8-10 nuclei thick to 1 nuclei thick within the space of 10 weeks.⁹⁰ However this would not explain cone loss in the human fovea. Furthermore this theory ignores the physical support Mue ller cells and RPE cells provide cone photoreceptors.⁹¹⁻⁹²

Oxidative stress

Photoreceptors have a very high rate of oxygen consumption, and this is supported by the highly vascular choroid. Choroidal blood vessels however lack the capacity for autoregulation in response to tissue oxygen levels. It is therefore argued that rod photoreceptor death, and hence reduced oxygen consumption, leads to an increase in oxygen tension in the outer retina and damage to cones through reactive oxygen species. This theory could also explain the retinal blood vessel constriction that is seen as a characteristic feature of RP, as retinal vessels do have the capacity for autoregulation. The theory would also explain why the peripheral retina, with its high rod/cone ratio, is first to be affected whilst the cone-dense fovea is not affected until late on. Intra-retinal oxygen levels have been found to be significantly increased in the RCS⁹³ and P23H rat⁹⁴ in association with rod degeneration. It is however challenging to demonstrate that hypoxia is the cause of subsequent cone-photoreceptor loss.

Shen *et al.* used immunofluorescent markers in a porcine model of RP to demonstrate evidence of lipid peroxidation, and other markers of oxidative damage, in degenerating cone photoreceptors.⁹⁵ It has also been demonstrated by Okoye *et al.*⁹⁶ and Yamada *et al.*⁹⁷ that subjecting mice to hyperoxia leads to photoreceptor loss and marked thinning of the outer nuclear layer.

The hypothesis would be strengthened further if it could be demonstrated that expression of antioxidants, specifically in the photoreceptor layers, did slow the secondary cone loss in models of RP. Peter Campochiaro's group have attempted this by generating rd10 mice with increased expression of superoxide dismutase (SOD2) and catalase in the photoreceptors.⁹⁸ Both these molecules

are normal components of the cellular antioxidant defence system and their expression was shown to reduce levels of free radicals in the outer retina of rd10 mice and reduce levels of protein markers for oxidative damage. Interestingly expression of these two molecules did not cause any apparent reduction on rod cell death as measured by ONL thickness at 2 timepoints; the first was at P25 when rod degeneration was well in progress and the second at P325 when the rod degeneration is ordinarily near completion. However, it was found that cone cell numbers and function were preserved. Cone numbers were determined with PNA staining, which binds to the extracellular matrix comprising the cone cell sheath,⁹⁹ and so does not itself necessarily indicate increased cone survival; an increase in photopic b wave was however demonstrated, following comparison to null-rd10, SOD2-rd10 and Catalase-rd10 controls. It was only the rd10 mice which expressed both SOD2 and catalase that had the increased response. This suggests that SOD2 and catalase can protect against cone photoreceptor loss. As rod photoreceptor loss was not reduced it does not appear that these molecules are acting just by non-specifically slowing apoptosis. Instead the study suggests oxidative damage was specific to cone photoreceptors.

Nutrition

In their study of the kinetics of cone photoreceptor death Punzo et al. evaluated four different mouse models with mutations in rod-specific genes (the P23H, rd, rhodopsin knockout and PDE- γ knockout mouse models).⁷⁵ In each of these models the major phase of cone cell death was coincident with upregulation of genes involved in cellular metabolism, and specifically in the mammalian target of rapamycin (mTOR) pathway. Furthermore the surviving cones had signs of autophagy, a self-digestion process, and molecular markers of cellular starvation. Rd mice treated with insulin had prolonged cone survival, whereas depletion of endogenous insulin (using streptozotocin injections that kill insulin-producing beta cells of the pancreas) had the opposite effect. These authors therefore presented multiple lines of evidence that the degeneration of cones is through molecular pathways at least in part related to shortage of nutrients.

The exact mechanism of how nutrient shortage would be triggered by the loss of rods has not been established. The authors hypothesised however that the cones could be dependent on rod-rpe interactions for the flow of nutrients into the retina.⁷⁵ In their experiments detailing the kinetics of cone photoreceptor loss Punzo et al. noted that the major phase of cone photoreceptor loss started only once rod degeneration was advanced to the extent that the ONL was just one cell thick. Possibly this could represent a threshold at which the number of outer segment-rpe interactions fall below a critical level and nutrient flow becomes insufficient. This could explain the apparent mutation-independent timing at which cone photoreceptor loss commences.

1.4.2 Molecular mechanisms of photoreceptor cell death

Despite the large variety of underlying mutations and primary pathologies causing RP it is evident that photoreceptor death, in most cases, is through common molecular pathways. These pathways therefore, like the mechanisms for secondary cone involvement, represent a shared feature for large numbers of patients with RP and thus would represent an attractive therapeutic target.

The classical pathways through which cells die are shown in Figure 1-11. Necrosis, the least controlled of the 3 major pathways, describes a form of cell death which is primarily externally driven. It is in effect a passive process of which the cell is not in control. The hallmarks of necrosis include osmotic swelling, precipitation of proteins and cell lysis. This results in unprocessed proteins being released into the extracellular space, an inflammatory reaction and damage to surrounding tissues. This is not a feature of retinitis pigmentosa where inflammation is limited and cells of the inner retina are largely preserved.⁸³

In contrast, cell death in RP is 'programmed'. The process involves an orderly sequence of events driven by the cell which is in the process of demise. Through this process the cell degenerates with limited impact on adjacent healthy tissue. There are both autophagy and apoptotic programmed cell death pathways which

share common features. Elements of the autophagy pathway (also known as the lysosomal pathway) are part of the cell's normal homeostasis mechanisms and involved in organelle turnover. The pathway is characterised by the formation of large vacuoles, some of which expand to capture intracellular organelles – hence the term autophagic vacuoles. Cathepsins and proteasomal enzymes are features of the autophagy pathway. Cells undergoing autophagy may subsequently undergo apoptosis.¹⁰⁰⁻¹⁰¹

Apoptosis, like autophagy, is an active process requiring protein synthesis and mitochondrial function.¹⁰² In developing cells genes for the apoptosis effector proteins such as ubiquitin are up-regulated as part of the process but in adult cells they are commonly ordinarily present but in an inactive state.¹⁰³⁻¹⁰⁵

Extrinsic and intrinsic pathways are described, on the basis of whether the trigger is activation of a cell surface receptor or mitochondrial depolarization respectively. Apoptotic pathways most often involve a family of cysteine proteases, known as caspases, that cleave key cellular targets leading to death of the cell.¹⁰⁶ There are also caspase-independent apoptosis pathways.¹⁰⁷⁻¹⁰⁸

Photoreceptor death in inherited retinal degenerations is primarily through apoptosis, which can be detected using features summarised in Table 1-2.^{44;109-114} Inhibitors of apoptosis have therefore gained interest as potential therapies.¹¹⁵⁻¹¹⁹ However other factors, atypical for classical apoptosis, have also been implicated in photoreceptor cell degeneration particularly from studies in the rd mouse.¹²⁰⁻¹²³ In particular calpain enzymes,¹²² poly(ADP-ribose) polymerase,¹²⁴ and cathepsin activity¹²⁵⁻¹²⁶ have all been implicated in photoreceptor death in the rd mouse. A complicating factor with studies in this mouse model is that the photoreceptor degeneration commences before the retina is fully developed and so will be concurrent with normal developmental patterns of cell death.¹⁰² This can make tissue-based detection methods challenging to interpret. None the less the implication of alternative cell death mechanisms raises questions as to how effective potential therapies will be that target single pathways, particularly in the presence of persistent cell death stimuli.

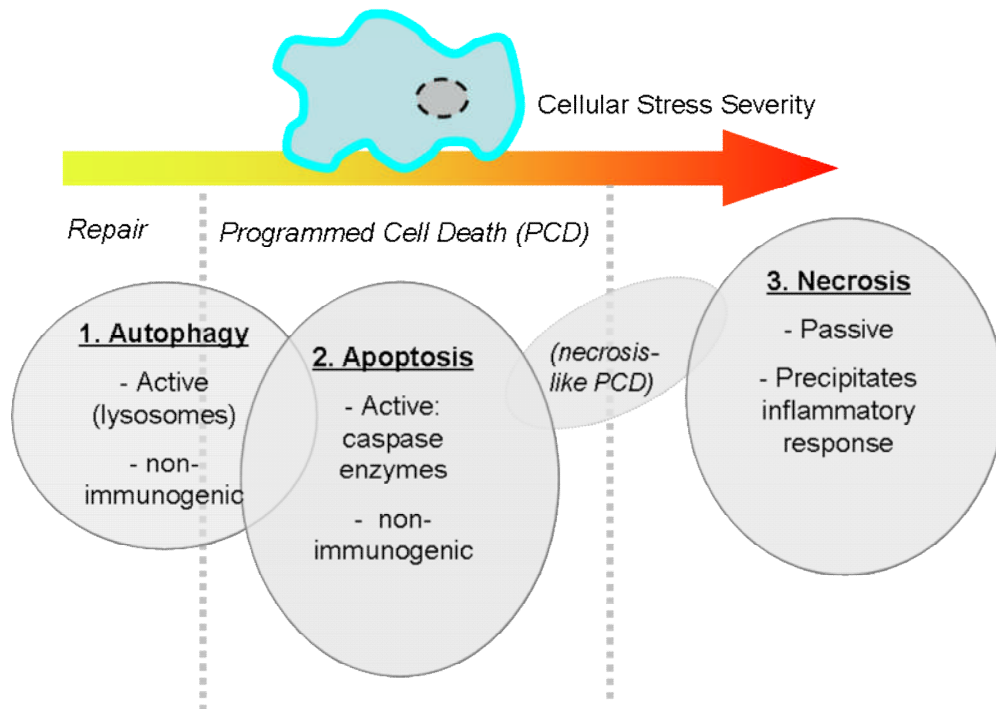


Figure 1-11 Classical pathways of cellular death. Cell death can proceed in an uncontrolled manner driven by external influences and known as necrosis, or in a controlled fashion known as programmed cell death (PCD). The latter achieves demise of the cell with minimal inflammatory reaction and disruption to surrounding tissues. It is an active process driven by the cell itself that is undergoing degeneration. Necrosis can also involve some enzyme activity (eg calpain enzymes) hence the term “necrosis-like PCD”. PCD primarily involves autophagy and apoptotic pathways which share some features and cells can readily move between these two pathways.

Indicator of Apoptosis	Means of Detection
<ul style="list-style-type: none"> • Cell shrinkage & membrane blebbing • Budding of whole cell to produce membrane-bound bodies in which organelles are initially intact. • Fragmentation of nuclei • Condensation & margination of chromatin 	Microscopy
<ul style="list-style-type: none"> • Exteriorization of phosphatidylserine 	Annexin V binding
<ul style="list-style-type: none"> • DNA cleavage & fragmentation 	Electrophoresis, in-situ end labelling, TUNEL
<ul style="list-style-type: none"> • Caspase enzyme activation 	Immunohistochemistry

Table 1-2 Markers of apoptosis. The terminal deoxynucleotidyl transferase dUTP nickend labelling (TUNEL) method is a particularly well known means of characterising apoptotic cell death. It is however not totally specific as in the advanced stages of cells undergoing apoptosis and necrosis can have overlapping features.¹²⁷⁻¹²⁸

1.5 Therapeutic approaches for retinal diseases

At present there are no effective treatments for inherited retinal degenerations. However, the identification of the underlying genes and molecular pathways for many of these diseases has provided a major impetus for research into treatments. Unsurprisingly some conditions are likely to be more amenable to treatment than others, and importantly different approaches are better suited in certain situations than others (Figure 1-12).

1.5.1 Gene replacement therapies

In many monogenic autosomal or X-linked recessive disorders the clinical phenotype results from absence of function of a specific gene. For such conditions expression of a wild-type version of the mutated gene offers the potential for a curative approach.^{2;129}

Viral vector mediated gene replacement therapy in the *rds* mouse was the first study to demonstrate restoration of photoreceptor structure and function in a model of retinal degeneration.¹³⁰ Mice homozygous for a null mutation in *Prph2* lack photoreceptor discs and outer segments and lose photoreceptors by apoptosis such that by 2 months there is minimal retinal function. In this study, subretinal injections of recombinant adeno-associated virus (AAV) encoding a *Prph2* transgene resulted in the formation of near normal outer segments sufficient for photoreceptor function.

Since then restoration of RPE or photoreceptor structure and function has been achieved in a number of animal models of RP using rAAV-mediated gene replacement therapy,^{1;131-133} and clinical trials have followed.²⁻⁵ However, interestingly in the majority of these trials the gene replacement therapy was not sufficient to significantly delay photoreceptor death. In part this may be related to strength of transgene expression as recent studies with more efficient viral vectors and promoters have demonstrated long-term prevention of photoreceptor loss, even in the presence of fast degenerations.^{131;133} It is also likely however

that the function of some genes is more readily replaced than others, due to levels or timing of expression for example.

1.5.2 Gene silencing

Other retinal degenerations are caused by a gain of function mutation having a toxic effect on the cell. Many of these are inherited as autosomal dominant traits. Inserting an additional wild-type version of the mutated gene for these disorders will not alone counter the effect of the existing mutated gene; instead a means of gene silencing is required. This can be achieved using a number of different molecular approaches including the use of single-stranded antisense oligonucleotides that are complimentary in sequence to the mutant transcript, or by expressing catalytic ribozymes specific to the mutant transcript. The latter technique was reported to delay photoreceptor degeneration in the P23H transgenic rat, with functional rescue demonstrated for up to 6 months.¹³⁴⁻¹³⁵ However these results have not been repeated or replicated in other models since.

Of greater interest recently has been the discovery of the RNA interference pathway through which short double-stranded RNA molecules can selectively degrade messenger RNA (mRNA) thereby suppressing translation and gene expression. Of note, a single molecule of short interfering RNA (siRNA) can initiate the degradation of multiple copies of mRNA. siRNA delivering therapies are already under evaluation in clinical trials for AMD¹³⁶⁻¹³⁷ and have been evaluated in pre-clinical studies for specific models of retinal degeneration.¹³⁸

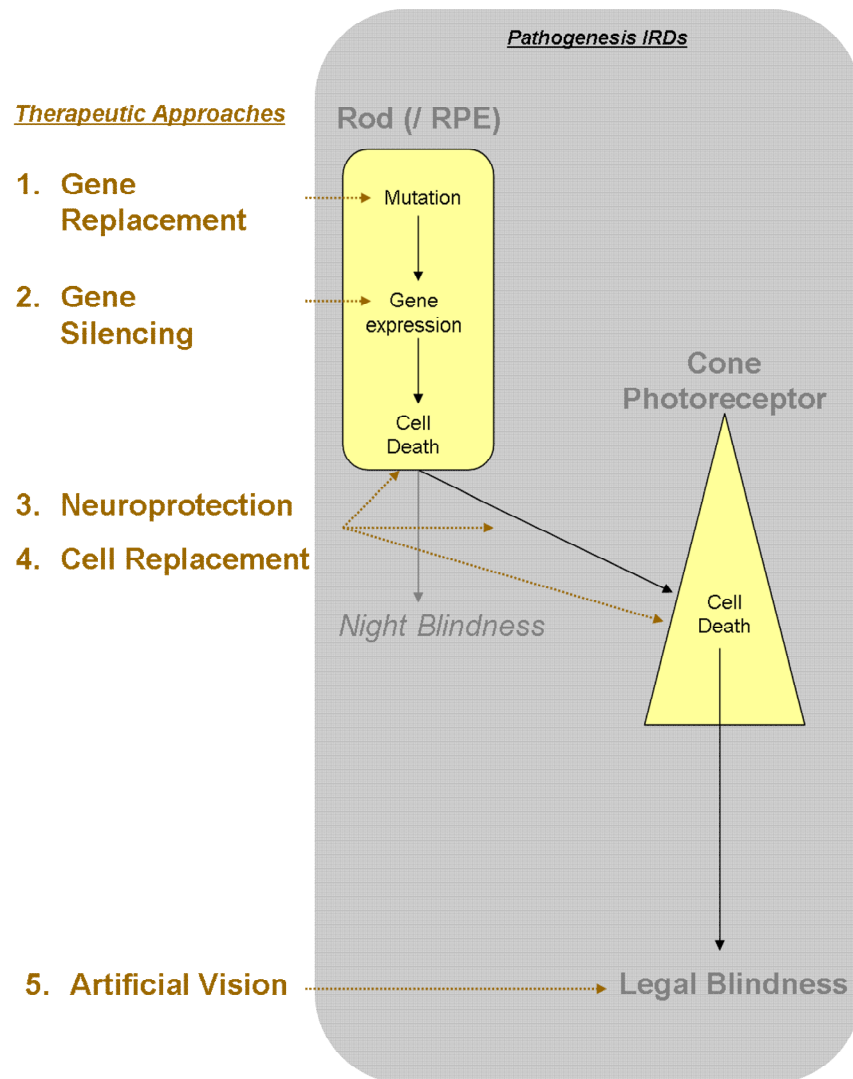


Figure 1-12 Therapeutic Strategies for IRDs. The majority of causative mutations for RP affect genes solely expressed in rods; a minority are expressed in RPE cells. Cone cell loss, and hence loss of central vision, visual acuity, colour perception and contrast sensitivity follows as a secondary consequence. Research into potential therapies can be regarded as focussing on 5 principal steps in the pathogenic pathway, namely: 1. Targeting the genome and inserting a ‘correct’ version of the mutated gene. 2. Targeting down-stream by silencing molecular expression of the gene. Further down the pathway the secondary consequence of photoreceptor death can be targeted (3), or subsequently attempts can be made to replace cells that have died (4). The end point of the pathway is irreversible visual loss, at which point supportive treatments or artificial vision are the principal focus of research.

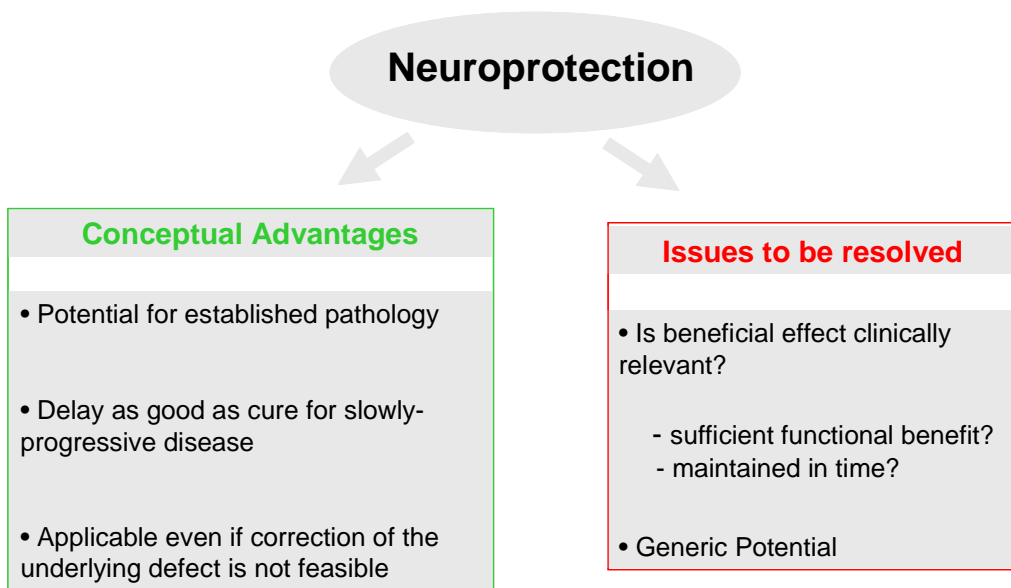


Figure 1-13 Summary of principal advantages and issues to be resolved regarding neuroprotection

1.5.3 Neuroprotection

Various approaches have been used to target the process of photoreceptor death, rather than addressing the underlying defect. Photoreceptors, as with other cell types, can tolerate some degree of insult and damage but there is a threshold above which apoptosis is more likely to follow. The idea behind neuroprotection is to raise the threshold required for the initiation of apoptosis, or interfere with the process of apoptosis so that completion becomes delayed or less likely.

Theoretical advantages of neuroprotection

As shown in Figure 1-13 there are a number of potential advantages that would make a neuroprotective approach an attractive alternative to means of addressing the underlying genetic or molecular defect. These are discussed in relation to the most prevalent causes of blindness:

1. Applicable for late presentation (eg once cell death / structural changes already established)

Most inherited retinal degenerations are slow processes that are typically well established by the time patients present with symptomatic visual loss. Targeting the underlying genetic mutation is often not feasible once the disease is symptomatic as rod photoreceptor loss is already well established. Targeting the later processes of the disease instead (i.e. secondary cone photoreceptor death) is more clinically relevant, and possibly more feasible, for patients with established pathology as it is specifically the loss of cones that precipitates loss of reading and driving vision, and the onset of legal blindness. Furthermore, substantial vision can remain even when most of the cone population has been lost¹³⁹ giving hope that even in advanced disease a slowing of cone cell death would prevent large numbers of people becoming blind.¹⁴⁰

2. For slowly progressive diseases cure may not be necessary or clinically relevant

The slow time course of visual loss in most inherited retinal degenerations, often over decades, means that even a relatively subtle slowing of the process may be all that is needed to preserve useful vision for the patient's lifetime – as long as the protective effect is maintained. Glaucoma is treated in much the same way, where the aim of treatment is not to stop ganglion cell death altogether, but instead treatment is titrated to limit loss just enough to minimise handicap for that patient's expected lifespan.

3. Applicable if correction of the underlying defect is not feasible

- rare
- unknown
- polygenic
- dominant mutation

One of the principal challenges of treating IRDs is the extensive genetic heterogeneity.¹⁴¹ Gene replacement therapies are inherently gene specific, and gene silencing techniques are sometimes mutation specific as well. Developing specific therapies for each mutation, or mutated gene, is not feasible in the near future. One of the attractions of neuroprotective therapies therefore, is that by targeting the the final common pathways of IRDs (regardless of the underlying mutation) they may offer the potential for a more widely applicable generic treatment. Indeed, a neuroprotective treatment could also be applicable to the large numbers of patients in which photoreceptor death results from other pathologies, such as age-related macular degeneration (AMD), which affects a substantial percentage of the population in developed countries over the age of 60.¹⁴² For many patients the underlying genetic mutations and molecular pathways are yet to be characterised. Mutation specific treatments may be decades away from fruition, if at all. In the meantime, more generic neuroprotective treatments could be more feasible for many such patients.

Limitations of neuroprotective factors

Before entering mainstream use it will have to be demonstrated that any neuroprotective agent has a beneficial clinical effect. For this the maintained neuronal cells will have to be functional, not just surviving. Furthermore, to be clinically relevant the effect will need to be maintained for a valuable period of time, and not rapidly over ridden by continuing cellular stresses secondary to the persistent underlying pathology. In the original description of an effect of fibroblast growth factor on photoreceptor degeneration it was evident that the effect was indeed diminished with time. Faktorovich *et al.* injected a single bolus into eyes of the RCS rat.¹⁴³ At one month post-injection photoreceptor numbers in the treated eyes were similar to pre-treatment, where as in control eyes most had been lost. However at two months following injection the number of photoreceptors in the treated eyes was diminished, as compared to treated eyes one month before. Previously preserved cells were therefore dying. Further assessments would be required to determine the rate of the photoreceptor death, and whether numbers would soon be as in untreated eyes, or whether there would

be a longer-lasting effect. This concept is illustrated in Figure 1-14.

Furthermore, the treatment effect may depend on the speed of the degeneration and nature of the underlying defect. It will therefore be of interest to see to what extent neuroprotective agents are indeed of generic, and mutation-independent, potential.

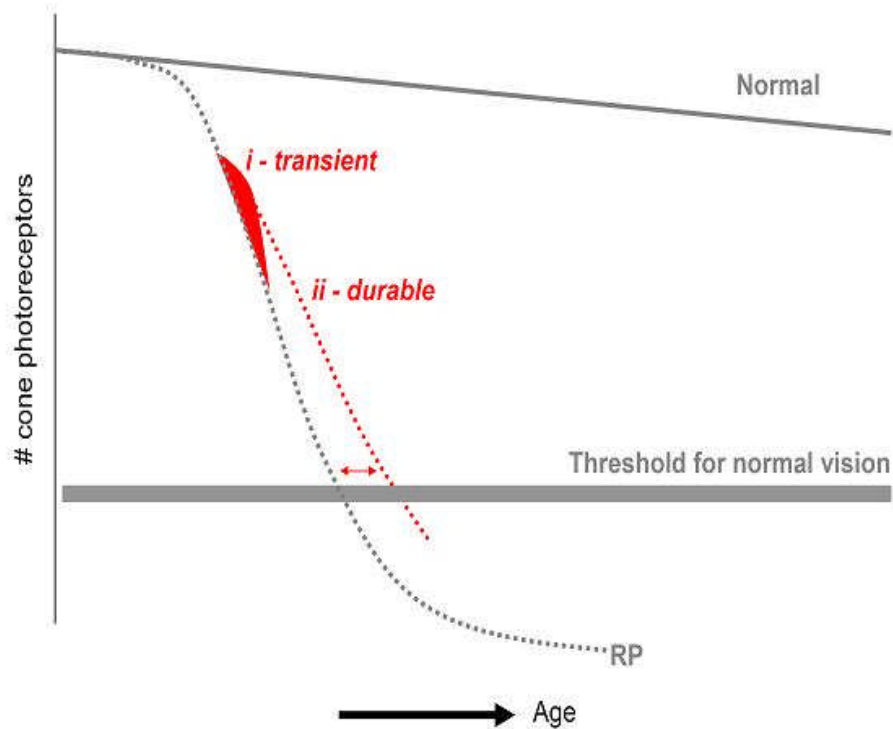


Figure 1-14 Duration of a neuro-protective effect. In this graph total cone numbers is shown on the y-axis. There is a normal age-related decline (top line) but within a patient's lifetime the number of cones is ordinarily adequate for 'normal' vision. In patients with RP there is a more rapid loss of cones such that there are insufficient functioning cones for normal vision, typically in the 4th decade of life. A transient therapeutic effect (red solid) could lead to a subsequent increased rate of photoreceptor loss such that soon cone numbers are as in untreated eyes. Alternatively, without a catch-up phase of increased cell death there would be a lasting benefit (red dotted line). The latter could lead to extra years of normal sight (red double arrows).

Neuroprotective factors for RP

The principal neuroprotective agents under investigation can be grouped together as trophic factors, anti-apoptosis factors, calcium channel blockers and vitamin A supplements. The understanding of how these agents modulate the photoreceptor microenvironment to promote survival is variable, and as the photoreceptor cell death mechanisms in IRDs are better understood additional approaches can be expected.

1. Trophic Factors

Proof of principle for the efficacy of trophic factors in IRDs comes from studies of fibroblast growth factor-2 (FGF-2, also variably referred to as bFGF). FGF-2 was initially found to act as a neurotrophic agent after axonal injury in several regions of the central nervous system,¹⁴⁴⁻¹⁴⁶ and is also found naturally in the retina.¹⁴⁷⁻¹⁴⁸ Supplementing this molecule has been found to induce histological photoreceptor rescue in the RCS rat and in a transgenic rat model with a rhodopsin mutation (the TgnS344ter-4 rat).^{143;149} However, it was also found to induce pathological neovascularisation and cataract formation and so interest has since focussed on finding alternatives.¹⁵⁰

Ciliary Neurotrophic Factor (CNTF) supplementation has also been shown to induce morphological photoreceptor rescue in a number of animal models. Its use is currently being investigated in clinical trials for RP and non-neovascular AMD.^{7;151} However animal model studies for this agent too have shown significant side-effects with a paradoxical negative effect on the ERGs of treated eyes.¹⁵²⁻¹⁵⁵ Glial cell line derived Neurotrophic Factor (GDNF) has also been shown to slow photoreceptor rescue in animal models, but apparently without significant negative side-effects.^{80;154;156-160} Furthermore GDNF has already entered the clinical domain as a CNS-delivered medication for Parkinson's disease,^{161;162} and so if it is effective for IRDs it would be an attractive neuroprotective agent with which to start clinical trials.

Whilst most neurotrophic agents are believed to target both rods and cones, Yang et al. evaluated the effect of RdCVF specifically on cone photoreceptor survival in the P23H rat.⁸¹ Sub-retinal protein injections repeated at 3 timepoints led to a preservation of cone cell numbers in this model of RP and a relative preservation of function on the ERG. Further studies are ongoing to evaluate the effect with more sustained, and clinically applicable delivery methods.

2. Anti-apoptosis Factors

Regardless of the underlying mutation, the final common pathway and key step prior to irreversible visual loss, is photoreceptor death involving the apoptosis pathway.^{44;112;113;163} Indeed, inhibiting apoptosis with the protooncogene bcl-2,¹¹⁵⁻¹¹⁸ the peptide inhibitor of caspase-3¹¹⁴ or expressing the x-linked inhibitor of apoptosis (XIAP)¹¹⁹ have all been shown to delay photoreceptor degeneration in rodent models of IRD. The oncogenic potential of these agents will raise concerns over their potential for clinical use, but if expression can be targeted specifically to a non-dividing cell population (such as photoreceptors) any oncogenic potential is likely to be significantly diminished.

3. Vitamin A

In a randomized, controlled, double-masked clinical trial oral vitamin A was found to slow, on average, the rate of retinal degeneration in patients with RP.¹⁶⁴ The mean rate of ERG decline was less in the treated group. The number of patients with known mutations was too small to assess from this study whether the effect varied with genotype, but work from mouse models does suggest that selected patients may benefit more than others.¹⁶⁵ Tiansen Li *et al* demonstrated that vitamin A supplementation preserved photoreceptor survival and ERG function in the T17M mouse, in which the degeneration results from mutant rhodopsin protein with reduced stability *in vitro* (a class II rhodopsin mutation). Vitamin A supplementation is believed to increase the bioavailability of the chromophore, 11-*cis*-retinal within photoreceptors, and binding of 11-*cis*-retinal to the mutant rhodopsin confers increased stability. In contrast treatment had no effect in an alternative mouse model (the P346S mouse) in which the primary

pathology is aberrant transport of the protein (a class I rhodopsin mutation). There were however other differences between the murine models treated, including speed of degeneration and stage of degeneration at the time of treatment, and so other mechanisms of action remain possible.

Even if a sub-population of patients could indeed be identified that gain a more predictable and significant effect from vitamin A supplementation there are concerns that long-term high doses of the drug could induce hepato-toxicity. Furthermore, in the presence of ABCA4 mutations (seen in atypical RP, cone-rod dystrophy and Stargardt disease) vitamin A supplementation may increase potentially harmful lipofuscin accumulation.¹⁶⁶

4. Calcium channel antagonists

Increased calcium levels are implicated in IRD photoreceptor death partly as a trigger for apoptosis, but also as a consequence of the raised cGMP levels found in at least some forms of RP.¹⁶⁷ cGMP activates the cationic membrane channels permeable to sodium and calcium, which ordinarily mediate the depolarizing current in photoreceptors responding to light stimuli.^{168;169} Excess activation of these channels, and a subsequent rise in intracellular calcium, may be related to the toxic effect of increased cGMP levels seen in the photoreceptors of the *rd* mouse^{170;171}

The function of cGMP gated cation channel is inhibited by diltiazem,¹⁷² a calcium channel blocker commonly used in the treatment of ischaemic heart disease, hypertension and cardiac arrhythmias. Frasson et al. therefore administered high doses of this drug systemically to *rd1* mice, and reported reduced rates of photoreceptor degeneration in the treated group.¹⁷³ However, the rescue effect was transient with preservation of the ERG for only up to 12 days, and in healthy retinas diltiazem leads to a considerable reduction in photoreceptor function (as measured by ERG b-wave amplitude). Furthermore the rescue effect described has not been a consistently repeatable result either in the same animal model¹⁷⁴ or in large animal studies.¹⁷⁵

1.5.4 Cell replacement therapies

Until recently sourcing sufficient numbers of non-immunogenic replacement cells has been one of the major limitations for cellular transplantation approaches to retinal diseases. The use of autologous cells for focal diseases¹⁷⁶ or cells from embryonic sources have been investigated, but have been met with significant practical and ethical challenges. The generation and subsequent neuronal differentiation of induced pluripotent stem (iPS) cells has however removed many of these limitations, raising the possibility that patients could be treated with replacement RPE or photoreceptor cells derived from a readily available source of their own such as fibroblasts or skin cells.¹⁷⁷⁻¹⁸⁰

Transplantation of replacement RPE cells has attractions for the treatment of AMD, where RPE compromise precedes the photoreceptor degeneration. However, to maintain differentiation the transplanted cells must bind to a suitable substrate and so replacing Bruch's membrane, which is also compromised with age alone and in AMD, presents one of the remaining problems for this field of stem cell research.¹⁸¹ Transplantation of photoreceptors for inherited retinal degenerations for example, would not only require that the transplanted cells survive and maintain their differentiation, but also that they form appropriate synapses. To an extent this has been achieved with transplantation of photoreceptor precursor cells, which led to a restoration of some basic visual function in a murine model of RP.¹⁸² It however remains to be convincingly demonstrated with embryonic stem cell-derived transplants.¹⁸³ Restoration of synapses presents an even greater challenge for attempts to replace ganglion cells which have proximal connections within the retina, as well as distal connections a relatively long distance along the optic nerve, the myelin in which is a known impediment to axonal growth.¹⁸⁴

An alternative to transplanting cells to restore their normal function is to use cell transplantation as a means of restoring beneficial paracrine effects. Cells transplants can be used as a means of achieving sustained local delivery of

beneficial trophic factors. Recently oligodendrocyte precursor cells¹⁸⁵ and Mueller cell-derived stem cells¹⁸⁶ have been used to slow optic nerve degeneration by integrating into the degenerating nerve fibre layer in the rat glaucoma model. Mohand-Said et al. transplanted sheets of rods into the sub-retinal space of mice with a retinal degeneration;^{77:187} although these rods did not integrate, and were in a non-physiological location, their presence did have a beneficial effect on cone survival which additional studies clarified was due to a positive paracrine effect.^{77:188}

1.6 Sustained delivery of therapeutic proteins to the retina

Systemic therapies typically only deliver low drug levels to the retina due to the blood-retinal barrier (formed by the endothelial cells of retinal blood vessels and RPE cells) and are often limited by the potential for systemic side-effects. The penetration of topical treatments such as eye drops is largely limited to the anterior chamber. Therefore current retinal treatments are commonly administered by intra-vitreous or peri-ocular injections. These are invasive procedures, and at present most of the drugs used have short half-lives but are being used to treat sub-acute or chronic diseases. Repeated injections are therefore commonly required. The large number of patients receiving anti-VEGF treatments for AMD, are usually injected every 4-6 weeks for the duration of their treatment. This is not without significant risk to the patient and challenges for health care providers. In the MARINA study assessing ranibizumab the rate of presumed intraocular infection, a potentially blinding complication, was 0.05% per injection. This risk is cumulative, and so over the 2 years of the study the risk was 1%.¹⁸⁹

Novel methods of achieving sustained delivery of therapies to the retina are now entering the clinical domain. Of note these include gene therapy to induce local expression of therapeutic proteins and implantable devices to effect the slow release of agents down a concentration gradient. In the future it may also be

possible to chemically modify selected drugs to facilitate topical or systemic delivery,¹⁹⁰ or even selectively disrupt the blood-brain barrier.¹⁹¹ The key requirements for all these approaches is to deliver the medicinal agent at therapeutic levels, which are sustained over time, to the required cell type or tissue without significant side-effects.

1.6.1 Direct gene transfer

Gene therapy is at present the only way to achieve sustained and intracellular expression of a therapeutic protein following a single procedure. As many of the cells within the retina are non-dividing the treatment gene need not be incorporated into the host genome in order to achieve long term expression, thus avoiding the risks of insertional mutagenesis.

The ideal recombinant vector used to introduce the therapeutic transgene should be non-pathogenic, non-immunogenic and effective at transducing the desired cell type.^{129;192} For these reasons recombinant adeno-associated virus (rAAV) is the most commonly used vector for retinal gene therapy at present, and was used in all 3 of the landmark clinical trials for RPE65 mutations. rAAV effectively transduces both rod and cone photoreceptors and the RPE.^{129;193} Serotype 2 (AAV2) is the most common serotype found in humans and many of the viral vectors in use now use the genome from this serotype. However by varying the capsid proteins in which the genome is packaged the transduction kinetics and specificity for different cell types can be varied; this process is known as pseudotyping and so for example combining the genome of AAV serotype 2 with the capsids from serotype 8 gives a viral vector (AAV2/8) with increased transduction efficiency in rod and cone photoreceptors.¹⁹⁴⁻¹⁹⁶ Other pseudotyped AAV vectors in common use include AAV2/5, AAV2/1 and AAV2/4 with the latter two being used to transduce RPE cells specifically.¹⁹⁵ Ocular gene therapy with AAV vectors results in sustained transgene expression for many years following a single injection in animal models,^{197;198} and now has an established safety and efficacy profile in humans.^{2;199}

Despite the success with viral vectors the reliable production presents technical challenges and concerns remain over insertional mutagenesis and inflammatory responses. Experimentally, a number of non-viral delivery systems are also used including the use of polymers such as polyethylenimine (PEI), nanoparticles or electroporation.²⁰⁰ Bejjani *et al.* reported short-term gene expression in RPE cells following intravitreal injection of plasmid-laden biodegradable nanospheres into the rat eye.²⁰¹ However, at present *in vivo* transduction efficiencies and longevity of expression are far from comparable with those already established for viral vectors, and the treatment effects demonstrated with these technologies have been limited.^{200;202}

1.6.2 Vitreous implants

Drugs that have good long-term stability such as dexamethasone, a synthetic corticosteroid, may be incorporated into vitreous implants. These can be biodegradable or non-biodegradable, with the latter usually requiring removal after a period of time. Ozurdex is a sustained-release dexamethasone implant manufactured by Allergan, and is licensed by the Federal Drugs Administration for treatment of retinal vein occlusion. The implant is biodegradable, and inserted into the vitreous cavity with a simple injection procedure.

Dexamethasone is released into the vitreous cavity for 6 months following implantation, with peak concentrations during the first 2 months.²⁰³

Delivering proteins or nucleic acids in this manner has been more problematic however, because they are particularly vulnerable to endogenous proteases or nucleases. One approach has been to embed amino or nucleic acids into polymers and carrier matrices that offer protection from endogenous enzymes.

^{190;204} The conformational structure of many small molecule therapeutics is essential for function, and so the challenge will be to preserve the structure and biological activity in the synthetic polymers.

An alternative approach for proteins has been to implant cells genetically engineered to continually produce the therapeutic agent. These have been used to investigate the effects of CNTF, GDNF and BDNF over relatively short-

timescales.^{7;156;157;205} If the cells are sequestered within a vitreous capsule the potential for removal remains but as with the slow release capsules any drug specificity must be inherent in the drug, as the delivery mechanism is itself non-specific. To achieve long-term expression the implanted cells must be protected from the host's immune system, but still receive oxygen and nutrients to maintain survival.

1.7 Rodent models of RP

The development of treatments for human retinal degenerations relies heavily on the use of animal models. Their use is a prerequisite for the development of stem cell and gene therapies where there is a significant risk of harm as therapies are developed, and where *in vitro* studies are insufficient to justify clinical investigations.

The widespread use of genetic modification with mice has allowed a broad selection of murine models of IRD to be established and well characterised. Many closely mimic the human pathology with an analogous retinal degeneration and similar pathophysiological defects. Those referred to extensively throughout this thesis are summarised in Table 1-3 and Table 1-4.

One of the challenges of translational research is to appreciate the significance of differences between the animal models in which disease mechanisms are studied and therapies developed, and the potential patients in which the therapies are to be used. Some of the more pertinent differences in relation to studies of RP are discussed below.

1. Anatomy. The principal anatomical difference between rodents and man with regard to the retina, lies in the fact that the rodent retina lacks a macula. This presents a challenge for the assessment of cone-related outcome measures in rodent models, and complicates studies related to the mechanisms of rod-cone degeneration. It is also true however that the macula in humans is only affected late on in RP and outside the macula the distribution of rods and cones in humans is similar to that in mice.

2. Timings and stage of disease. Experimental treatments tend to be evaluated in young animal models and in early stage of the disease. Differences in life-span and metabolic rate between animal models and humans are largely predictable and can be adjusted for, but it is matching the stage of disease that is of greatest relevance. In advanced disease accumulated cell damage (related to the disease process or ageing), cell death or cellular stress responses can all affect the response to interventions. This was well demonstrated in one of the RPE65 gene studies where a dog aged 30 months was treated, and in contrast to the younger animals, did not gain any functional improvement despite evidence of transgene expression.²⁰⁶

3. Type of mutation. The retinal degeneration (rd) and retinal degeneration slow (rds) murine models have mutations in genes that are commonly affected in patients with RP and have proved valuable models to study disease mechanisms and potential therapies. Of note however, both these models have null mutations, where as in patients missense mutations are more common. This causes differences in the phenotype severity and rate of progression. In addition the disease mechanisms and responses to interventions may also differ. Null mutations lead to the gene not being transcribed into RNA, or the transcript not being translated into a protein product. In contrast, missense mutations can lead to mutant protein accumulating in a cell, from where they can induce a variety of cellular responses including apoptosis, impact on gene expression and potentially compete with iatrogenically introduced therapeutic copies of the gene.^{207;208}

4. Heterogeneity. Colonies of animal models are typically extensively inbred and thus relatively genetically homogenous. For digenic conditions, or others heavily influenced by modifier genes, this could account for differences in phenotypes and responses to treatments between animal models and corresponding patients. Likewise environmental (including dietary) influences are similarly homogenous in experimental animals but much more variable for patients.

Murine models of retinal degeneration			
	<i>rd1</i> or rd	<i>rd10</i>	<i>rds/ Prph2^{rd2/rd2}</i>
Mutation	Null mutation in <i>Pde6b</i> ^{209;210}	Missense mutation in exon 13 of <i>Pde6b</i> . ²¹¹	Null mutation in <i>Prph2</i>
Photoreceptor degeneration	Lack of functional rod PDE ⁷² leads to a toxic accumulation of cGMP and rod photoreceptor death. ^{167;170;171} ^{112;113;163} Rapid loss of rods begins postnatal day 10 and is almost complete by PN20. ²¹² There follows a slower loss of cones between PN60-PN180, though 5% of cones last over 6 months. ²¹³	Photoreceptor loss is slower than that in the rd mouse. Rod loss commences at P14 and is maximal at P28. ²¹⁴ By P30 rod function is decreased by 70%, and cone function by 50%. ²¹¹ Rod degeneration is largely complete by P40, ²¹¹ but cones last up to 9 months of age. ²¹⁴	Absence of normal peripherin/RDS means outer segments fail to develop. ²¹⁵⁻²¹⁷ ERG function is greatly diminished, and almost completely lost by P60. Photoreceptor cell loss is maximal between P11 & P28 but then followed by a slower phase that lasts 8 to 11 months. ²¹⁸
Relevance to humans	PDE6B mutations in patients are a cause of autosomal-recessive RP. ^{72;219} They have also been associated with dominant congenital stationary night blindness. ^{220;221} The <i>rd10</i> mouse however, with a missense mutation and slower degeneration, is the more representative of the human disease than the <i>rd1</i> mouse.		<i>PRPH2</i> mutations are a cause of AdRP, (accounting for approximately ~5% human RP patients), but can also cause a large variety of other phenotypes including cone-rod dystrophies. ^{56;60;61;222;223} However, as for the rd mouse, the null mutation and failure of normal photoreceptor development is not representative of typical RP.

Table 1-3 Summary of relevant murine models of retinal degeneration. Timings are approximate as there is variation between strains in different research institutions; those for the *rd10* mouse are quoted for the mutation on a C57BL/6J background.

Descriptions are for mice homozygous for each mutation.

Rat models of RP		
	P23H	S334ter4
Mutation	This transgenic carries a rhodopsin transgene with a single amino acid substitution at amino acid position 23 (histidine for praline) ²²⁴	This transgenic carries a rhodopsin transgene with a premature termination codon at residue 334 of the opsin transgene
Photoreceptor degeneration	Experimental animals are typically heterozygotes. These have a slow rod degeneration with initially normal cone function. ²²⁵ P23H is a class II rhodopsin mutation. The mutant protein is mis-folded leading to aggregation and subsequent degradation via the cellular ubiquitin proteasome system. ^{226;227}	Experimental animals are typically heterozygotes. The retinas typically develop normally and then have a degeneration that starts at P15 and is fast until about P60. This is followed by slower progression. S334ter4 is a class I mutation. Rhodopsin protein formed from the transgene lacks 15 carboxy-terminal amino acids that are ordinarily involved in protein trafficking to the outer segments and in the deactivation of the rhodopsin protein after light absorption. ²²⁸ ²²⁹
Relevance to humans	Same mutation is causative in most prevalent form of adRP in north America. ~12% human cases. ²²⁵	Multiple mutations within the C terminus have been identified in patients. Class I mutations are however less common than class II rhodopsin mutations.

Table 1-4 Commonly used rhodopsin transgenic rat models of RP. As expected for transgenics, the rate of variation varies considerably between different lines.

1.8 Thesis aims

Cone photoreceptor death, secondary to disease in another cell type within the retina, is an important cause of blindness. A treatment to slow or prevent the secondary loss of cone photoreceptors could benefit millions of people by delaying or preventing the onset of legal blindness.

Therapies targeting cell death pathways have shown promise in animal model studies. However, it remains unclear why healthy cones degenerate following a rod degeneration and whether their sustained survival is possible without restoring the rod photoreceptor population. Furthermore to be clinically valuable any treatment would need to produce a sustained protective effect on cone numbers and function.

The aim of this thesis is to investigate neuroprotective treatments as potential therapies to preserve cone-mediated vision. A novel murine model of rod-cone degeneration will be used to enable study of specifically the cone photoreceptor population at repeated time points. This will allow evaluation of whether any treatment effect is preserved with time.

Chapter 2 Materials & methods

2.1 Buffers & media and solutions

Buffers were prepared in dH₂O and autoclaved. Antibiotics were added following autoclaving, and once solutions had cooled to less than 50°C.

<i>Buffer/Medium</i>	<i>Constituents</i>
Blocking solution (immunohistochemistry)	1% bovine serum albumin (BSA), 3% normal goat serum (NGS), 0.1% triton
Blocking solution (western blot)	1x phosphate buffered solution (PBS), 3% dried milk powder (fat-free), 0.5% tween
Church mix	0.24M SDS, 0.5M EDTA, 0.34M Na ₂ HPO ₄ , 0.16M NaH ₂ PO ₄
D10	Dulbecco's Modified Eagle's Medium (DMEM) supplemented with 10 % heat inactivated foetal bovine serum (FBS), 100 U/ml penicillin and 0.1 mg/ml streptomycin.
ELISA blocker	1x PBS, 1% BSA, 5% sucrose, 0.05% NaN
G10 growth medium	BHK-21 media supplemented with 10 % FBS, 100 U/ml penicillin and 0.1 mg/ml streptomycin, 5 % tryptose phosphate broth, 2 mM L-glutamine and 0.25 mg/ml geneticin G418.
2x hepes buffered saline (HBS)	280 mM NaCl, 10 mM KCl, 1.5 mM NaH ₂ PO ₄ , 12 mM D-(+)-Glucose, 50 mM HEPES
Laemmli buffer (2x)	4% SDS, 20% glycerol, 10% 2-mercaptoethanol, 0.004% bromophenol blue, and 0.125 M Tris HCl
LB broth	Prepared using 25g/l of LB-Broth preparation (Sigma-Aldrich, Gillingham, UK). Preparation contains Casein enzymic hydrolysate 10 g/l, yeast extract 5g/l and NaCl 10 g/l)

<i>Buffer/Medium</i>	<i>Constituents</i>
LB culture plates	15g/l of agar (VWR International, Leicestershire, UK) was added to LB medium prepared as above. Ampicillin (100 µg/ml) was added following autoclaving and then the LB-agar mix was set in 9cm diameter plates and stored at 4°C.
PBS	8g NaCl, 0.2g KCl, 1.44g of Na ₂ HPO ₄ , 0.24g, KH ₂ PO ₄ in 1 litre distilled water.
PBS-MK	1xPBS, 2.5mM KCl, 1mM MgCl ₂
POROS buffer A	20 mM Bis-Tris Propane, 20 mM Tris Base
POROS 10% buffer B	20 mM Bis-Tris Propane, 20mM Tris Base, 0.3M NaCl
POROS 100% buffer B	20 mM Bis-Tris Propane, 20mM Tris Base, 3M NaCl
Proteinase K buffer	100 mM Tris (pH7.4), 50mM EDTA, 0.5% SDS
Running buffer	182g/L Tris Base and 4g/L SDS. This solution was filtered (0.45µm) and HCl was added drop wise to give a pH of 8.8
Sodium phosphate buffer (1M)	97.1 g/L Na ₂ HPO ₄ and 43.6 g/L NaH ₂ PO ₄ . pH 7.2
TD buffer	140mM NaCl, 5mM KCl, 0.7 mM K ₂ HPO ₄ , 3.5mM MgCl ₂ , 25 mM Tris.
TE buffer	10 mM Tris (pH 8.0) + 1 mM EDTA in dH ₂ O.
TBE buffer (10x)	108g Tris base, 55g Boric acid, 9.3g Na ₄ EDTA
Transfer buffer	Running buffer + 20% methanol

Table 2-1 Buffers, Media & Solutions

2.2 Molecular biology

2.2.1 mRNA extraction

To prepare mRNA from retinal tissue enucleated eyes were rapidly dissected and the retina snap frozen in liquid nitrogen. Samples were stored at -80°C prior to further steps. At the time of mRNA extraction 1ml of Trizol (Invitrogen) was added to each frozen retina in order to preserve mRNA integrity during cell membrane disruption. The retina and trizol mix was pipetted up and down, and vortexed, to achieve tissue homogenization. 200 μl of chloroform was subsequently added followed by centrifugation (15 minutes at 14 000g) to separate the mixture into an aqueous phase (containing the mRNA) and an organic phase (which is discoloured and of greater density relative to the aqueous phase). The aqueous phase, mixed with an equal volume of isopropanol was frozen at -20°C overnight to achieve mRNA precipitation. An mRNA pellet was isolated by centrifugation (14 000g for 10 minutes), and the supernatant removed. This was followed by an ethanol wash (1ml 70% ethanol was added and the mixture centrifuged at 14 000g for 5 minutes) followed by air drying (for 5 minutes). The resultant pellet was then resuspended in RNase-free water or EB buffer (QIAGEN Ltd., UK, 10 mM Tris-Cl, pH 8.5). The resuspension volume was typically 50 μl . In the event of poor re-suspension the solution was heated to 55°C for up to 10 minutes to aid the process. An alternative means of mRNA isolation was to use the RNeasy Mini Kit (QIAGEN Ltd., UK). RNA samples were quantified by measuring absorbance at 260 nm (A_{260}) in a spectrophotometer, and purity was estimated by comparing the ratio of readings at 260nm and 280 nm (Nanodrop[®] apparatus, LabTech International). Samples were stored at -80°C prior to further use.

2.2.2 Generation of cDNA

Complimentary DNA (cDNA) was generated from RNA samples using the Quantitect Reverse Transcription kit (Qiagen, Crawley, UK). RNA samples were first treated to remove contaminating genomic or viral DNA by incubation for 2 minutes at 42°C with diluted Qiagen gDNA wipeout Buffer. Reverse transcription was then performed in a mix containing the Quantiscript reverse

transcriptase enzyme (an RNA-dependent DNA polymerase, 1 μ l), Quantiscript RT buffer (4 μ l), primer mix (1 μ l) and 1 μ g of the purified RNA sample (in 14 μ l) (total volume 20 μ l). The reaction was allowed to run for 15 minutes at 42 $^{\circ}$ C before the enzyme was inactivated by incubation at 95 $^{\circ}$ C for 3 minutes. cDNA was stored at -20 $^{\circ}$ C.

2.2.3 Plasmid preparation

Maps for the plasmids used and produced are shown in the supplementary data chapter.

GDNF plasmids

Murine GDNF cDNA was subcloned from an existing plasmid into the pd10 backbone with a CMV promoter. The sequence of the cloned plasmid was confirmed with restriction enzyme digests, and by sequencing using a CMV forward primer and a GDNF forward primer.

XIAP plasmids

Human XIAP cDNA was obtained from a plasmid kindly provided by Professor Catherine Tsilfidis (University of Ottawa, Canada). PCR reactions were performed to insert the ApaI and BsrG1 restriction enzyme sites at the 5' and 3' ends of the XIAP cDNA respectively. This permitted subsequent ligation into a pre-existing pd10 plasmid containing a CMV promoter. The PCR primers used were manufactured to order by Sigma-Aldrich (Dorset, UK) and used in the PCR mix shown in Table 2-2. The KOD polymerase enzyme was used because of its proof reading properties and low PCR error rate. The sequences of the 5' and 3' primers used are CC GAG CTC GGG CCC ATG ACT TTT AAC and G GGC CCT GTA CAT GCA TGC TCG respectively.

	μl
10x Reaction Buffer	5
dNTPs	5
MgSO ₄	3
Primers (10 μ M)	1 each of forward & back
DNA	1
H ₂ O	33
KOD polymerase	1

Table 2-2 KOD polymerase PCR reaction

Following an initial denaturation step (5 minutes at 95°C) 30 cycles of PCR were performed using the following conditions:

- Denaturation: 30 sec at 95°C
- Annealing: 30 sec at 50-60°C
- Extension: 2 minutes at 65°C
- Final extension: 5 minutes at 68°C

The PCR products were sized by electrophoresis and digested prior to ligation into a CMV-containing pd10 plasmid. Sequencing of the entire CMV and XIAP containing regions was performed to confirm accuracy of the PCR reactions and cloning.

Rhodopsin plasmid

cDNA for human rhodopsin was subcloned into a pd10 plasmid containing the bovine rhodopsin promoter sequence using the AfeI and SexAI restriction enzyme sites. The latter is sensitive to *dcm* methylation and so DNA was prepared in methylation deficient *E.coli* cells. Restriction enzyme digests and DNA sequencing was used to confirm the plasmid sequence. The insertion of an

SV40 intron sequence, and modifications to the transgene sequence to optimise protein expression, were performed commercially by Genscript, New Jersey, USA.

2.2.4 Electrophoresis, gel extraction & ligation of DNA

DNA products were separated on agarose gels containing ethidium bromide (1 μ l of 10 mg/ml concentration per 50 ml of gel) in order to visualise nucleic acid bands. Bands were sized by comparison with commercial DNA ladders (Promega, UK), and both the DNA samples and the ladders were loaded with 6x loading dye (Promega, UK) to allow visualisation of the bands under UV light. In most instances 1% agarose (w/v) gels were used but for more detailed examination of small or large fragments the agarose percentage was increased or decreased respectively.

The gels were prepared by adding the agarose (VWR International, UK) to 0.5% TBE (Table 2-1). The mixture was heated in a microwave and intermittently mixed until the agarose was completely dissolved. Following cooling the ethidium bromide was added and the gel set in a plastic mould. Gels were run at 180V until the required bands could be resolved (typically 60-90 minutes).

DNA bands were excised from the agarose gel use a clean scalpel under a UV light. DNA was isolated using a QIAquick[®] Gel Extraction Kit (Qiagen, Crawley, UK). The protocol entailed dissolving the agarose-based fragment in buffer at 55°C. Following addition of isopropanol the solution was passed through a binding column followed by washes to remove traces of agarose and high salt concentration contaminants. DNA was then eluted in a tris buffer. The size and quality of collected DNA was determined by spectrophotometric analysis (using Nanodrop[®] apparatus, LabTech International) to determine the concentration and pattern of absorbance, and by running a sample on an agarose gel. DNA samples were stored at -20°C.

2.2.5 Amplification of DNA in bacteria

Transformation of competent cells

Chemically competent cells (α -Select gold efficiency, Bioline, London, UK) were preferentially used to transform cloned cDNA into bacterial cells. In selected instances *dam* and *dcm* methylation deficient *E.coli* cells (*dam*-/*dcm*-competent *E.coli*, New England Biolabs) were used instead to grow plasmids free of Dam and Dcm methylation. This was necessary when plasmids were to be digested using restriction enzymes sensitive to methylation (as was the case for the rhodopsin plasmid).

Competent cells were stored at -80°C . Prior to use cells were thawed on ice, and incubated with plasmid DNA for a further 15 minutes on ice. The cells were heat shocked for 45 seconds at 42°C using a pre-warmed heat block. The cells were immediately transferred back to ice for a further 3 minutes. 100 μl of SOC medium (Sigma-Aldrich, UK) was added and the cells incubated at 37°C for 1 hour to maximise transformation efficiency, before being spread onto an LB-agar plate. In cases where a blue-white colony selection was required (i.e. when using the pGEM[®]-T Easy system for sub-cloning) 50 μl of X-gal solution (20mg/ml) was spread over the plate before addition of the transformation mix. Plates were incubated overnight at 37°C to allow growth of bacterial colonies.

Amplification and recovery of recombinant plasmid DNA

Bacterial colonies were inoculated into 5ml of LB medium containing 100 $\mu\text{g/ml}$ of ampicillin, and incubated at 37°C with shaking for 12-16 hours.

For small-scale preparations, DNA was isolated using a GenElute[™] Plasmid Miniprep Kit (Sigma-Aldrich, UK) using the standard protocol. This entailed harvesting a pellet of *E.coli* cells by centrifugation of the inoculated LB medium; the pellet was then resuspended and the cells lysed by alkaline lysis to release the plasmid DNA into solution. A neutralisation and binding solution was added to

precipitate unwanted cell debris, which was then separated from the supernatant by centrifugation. The supernatant was passed through a primed DNA-binding column and subsequently washed with an ethanol based solution to remove residual salts and contaminants. DNA was harvested from the column by passing through a small volume of elution solution.

For larger preparations 200µl of the 5 ml LB culture following transformation, or a pipette tip dipped in frozen glycerol stock, was used to inoculate a further litre of LB, which was incubated as above. For these larger preparations plasmid DNA was recovered using a GenElute™ Plasmid Mega Kit (Sigma-Aldrich, UK); this uses a similar protocol to above. Bacterial cells were isolated by centrifugation, then resuspended and lysed. Again the genomic DNA, proteins and cell debris was precipitated and separated from the suspended plasmid DNA by centrifugation. The supernatant was passed through a primed anion-exchange resin column which binds DNA, and subsequently washed. DNA was eluted in a high salt buffer and precipitated using isopropanol to concentrate the DNA and separate it from residual salts and buffer. The DNA pellet was washed in 70% ethanol in endotoxin-free water and redissolved in EB-buffer (Sigma-Aldrich, UK).

The size and quality of collected DNA by either technique was determined by spectrophotometric analysis (using Nanodrop® apparatus), agarose gel electrophoresis and with selected restriction enzyme digests. The spectrophotometer was used to determine the ratio of absorbance at 280nm and 260nm, with 1.7 to 1.9 being considered the acceptable range. DNA samples were stored at -20°C.

2.2.6 Restriction enzyme digests

Restriction enzymes were purchased from Promega (WI, USA) and New England Biolabs (NEB) (Hitchin, UK). Digests were typically performed using 1.0 µg of plasmid DNA, 1µl of enzyme and the appropriate concentration of the manufacturer's recommended buffer for 1-4 hours at either 25 or 37°C. Digests

were terminated, and salt in the buffers removed by DNA precipitation. Restriction enzyme products were analysed using agarose gel electrophoresis and comparison of fragment size with a commercial DNA ladder (Bioline, London, UK)

2.2.7 DNA precipitation

DNA was precipitated following restriction enzyme digests by adding 1/10th volume of 3M Sodium Acetate (pH5.2) and 2.5x volume of 100% ethanol. The mixture was then kept at -20°C for 30 mins prior to centrifugation at maximal speed for a further 10 minutes. The supernatant was removed by pipetting following repeated spins allowing a DNA pellet to be precipitated; the pellet was then resuspended in sterile water or elution buffer.

2.2.8 DNA Sequencing

DNA plasmids were sequenced commercially by Eurofins Laboratories Ltd. (Acton, U.K.) or Beckmann Coulter Genomics (Takeley, U.K.).

2.3 Cell culture

Baby Hamster Kidney (BHK) and HEK-293T cells were used for rAAV 2/2 and rAAV 2/8 production respectively. BHK, HEK-293T cells and HELA cells were used for *in vitro* testing of plasmids, and BHK and HELA cells were used for *in vitro* testing of rAAV 2/2 viruses. All cell lines were grown in incubators maintained at 37°C with 5% CO₂, and steps were performed in sterile tissue culture hoods. The media used for each cell line are shown in Table 2-3. Confluent cells were split approximately 1:3 every 48 hours, or 1:5 every 72 hours to maintain healthy growth.

Cell line	Growth Medium Used
BHK	G10 (see Table 2-1)
HEK-293T	D10 (see Table 2-1)
HELA	D10

Table 2-3 Growth media used for cell culture

2.4 rAAV production

Recombinant adeno-associated viral (rAAV) vectors, containing single-stranded DNA, were used to transduce cells *in vitro* and *in vivo*. AAV viruses are replication-deficient and so are dependent on co-infection with “helper” viruses, such as adenovirus or herpes simplex virus, to effect the steps of viral replication, genome packaging and to an extent host cell lysis. Recombinant AAV vectors additionally lack the normal *rep* and *cap* genes of the AAV genome. In wild type AAV the *rep* gene is required for integration, replication and packaging, and the *cap* gene encodes the three proteins (VP 1-3) that form the normal 20nm icosahedral AAV capsid.

To produce rAAV vectors *in vitro* host cells were transfected with the “transgene” plasmid (containing the gene of interest, a promoter and the viral inverted terminal repeats (ITRs) required for viral replication) and a plasmid containing the AAV *rep* and *cap* genes. To produce rAAV2/2, the transfected cells were also infected with a helper virus (Figure 2-1). To produce rAAV2/8, the host cells were instead co-transfected with a further plasmid containing genes required by the host cell to perform the helper virus functions. Helper virus infection was therefore not required for rAAV2/8 production.

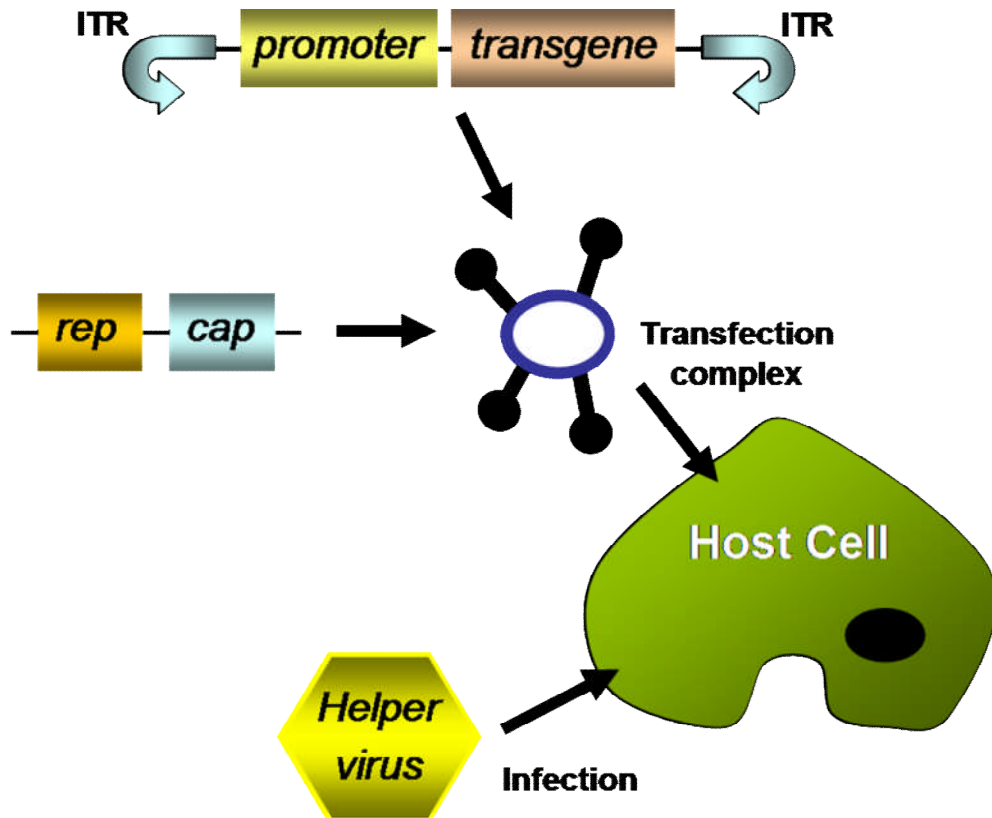


Figure 2-1 *In vitro* rAAV2/2 vector production. Host cells were transfected with plasmids containing the AAV *rep* and *cap* genes that are absent in recombinant viruses, and the “transgene” plasmid which contained cDNA for the gene of interest and the AAV inverted terminal repeats (ITRs) required for viral replication. For rAAV2/2 production BHK cells were co-infected with helper virus. rAAV2/8 production is similar, except that the host cells are 293T cells and they are co-transfected with a helper plasmid instead of being infected with helper virus. Plasmid DNA entry into cells was achieved using transfection complexes; the constituents of these complexes varied with the cell type being targeted.

2.4.1 rAAV 2/2 production

rAAV 2/2 was produced using protocols based on previously published methods.^{131;133;230} 20 plates of BHK cells were used per batch of virus. Virus particle production was achieved using *rep* and *cap* genes from the replicating Herpes Simplex virus (HSV) amplicon pHAV7.3 in association with disabled infectious single cycle HSV (DISC-HSV) helper virus.

Transfection

Transfection was performed when the plates of BHK cells were approximately 60% confluent (giving approximately 10^7 cells per 150mm plate); this was achieved by splitting plates of confluent cells 1:2 the day prior to transfection.

A transfection mix was prepared in the ratios shown in Table 2-4 and added to the BHK cells for a period of 4 hours before being removed and replaced with fresh B10 medium containing the helper virus (DISC-HSV) in the ratio of 10 infectious units per cell. The cells were then left for a further 36 hours for rAAV production.

Component	Quantity per 150mm plate of BHK cells
Optimem medium	15 mls
Peptide 6 ((K16)GACRRETAWACG) (an integrin-targeting peptide)	250 µg
Construct DNA	30µg
pHAV7.3 DNA	30µg
Lipofectin reagent	45µl

Table 2-4 Transfection mix for AAV2/2. The peptide 6 has a lysine tail contributing to the peptide having a positive charge of +17 which aids binding to DNA; peptide 6 also binds to cell surface integrin proteins. Lipofectin reagent (purchased from Invitrogen, Paisley, UK) is lipid based and aids binding of the transfection complex to cell surface membranes and subsequently the endosomal membrane prior to release of DNA from the endosome.

Harvesting and Purification

After 36 hours of virus production cells were scraped off the plates and aspirated. Following centrifugation isolated cell pellets were resuspended in 1ml per plate of Optimem, and subjected to 3 freeze-thaw cycles (at -80°C and 37°C respectively) with vigorous vortexing in between to ensure lysis of the cells.

The cell lysate was treated with 50 units per ml of Benzonase (Sigma, Dorset, UK) and incubated at 37°C for 30 minutes to remove cellular DNA. This was then spun at 4000g until the supernatant was clear (typically 30 minutes). The supernatant, containing the virus, was then further cleaned by adding 0.5% deoxycholic acid (DCA, Sigma-Aldrich, Dorset, UK) and incubation at 37°C for a further 30 minutes. The DCA also aids subsequent binding of vector particles to the heparin columns. The supernatant was then filtered through 5µm and then 0.8µm syringe filters (Millipore, Watford, UK) to remove cellular debris. rAAV particles were then purified using a heparin-agarose column (Sigma-Aldrich, Dorset, UK) and pre-washed with 10 ml PBS-MK (Table 2-1).²³¹ The column with the bound virus is then washed with 10 ml PBS-MK + 0.1M NaCl before being eluted in 6 ml of PBS-MK + 0.4M NaCl (the first 2mls of which are discarded due to the dead-space of the column).

The virus elute was concentrated by applying to Amicon Ultra-4 filter columns (Millipore, Watford, UK) and centrifugation at 5000x *g* until the residual volume was less than 200µl. The virus was then washed by adding a further 2 mls of PBS-MK to the concentrated virus in the Centricon columns, and spinning in the centrifuge at 5000x *g* until the residual volume of PBS-MK containing virus was approximately 100µl. This was then aliquoted and frozen at -80°C.

2.4.2 rAAV 2/8 production

rAAV2/8 was produced by transfecting HEK-293T cells. The cone arrestin-GFP vector was produced following a transfection using a calcium chloride. For all other rAAV2/8 vectors cells were transfected using polyethylenimine (PEI). In

both cases the transfection mixture was added to the cells once they were approximately 70-80% confluent. 20 plates (of 150mm diameter) were typically used per batch of virus. To ensure the cells are growing at the time of transfection the plates were split on the day prior to transfection.

Calcium chloride transfection

The calcium chloride-based transfection mix used is shown in Table 2-5. Particular care was needed when making this mix to avoid protein precipitation. Under sterile conditions the required volumes of plasmid DNA were first mixed in a sterile flask, before adding the dH₂O and then finally CaCl₂. The flask containing this mixture was then continually vortexed whilst 2xHBS (which had been fully equilibrated to room temperature) was added slowly drop by drop. The transfection mix was left to stand at room temperature for 30 minutes, during which time complexes formed giving it a partially opaque appearance. The required volume of D10 medium was added, which stops the complexing reaction, before the mixture was added to the 293T cells (5mls per plate). The transfection mix was left on the cells for approximately 24 hours before being replaced with fresh D10 medium.

Component	per 20 plate transfection
Transgene plasmid DNA	200µg
AAV packaging plasmid (<i>rep</i> and <i>cap</i> genes)	200µg
Helper Plasmid	600µg
2xHBS	25 mls
2.5M CaCl ₂	2.5 mls
dH ₂ O (autoclaved)	22.5 mls
D10 Medium	50 mls

Table 2-5 rAAV2/8 calcium chloride transfection mix

PEI transfection

To transfect cells using PEI transgene, AAV8 packaging and helper DNA were prepared in the ratio 1:1:3. A total of 50µg of DNA was used per plate of cells. Plasmid DNA was added to DMEM (2.5mls/plate) and then PEI was added last

(2.25 μ g of PEI per μ g of DNA). The transfection mix in DMEM was gently mixed and left still for ten minutes for the formation of PEI-DNA complexes. The transfection mix was added to cells for 24 hours before being replaced with fresh D10 medium.

293T cell harvesting

Cells were harvested 72 hours following transfection or earlier if they were on the verge of lysis (as evidenced by the cells adopting a rounded morphology and starting to lift off the cell culture plates). Harvested cells were concentrated by centrifugation (5 minutes at 2000 rpm) before the cell pellet was resuspended in 1xTD buffer. Cell pellets were stored at -80°C prior to purification.

Vector purification

As for AAV2/2 production, cell lysis was achieved with repeated (typically 4) freeze-thaw cycles with vigorous vortexing in between cycles. The cell lysate was then treated with a detergent (1% Triton), before being incubated with Benzonase at 37°C for 30 minutes to breakdown any residual free DNA. The sample was then repeatedly spun down and then filtered to separate cell debris. After each spin the supernatant was removed and the cell debris pellet discarded prior to the next step. The spin / filter protocol was as follows: spin at 3220g 10 minutes, respin supernatant at 7500g 15 minutes, pass through 5 μ M filter, spin at 7500g 15 minutes, filter through 0.45 μ M and 0.22 μ M filters and finally 2 final spins at 20 000g for 30 minutes each. These final spins were repeated if necessary until there was no debris pellet visible in the tube at the completion of the spin. The additional two-phase separation step described below was performed at this stage when used.

Residual supernatant containing the suspended virus was then concentrated and purified in a 2 step process using a Sephacryl column for size exclusion, and then passage through an anion exchange column. Flow through the columns was

driven by a fast protein liquid chromatography (FPLC) machine (GE Healthcare, UK)

A Sephacryl S300 column was first prepared by equilibration with 50% Poros buffer B (Table 2-1). This was run at 5-10 mls/minute until the conductivity and UV spectrophotometer readings had equilibrated (which typically took up to 2 hours). The filtered lysate was then loaded on to the column which separates the lysate by size with larger items being impeded less by the medium and hence coming off first. 50% Poros buffer B was also used to push the lysate through the column.

The passage of virus was detected on the UV spectrograph, and pooled into distinct collection tubes. These were then diluted 1 in 4 with Poros Buffer A (Table 2-1) and stored at +4°C until ready for use, whilst the Sephacryl column was re-equilibrated using 50% Poros buffer B and then washed with 20% ethanol.

The diluted virus containing lysate was then loaded onto the Poros anion exchange column, which had been equilibrated with 15% Poros buffer B. The virus was washed through with further 15% Poros buffer B and then eluted with 60% Poros buffer B. Eluted virus was concentrated using Vivaspin 4 10kDa concentrator tubes and centrifugation; for this, the eluted virus was loaded onto the concentrator tube and spun until the residual volume was less than 200µl.

Concentrated virus was washed with 2mls PBS-MK by adding the PBS-MK to the concentrate in the Vivaspin tube and spinning at 5000g until all but 50-100µl had passed through the filter. This residual volume was placed in a sterile eppendorf whilst the concentrator tube was washed with a further 100µl of PBS-MK. The virus-containing PBS-MK samples were pooled, aliquoted and stored at -80°C.

Two phase separation for ultra pure virus

When used this additional step was performed following the spin / filtering protocol for lysed virus samples, and prior to passage through the size exclusion and anion exchange columns.

Viral suspension was added to approximately 5mls of a 1M ammonium sulphate and 20% PEG4000 mix. This was left to settle for over 3 hours at room temperature before being spun at 1000g for 5 minutes. The mix was left overnight at 4°C for separation of the 2 phases. The lower (aqueous) phase was drained and passed through a 0.22µM filter before a further spin at 20000g for 30 minutes. Collected supernatant was concentrated from approximately 5mls to 1-2mls by spinning in a 300kDa Vivaspin column, before being suspended in approximately 6mls of TD buffer for passage through the size and anion exchange columns.

2.4.3 Vector genomic titres

Vectors were quantified by determining the number of genome copies per ml of the vector preparation, using dot-blot assays and a probe specific for a segment of the genomic DNA. In brief vector DNA was first extracted from the rAAV particles by enzymatic digestion of the capsid, and then quantified relative to serial dilution of a known concentration of plasmid DNA. The number of DNA-containing particles is calculated based on the fact that each virion carries one single-stranded DNA molecule. This 'physical' method of quantification has advantages over 'biological' assays of infectivity which are highly dependent on vector properties and laboratory conditions (such as promoter strength as well as the cell type and helper virus used for infection).

Generation of Biotinylated Probe and Dilution Series

A segment of the plasmid DNA used to make the virus was cut using restriction enzyme digests, and isolated by agarose gel electrophoresis and gel extraction. In order to tag the probe DNA with biotin the double-stranded molecule was first

denatured (95°C for 2 min then cooled on ice) before being mixed as follows: 34µl of denatured probe DNA, 10µl of 5x labelling mix (contains random octomers), 5µl dNTP mix (containing biotin-dATP) and 1 µl Klenow (all reagents purchased from New England Biolabs, Herts, UK). The biotinylation mixture was incubated for in excess of 1 hour at 37°C, and then the reaction was terminated with 5µl of 0.2M EDTA (pH8). Biotinylated probe was then precipitated by mixing with 5µl NaOAc (3M) and 150 µl of 100% ethanol and incubating at -20°C for 20 minutes, followed by centrifugation at 14000 rpm for 10 min. Precipitated DNA was washed with 70% ethanol and resuspended in 20µl of TE buffer (Table 2-1).

The precise concentration of the plasmid DNA used for the standard was determined using Nanodrop[®] apparatus (LabTech International); knowing the concentration and size of the plasmid DNA (ng/µl) allows calculation of the volume required to give a specific number of molecules per well of the dot-blot apparatus. (This is calculated knowing that 1 mole of any nucleotide weighs 325g, and that 1 mole consists of 6×10^{23} molecules (Avogadro's constant)). The plasmid DNA used for the standard was subsequently pipetted out to give a dilution series between 10^{12} and 10^5 molecules per well.

Virus DNA extraction

1µl and 5µl samples of virus were digested with proteinase K enzyme using the protocol shown in Table 2-6.

	μ l
Virus	1 or 5
Proteinase K Buffer (2x)	100
dH ₂ O	99 or 95 (for 1 μ l and 5 μ l samples respectively)
Proteinase K enzyme	1

Table 2-6: Proteinase K digest of rAAV. The proteinase K enzyme and buffer was manufactured by Sigma-Alrich, Dorset, UK. The digest was incubated at 56°C for 30 mins.

To precipitate out the genomic DNA the digested virus was mixed with 20 μ g glycogen, 21 μ l of NaOAc (3M), 260 μ l of EtOH and incubated at -20°C for 30 minutes, prior to centrifugation at 14000 rpm for 10 min. Precipitated viral DNA was washed with 70% ethanol and centrifuged for 5 mins at 14000 rpm, before being resuspended in 200 μ l of 0.4M NaOH and 10mM EDTA. The DNA was denatured as above (2 min at 95°C then cooled on ice).

DotBlot Assay

A nylon transfer membrane (Amersham Biosciences, Bucks, UK) was placed in a Dotblot apparatus (BioRad). Wells to be used were filled with 200 μ l dH₂O and a vacuum applied to the apparatus. The prepared samples and standards were pipetted in the wells, and drawn into the membrane under vacuum. Wells were washed with 200 μ l 0.4M NaOH + 10 mM EDTA, also drawn into the membrane under vacuum.

DNA cross-linking to the membrane was induced by drying the membrane between sheets of Whatman paper (VWR, Leicestershire, UK) at 37°C for in excess of 20 mins.

The membrane was soaked in ddH₂O and transferred to a hybridisation bottle with 50 ml of hybridization buffer (Church mix, Table 2-1). Both the bottle and buffer are pre-warmed in advance to 65°C. The bottle, mix and membrane are kept in a rotating hybridisation oven for 30 minutes, which comprises the pre-hybridisation step of the protocol. 5µl of the denatured biotinylated probe is added, and the bottle and blot are left in the oven overnight for the hybridisation reaction to occur.

The membrane was then washed 3 times (each using 50ml of 33mM sodium phosphate buffer) for 5 minutes per wash. The membrane was then processed using the Phototope-Star Detection kit (New England Biolabs, Herts, UK) using the protocol summarised in Table 2-7.

<i>Step</i>	<i>Procedure</i>
A. Blocking	Membrane soaked in blocking solution (5% SDS, 125mM NaCl, 25 mM sodium phosphate, pH7.2) for 5 minutes with shaking.
B. Incubation 1	Streptavidin (1:1000 in blocking solution) applied for 5 minutes with shaking
C. Washes	2 x 5 minutes washes with Wash Solution I (=block solution diluted 1/10)
D. Incubation 2	Biotinylated Alkaline phosphatase (1/1000 in blocking solution) applied for 5 minutes with shaking
E. Washes	x 1 with block solution then x 2 with wash solution II (10mM Tris-HCL, 10 mM NaCl, 1 mM MgCl ₂ , pH 9.5). Each wash for 5 minutes
F. Substrate application	CDP-Star reagent (1:1000) applied to membrane for 5 minutes without shaking

Table 2-7: DotBlot Labelling protocol

The membrane was read using an X-ray film or a chemifluorescence imager. Digital scanning and densitometry (AIDA Image Analyzer, Raytest, Straubenhardt, Germany) was used to compare signal intensity from the virus samples with that from points on the standard curve. Titres were described in terms of numbers of viral genomes per ml (vg/ml). This is preferable to methods of quantifying vector particles per ml (vp/ml) as it avoids including empty, and hence non-functional, vector capsids.

2.4.4 Polyacrylamide gel electrophoresis (PAGE) and protein stain

Sodium dodecyl sulphate (SDS)-PAGE and a fluorescent protein stain were used to examine the protein content of vector preparations. Vector samples were first incubated with Laemmli buffer (which contains β -mercaptoethanol and SDS, Table 2-1) so that proteins are denatured and their positive charges neutralised; this allows proteins to be sorted specifically by size and not by shape or charge. 1-3 μ l virus samples were mixed with 5 μ l Laemmli buffer (2x), and the final reaction volume made up to 10 μ l with dH₂O, before being incubated at 37°C for 30 minutes.

Samples were loaded into a 10% w/v reducing SDS polyacrylamide electrophoresis gel (prepared in advance with 2.5mls Protogel (Bisacrylamide 0.8%, acrylamide 30%), 1.875mls Tris/SDS running buffer (Table 2-1), 3.125mls dH₂O, 35.25 μ l 10%APS and 7.05 μ l Temed (Tetramethylethylenediamine, Sigma). A commercial protein ladder was run alongside (Bio-rad). Bands were run to establish protein band separation over approximately one hour at 120 volts.

The gel was washed and fixed with 2 half hour washes in gel fixing solution (50% Methanol, 7% Acetic acid in distilled water). The washed gel was stained overnight with Spyro Ruby protein gel stain (Invitrogen), before further washes

in the same wash solution (for 1 hour) and in distilled water to decrease background fluorescence.

The Spyro Ruby protein gel stain has excitation peaks at 280 nm and 450 nm and an emission maxima close to 610 nm. The stained gel was therefore visualised using a UV transilluminator.

2.4.5 Transmission electron microscopy

Viral vectors were examined using transmission electron microscopy and a protocol based on previously published methods.²³² Purified rAAV virus was placed on a 300 mesh electron microscopy grid pre-coated with carbon and 1% formvar. Grids were then washed with PBS-MK (3x 30 second washes) and stained with 4% uranyl acetate for 1 minute. Excess uranyl acetate was removed by placing the stained grid onto a drop of ddH₂O, and then blotting away residual fluid with filter paper followed by air drying. Virus particles were observed using a JEOL 1010 transmission electron microscope (Jeol Ltd, Akishima, Japan) with an accelerating voltage of 80kV.

2.5 PCR

2.5.1 Primer design and manufacture

Primers were designed manually from the sequence or using commercial software (eg the Roche website). Prospective primers were evaluated for melting temperatures and the risks of forming primer dimers or secondary structures using primer select software (Lasergene). Primers were manufactured to order by Sigma-Alrich, UK.

2.5.2 Standard PCR

PCR reactions using the human and murine XIAP primers were run using 0.5µl of sample cDNA or linearised plasmid DNA, 10µl of Roche mastermix, 1µl each of the forward and reverse primers at a concentration of 20µM, and 7.5µl of water to give a total reaction volume of 20µl. The PCR reaction was run following 3 minutes of initial denaturation at 94°C. There then followed 40 cycles of 15 seconds at 94°C followed by 1 minute at the desired temperature (62°C, unless otherwise stated) and a final extension step of 5 minutes at 72°C.

The murine and human xiap primers used gave amplicons of 110 and 445 bp respectively. The products of these pcr reactions were therefore detected and sized by running on a 2% agarose gel with a 100bp commercial dna ladder.

2.5.3 Real-time PCR

cDNA from each sample was loaded into a 96 well plate along with FastStart TaqMan® Probe Mastermix (ROX) (Roche, UK), forward and reverse primers for amplification of the gene of interest, a hydrolysis probe that binds the amplified area and dH₂O to make the final reaction volume up to 30 µl. For quantification of XAF1 and β-actin expression, primers were used at a final concentration of 900 nM each, and the hydrolysis probe at a final concentration of 250 nM. Quantitative real-time PCR was run on an ABI Prism 7900HT Fast Real-time Sequence Detection System (Applied Biosystems, UK). The reaction cycle at which the fluorescence signal in each reaction reached a defined level, known as the “threshold cycle” (C_t) was determined using the manufacturer’s software (SDS 2.2.2). The relative expression between comparable samples in relation to the expression of genes of interest was calculated using the “Comparative C_t ” method and formulae provided by the manufacturer (Applied Biosystems).

2.6 Testing of plasmid and vector transgene expression

in vitro

293T cells were used preferentially because of their high susceptibility to plasmid transfection or infection by AAV2/2 virus. Cells were seeded on to a 24 well plate 24 hours prior to transfection or infection, such that there were approximately 75 000 cells per well (as determined using a haemocytometer).

2.6.1 Cell culture transfection with plasmids

Transfections were performed using either a peptide-lipofectin-DNA complex or using Polyethylenimine (PEI).

Lipofectin transfection mixes were prepared as in Table 2-8. The transfection mix was used to replace the normal growth medium for a period of 4 hours before being removed, and replaced with D10 until cell or supernatant harvesting after approximately 48 hours.

	<i>Per single well (of 24 well plate)</i>
Lipofectin (1µg/µl)	0.75µl
Peptide 6	42µl
Plasmid DNA (added last)	1µg
Medium	500µl of Optimem (no additives)

Table 2-8 Lipofectin Transfection mix

PEI transfection mixes were prepared as in Table 2-9 and left still to complex for 10 minutes before being added to the cell culture. In contrast to the lipofectin transfection mix, this mix was not changed until supernatant or cell harvesting.

	<i>Per single well (of 24 well plate)</i>
Plasmid DNA	3.3µg
Medium	0.756mls of DMEM (no additives)
Polyethylenimine (PEI)	36.8µg

Table 2-9 PEI Transfection mix

2.6.2 Cell culture infection and superinfection with AAV2/2

The 293T cell line consists of human kidney cells transformed with adenovirus 5 DNA (ATCC Product Information Sheet for CRL-11268). The cells can therefore be infected in the absence of additional helper virus. However, to increase infection efficiency, and increase the chance of detectable levels of transgene expression before cell culture overgrowth, *in vitro* infections can be performed with concomitant adenovirus application; this technique is known as ‘superinfection’.

Standard infections were performed by adding 1µl of AAV2/2 (with a titre of approximately 1×10^{12}) to each well of cells. For superinfections adenovirus was added concomitantly at a ratio of between 10-20 virus particles per cell (i.e. multiplicity of infection (MOI) of 10-20).

2.7 In vivo procedures

All animal procedures were approved and licensed by the Home Office.

2.7.1 Anaesthesia and recovery

The general anaesthetic used for mice procedures consisted of Dormitor (1mg/ml medetomidine hydrochloride, Pfizer Pharmaceuticals, Kent UK), Ketamine (100 mg/ml, Fort Dodge Animal Health, Southampton, UK) and sterile water for injection prepared in the ratio of 1.0 : 0.6 : 8.4 respectively. 0.10-0.15 ml of the

anaesthetic was administered by a single intra-peritoneal (i.p.) injection to adult mice; for pups <14 days old 0.1ml of anaesthetic diluted 1/5 was used.

Mice were recovered by an equal-volume i.p. injection (0.15ml) of recovery mix (containing 0.25ml Antisedan (5mg/ml Atipomezole hydrochloride, Pfizer Pharmaceuticals, Kent UK) per 12 ml sterile water for injection). During recovery mice were kept warm using heat pads and free access to water and food was ensured.

2.7.2 Electroretinogram

Electroretinogram (ERG) recordings can be used to study specifically rod or cone function by varying the background light intensity, and the intensity and frequency of flash stimuli.²³³ In the dark-adapted scotopic state any ERG response to dim stimuli is exclusively from rod photoreceptors.²³⁴ In contrast following light adaptation and under bright background (photopic) conditions the rod pathway is suppressed and the ERG response is mediated by cone photoreceptors.²³⁵

ERGs were recorded from anaesthetised mice using the commercially available Espion E² system with a ColorDome Ganzfeld Stimulator (Diagnosys, UK). A purpose built platform, with moveable stands for the positioning of electrodes, was used to position the mouse (Figure 2-2). Following the onset of general anaesthesia the pupils of both eyes were dilated with a single drop of 1% tropicamide. 2% hydroxyl-propyl-methyl-cellulose (HPMC) was then placed onto each cornea to maintain hydration for the duration of the procedure and improve electrical contact with the electrode.

The anaesthetised mouse was placed onto a heat pad aligned with the middle of the ganzfeld bowl, and a rectal thermometer inserted. The heat pad and thermometer were part of the commercially available Homeothermic Blanket system manufactured by Harvard Apparatus Ltd (Edenbridge, Kent, U.K.). This system was set up such that the mouse body temperature was maintained within 1 degree of 36.9⁰C throughout the electrodiagnostic assessment.

Corneal contact electrodes, a midline subdermal ground electrode (placed above the base of the tail) and a sub-lingual reference electrode were placed and the impedance of the contacts checked; electrode contacts were adjusted to ensure that the impedances for each recording channel (1 for each eye) were equal, and low (between 5 and 8 KOhm). The electrodes were fashioned in house from platinum wire.

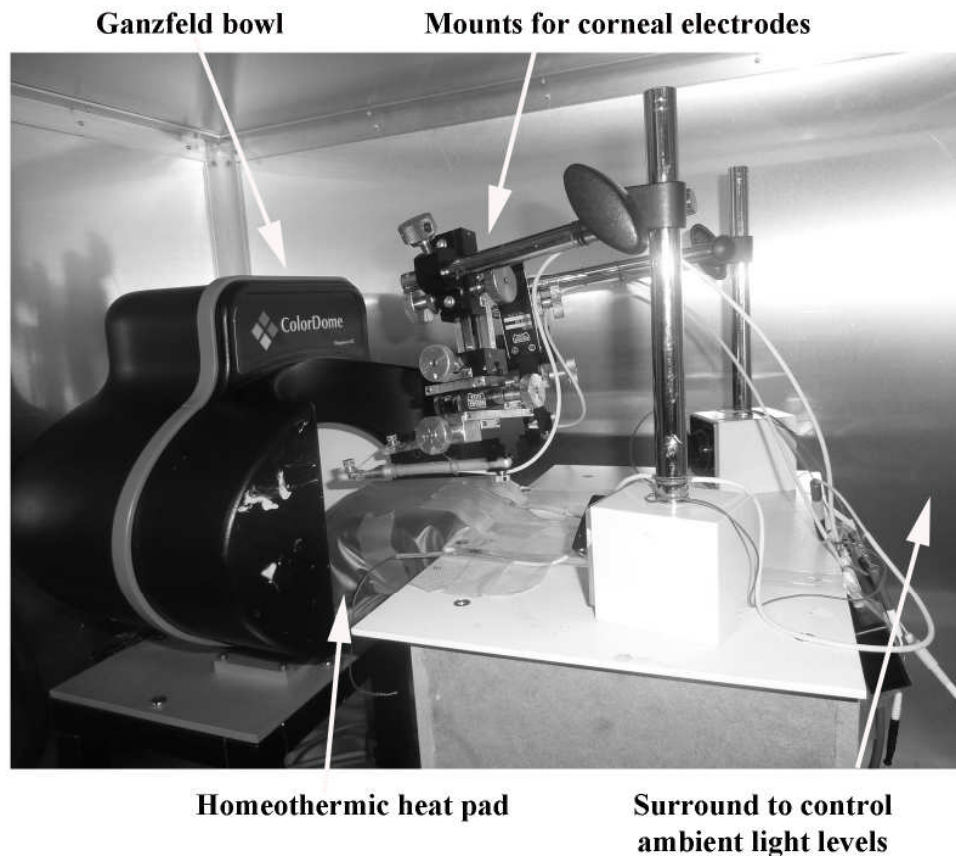


Figure 2-2 ERG recording apparatus. A custom built platform was used to position the mouse in the centre of the Ganzfeld recording bowl. A heat pad was positioned between the mouse and the platform surface. Mounts on the platform were used to position electrodes. The recording apparatus was all within a metal Faraday box to help control ambient light levels and reduce electrical interference.

Scotopic series were performed in animals that had been dark adapted over the preceding 16 or more hours. Red LED headtorches (Silva, Sollentuna, Sweden) were used to prepare the animal for scotopic examinations so as to avoid compromising the dark adaptation prior to recordings. Responses to stimuli over a 4 log unit range (0.001 to 10 cd.s/m^2) were recorded, with 10 trials averaged at each step. Each trial was recorded over 400ms, and the recordings were filtered from 0-1KHz with a sampling frequency of 5kHz to reduce interference from the

mains electrical supply. The first 10ms of each recording were used to establish the baseline prior to stimulus presentation.

Prior to photopic examinations the animal was light adapted for 10 minutes with a background white-light stimulus of 20 cd/m² intensity. In the photopic flash protocol responses were recorded to stimuli of increasing intensity, with 25 trials averaged at each step. Example traces are shown in Figure 2-3.

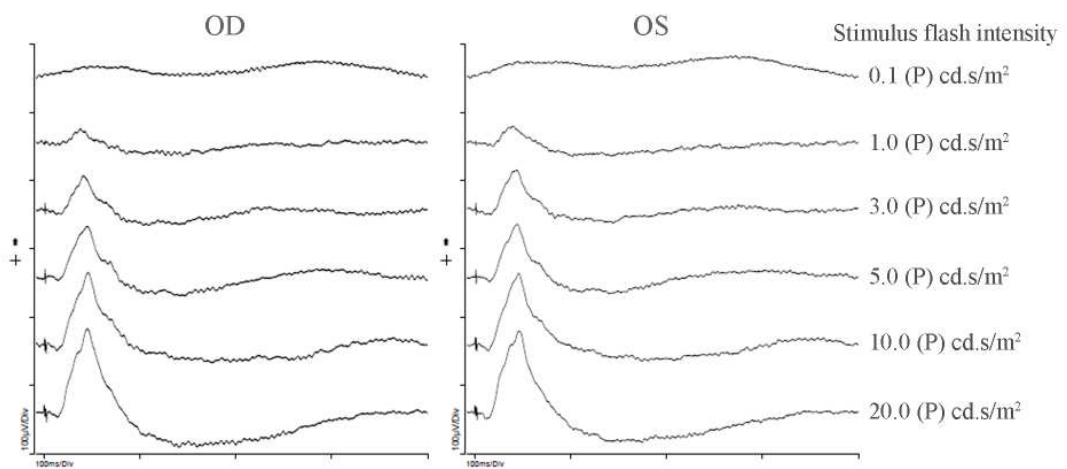


Figure 2-3 Example of photopic flash traces. Averaged recordings from a series of flash intensities are shown for the right (OD) and left (OS) eyes.

Photopic flicker examinations were performed in light-adapted animals, following the photopic flash protocol. Responses were examined to standard white light flashes of 0.5, 2.0, 5.0, 10.0, 15.0 and 30.0Hz frequency, all at an intensity of 3 cd.s/m². Analysis of amplitudes and implicit times was performed on the averaged trace of 25 recordings from the 10Hz stimulus, as this response typically shows the greatest amplitude in mice.²³⁶

Analysis of recordings was performed using the Espion E² software. The principal variables studied were A and B waves which were recorded relative to the baseline and A wave trough respectively (Figure 2-4).

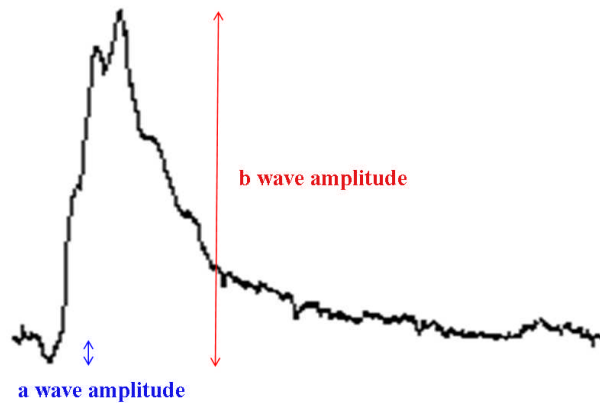


Figure 2-4 The a and b waves demonstrated on a typical ERG waveform to a bright flash from the rhodopsin knockout

2.7.3 Sub-retinal and intra-vitreous Injections

Sub-retinal injections were performed under general anaesthesia and following pupil dilation with 1% tropicamide. HPMC and a coverslip were placed onto the cornea to maintain clarity of view and to protect the cornea from drying. Under direct retinoscopy through an operating microscope the tip of a 1.5 cm 34-gauge hypodermic needle (Hamilton) was guided under the coverslip and then tangentially through the sclera to produce a self sealing wound tunnel. The needle tip was slowly advanced so as to rest between the retina and retinal pigment epithelium. 0.5-1.5 μ l of virus suspension was then injected to produce a bullous retinal detachment (typically covering 30-40% of the fundus), and care was taken to minimize reflux on withdrawal of the needle.

Intra-vitreous injections were performed as above but with the site of injection 1 mm posterior to the limbus. The needle was advanced posteriorly towards the optic disc under direct visualisation to avoid damage to the retina or lens.

To perform injections in mice before separation of the eyelids, the eyelids were divided using a sharp needle and manual retraction.

2.7.4 Confocal scanning laser ophthalmoscopy

Confocal scanning laser ophthalmoscopy (cSLO) allows high quality retinal images to be obtained quickly in patients and in animal models. With this technology, a laser is used to illuminate the retina and the reflected image is then captured through a fine pinhole (approximately 400 μ m in diameter). The small aperture of the pinhole ensures that scattered light, or light from outside the focal plane, is excluded. The image formed on the detection unit is therefore exclusively from a single focal plane illuminated by the stimulating laser (hence the term confocal), resulting in high contrast optimally focussed images (Figure 2-5). To image across the retinal surface the emitted laser beam is redirected horizontally (in the x-axis) and vertically (in the y-axis) along a plane of focus perpendicular to the optic axis (conventionally the z-axis). This is performed using oscillating mirrors, and allows the illuminating and confocal detection system to effectively scan across an area of the retinal surface. As only a limited area is imaged at any one time the illumination used can be brighter than would be tolerated with conventional photography, which also contributes to the images obtained being more clearly defined.

In these experiments cSLO was performed with the Heidelberg Spectralis hardware and software (Heidelberg Engineering, Dossenheim, Germany). This was used as is it is in hospital clinics, except that the chin rest was replaced with a custom-made platform and heat pad on which to position mice. (Figure 2-6). In the human eye this system can achieve a detection resolution of 5 μ m (www.heidelbergengineering.com), though the different optics of the murine eye will be likely to affect this. In these experiments the infra-red and fluorescein angiography modes were used for cSLO, which use the 820nm and 488nm stimulating lasers respectively.

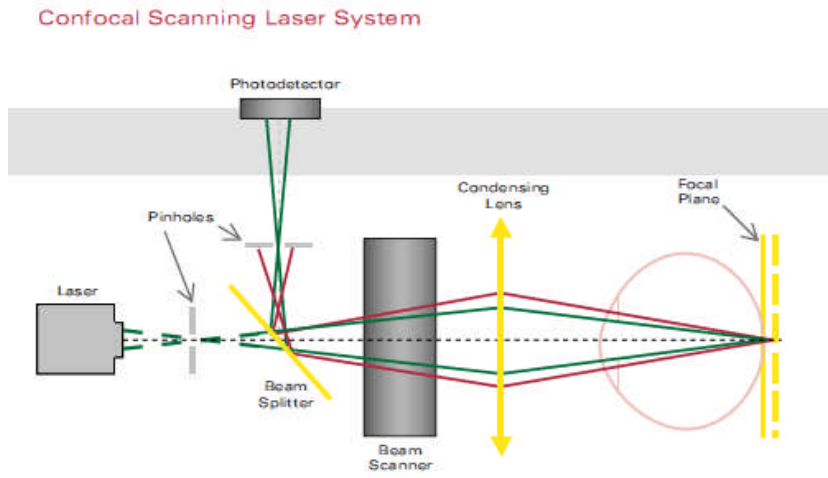


Figure 2-5 Schematic diagram of a confocal scanning laser system. From www.heidelbergengineering.com.

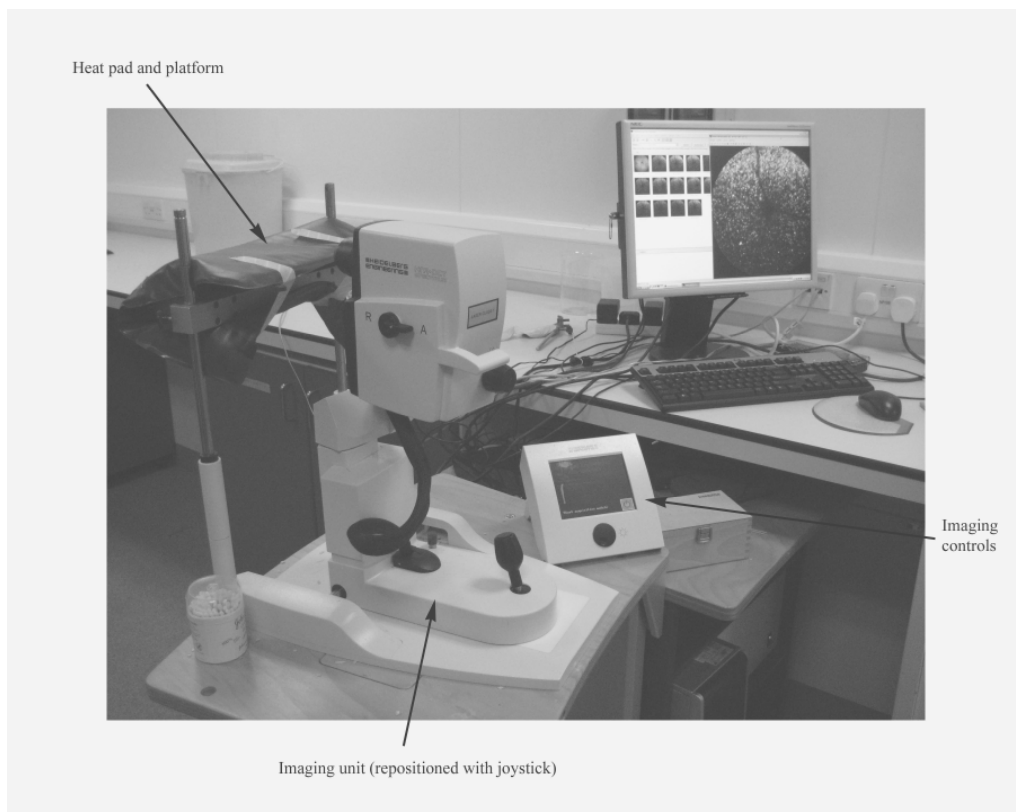


Figure 2-6 The Heidelberg Spectralis adapted for use with animal models.

Prior to imaging mice were anaesthetised with a general anaesthetic and the pupils dilated with 1% tropicamide. Drops of Hypromellose (0.3%) (Tubilux Pharma, Pomezia Italy) were applied to the corneas of anaesthetised animals to prevent drying during the imaging procedure.

Infra-red cSLO was employed in order to focus on the retina and orientate the imaging unit and mouse eye such that the optic disc was in the centre of the image and that as far as possible the image clarity was equal across the field of view (Figure 2-7). Imaging with infra-red has many advantages over conventional ophthalmoscopy; of particular relevance for imaging the mouse eye the infra-red illumination is better able to penetrate unclar media, and high quality images are less dependent on the extent of pupillary dilation. We have previously found that the combination of general anaesthetic, pupillary dilation and corneal exposure readily predispose to corneal opacity in the mouse eye, which can be challenging to prevent even with the frequent application of lubricating drops. The use of infra-red ophthalmoscopy therefore assisted in obtaining high quality images. In addition, the absence of a bright flash light reduces stimulation of the subject being imaged.

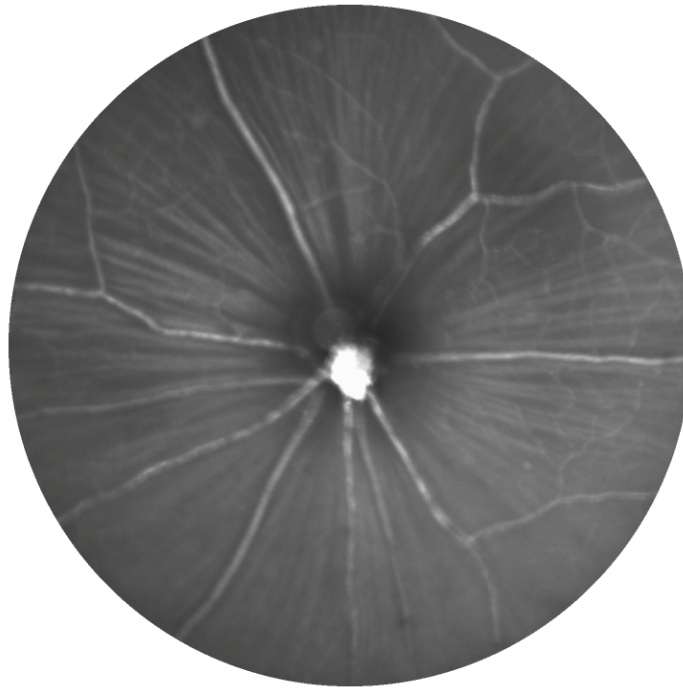


Figure 2-7 *In vivo* infra-red imaging of the murine retina.

To detect GFP the fluorescein angiography mode was used for cSLO; in this mode a 488 nm laser is used to illuminate the retina, and a 500nm barrier filter is inserted prior to the detection unit. Clinically this setting is used to image fluorescence from pre-injected fluorescein dye, and so image retinal vasculature and detect leak of the dye from vessels. The peak of the fluorescein absorption spectrum is approximately 490 nm, and the peak of the emission spectrum is approximately 521 nm. By detecting only light of a wavelength greater than 500 nm reflected 490 nm light is excluded. Fluorescence by fluorescein is however still detected and so the morphology and leakiness of retinal vasculature can be visualised in detail. GFP has similar peaks of absorption and emission spectra (475 and 509 nm spectrum), and so can be imaged using the same settings. In these experiments cSLO with the 488 nm laser was used to image *in-vivo* GFP expressed in transgenic mice, and in wild type mice following gene therapy. To achieve consistency between different images sensitivity settings were kept constant (4.7 scans/second, 100% laser power, 100% sensitivity, high resolution setting selected). Saved images were an average of 33 frames each.

For analysis of cone cell densities images were subsequently analysed using Photoshop (Adobe) and Image Pro-Plus (Media Cybernetics) software. In a separate and overlying image individual hyperfluorescent spots were marked, and the area corresponding to 75% of the field of view centred on the disc was also delineated. The hyperfluorescent spots within this defined area were then counted using Image Pro-Plus.

2.7.5 Optical coherence tomography

Optical coherence tomography (OCT) is a means of obtaining detailed cross-sectional images from analysis of scattered light *in vivo*. 3D reconstructions can then be created. Long wavelength (near-infrared) light is used which is able to penetrate into ocular tissues, and so from the pattern of scatter the composition of retina, RPE and choroid can be examined repeatedly in living subjects.

Spectral (or Fourier)-domain OCT (SD-OCT) technologies are able to simultaneously measure multiple wavelengths of reflected light, hence the name spectral-domain. These have largely superseded previous time-domain OCT (TD-OCT) technologies that used a moving reference mirror to measure the time taken for light to be reflected, and produced lower quality images.

The SPECTRALIS system used in these experiments integrates SD-OCT with cSLO, to allow eye tracking and reduced motion artefact. In addition noise artefact is reduced by averaging repeated scans at precisely the same location,²³⁷ and in humans the system has been demonstrated to have very high repeatability and reproducibility with a repeated thickness measurements varying by less than 1 μm .²³⁸ Although the tracking laser is not known to pose any safety hazards, the imaging time for a single session is limited to 300 seconds. This was found to be more than enough to obtain high quality images in mice.

2.8 Immunohistochemistry

2.8.1 Tissue preparation

Animals were sacrificed according to Schedule 1 of the Animals (Scientific Procedures) Act 1986. The superior aspect of each eye was marked by cautery of the peri-limbal tissues prior to enucleation or by placing a suture under the superior rectus muscle.

For the preparation of flatmounts enucleated eyes were dissected whilst in 1% PFA under the operating microscope. Whole retinas were carefully separated from underlying RPE, choroid and sclera and incised with 3-4 radial incisions to allow flattening of the retinal sheet. The superior incision would approximate closest to the optic disc to allow subsequent orientation. The retinal sheet was then transferred onto a glass slide using a Pasteur pipette and 1% PFA. To fix the retina as a flat sheet a cover slip was gently applied over the retina and 4% PFA applied around the edges which subsequently fixes the tissue by capillary action.

For the preparation of frozen sections the cornea, iris and lens was removed from enucleated eyes whilst immersed in 1% PFA. The remaining eye-cups were then fixed for 15 minutes to 1 hour in 4% PFA. Cryo-protection, when used, was performed by incubation in 10% sucrose solution overnight. Eyes were then embedded in O.C.T (R A Lamb, East Sussex U.K) with care to maintain track of the orientation. Eyes were then frozen in iso-pentane which had been pre-cooled in liquid nitrogen. Specimens were stored at -20°C and prior to examination 12-20 µm thick sections cut using a Bright cryostat.

2.8.2 Antibody staining

Tissue, from flatmounts or frozen sections, was immersed in blocking solution (Table 2-1) at room temperature for 2 hours prior to immunohistochemistry. The tissue was incubated overnight at 4°C with the primary antibody (Table 2-10) diluted in blocking solution. 3 washes in PBS were performed (each ≥ 15

minutes) before incubation with secondary antibody for 2 hours at room temperature. Further washes in PBS were performed (3, each ≥ 15 minutes). Secondary antibodies (goat anti-rabbit, goat anti-chicken and goat anti-mouse) were purchased from Invitrogen and used at 1/1000 concentration in blocking solution unless otherwise stated. For rhodopsin immunohistochemistry the goat anti-mouse secondary was used at 1/250, for caspase 3 staining the rabbit anti-mouse secondary was used at 1/200, and for PNA staining the streptavidin-546 secondary was used at 1/200.

To stain nuclei sections were counterstained with 4',6-diamidino-2-phenylindole (DAPI); this binds strongly to DNA, preferentially within AT-rich regions, and has a blue fluorescence.²³⁹

Epitope	Background	Manufacturer	Concentration used at (in Blocking solution)
a-subunit of cone transducin (Gt2)	Rabbit	Santa Cruz Biotechnology	1/500-1/1000
Caspase 3 (active)	Rabbit	AbCam	1/20
Cone Arrestin	Rabbit	Gift	1/2000
Cone-opsin (red-green)	Rabbit	Chemicon	1/1000
Cone-opsin (blue)	Chicken	Gift	1/4000
Cone-opsin (short)	Rabbit	Chemicon	1/1000
Hemagglutinin (HA) tag (polyclonal)	Rabbit	Abcam	1/200-1/1000
Rhodopsin	Mouse	Gift	1/100
Peanut agglutinin (PNA)	Goat	Vector laboratories	1/200-1/1000

Table 2-10 Primary Antibodies

2.8.3 Histology

Lectin

Lectin staining (Lectin from *Bandeiraa simplicifolia*, TRITC conjugated, Sigma, UK) was used for orientation of retinal flatmounts by staining the vasculature. Fixed retinal sheets were immersed in lectin (0.1mg/ml in PBS) at 4°C for 12-16 hours, prior to repeated washes in PBS (6x 1 hour washes). Prior to mounting on microscopy slides, retinal flatmounts and sections were stained with the Hoechst 33342 DNA stain (used at 1/1000 dilution in PBS). In addition DAPI (1/100 w/w) was added to the fluorescent mounting medium used (DAKO, Ely, UK).

Haematoxylin and Eosin (H&E)

Prior to staining cryosections were washed in running water to remove OCT medium; paraffin sections were instead washed in xylene to remove the wax, followed by alcohol and water washes to rehydrate the tissue. Slides were immersed in Hematoxylin (Fisher Scientific, Loughborough, UK) for 5 minutes to over-stain the tissue, before 2 minute rinses in water and acid alcohol (1% HCL in 70% alcohol) to differentiate the staining by removing Haematoxylin from non-basic tissue components. Following a further wash in water the slides were immersed in ammonia water (1ml NH₄OH in 1L H₂O) to alkalinise the tissue and turn the Haematoxylin blue. Slides are washed in water and rehydrated with 95% alcohol prior to staining with Eosin (Fischer Scientific). The staining is differentiated by immersion in 95% alcohol to remove excess eosin. Finally the slides are immersed for 2 minutes in Xylene to aid fixation of the aqueous based dyes, before being mounted in a Xylene-based mounting medium (DEPEX, BDH chemicals, distributed by VWR International Ltd, Lutterworth, Leicestershire).

2.9 Protein Detection

2.9.1 Evaluation of Protein Concentration

Total protein concentrations were determined by examining samples in triplicate with a commercial calorimetric protein assay (DC protein assay kit, Biorad, Hemel Hempstead UK). Sample concentrations were compared to a bovine serum albumin standard curve and diluted in assay buffer to bring the concentration to within the linear portion of the standard curve for quantification. Bovine serum albumin used for the standard curve was supplied at 10mg/ml (Promega, Madison, WI, USA). Measurement of optical density was performed using the Emax ELISA reader (Molecular Devices Ltd, Berkshire, UK) to quantify absorbance at 650 nm.

2.9.2 ELISA

GDNF and XIAP proteins were detected, and concentrations determined, using commercial immunoassays manufactured by R&D Systems Europe Ltd., Oxford, U.K. (human GDNF ELISA DuoSet[®] and total human XIAP DuoSet[®]). Kits were used according to manufacturer's instructions. A 96 well plate was first coated with 'Capture' antibody. A high-protein blocking solution was then used to bind to any remaining areas of plastic on the 96 well plates. Samples were then applied for 2 hours incubation at room temperature prior to washing with wash buffer (0.05% (v/v) Tween[®] 20 in PBS) . A biotinylated 'Detection' antibody was then applied for a further 2 hours prior to repeated washes. Samples were incubated with streptavidin conjugated to horseradish-peroxidase and detected using a chromogenic substrate. The colour change was measured at 450 nm using a spectrophotometer (Immunoscan, Cellular Technology Ltd).

2.9.3 Western Blotting

Cells from *in vitro* and *in vivo* samples were lysed in a commercial RIPA buffer with added protease inhibitor (both from Sigma Aldrich, Gillingham, UK). Cell membranes were disrupted using a sonicator (Soniprep 150, MSE London UK) with the samples maintained on ice, prior to storage in aliquots at -80°C .

Equal amounts of protein were loaded into wells of a reducing SDS polyacrylamide electrophoresis gel (typically 9% w/v) and run to establish protein band separation over approximately one hour at 120 volts. Bands were then transferred to a PVDF membrane (Millipore Watford UK) and blocked in 5% milk for one hour at room temperature with mixing. Primary and secondary antibodies were used as in Table 2-11 prior to imaging of the membrane with a chemifluorescence reader or x-ray developer.

	Concentration used	Incubation Conditions
Primary Antibodies		
- anti HA	1/2000	Overnight at 4°C
- anti XIAP	1/500-1/1000	Overnight at 4°C
Secondary Antibodies		
- anti Rabbit secondary	1/5000 in TBS Tween and 2% goat serum	2 hours at room temperature

Table 2-11 Antibodies used for Western Blotting

Chapter 3 A novel model for the *in-vivo* study of rod-cone degeneration

3.1 Introduction

A challenge to the study of cone photoreceptors in the mouse is that they constitute only 3% of the total photoreceptor population, and are diffusely spread throughout the retina.^{13;14} Retinal sections are therefore dominated by rod photoreceptors, and the magnitude of cone-specific functional responses is small in comparison to rod responses in wild-type mice.

A novel mouse model was therefore generated to facilitate the study of specifically cone photoreceptor survival and function in the course of a rod-cone retinal degeneration. The mouse model is a double transgenic, homozygous for a targeted disruption of the rhodopsin gene and heterozygous for green fluorescent protein (GFP) expression driven by a cone specific promoter. The rhodopsin knockout mutation gives the mouse model a rod-cone degeneration analogous to that seen in patients, in which a mutation expressed specifically in rods leads first to rod photoreceptor death and then to a subsequent secondary loss of healthy cone photoreceptors. The advantage of using this specific rhodopsin mutation is that it renders the rods non-functional and so specifically cone function can be assessed with confidence. The advantage of the cone promoter driven GFP expression is that it permits *in vivo*, and hence repeated, quantification of cone-photoreceptor survival during the course of the degeneration.

The mouse line was derived by inter-breeding the pre-existing 'Rhodopsin Knockout' and '*Opn.gfp*' strains.

The Rhodopsin Knockout Mouse

This mouse line, with a targeted disruption of the rhodopsin gene, was generated by Humphries *et al.* and has been widely used since as a model of human retinitis pigmentosa.⁹⁰ The gene was disrupted by generating a vector that incorporated a neomycin cassette at codon 135 in exon 2 of the rhodopsin gene. Southern blots were used to identify embryonic stem cell clones and subsequently chimeric mouse off-spring with DNA containing the targeted disruption. In addition absence of rhodopsin expression in ocular tissues was confirmed with reverse transcriptase PCR, with primers spanning the insertion in exon 2, and rhodopsin immunohistochemistry. These experiments confirmed that there was no rhodopsin in the homozygous knockouts (*Rho*^{-/-}), in contrast to the heterozygotes and wild types (*Rho*^{+/-} and *Rho*^{+/+} respectively).

Rhodopsin has structural roles essential for photoreceptor morphogenesis, in addition to its role in phototransduction,²⁴⁰ and so rhodopsin knockout mice lack rod outer segments.⁹⁰ The outer nuclear layer however, which is principally rod photoreceptor nuclei,^{13;241} is nevertheless still about 80% of its normal thickness at 24 days of age; this degenerates with time such that by 48 days it has decreased in thickness by 50%, and by 90 days the ONL is just one cell thick indicating that rod photoreceptor degeneration is essentially complete. In keeping with the histological findings ERG analysis shows no evidence of a rod response in the *Rho*^{-/-} animals.^{90;242} In contrast, the cone ERG response is initially equal to that in wild type mice, until about P47 when it then progressively declines to reach 1-2% of the wild type response by P80. Punzo *et al.* characterised the course of cone loss using quantitative real-time PCR to short wavelength sensitive opsin transcript, and using whole-mount immunohistochemistry to medium wavelength sensitive opsin and peanut agglutinin lectin (PNA).⁷⁵ Cone photoreceptor loss was found to commence only once the rod loss was largely complete and the ONL just one cell thick. Cone loss commenced in the central retina and was only complete across the whole retinal surface by about 80 weeks of age.

The *Opn.gfp* mouse

This mouse strain was purchased from the Mutant Mouse Research Resource Centre (www.mmrrc.org) and is referenced by the strain name of “*B6.Cg-Tg(OPN1LW-EGFP)85933Hue/Mmmh*”. The mutant mice contain a modification of the *Aequorea victoria* jellyfish green fluorescent protein (GFP) transgene under control of the human long-wavelength-sensitive cone opsin promoter (OPN1LW-human). GFP, and in particular the variant used in this mouse strain known as enhanced green fluorescent protein (eGFP), is a valuable cellular and protein marker due to it being both highly fluorescent and soluble.

The strain was initially developed by Fei and Hughes²⁴³ by injecting a plasmid DNA construct into the pronuclei of F1 mouse embryos; transgenic mice were identified using PCR, epifluorescence microscopy and immunohistochemistry.

Fei and Hughes found that only cone photoreceptors contained detectable levels of GFP. No GFP was found in the RPE, suggesting that the GFP released during disc shredding is rapidly degraded or loses its fluorescence due to the pH of the endosomal pathway.²⁴⁴ The effect is that the GFP expression is found very specifically in cones, and not in the RPE cells or macrophages even though they are involved in cone photoreceptor outer segment phagocytosis.

Fei and Hughes also found that

- The subset of the cone population that express GFP are found in greatest density in the dorsal retina, and were relatively sparse in the more peripheral ventral retina (in a similar pattern to M opsin expression).
- The level and distribution of expression was stable through successive generations. Only heterozygotes for the transgene were studied (personal communication).
- The cells (on the basis of histological appearance) appeared healthy and normal despite the quantities of GFP seen.

3.2 Colony Generation and Maintenance

Mice homozygous for the rhodopsin disruption were selected for by performing scotopic ERGs following 12 hours of dark adaptation (example traces shown in supplementary data chapter). In contrast to wild types or heterozygotes, homozygous rhodopsin knockout mice are distinctive in having no a-wave;^{90;242} this is likely to be because the a-wave is a direct measure of the photoreceptor response, and in mice lacking functional rods the a-wave generated by the relatively sparse cones is too small for detection using standard ERG protocols. Selection for retinal GFP expression was achieved by fundal imaging of fluorescence using the scanning laser ophthalmoscope.

Experimental animals were all bred from crosses where one parent had no GFP expression to ensure that only *Opn.gfp* heterozygotes were used. This was to avoid variability in levels of GFP expression that could potentially result from including *Opn.gfp* homozygotes. Breeding pairs were confirmed to be homozygous for rhodopsin gene disruption and so all GFP-expressing off-spring (i.e. the experimental animals) had the *Rho-/-Opn.gfp+/-* genotype. Experimental animals, with this genotype, are here-in referred to using the “*Rho-/-Opn.gfp*” abbreviation.

3.3 Cone-specific GFP expression

In order to confirm the cell population in which eGFP is expressed *Rho*^{-/-} *Opn.gfp* animals were culled at 6 weeks of age, and cryosections prepared along the superior-inferior axis.

These showed the eGFP to be strongly expressed in specifically cone photoreceptors, as determined by cellular morphology, location and counter-staining with cone-specific antibodies (Figure 3-1 to Figure 3-3). eGFP is excluded from nuclei and so in Figure 3-1 part B a negative image of the lobular nucleus can be seen, which is a characteristic features of cone photoreceptors.¹³ It can also be seen that the cone photoreceptors are localised to a single plane at the outer edge of the outer nuclear layer; this means that a single confocal image, with the focal plane at this level, can be expected to detect a high percentage of the cone photoreceptors.

Also in Figure 3-1 the eGFP is seen to be strongly expressed throughout the cone photoreceptor except in the outer segment where expression was reduced. An antibody to red/green opsin was used to delineate cone outer segments. As expected eGFP expression driven by the human long-wavelength opsin promoter largely corresponds to cone outer segments expressing red/green opsin.

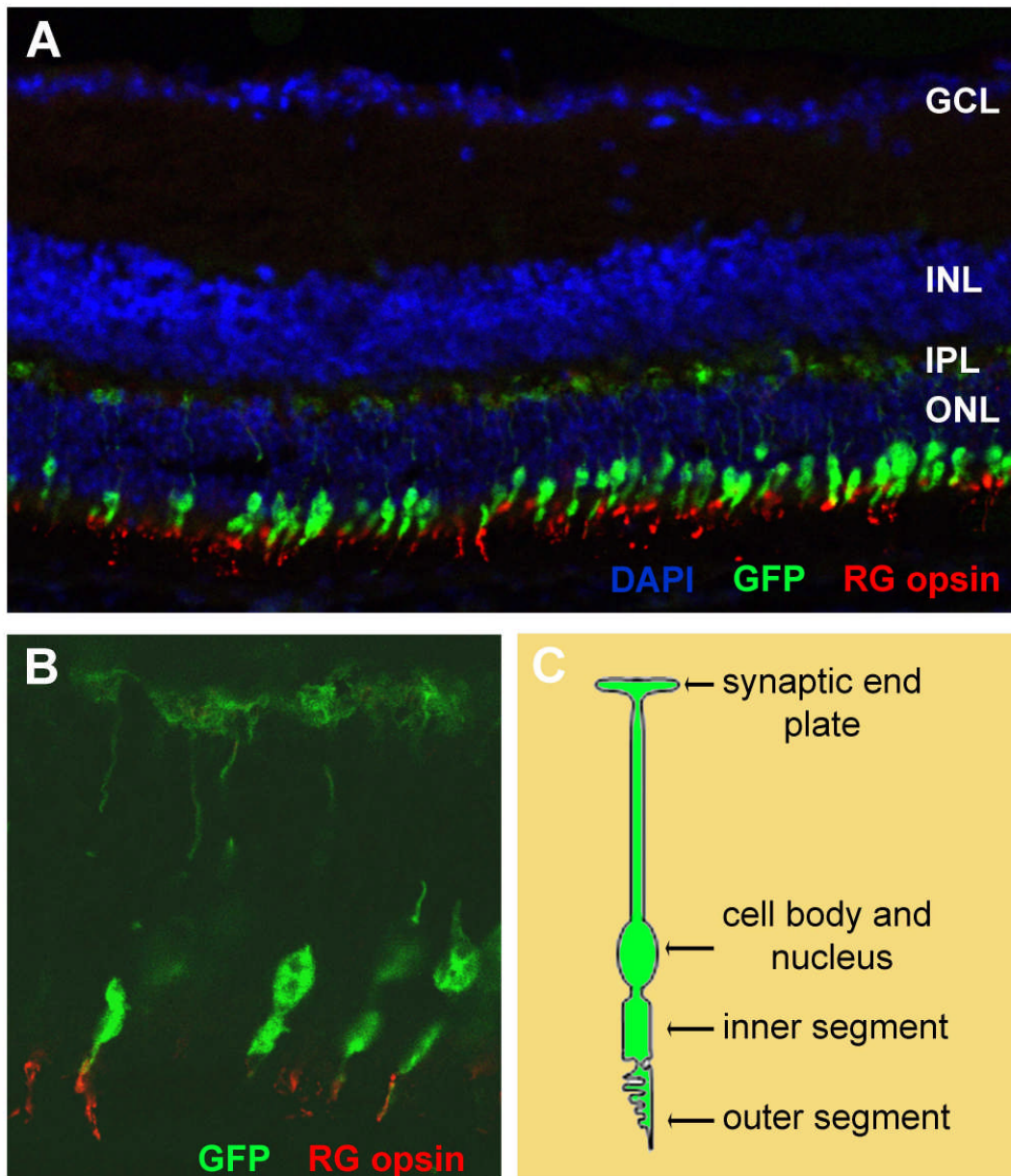


Figure 3-1 GFP expression in cone photoreceptors of the *Rho*^{-/-}*Opn.gfp* mouse. A cryosection of adult retina has undergone immunohistochemistry for opsin protein (A and B). Strong GFP expression is seen in cone cell bodies, synaptic end plates and inner segments (shown at low power, high power and schematically in panels A, B and C respectively). The typical cone photoreceptor morphology, with multi-lobed nuclei localised to the outer limit of the outer nuclear layer (ONL), is well demonstrated in this figure. Red-green opsin expression (demonstrated using immunohistochemistry and shown in red) is seen in the outer segments of cones expressing GFP (A and B).

Peanut agglutinin (PNA) lectin selectively binds to the protein sheath and interphotoreceptor matrix surrounding cone photoreceptors, and not rod photoreceptors.²⁴⁵ It was therefore used to identify the total cone population, regardless of opsin subtype expressed in the sections of *Rho-/-Opn.gfp* retina (Figure 3-2). In keeping with findings from other mouse strains the cones were found to be evenly distributed across the retinal surface.^{13;14} The eGFP expression however, followed a superior-inferior gradient with greatest expression in the superior retina and posterior pole (Figure 3-2). This pattern approximates previously described patterns of M-opsin expression in the mouse eye, and is as expected given that the eGFP expression is driven by the human long-wavelength-sensitive opsin promoter.^{12;246} These sections clarified therefore that the eGFP is expressed in a sub-proportion of the total cone population.

To elucidate this further, additional sections were counter-stained with an antibody to the S-opsin protein (Figure 3-3). In the mouse eye S-opsin is primarily expressed in the ventral retina, with only scattered expression in the dorsal retina.^{12;246} This pattern of expression is evident in Figure 3-3.

Thus although cone photoreceptors are evenly distributed along the superior-inferior axis of the *Rho-/-Opn.gfp* mouse eye, cones expressing eGFP are found at greatest density in the superior retina and posterior pole. This distribution is approximately proportional to the gradient of M opsin expression, and inversely related to the gradient of s-opsin expression. Therefore the eGFP is principally a marker of M opsin expressing cones, and not of cones expressing high levels of s-opsin.

Legend to Figure 3-2 (following page). The 6 week old *Rho*^{-/-}*Opn.gfp* eye has been sectioned along the superior-inferior axis at the posterior pole of the eye. Peanut agglutinin lectin (red) was used to show the cone sheaths of all cones regardless of cone subtype. A composite image is shown (middle right) along with 6 surrounding enlargements from the different regions. GFP expressing cones are seen throughout the retina, but are most numerous at the posterior pole of the eye, and in the superior retina. The insert (*) is a high power magnification from the image to its right, showing the morphology of GFP expressing cones. Cone cell bodies are aligned at the outermost edge of the ONL. PNA (red) is seen to surround and overlie the outer segment of GFP expressing cones, which is seen as yellow on the image.

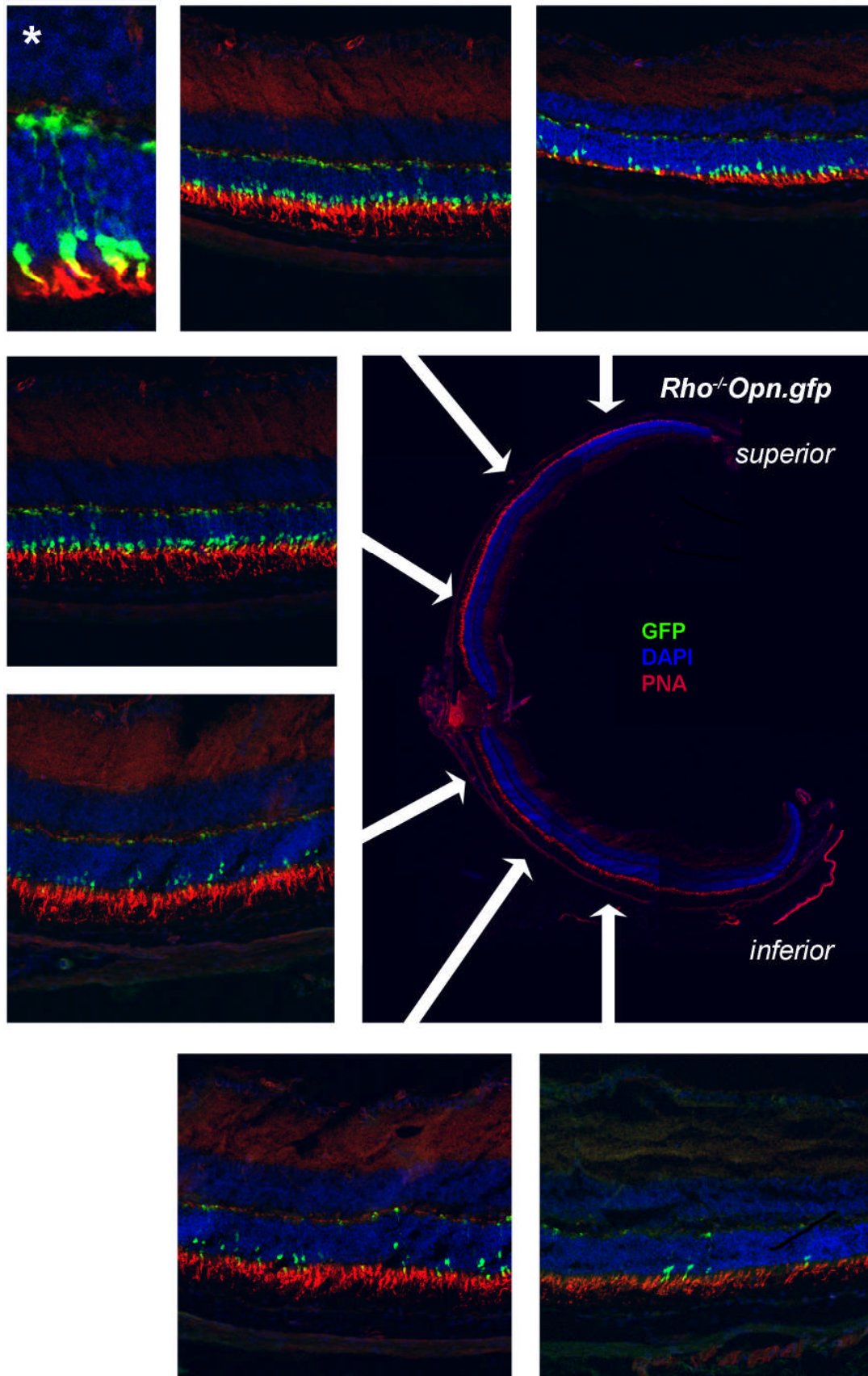


Figure 3-1 GFP and PNA in the *Rho^{-/-}Opn.gfp* mouse at 6 weeks of age. (Legend on previous page).

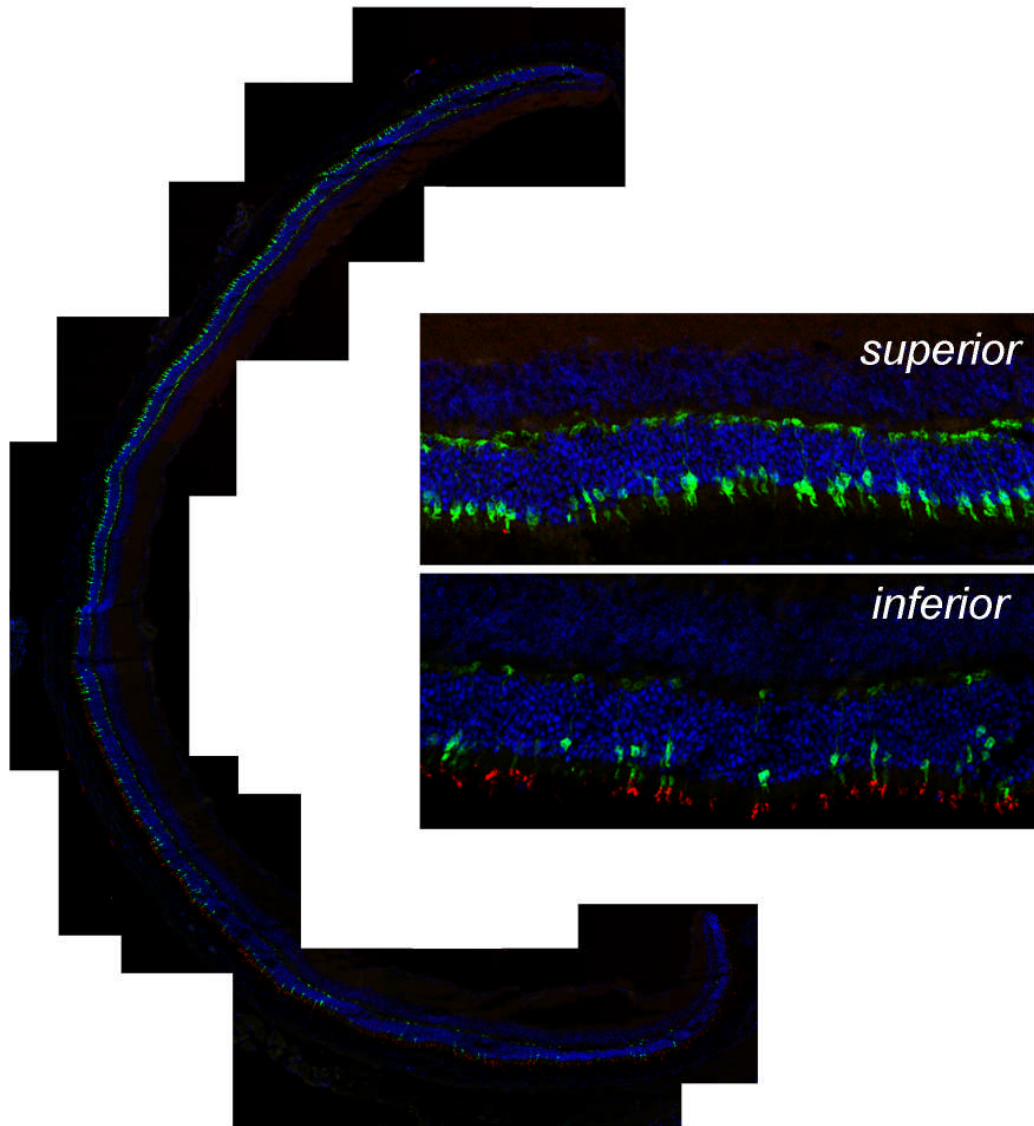


Figure 3-3 Composite image along the superior-inferior axis of the eye of a 6 week old *Rho*^{-/-}*Opn.gfp* mouse. Antibody staining to s-opsin is shown in red. GFP expression is seen to be most dense in the superior retina and posterior pole. S-opsin expression was seen to be more dense in the inferior retina (lower-most inset) than in the superior retina (upper-most inset).

3.4 In-vivo imaging of cone photoreceptors

Having ascertained the specificity of eGFP expression in histological sections the aim was to establish an *in vivo* monitoring method for these cone photoreceptors. This was achieved using the Scanning Laser Ophthalmoscope (SLO), and specifically the autofluorescence mode in which light of 500nm or above is detected following stimulation of the retina at 488nm (the peak absorbance for GFP) (Figure 3-4).

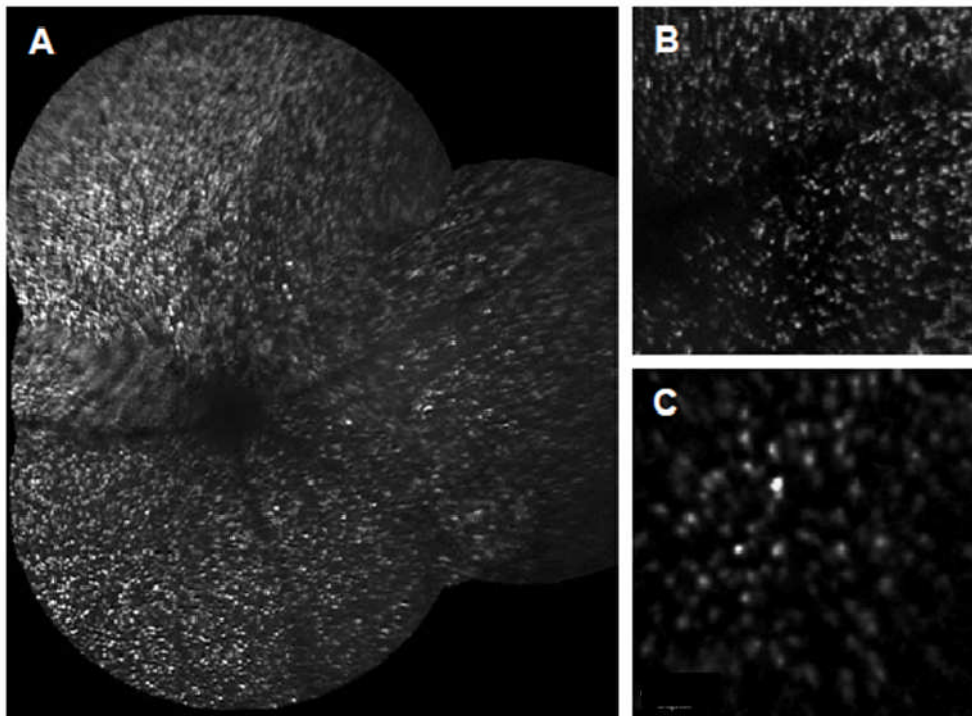


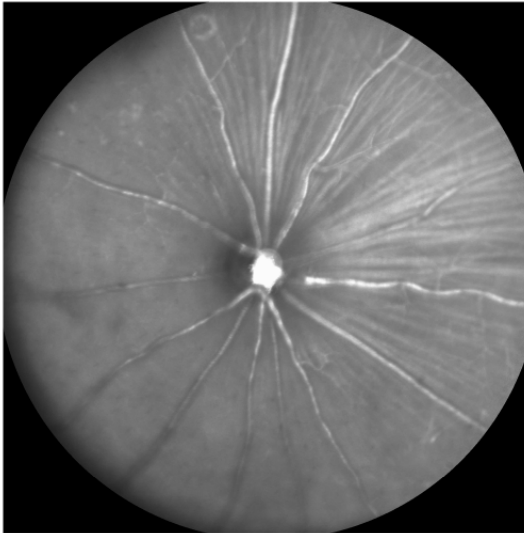
Figure 3-4 Autofluorescence image of the retina of a *Rho*^{-/-}*Opn.gfp* mouse at low(A), intermediate (B) and high (C) magnification. Images were taken from an anaesthetised mouse a Heidelberg confocal scanning laser ophthalmoscope. GFP expressing cells, in this case cone photoreceptors, can be seen as distinct entities.

In order to count the number of GFP-expressing cones in a defined area of the retina, and maintain consistency between examinations, the retina was first imaged with the infra-red mode of the scanning laser ophthalmoscope. As seen in Figure 3-5, this allows for the optic disc and retinal blood vessels to be used for orientation of the images and to accurately centre images on the optic disc. Autofluorescence images were then taken at the same location.

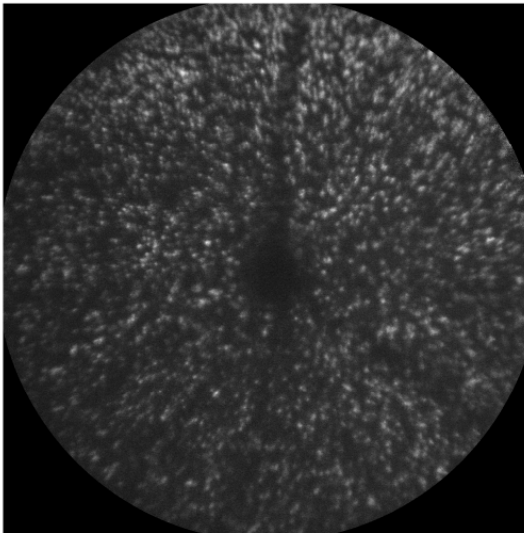
Cone photoreceptor counts were performed using Photoshop (Adobe) and Image Pro-Plus (Media Cybernetics) software. An overlay was applied to cover the central 75% of the field of view, and centred on the optic disc. Discrete hyperfluorescent spots were counted within this defined area. Only the central 75% of the field of view was counted so that counts were not compromised by small variations in positioning and centring of the original image, or by edge artefacts (as at the edge of the SLO image there can be some blurring which making fluorescent spots less distinct).

Legend to Figure 3-5 (following page). In vivo retinal imaging of a *Rho^{-/-}Opn.gfp* mouse. Infra-red imaging (uppermost) was used to visualise the optic disc and retinal blood vessels that were used for orientation. GFP fluorescence was visualised with a 488nm laser and 500nm barrier filter (middle image). Discrete hyperfluorescent spots were counted in the central 75% of the visual field (indicated by overlay, lower image). The red spots have been added in Photoshop to overlie discrete spots of hyperfluorescence; these are then counted using image processing software (Image Pro-Plus).

Rho-/-Opn.gfp [aged 10 weeks]

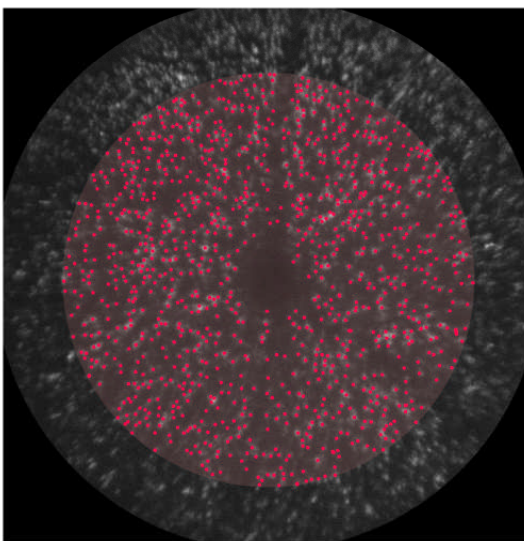


Infra-red image



Auto-fluorescence image

(488 nm excitation laser; 500nm barrier filter)



n=1108

area counted = 75% field of view

Figure 3-5 *In vivo* imaging of cone photoreceptors. (Legend on previous page)

To confirm that the distinct fluorescent spots seen with the SLO were indeed individual GFP expressing cones (rather than clusters for example), experiments were performed to compare *in vivo* images with subsequent histological images from the same eyes.

Both fundi of both 4 *rho^{-/-}Opn.gfp* mice, of 10 weeks of age, were imaged prior to the animals being sacrificed on the same day. The retinas were dissected out and prepared as flat mounts with care to avoid distortion of the tissues or damage to the imaged area surrounding the optic disc. Lectin staining (Figure 3-6) was used to show the retinal vasculature on the flat mounts and thus allow images from the flat mounts to be correctly sized and orientated prior to being overlaid on the SLO images where the branching pattern of the vasculature can also be seen.



Figure 3-6 Lectin staining was used to show in detail the retinal vasculature and branching pattern in flatmounted retinas

These correlations of the flat mounted retinas and the SLO images showed that the area of imaged retina, with the SLO focussed on the hyper fluorescent spots, was 4.3mm^2 (sd 0.95mm^2), giving a value of 2.4mm^2 (sd 0.53mm^2) for the area of each image in which fluorescent cones are counted.

Overlying corresponding areas of the vascular tree in retinal flat mount and SLO images demonstrates that the hyper fluorescent spots seen on the SLO are individual cones (Figure 3-7). The SLO images obtained can therefore be used to monitor *in vivo* the survival of individual cones over time, as well as give quantitative data on the survival of the cone photoreceptor population within a defined area of the posterior pole.

Four sample points were identified where there was distinctive vasculature evident on the retinal flat mounts that had also been seen *in vivo*. These were

used to compare *in vivo* counts with histological counts of GFP expressing cells in corresponding fields of view. At these sample points, all within the posterior pole of the eye, the *in vivo* count was 67% (sd 12.3) of the histological count.

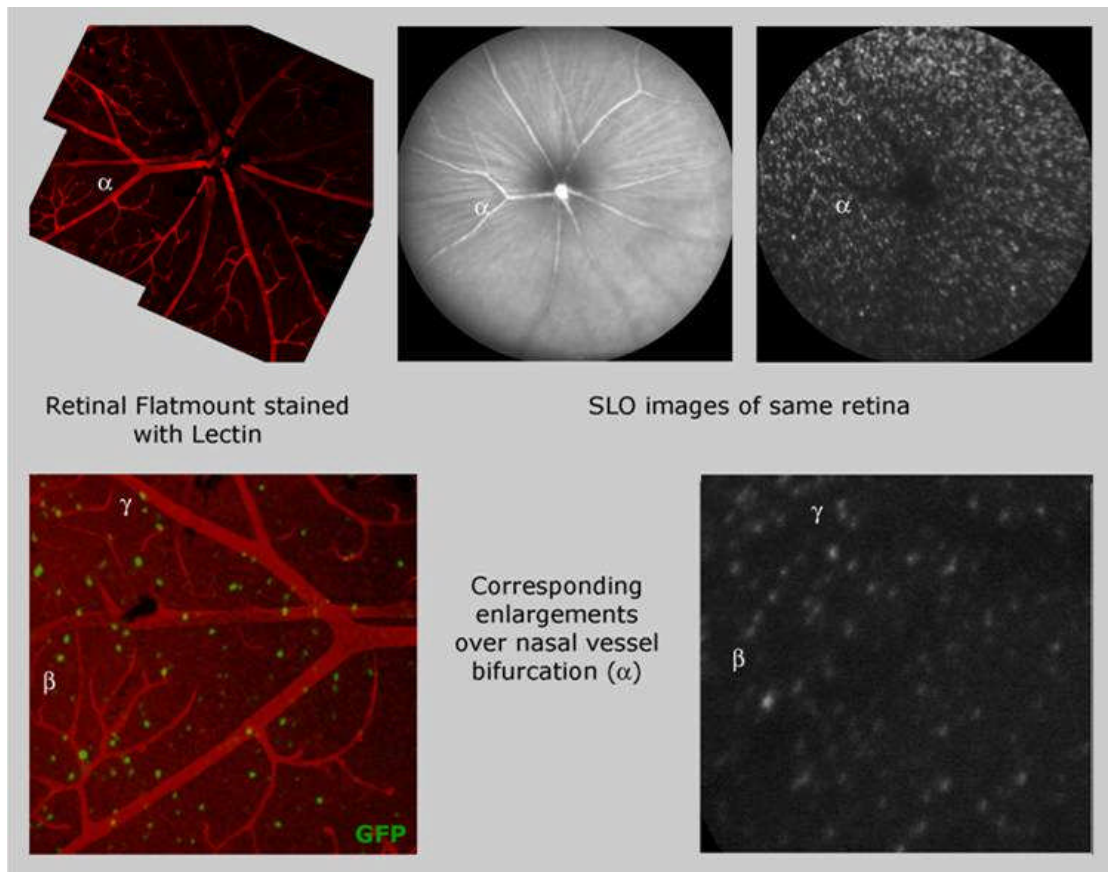


Figure 3-7 Histopathological correlation of the SLO image. Retinal flatmounts were stained with lectin (red) to demonstrate the retinal vasculature, and in the lower image the underlying GFP-expressing cones (green) are also shown. The vessel bifurcation, with an intersecting vessel over the upper branch (α), can be seen in the histological sections as well as the *in vivo* SLO images. Enlargements of the histological and SLO images (lower row) in this area demonstrate that distinct patterns of hyperfluorescent spots seen *in vivo* [eg straight line (β) and curved line (γ)] correspond exactly to individual *gfp* expressing cones in the flat mounted retina.

3.5 Characterisation of the cone degeneration in the

Rho^{-/-}*Opn.gfp* mouse

To better understand the time course of the cone degeneration secondary to a rod-specific mutation *Rho*^{-/-}*Opn.gfp* mice were studied at repeated time points with functional assessments (ERG), and *in vivo* counts of GFP positive cones. At selected time points mice were sacrificed for histological correlation of the findings. To control for the effects of GFP expression on degenerating cones *Rho*^{-/-}*Opn.gfp* mice were compared to uncrossed rhodopsin knockout mice that lacked GFP expression.

3.5.1 Loss of cone function

Scotopic ERGs in the *Rho*^{-/-}*Opn.gfp* mouse confirmed the absence of rod function (example trace in supplementary data chapter). To determine the time course of cone degeneration in the *Rho*^{-/-}*Opn.gfp* mouse cone-specific ERG assessments were performed at repeated timepoints, and the b-wave amplitude compared over time. The degeneration in cone function in a cohort of *Rho*^{-/-}*Opn.gfp* mice is shown in Figure 3-8. Cone function was approximately stable until day 52 of age, after which there was a steep decline. Whilst b-wave amplitudes could be consistently identified, a-waves were less distinct and more variable. b-wave data only is presented in this thesis. The last data point shown is for day 73, at which time mean b-wave amplitude to a 10cd.s/m² flash was 30.1 μ V (sd 19.3). By day 77 function in most animals was at the detection limit of the apparatus, as indicated by lack of a distinct b-waves in comparison to background noise on the recording baseline.

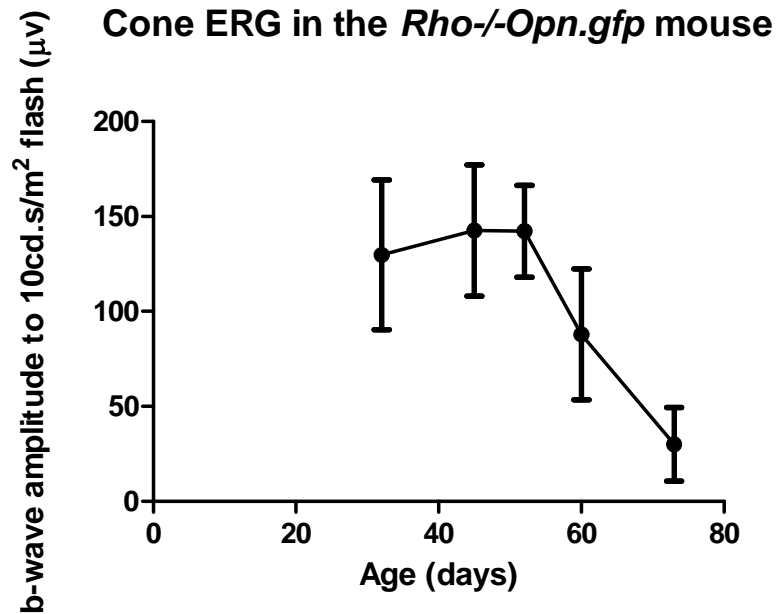


Figure 3-8 Degeneration in ERG cone function in the *Rho*^{-/-}*Opn.gfp* mouse. Mice were examined after light adaptation and in photopic conditions at repeated timepoints. Mean b-wave amplitude (\pm sd) to a single flash intensity is shown (n=11).

To examine the effect of GFP expression on cone function a *Rho*^{-/-}*Opn.gfp*^{+/-} male was crossed with a *Rho*^{-/-} female (i.e. a rhodopsin knockout female without GFP expression). Cone function was assessed in littermates which were then imaged to determine which expressed GFP. As shown in Figure 3-9 cone function in GFP expressing mice was diminished as compared to non-GFP littermates. The number of littermates was small, and so results from multiple litters were also compared. These also showed GFP expression to be associated with reduced cone function. This could be directly due to high levels of GFP protein within the cell compromising function, light absorption by the GFP protein reducing opsin stimulation or from an unrelated gene or consequence of transgene integration being inherited in association with the GFP transgene. This has not been investigated further, but Rex *et al.* likewise found cone function in the *Opn.gfp* mouse to be reduced as compared to age-matched wild types from the same genetic background.²⁴⁷ It is also of note that the ERG amplitudes in the cohorts of animals shown in Figure 3-9 are lower than those examined separately

in Figure 3-8. This could be due to variation between litters or changes in the ERG apparatus which occurred between separate experiments. To limit such variation ERG maintenance changes (such as replacement of corneal electrodes and the heat pad) were avoided during longitudinal time courses. They however could still account for differences between separate experiments.

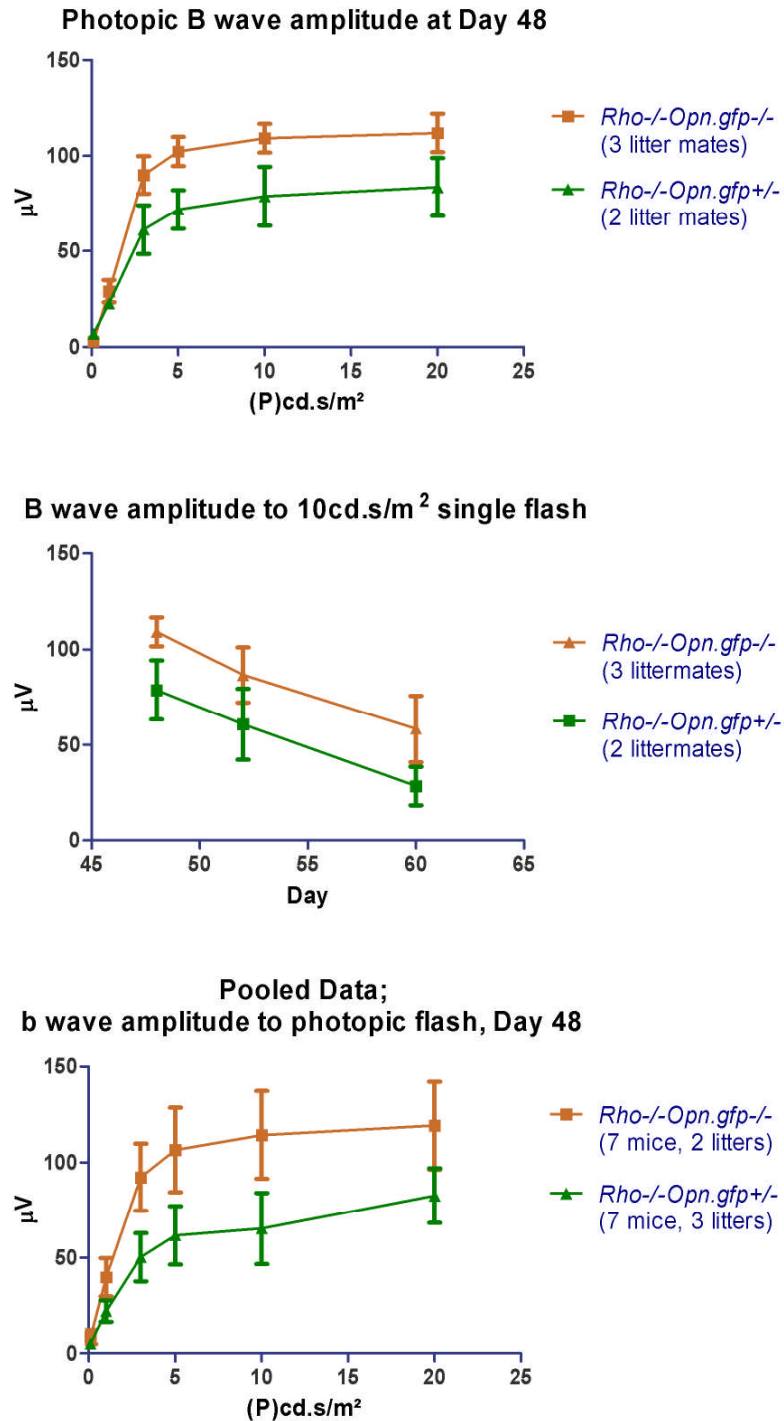


Figure 3-9 The effect of GFP expression on cone function. Cone function was compared in litter mates with and without GFP expression (top and middle graphs). In the top graph b-wave amplitudes are shown for all flash intensities at day 48. The time course of degeneration is shown with b-wave amplitudes to a single flash intensity at 3 timepoints. In the lower graph data from multiple litters is compared.

3.5.2 Cone photoreceptor survival

To examine the time course of cone photoreceptor loss *Rho*^{-/-}*Opn.gfp* mice were imaged with the SLO at weekly intervals commencing from the start of functional loss (week 7 of age). These initial investigations showed that GFP expression continued at approximately stable levels until week 11, before degenerating over the subsequent 6 weeks. To quantify this, GFP-expressing cones were counted at weekly intervals in a cohort of *Rho*^{-/-}*Opn.gfp* mice and in a comparison group of age-matched *Opn.gfp* mice (which lacked the rhodopsin knockout genotype/phenotype). The SLO counts from both eyes of each animal are presented in Figure 3-10. Corresponding example images from each mouse model, at weeks 11 and 17, are shown in Figure 3-11.

In the *Rho*^{-/-}*Opn.gfp* mouse there was a steep and progressive decline in cone numbers at the posterior pole of the eye. At week 11 the mean central cone count was 1048 (sd 313) as compared to 36 (sd 47) at week 17. There was also a more limited decline in cone counts in the *Opn.gfp* mouse. Mean counts at week 11 and 17 were 942 (sd 178) and 631 (sd 189) respectively. Two way ANOVA analysis with Bonferroni post-tests confirmed the *Opn.gfp* and *Rho*^{-/-}*Opn.gfp* counts to be significantly different from one another ($p < 0.01$). At week 17 cones in the *Opn.gfp* mouse remained approximately equally distributed across the field of view, where as in the *Rho*^{-/-}*Opn.gfp* mouse residual cones were primarily in the superior retina (Figure 3-11). The steep loss in cone numbers in the *Rho*^{-/-}*Opn.gfp* mouse occurred approximately 4 weeks after the degeneration in cone function. Cone photoreceptors were therefore losing function weeks before losing GFP expression. The decline in cone numbers in the *Opn.gfp* control is discussed in 3.6.

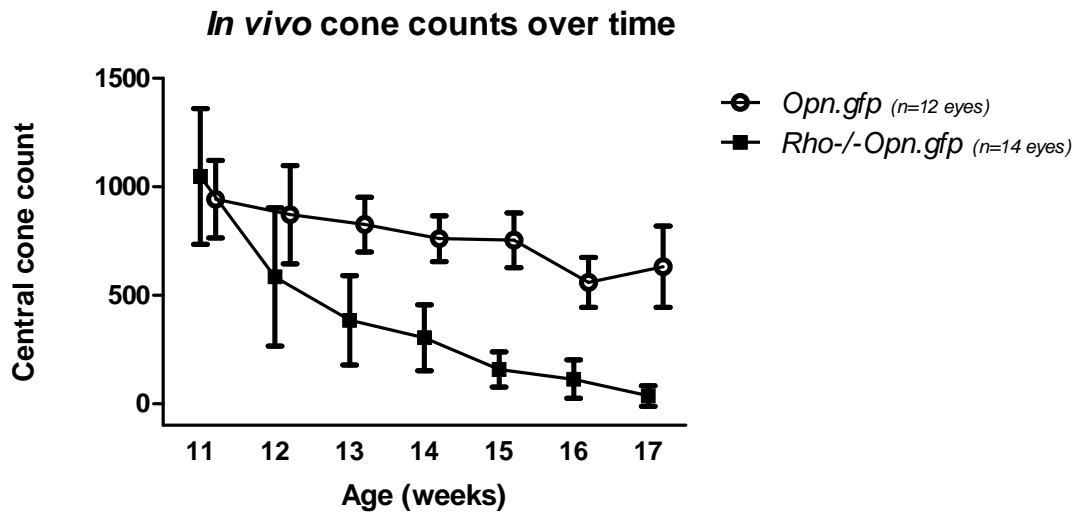


Figure 3-10 Cone counts over time. *Rho*^{-/-}*Opn.gfp* and *Opn.gfp* mice were imaged on a weekly basis between 11 and 17 weeks of age, and the number of discrete cones quantified. The cone counts reveal a fast degeneration in the *Rho*^{-/-}*Opn.gfp* mice, and a statistically significant slower decrease in GFP signal from the *Opn.gfp* mice.

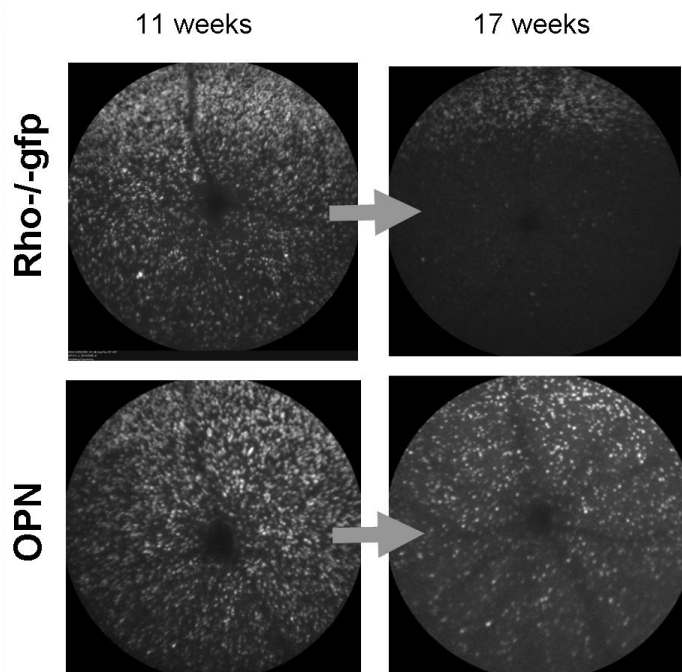


Figure 3-11 Example cone degeneration images from *Rho*^{-/-}*Opn.gfp* and *Opn.gfp* mice. There was a marked cone degeneration in the *Rho*^{-/-}*Opn.gfp* mouse, and at 17 weeks the density of residual cones was maximal in the superior retina. In the *Opn.gfp* mouse there was a more limited change in cone density.

3.5.3 Non-functional cones

To investigate why cones in the *Rho*^{-/-}*Opn.gfp* mouse lose function weeks before cell death eyes were examined histologically at weeks 6 and 13 of age. At the former timepoint function is approximately maximal, whilst at the latter cone function was no longer detectable. Immunohistochemistry was performed to examine expression of proteins integral to the phototransduction pathway, and visualise outer segments.

The G-protein transducin is directly activated by photo-excited visual pigment, and in rods the rate of its activation is a critical determinant of the cellular light sensitivity. Translocation of transducin out of the outer segment and in to the inner segment allows rods to operate in light conditions that would otherwise lead to saturation of the response.²⁴⁸ In contrast in cones levels of transducin activation are controlled by other means, and transducin is consistently compartmentalized in the outer segment.²⁴⁹⁻²⁵¹ This is evident in the wild type controls in Figure 3-12. In the *Rho*^{-/-}*Opn.gfp* mouse limited transducin expression, also within the outer segment, is evident at 6 weeks of age when cone function is approximately maximal (Figure 3-8). In sections from 13 week old *Rho*^{-/-}*Opn.gfp* mice, in which the rod-cone degeneration has progressed, the ONL is only approximately 2 nuclei thick. Residual GFP expression is evident demonstrating that surviving cones remain but that the normal morphology has been lost. Of note though, there is no evidence of persistent transducin expression in these residual cones, which will help explain the absence of cone function at this timepoint.

The phototransduction protein arrestin is also translocated between inner and outer segments in rods, but in the opposite direction to transducin. Thus in the dark adapted state rod arrestin is found in the inner segments, but on exposure to light there is a translocation to the outer segment.²⁴⁹ In cones the distribution of the arrestin protein is less compartmentalised, and in the light-adapted mouse the protein is found in both the inner and outer segment, cellular processes and in the synaptic end plate.²⁴⁹ The sections in Figure 3-13 are from light adapted mice, and demonstrate this pattern of expression. In the wild type mouse cone arrestin

expression is seen at high levels throughout cone photoreceptors. In the 6 week old *Rho*^{-/-}*Opn.gfp* mouse the expression is reduced as compared to the wild type, but is still evident throughout the cell body of selected cone photoreceptors. By 13 weeks however, this expression too is much reduced, which is again in keeping with the absence of function in *Rho*^{-/-}*Opn.gfp* mice of this age. The reduced transducin and arrestin expression could be due to down-regulation of their respective promoters or due to post transcriptional regulation of mRNA processing or protein translation.

It is also evident from Figure 3-12 and Figure 3-13 that the morphology of the cone photoreceptors is altered during the degeneration. In the images from 6 week old *Rho*^{-/-}*Opn.gfp* mice cones are evident with long long straight processes extending across the outer nuclear layer. However by week 13 this normal morphology is lost. The change in morphology is further illustrated in Figure 3-14 in which GFP expressing cones are shown at weeks 6, 14 and 17. At the later time points the ONL is thinner and the cones can be seen to be shortened and apparently angulated. Whilst the shortening is likely to be real the angulation could also be a sectioning artefact secondary to shearing of the degenerate retina during cryosectioning.

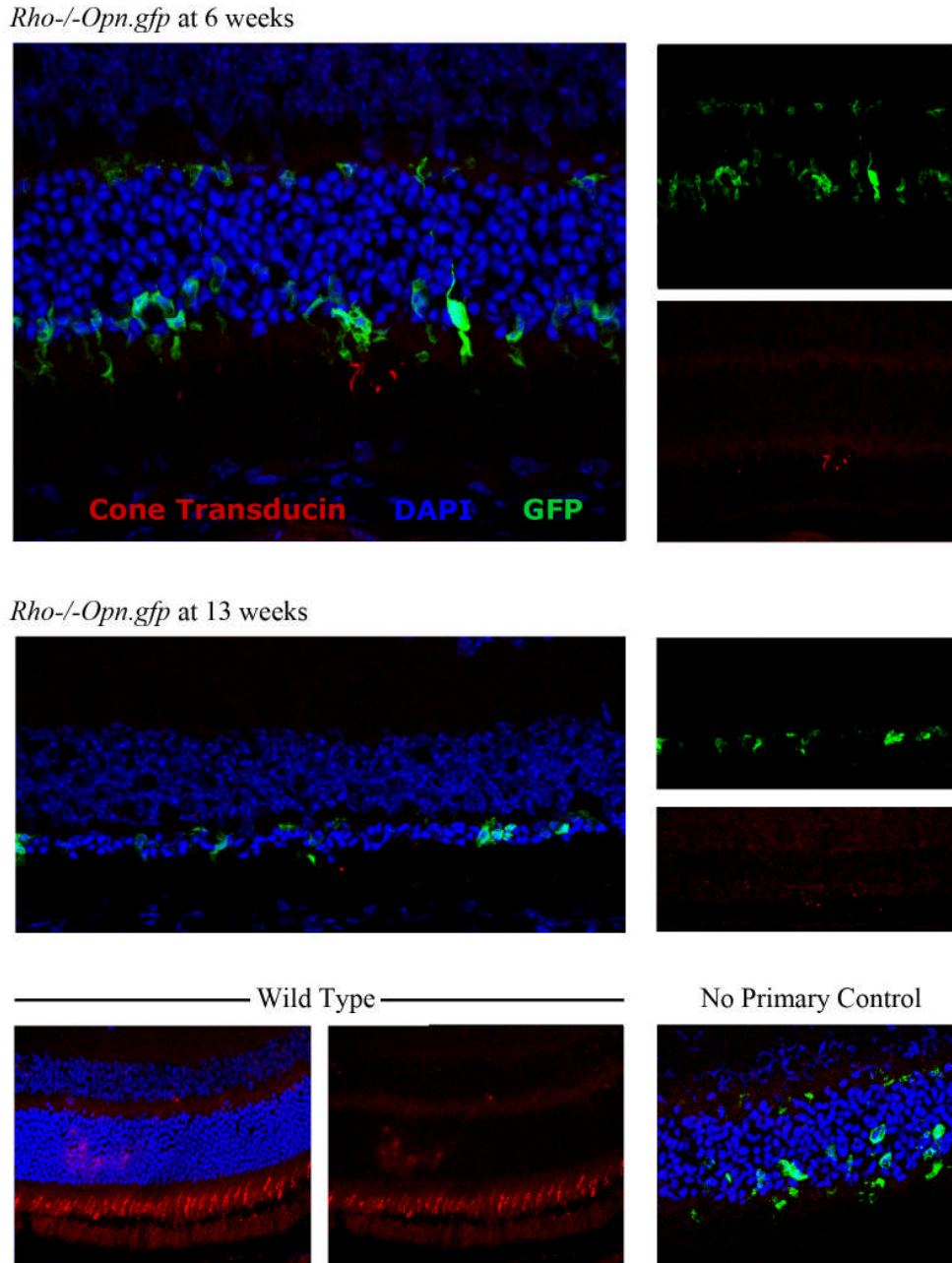
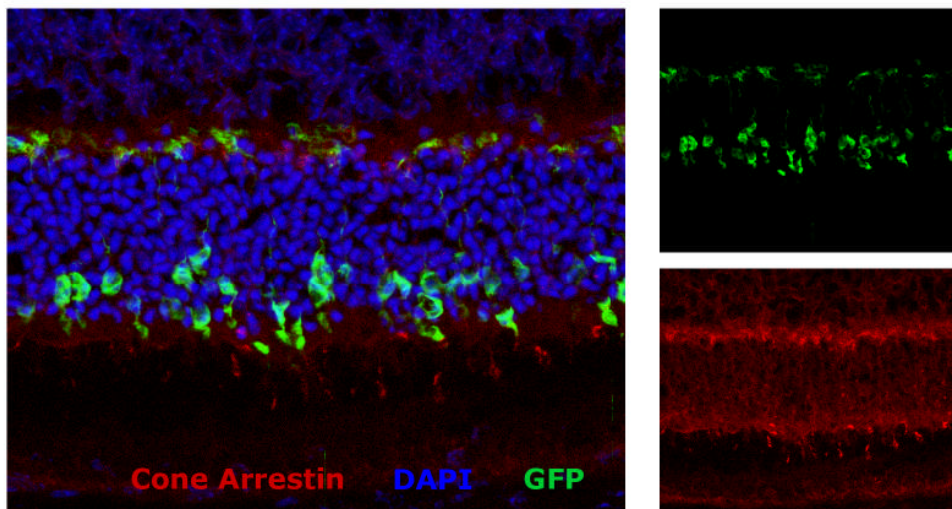


Figure 3-12 Cone transducin expression in the *Rho*^{-/-}*Opn.gfp* and wild type mouse. Cone transducin is expressed in cone outer segments of the wild type and 6 week old *Rho*^{-/-}*Opn.gfp* mouse. Levels in the latter are diminished relative to the wild type. By 13 weeks of age residual GFP expression driven by the OPN promoter is still evident but there is little evidence of continued transducin expression. To control for specificity of the secondary antibody, sections from a 6 week old *Opn.gfp* mouse without primary antibody were stained in the same antibody run. Cryo-sections are from the mid-superior retina.

Rho^{-/-}*Opn.gfp* at 6 weeks



Rho^{-/-}*Opn.gfp* at 13 weeks

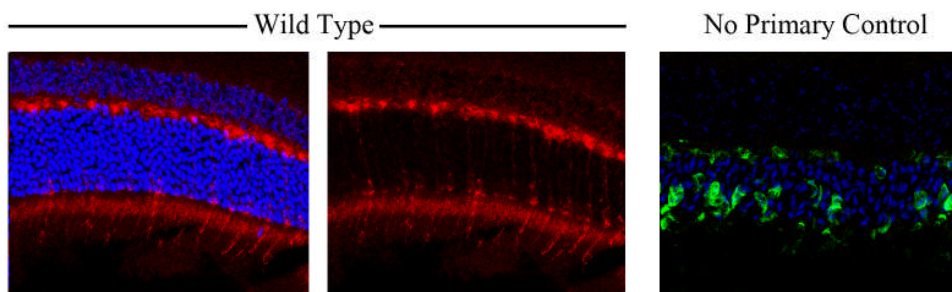
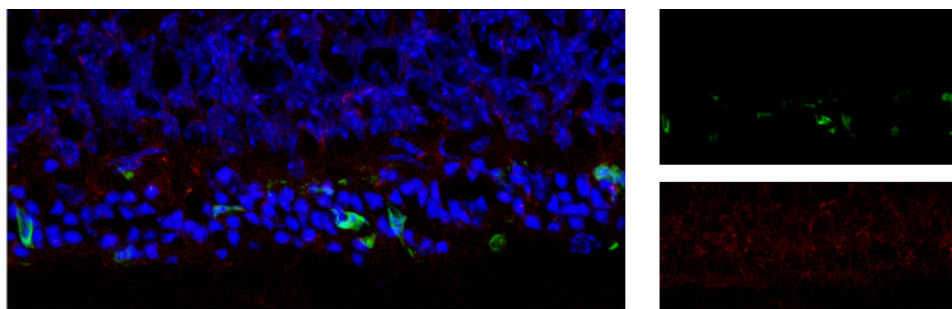


Figure 3-13 Cone arrestin expression in the *Rho*^{-/-}*Opn.gfp* and wild type mouse. In the 6 week old *Rho*^{-/-}*Opn.gfp* mouse cone arrestin is expressed in cone outer segments, cell bodies and synaptic regions. An identical distribution is seen in the wild type mouse, but with greater levels. At 13 weeks of age GFP expression driven by the OPN promoter is still evident but there is no evidence of continued cone arrestin expression. To control for specificity of the secondary antibody sections from a 6 week old *Opn.gfp* mouse without primary antibody, were stained in the same antibody run. Cryo-sections were obtained from the mid-superior retinal where *opn.gfp* expression was maximal.

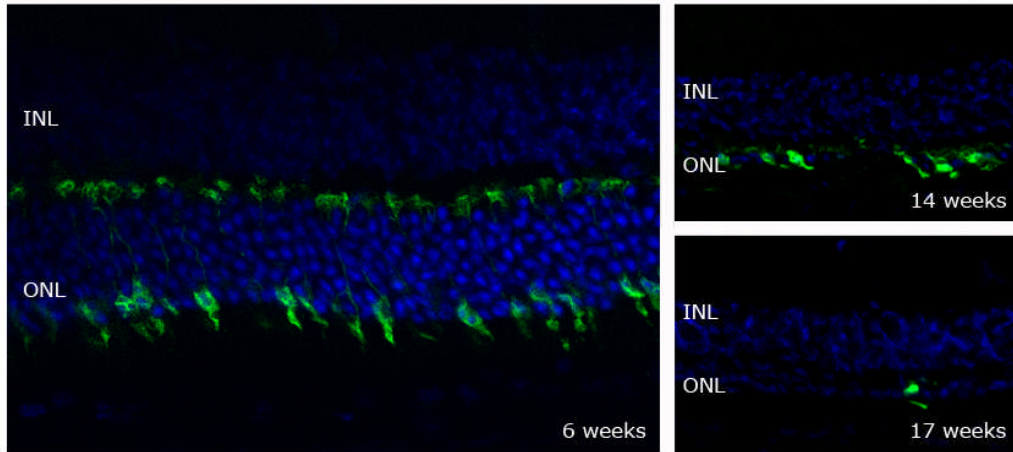


Figure 3-14 Changes in morphology of the *gfp* expressing cones over time in the *Rho*^{-/-}*Opn.gfp* mouse. Cryosections are shown from 6 week old, 14 week old and 17 week old mice, and have been counterstained with DAPI only in order to show nuclei. eGFP expressing cones are seen to display typical cone photoreceptor morphology in the 6 week old mouse, but this is lost in older mice coincident with loss of the ONL.

3.6 The *Opn.gfp* mouse

The decrease in central cone counts in the *Opn.gfp* mouse, as seen in Figure 3-10, is suggestive of a slow cone degeneration in this mouse model which lacks the rhodopsin knockout mutation. This commercially available mouse line has been used by at least two different research groups previously. Rex *et al.* found these mice to have reduced cone function on ERG, as compared to wild types, at 6-8 weeks of age but commented there was no histological evidence of a degeneration at this timepoint (as evidenced by normal layer thickness, cone density and PNA staining).²⁴⁷ Beck *et al.* using the same mouse line, but referred to as ‘RG-GFP, reported normal ERG function at 8 weeks, but that by 10 months of age the GFP signal and photopic function had diminished.²⁵² Further investigations of the *Opn.gfp* mouse, from which the experimental *Rho*^{-/-}*Opn.gfp*

mice were derived, were therefore performed in order to investigate the aetiology of photoreceptor degeneration.

At day 48 of age, cone function in the *Opn.gfp* mouse was found to be equal to that in wild type mice and in rhodopsin knockout mice prior to the onset of cone degeneration (Figure 3-15). Cone function was similar in one year old wild type mice (n=3, Figure 11-17). However in two one year old *Opn.gfp* mice cone function was absent, despite preservation of rod function (Figure 3-16). Rod function (as measured by b-wave amplitude to a 0.01 cd.s/m² flash under scotopic conditions) was equal in the 1 year old *Opn.gfp* mice to that in age-matched wild type mice [mean b-wave amplitude 180 μ V (sd 20) (n=2) and 150 μ V (sd 45) (n=3) respectively, p(difference)=0.20 (t-test)]. There was evidence therefore of a slow cone photoreceptor specific degeneration in the *Opn.gfp* mouse, that was not secondary to rod degeneration.

Cryosections of the year old *Opn.gfp* retinas (n=4) were analysed with immunohistochemistry for M/L and S opsin expression. There was no evidence of these cone-specific proteins or GFP expression in the year old *Opn.gfp* mice. In sections of an 8 month old *Opn.gfp* mouse S and M/L opsin were expressed but they and GFP were only sparsely distributed in the retina (Figure 3-17)

The histological findings are in keeping with the functional data, and indicate there is a slow cone degeneration in the *Opn.gfp* mouse. Duisit *et al.* have previously reported RPE cell toxicity after the expression of high levels of eGFP.²⁵³ In this study rat RPE cells were transduced following the sub retinal injection of lentiviral constructs. High levels of eGFP expression were seen for approximately one month, after which expression diminished and there was histological evidence of RPE loss in the transduced area. The use of the same vector types with an alternative form of GFP (derived from the sea pansy *Renilla reniformis*) lead to stable GFP expression within the RPE for at least six months without signs of toxicity. The toxicity in the first set of experiments was therefore attributed to eGFP. However in contrast Rex *et al.* did not find evidence of toxicity, at least in the short-term, with quantified and high levels of

expression within either RPE or photoreceptor cells;²⁴⁷ in these experiments eGFP cDNA was integrated into the genome (transgenic mice) or predominantly episomal following viral vector mediated transduction; they found no evidence of altered morphology or altered function with thorough investigations that included single cell recordings as well as whole field ERGs. Their animals were however only evaluated up to P30, and so a slow degeneration was not excluded.

In the experiments here *Rho*^{-/-}*Opn.gfp* littermates expressing eGFP in cones had reduced cone function compared to GFP-negative littermates. eGFP expression could therefore have negative effects that impair cone survival. However expression was still strong at week 17, and still evident in the 8 month old *Opn.gfp* mouse. Thus despite strong transgenic expression any toxicity is not as potent in the cone photoreceptors as that described by Duisit *et al.* following lentiviral infection of RPE cells. Furthermore in the experiments here there was no evidence of any cone function or opsin expression in year old *Opn.gfp* mice. Thus non-GFP expressing cones had also been lost. It is likely therefore that the *Opn.gfp* mouse has a slow cone degeneration that is not directly related to eGFP protein.

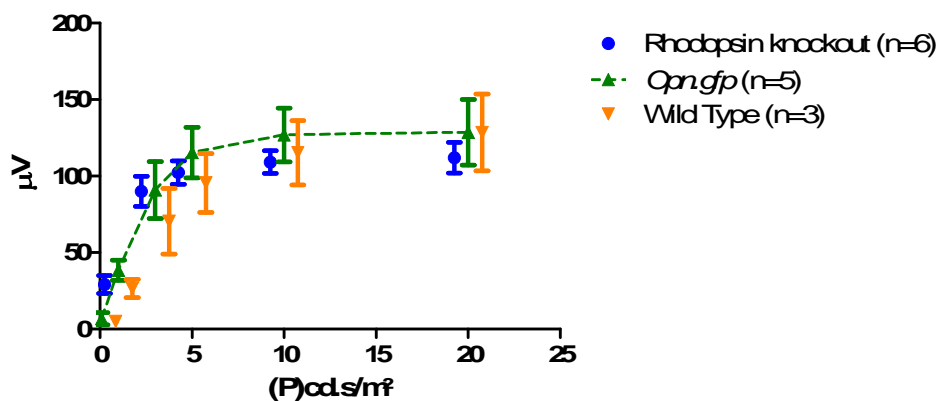


Figure 3-15 Comparison of cone function in the *Opn.gfp*, wild type and rhodopsin knockout (KO) mouse. Mean ERG b-wave amplitude (\pm sd) at day 48 is plotted on the y-axis and flash intensity on the x-axis. There is no difference in cone function between the three different types of mice at this timepoint.

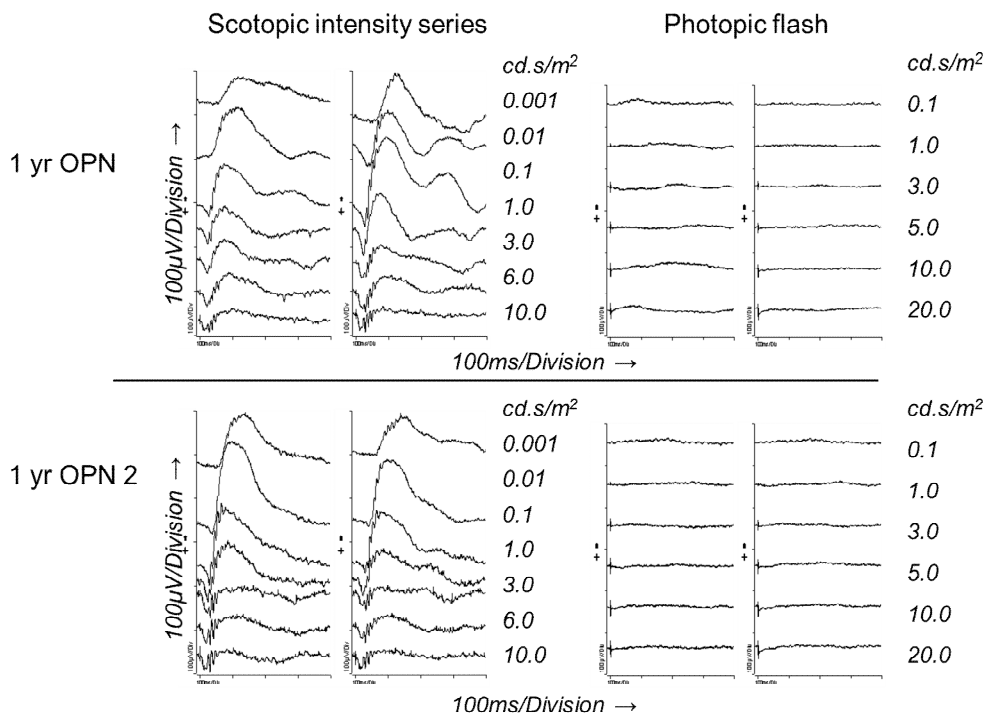


Figure 3-16 ERGs in two *Opn.gfp* mice at one year of age. Scotopic ERGs were performed with flash intensities of 0.001, 0.01, 0.1, 1.0, 3.0, 6.0, 10.0 cd.s/m^2 . Photopic ERGs were performed with flash intensities of 0.1, 1.0, 3.0, 5.0, 10.0 and 20.0 cd.s/m^2 . Averaged traces are shown.

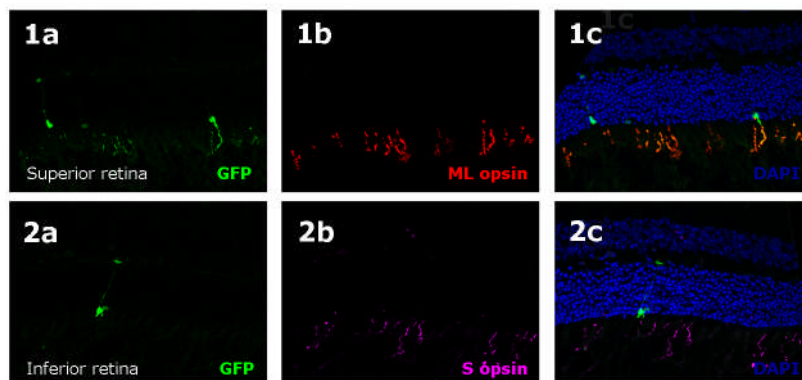


Figure 3-17 Cryosections from an 8 month old *Opn.gfp* mouse. Sections from superior (1) and inferior (2) retina are presented showing GFP expressing cones (a), opsin immunoreactivity (b) and combined images with DAPI staining (c). GFP expressing cones were seen but at reduced density when compared to sections from 10 week old *Opn.gfp* mice. Immunohistochemistry for ML and S opsins confirmed that both cone subtypes were still present in this aged retina.

3.7 Discussion

3.7.1 Cone photoreceptor degeneration

The experiments here show cone function in the *Rho*^{-/-}*Opn.gfp* mouse to be approximately stable until P52 and then rapidly decline over the following 4 weeks. These results are in keeping with published literature as to the effect of the rhodopsin knockout genotype on cone photoreceptors. In the original description of the rhodopsin knockout phenotype by Toda *et al.* the cone ERG was likewise found to be normal until approximately week 7 before degenerating, in their series, over the following 5 weeks.²⁴²

In the experiments here *in vivo* imaging of the cone photoreceptors illustrated that eGFP expression, driven by a cone opsin promoter, was persistent despite near complete loss of rod photoreceptors. Cone photoreceptors, particularly in the superior retina, continued to survive and produce eGFP for weeks after all detectable cone function was lost and the ONL was just one cell thick. This is of interest in relation to theories of rod-cone degeneration and in view of potential treatment approaches for advanced RP.

It is suggested that if a rod-derived survival or toxic factor were central to cone photoreceptor loss one would expect a short time lag between the major phases of cell death. Instead in the *Rho*^{-/-}*Opn.gfp* mouse cone photoreceptors persists for up to approximately 6 weeks in the posterior pole of the eye after rod photoreceptor degeneration is largely complete. This is a common feature across a variety of rod-cone degeneration models. Punzo *et al.* quantified cone photoreceptor loss in four models of rod-cone degeneration, using quantitative PCR of S-opsin mRNA levels and histological assessments of M/L opsin and PNA expression.⁷⁵ In all cases cone loss only progressed after the major phase of rod photoreceptor loss. If rod-derived trophic or toxic factors are the primary determinants of cone photoreceptor fate one would therefore expect there to be a threshold level with cones dying only after this has been reached. Alternatively there could be a considerably delayed biological effect. It is of note that in both

humans and mice the cone photoreceptor loss lags behind that of rods, despite the different spatial distributions. This indicates that the presence of a cone-only fovea is not central to the reasons for a delayed loss of cone photoreceptors.

Persistent cone photoreceptors have also been found in patients with advanced RP, and little if any residual vision. Researchers have therefore been developing approaches to restore function in these residual photoreceptors. Recently Busskamp *et al.* reported restoration of light sensitivity in surviving but non-functional cones through the expression of an alternative light-sensitive protein, the bacterial protein halorhodopsin.²⁵⁴ This was performed in fast (rd) and slow (*Cnga3*^{-/-} *Rho*^{-/-} double knockout) murine models of retinal degeneration using AAV. Protein expression was also induced *ex vivo* in photoreceptors of human retinal explants. To be of broad application, this approach is dependent on the presence of residual non-functional cones in significant numbers of patients with advanced RP. In their paper Busskamp *et al.* demonstrated such residual cones in the macula of a patient with advanced sporadic RP, and they have previously been well reported in the rd murine model of retinal degeneration as well.^{213;255-258} It remains to be demonstrated however how general a finding this is. Conceivably certain mutations could be much more likely to result in surviving non-functional cones than others. It is therefore of note that even in the rhodopsin knockout mouse, with an absence of one of the most highly expressed proteins in the outer retina and a fast retinal degeneration, cone photoreceptors survive for weeks after loss of function.

The data presented here also demonstrates that although cones were surviving for many weeks after loss of function, they had highly abnormal morphology and the expression of selected functional proteins (cone transducin and arrestin) was reduced. This will present a challenge for other treatment approaches, including neuroprotection, that aim to maintain cone photoreceptors in their normal functional state and sustain function using the natural cone photoreceptor apparatus. The shortening of cone photoreceptor outer segments during the course of retinal degeneration has been reported previously in animal models.⁷⁵ It has also been seen in the retina of a patient with relatively early RP and good visual acuity (20/60 4 months prior to death), in which only very small or no

cone outer segments were visible.²⁵⁹ Potential treatments are likely to need to halt, or possibly reverse, cone outer segment shortening and this is a potential outcome measure for the evaluation of treatments and monitoring of disease progression. However these images from the *Rho^{-/-}Opn.gfp* mouse also show how the cell body and inner segment are also seen to collapse and become folded during the degeneration. This is possible to see in the *Rho^{-/-}Opn.gfp* mouse as eGFP is distributed widely in the cell body and inner segment. In contrast more traditional methods of following cone degeneration with PNA stains for the surrounding protein sheath or antibody stains for outer segment opsin proteins do not show such detail. The likely cause for the cone cell body and inner segment collapse is loss of the surrounding rod photoreceptors that ordinarily constitute the bulk of the outer retina in rodent retina. It may be impossible to restore physiological cone function in the absence of a near normal ONL and the mechanical support it ordinarily provides. The study by Busskamp *et al.* however indicates that non-physiological phototransduction, using an alternative light-sensitive protein, is achievable.

If physical collapse and a loss of surrounding structural support is indeed a reason for loss of cone function that could explain why rod-cone degenerations in humans cause loss of peripheral cone function first with relative sparing of the fovea until advanced stages of the disease; in humans peripheral cones are surrounded by a high density of rods, and so loss of the rod photoreceptors will cause thinning of the ONL as seen in the *Rho^{-/-}Opn.gfp* mouse. However in the human fovea the lack of rod photoreceptors means that the cones are more reliant on one another and Mueller cells for structural support.

3.7.2 Ventral-dorsal gradient

Histological characterisations of the spatial patterns of cone photoreceptor loss can be hampered by substantial variability between animals.^{255;258} The *in vivo* counts presented here, examining only the posterior pole, likewise showed greater variability in the *Rho^{-/-}Opn.gfp* degenerating retina than the OPN controls (Figure 3-10). However a distinctive feature in the degenerating retina

was a superior-inferior gradient in GFP distribution, most marked at the latter stages of the degeneration (Figure 3-11). In part this will have been due to GFP expressing cones being found at greatest density in the superior retina pre-degeneration (Figure 3-2) however the distinction between superior and inferior retina is more distinct at the end of the degeneration than at the start (Figure 3-11). Superior-inferior, or dorsal-ventral, distributions of surviving M/L cones have been described previously in the *rd* mouse, the rhodopsin knockout mouse, the PDE- γ knockout mouse (which lacks the γ -subunit of PDE) and the P23H rat model of rod-cone degeneration.^{75:255;257} However this pattern of M/L cone photoreceptor loss is not specific to rod-cone degenerations. The cone photoreceptor function loss 1 (CPFL1) mouse (which carries a mutation in cone specific phosphodiesterase 6 (Pde6c))²⁵² and guanylate cyclase-1 knockout mouse,²⁶⁰ which both have mutations expressed in cone photoreceptors, have similar patterns of cone loss. A dorsal-ventral gradient of residual cones has also been described in the RPE65^{-/-} mouse in which there is a rod-cone degeneration secondary to a mutation expressed in RPE cells,²⁶¹ and in the *Rdh8^{-/-}Abca4^{-/-}* mice in which there is disrupted all-*trans*-retinal clearance in both rod and cone outer segments, and subsequent RPE and photoreceptor degeneration.³⁰ The apparent increased susceptibility of cones in the inferior or ventral retina may therefore not be related to the underlying genetic mutation, or an inherent characteristic; instead it may reflect a common external or environmental influence, such as increased light exposure in the inferior retina which has been found to accelerate selected degenerations.^{30:262-267}

An inferior-superior gradient of disease progression has also been reported in selected patients and families with RP.²⁶⁸⁻²⁷⁰ It is hypothesised that mutations causing increased cell activation may be more predisposed to the effects of light than others. The significance of this for treating patients is that targeting of the superior retina may be more likely to improve vision because of a relative preservation of cell architecture. It also means that experiments to evaluate potential treatments need to compare corresponding regions in treated and untreated eyes. Light exposure is a potential confounding variable. Therefore in the following experiments using the *Rho^{-/-}Opn.gfp* model, mice were kept in

standardised lighting conditions (14 hours light per 24 hours at 200-300 lux directly under the ceiling lights, and approximately 40 lux within the cage). Eyes with corneal opacities or cataracts were excluded from analysis. Furthermore, interventions having a localised effect, such as subretinal injections, were performed in both superior and inferior hemispheres.

3.7.3 A valuable model to evaluate cone-related outcome

measures

The experiments here have shown that the *Rho^{-/-}Opn.gfp* mouse allows repeated assessments of cone function, cone numbers and cone morphology in degenerating retina. The *in vivo* findings were corroborated with histological examinations to confirm that it is individual cone photoreceptors that can be visualised and counted *in vivo*. Sample points from the posterior pole of the eye identified that 67% of GFP expressing cones detected on retinal flat mounts had been seen *in vivo*. A previous study imaging GFP expressing ganglion cells in the rat retina with a similar scanning laser ophthalmoscope found that 60% of the GFP expressing ganglion cells had been detected *in vivo*.²⁷¹ The *in vivo* counts are a representative sample of the M/L opsin-expressing cones at the posterior pole of the eye and can be used to compare rates of degeneration between eyes.

Traditionally studies of cone degeneration have used immunohistochemistry to identify cone specific proteins or the surrounding interphotoreceptor matrix in order to identify and image the cones. These techniques principally identify the cone outer segments. In the *Rho^{-/-}Opn.gfp* mouse the eGFP is expressed in a larger proportion of the cell (see Figure 3-1) meaning that changes in cell morphology can be seen in greater detail, and cones can still be effectively visualised when outer segments, and the proteins predominantly expressed within them, have been lost (Figure 3-12 and Figure 3-13).

The degeneration in cone function was found to have a similar time course to that in rhodopsin knockout mice that have not been crossed onto the OPN line. However, evaluations of the *Opn.gfp* mouse also identified a slow cone

degeneration, that was not secondary to rod degeneration. The *Rho^{-/-}Opn.gfp* mouse, derived from a cross of *Opn.gfp* and rhodopsin knockout mice, may therefore have stimuli for a cone degeneration in addition to the rhodopsin knockout mutation. However, the results show that cone loss secondary to the rhodopsin mutation is fast leading to loss of function within approximately 11 weeks and loss of cone cell bodies over approximately 17 weeks in the posterior pole of the eye. In contrast the cone loss in the *Opn.gfp* mouse was very slow, over approximately 12 months, with limited impact in the young adult mouse (Figure 3-10). Cone loss in the *Rho^{-/-}Opn.gfp* mouse, which is largely complete within 4-5 months, is therefore likely to be predominantly if not exclusively secondary to rod degeneration.

The ability to study cone numbers and function *in vivo* in the *Rho^{-/-}Opn.gfp* mouse allows repeated assessments in individual animals; this can be expected to be a valuable tool in evaluating whether the magnitude of any treatment effect on cone photoreceptors changes in time. The *Rho^{-/-}Opn.gfp* mouse therefore allows interventions to be assessed with clinically important outcome measures that have historically been difficult to assess in rodent models.

Chapter 4 GDNF as a potential therapy for retinitis pigmentosa.

4.1 Introduction

Neurotrophic factors, released by glial cells, ordinarily act on neuronal cells to sustain growth, differentiation and survival.²⁷² As an absence of such factors has been linked with increased rates of apoptosis, it has long been hypothesised that augmenting levels could have neuroprotective effects in conditions of increased apoptosis.¹⁴³

One such protein, glial cell-line-derived neurotrophic factor (GDNF) was first identified as a stimulant of dopaminergic neurons *in vitro*.²⁷³ It has subsequently been identified as protecting a wide variety of cell types from apoptosis under diverse experimental conditions.²⁷⁴⁻²⁷⁷ The greatest interest in GDNF has stemmed from its protective effects in *in vivo* models of Parkinson disease,²⁷⁸⁻²⁸⁰ and clinical trials have followed.¹⁶¹ It is also however, synthesized in the retina²⁸¹ and has been found to promote photoreceptor survival and morphology both *in vitro*^{282;283} and *in vivo* in models of retinitis pigmentosa.^{80;154;158;160}

The GDNF protein, in its non-glycosylated state, has a molecular mass of approximately 15kD.²⁷³ It is highly conserved between species and is a member of a group of 4 structurally related neurotrophic factors known as the GDNF family of ligands (GFLs), all of which belong to the transforming growth factor β super family. The other 3 GFLs are neurturin (NTN), persephin (PSPN) and artemin (ARTN). GDNF, and the other GFLs, act by binding to a 'GDNF family α receptor' of which there are 4 subtypes (GFR α 1-4).^{277;284;285} It is GFR α -1 which has the greatest affinity for GDNF.^{277;286} Bound receptors in turn activate the membrane bound tyrosine kinase 'Ret' (rearranged during transfection)²⁸⁷

leading to activation of intracellular signalling pathways. In particular GDNF mediated Ret activation has been shown to lead to interactions with signalling molecules of the src-family of protein-tyrosine kinases through phosphoinositide-3 kinase (PI-3K) dependent pathways.²⁸⁸ Phosphatidylinositol 3-kinase/Akt (PKB) and mitogen-activated protein kinase (MAPK) pathways are also implicated.^{276;277;289} The GFR α receptors may alternatively bind to another trans-membrane protein p140^{NCAM} (an isoform of the neural cell adhesion molecule NCAM)^{290;291} but the physiological relevance of this binding for downstream intracellular signalling remains uncertain.²⁹²

The secondary pathways activated by GDNF are able to inhibit cell death through the intracellular expression of anti-apoptotic proteins belonging to the inhibitor of apoptosis (IAP) family.²⁹³ In particular, inhibition of the X-linked inhibitor of apoptosis (XIAP) and neuronal apoptosis inhibitory proteins (NAIP), using anti-sense mRNA, is found to prevent the neuroprotective effects of GDNF.²⁹³

4.1.1 GDNF pathways in the retina

GDNF has been shown to slow rod photoreceptor death in several different animal models of RP.^{80;154;156;159;160} There is uncertainty however, over the molecular pathways through which these effects are mediated.

GDNF receptors are found on photoreceptors, and *in vitro* it is through these receptors that GDNF-induced effects can be demonstrated on isolated photoreceptor preparations.^{282;283;294-297} However many studies on whole mammalian retina have found the GDNF receptor components to be most prevalent in the Mueller glia, with a lower density in the ganglion cell layer and only a sparse distribution in the photoreceptor layer.^{212 298 292} This is not always the case as for example Harada et al. found immunoreactivity to GFR α 1 and α 2 to be predominantly in the photoreceptor layer of the Wistar rat,²⁹⁹ though in the presence of light-degeneration expression was strongly up-regulated in the Mueller glial cells as well.^{299 300} These findings have contributed to theories

(reviewed by Bringmann and Reichenbach)¹⁷ that the action of GDNF on photoreceptors is predominantly indirect, acting via the Mueller glia. It is postulated that GDNF stimulated Mueller glia in turn release secondary intermediate factors which directly stimulate photoreceptors. In keeping with this, GDNF supplementation does increase glial fibrillary acidic protein (GFAP) staining in Mueller glia.⁸⁰ GFAP is an intermediate filament protein, and up regulation of its expression is a marker of increased cell activity and up regulation of gene expression in general. Fibroblast growth factor, which itself promotes photoreceptor survival *in vivo* and *in vitro*,^{292 143;149;301;302} is one of the genes up regulated in activated Mueller glia and so is a candidate for the postulated secondary messenger.

4.1.2 Anti-apoptotic effects in the retina

Optic nerve transection is a commonly used model of neuronal apoptosis in the adult central nervous system, as following transection approximately 90% of the retinal ganglion cells (RGCs) undergo apoptosis within 2 weeks.³⁰³ Multiple studies have demonstrated that GDNF reduces apoptosis and enhances survival of axotomized RGCs.^{298;304-306} Analogous results are seen with GDNF treatment of axotomized motor neurons²⁹³ and in models of chemically induced oxidative damage¹⁵⁸ which are also acute models of apoptosis.

However, in inherited retinal degenerations photoreceptor apoptosis is less acute, instead occurring more gradually over a sustained period of time.^{75;307} The most convincing evidence of a GDNF-mediated neuroprotective effect in this context comes from a study in a rat model of RP where the treated eyes had morphological and functional evidence of rod photoreceptor rescue (increased ONL thickness and an improvement in scotopic a and b wave amplitudes in the treated group).¹⁶⁰ The animal model used for these experiments was the TgN S334ter-4 transgenic rat which expresses a mutated rhodopsin gene in which there is a premature stop codon (at residue 334 of the opsin transgene). The rhodopsin protein formed lacks 15 amino acids at the carboxy-terminal of the protein, which is believed to compromise trafficking of the protein to the outer

segments resulting in photoreceptor cell death by a caspase-3-dependent mechanism.^{114;228} The retina of these animals develops normally and then a degeneration starts at approximately p15 that is slower than that seen in the *Rho-/-Opn.gfp mouse*. Although the eyes treated with sub-retinal AAV.CBA.GDNF had evidence of reduced photoreceptor loss compared to control (i.e. AAV.CBA.GFP) treated and untreated eyes, there was no direct comparison to pre-degeneration animals or wild types to help assess the physiological relevance of the rescue effect. In addition the treatment effect was only demonstrated at one timepoint (p60). None-the-less the relative preservation of ONL thickness and rod function does indicate that GDNF can exert a neuroprotective effect on at least rod photoreceptors, and furthermore can do so in a sub-acute model of cell death, as well as the acute axotomy models.

GDNF as a therapy

A variety of growth factors and cytokines have been identified as potential neuroprotective agents. GDNF is notable however in having a favourable safety profile to date,^{160;308} including from clinical trials in patients with Parkinson's disease.^{152-155;309} This is in contrast to CNTF and FGF in particular, for which side-effects of impaired photoreceptor function^{154;309;310} and neovascularisation³¹¹ have been demonstrated respectively.

The work on GDNF supplementation in inherited retinal degenerations highlights some of the potential limitations and unknowns of neuro-protective therapies in general. In particular it is largely unknown how long beneficial effects are maintained for, and how broadly applicable they are to different diseases and underlying mutations. Additionally, in the context of rod-cone degenerations, it is not known if neuroprotective therapies are effective at slowing the secondary cone photoreceptor loss that has the greatest functional impact in patients.

Functional potential of GDNF monotherapy

GDNF-mediated preservation of photoreceptor function has been demonstrated in the rd mouse,^{80;159} RCS rat^{154;156;312} and TgN S334ter-4 rat^{157;160} models of retinal degeneration, and in mice treated with chemical inducers of oxidative damage.¹⁵⁸ In these studies GDNF was shown not only to slow photoreceptor loss, as compared to untreated or control-injected eyes, but also lead to a relative preservation of photoreceptor function. Thus photoreceptors were maintained in a functional state.

However, the neuroprotective effect of GDNF is partial, resulting in a slowing rather than cessation of the retinal degeneration. This is to be expected as the underlying defect has not been corrected and so there are continued stimuli for photoreceptor degeneration. Prolonged functional preservation will be dependent on the prevention of cell death in the cells concerned, and so it is important to have longitudinal studies that determine the magnitude of the neuroprotective effects over time. Only longitudinal studies can assess for how long the neuroprotective effect of GDNF is functionally relevant, but to date most of the studies have reported outcomes at single timepoints only. Buch et al. did however evaluate the effect of AAV2/2.CBA.GDNF in the RCS rat at repeated timepoints and found that the initial functional benefit over untreated fellow eyes was lost within 2 weeks.¹⁵⁴ It remains to be demonstrated whether higher levels of GDNF expression, or indeed studies in different models of retinal degeneration, achieve more long-lasting benefits.

In addition, although GDNF and neuroprotective therapies in general, are considered as potential treatments for a wide variety of IRDs it is important to emphasise that they, when used alone, can only be expected to achieve functional benefits in models, or stages of disease, where function still remains. Thus for example in the rds mouse, in which the lack of peripherin prevents formation of photoreceptor outer segments,²¹⁷ GDNF supplementation has no functional effect unless combined with gene replacement therapy.¹⁵⁴ The studies demonstrating functional benefits of GDNF are in animal models with milder phenotypes and with treatment at early stages of disease when function still exists.^{80;156;157;159;160}

These functional benefits are unlikely to translate to more advanced RP where there are residual but non-functional photoreceptors.^{83;254;255}

Neuroprotection without function

To date neuroprotective agents have been primarily evaluated as single-line therapeutic agents, and in this context functional effects are fundamental to the value of the treatment. However, many more complex diseases are best treated with combination therapies, and in this context even an effect that preserved cells but was not sufficient to maintain function would be valuable.

Dong et al. studied the effects of GDNF supplementation in the context of oxidative stress induced retinal degeneration.¹⁵⁸ Transgenic mice with doxycycline inducible expression of GDNF were treated with paraquat to promote oxidative stress and apoptosis within the retina. GDNF expression in this model lead to only a modest functional benefit as measured by the ERG, but the histological evidence of neuroprotection was much more striking, with almost normal appearing outer nuclear layers. Most of the preserved cells may therefore have been non-functional.

In contrast gene replacement for selected proteins has proved much more effective at restoring function than preventing cell death,¹³⁰ and combining the gene therapy with neuroprotection can improve the outcomes. In the study by Buch et al. rds mice were treated with rAAV.GDNF both alone and in combination with gene replacement (rAAV.Prph2).¹⁵⁴ Eyes treated with the combination of GDNF and gene replacement had significantly greater ERG function at 8 weeks and 3 months following injection than eyes treated with the replacement vector alone. At least in part this was because of a larger number of surviving photoreceptors (at 4 months post treatment photoreceptor numbers in the GDNF and gene replacement group were 74% greater than in the gene replacement only group). Analogous results were also shown in the RCS rat treated with lenti-viral vector mediated *MERTK* expression with and without rAAV.GDNF. Both ERG function and numbers of surviving photoreceptors

were greater in the eyes treated with the combination of *MERTK* and GDNF, than in eyes treated with *MERTK* gene replacement alone.

Furthermore, even for patients for whom gene replacement therapy is not an option, due to the nature of the mutation or stage of disease, it may soon be of benefit to preserve cone photoreceptors in a non-functional state. In a recent Science paper Busskamp et al. demonstrated that expression of halorhodopsin in light-insensitive cones was sufficient to restore not only light-sensitivity but also sophisticated retinal circuitry functions including ON and OFF responses and directional sensitivity.²⁵⁴ Halorhodopsin is a light activated chloride pump found in archaebacteria, and so the reactivated cones were functioning by bypassing the native phototransduction pathways. This approach is being carried forward into clinical trials but of note there is no evidence to suggest that this strategy will prolong the life of the cone photoreceptors. Benefits from the therapy would therefore be transient in patients with RP. These developments too therefore demonstrate a need for neuroprotective therapies even, or potentially especially, if they don't maintain native means of phototransduction.

Differential effect on rods and cones

The majority of photoreceptor outcome measures in rodent models of retinal degeneration are rod-dominated, as rods far outnumber the cones and unlike in higher animals there is no cone-rich area to facilitate assessment of cone-specific outcomes. Thus, for example, in the study by McGee Sanftner of AAV.CBA.GDNF in TgN S334ter-4 transgenic rats the outcome measures (ONL thickness and scotopic ERG function) inform us that GDNF had a neuroprotective effect on rod photoreceptors, but do not indicate whether there was any effect on cones.¹⁶⁰

Layer and colleagues have however studied the effects of GDNF in chicken retina, which has a reversed rod-cone ratio to that seen in rodents, such that cones are far more numerous.^{294,27} Working *in vitro* with retinal aggregates derived from embryonic chicken retinas they too found that GDNF supplementation

enhanced rod photoreceptor survival and rhodopsin expression, and conversely that down-regulation of expression (using antisense oligonucleotides) was found to decrease rhodopsin expression (and the number of rhodopsin staining cells seen with immunohistochemistry). However, no effect was demonstrated on the cone photoreceptors. The absence of a demonstrable effect on cone survival does not however preclude an effect in the degenerating adult retinas of rodents or humans; Layer et al. were working with embryonic tissue *in vitro*, and there is evidence that in this experimental model the development of rods is highly dependent on micro-environmental changes and spatial proximity of cones, whereas that of cones is less so;^{313;314} the susceptibility to survival factors may well be different *in vivo*. Furthermore, as the cones develop earlier than rods, at least some will have been at a different embryonic stage to the rods at the time of the GDNF supplementation or down-regulation, which could influence sensitivity to GDNF. In addition, the stimuli and mechanisms for cone photoreceptor loss are likely to have been very different in the *in vitro* retinal aggregates to the situation in rod-cone retinal degenerations. In particular the secondary loss of cones *in vivo* in rod-cone degenerations is at least in part through oxidative damage,⁹⁵ and the delivery of systemic antioxidants has been shown to slow this in both fast and slow murine modes of retinal degeneration.^{315;316} GDNF is protective against oxidative retinal damage induced in mice with paraquat, iron or hypoxia.¹⁵⁸ Although this latter study too used rod dominated outcome measures (ONL thickness and scotopic ERGs), it is plausible that if these effects were on cones as well as rods then GDNF would be protective for the oxidative damage that occurs in cones during rod-cone degenerations.

Even if in contrast to rods, cones are not directly sensitive to GDNF, it is conceivable that GDNF expression in rod-cone degenerations could lead to an indirect effect on cone survival by augmenting rod survival. By enhancing rod survival in this situation, GDNF would diminish the stimulus for cone degeneration. Such an indirect action would not have been apparent in the study by Layer et al. because of the reversed ratio of rods to cones. In the retinal aggregates used by Layer the cones were far more prevalent and so will have

been less dependent on surrounding rod photoreceptors for structural and metabolic support.

It is of both interest and clinical importance to identify whether this difference in GDNF sensitivity of rods and cones in embryonic chicken retinal aggregates does correspond to a difference in degenerating adult mammalian retinas. Whether any effect on cones is direct, or indirect by augmenting rod survival, could then be tested by inducing cone specific expression of one of the downstream effectors of GDNF mediated effects. XIAP would be a suitable candidate for this as its inhibition can prevent the neuroprotective effects of GDNF,²⁹³ and furthermore it is an intracellular protein and so cell-specific expression could be achieved.

4.1.3 Aims

It remains to be demonstrated whether GDNF treatment does or does not delay secondary cone degeneration in models of RP. A treatment effect on cones is potentially more feasible than one in rods as, in rod-cone degenerations, the cones themselves express no genetic mutation and are initially healthy prior to degenerating secondary to the rod photoreceptor loss. However the models used previously have not facilitated an assessment of cone-specific outcome measures, and one of the principal aims is to address this. This is a clinically relevant question to address as even the most effective means of preserving rod photoreceptors will be of limited clinical relevance in the absence of a concomitant effect on cone photoreceptor function, and hence colour and high acuity central vision.

Assessing cone function in the *Rho*^{-/-}*Opn.gfp* mouse, following treatment with GDNF, will allow an assessment of whether there is an effect on the secondary cone degeneration. Furthermore, if there is an effect, it will be possible to monitor the magnitude of the effect over time, potentially addressing further unknowns as to the duration of GDNFs effects on apoptotic photoreceptors.

4.2 GDNF receptor expression

Before embarking on GDNF treatments the first experiments were designed to test whether the GDNF receptors were still expressed in the degenerating retina during the time period of cone degeneration. Previously Jomary et al. reported that GFR α 2 mRNA expression levels were lower in the rd mouse retina than in wild types, as detected with in situ hybridisation.²¹² Furthermore, whilst it looked as though there may be expression within photoreceptors in the adult wild type retinas, this was not evident in the rd mouse. Down-regulation of the sensitive receptors during the cause of the degeneration could limit the potential efficacy of GDNF as a potential therapy. However in situ hybridisation is no longer the most reliable means of quantifying and comparing levels of expression. Furthermore, whilst down-regulation of expression may be expected to cause decreasing expression of GFR α 2 signal with time in the rd mouse, this is not what was found. Instead, the authors found the GFR α 2 signal to be less widespread in the rd retinal images, than in the age-matched wild type retinas at early timepoints. However, during the degeneration (p17 and p20) and in adult rd retinas (p60) in which photoreceptors are lost increasing expression was seen within the inner retina. The same research group went on to examine GFR α 2 expression levels in a rat-model of light-induced retinal degeneration, and found essentially the opposite of the findings in the rd mouse; in the rat model of light-degeneration GFR α 2 expression increased during the course of the degeneration, and this was particularly evident in the photoreceptors.²⁹⁵ These conclusions were well supported with western blot analysis and immunocytochemistry. No variation in GFR α 1 expression levels was seen.

Whether GFL receptors are present in inherited retinal degenerations is of relevance for the therapeutic potential of neurotrophic factors such as GDNF. The relevance of where they are expressed is less clear as the mechanism of action may be indirect via Mueller cells, and furthermore the GFR receptors may be secreted and, once bound to GDNF, be able to stimulate other neuronal cell types expressing RET.^{282;317} The first line of experiments was therefore to

identify if GFR α 1 and GFR α 2 are present or not in the degenerating retina of the rhodopsin knockout cone-GFP mouse.

4.2.1 Primer design and testing

Primers were designed to bind to murine GFR α 1 or GFR α 2 mRNA. To test these primers whole eyes from an 8 week old wild type and 11 week old *Rho*^{-/-}*Opn.gfp* mice were enucleated, and mRNA isolated and quantified. cDNA was then generated for primer testing.

Amplicons of the expected size were detected with cDNA from both mouse lines confirming presence of the GFR mRNA in both samples. Control PCR reactions for β -actin were run alongside to test for successful cDNA generation and PCR reactions.

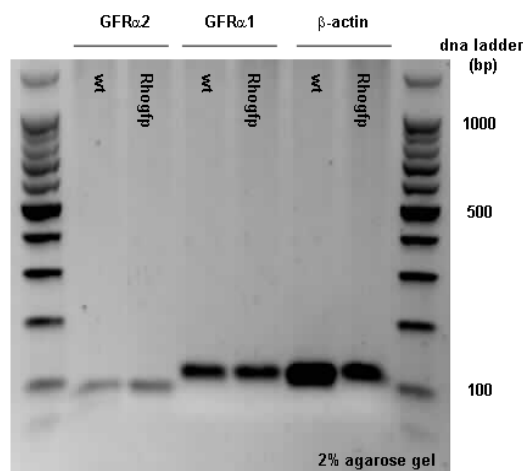


Figure 4-1 Validation of primers for murine GDNF receptors. PCR reactions were performed with GFR α 1 and GFR α 2 primers, and cDNA from adult wild type (wt) and 11 week old *Rho*^{-/-}*Opn.gfp* eyes. B-actin primers were used as positive controls.

4.2.2 GFR α 1 and GFR α 2 expression in the *Rho*^{-/-}*Opn.gfp* mouse over time.

To look for GFR α 1 and GFR α 2 mRNA in specifically the retina, and whether it is maintained in time *Rho*^{-/-}*Opn.gfp* eyes were isolated at 10 days of age, 13 weeks of age (approximate age of maximal cone photoreceptor loss) and 17 weeks of age (approximate endpoint of cone degeneration). An adult wild type eye was also enucleated to be used as a positive control. Retinas were dissected out in RNA later immediately following enucleation and stored at -80⁰C prior to mRNA isolation and cDNA preparation. These PCR reactions confirm that the GFR receptors to which GDNF has the greatest affinity are present throughout the rod-cone degeneration in the *Rho*^{-/-}*Opn.gfp* model of retinitis pigmentosa.

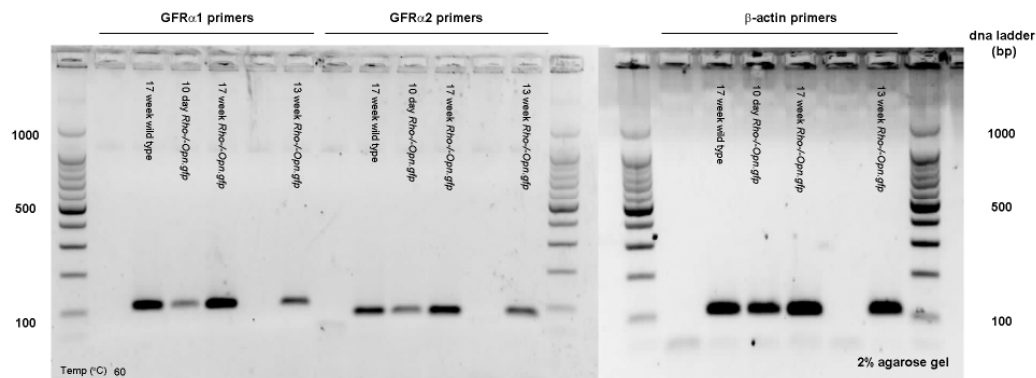


Figure 4-2 Detection of GFR α 1 and GFR α 2 mRNA. cDNA from wild type retina and *Rho*^{-/-}*Opn.gfp* retina at repeated timepoints confirmed the presence of GFR α 1 and GFR α 2 mRNA. β -actin control PCR reactions were run alongside for each sample to test for the presence of cDNA, and successful PCR reactions.

4.3 Intra-vitreous delivery of recombinant protein.

A minimally invasive means of delivery of GDNF to the retina is with an intra-vitreous injection of the recombinant protein. This means of delivery has the advantages of being relatively technically undemanding to perform, and comparatively safe as evidenced by the complication rates in clinical trials of

Ranibizumab.¹⁸⁹ In addition the timing and dose of drug delivery is highly controlled. It is therefore a favoured means of delivering therapeutic agents both experimentally and in clinical practice.

For a therapeutic agent delivered to the vitreous cavity to act within the retina, sufficient levels must pass through the structural and cellular barriers of the vitreal-retinal interface (including the internal limiting membrane) and inner retina. In comparison to the highly effective anti-VEGF agent ranibizumab, which has a molecular weight of 48 kDa, GDNF is relatively small with a molecular mass of 15kDa.²⁷³ Furthermore, where as ranibizumab has to reach the outer retina to exert its therapeutic agent GDNF may only have to reach the inner retina, if indeed its action on photoreceptors is via the Mueller cells whose processes transverse the retina. Evidence that GDNF protein delivered to the vitreous cavity can indeed be effective in photoreceptor neuroprotection comes from animal model studies of slow-release capsules implanted into the vitreous cavity.¹⁵⁷

4.3.1 Validation of assay

In order to be able to quantify levels of murine GDNF a commercial enzyme-linked immunosorbent assay (ELISA), previously validated with human and rat GDNF, was first tested with recombinant murine GDNF. Homology between murine and human forms of GDNF is 92.2% for the amino acid sequence, and 98.5% for the mature GDNF formed following cellular proteolytic processing prior to secretion.³¹⁸

Recombinant murine GDNF was purchased from Peprotech (London, UK) and reconstituted in autoclaved PBS to produce a working solution of 500µg/ml. The GDNF ELISA kit used, with human GDNF standards, was purchased from R&D systems. In a 96 well plate a dilution series of the recombinant murine protein was produced in triplicate along side the recombinant human protein standard (in duplicate). Concentrations were measured using the ELISA kit and compared to calculated concentrations to assay the sensitivity of the assay (Figure 4-3). The

apparent increased sensitivity for the murine GDNF is likely to be an experimental artefact (possibly relating to the manufacturer's aliquoting of the recombinant protein or preparation of the dilution series). The results validate the ELISA prep used as a valid means of assaying murine GDNF.

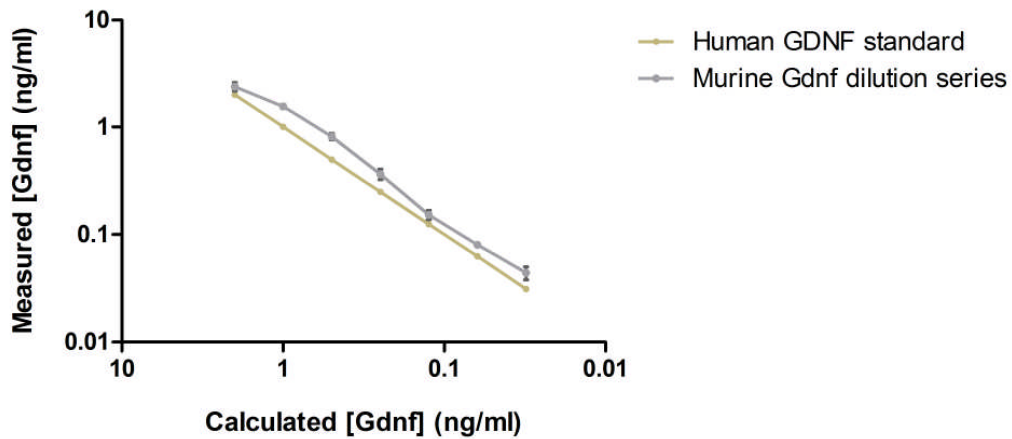


Figure 4-3 Comparison of ELISA detection of human and murine recombinant GDNF protein. Error bars (+/- standard deviation) are shown for the murine GDNF series. Concentrations of human and murine GDNF were measured to very similar, validating the use of the assay for either protein.

4.3.2 Pharmokinetics

To establish the half-life of GDNF in the mouse eye wild type mice were injected with recombinant protein, and the eyes harvested for analysis at six subsequent timepoints.

For this experiment, 18 wild type mice were injected intravitreally with 500ng of recombinant murine GDNF in 1 μ l of PBS, at 38 days of age. At each of the 6 timepoints (midday on days 1, 2, 5, 8, 16 and 33) 3 mice were culled and the eyes snap frozen in liquid nitrogen. At completion of the time series treated eyes were crushed whilst still frozen and then suspended in 120 μ l of reagent diluent with 1/100 protease inhibitor. Following vortexing samples were spun at 10 000 rpm for 5 minutes and the supernatant used for ELISA to determine the concentration of GDNF.

For the day 1 and day 2 samples supernatants were analysed at 1/100, 1/1000 and 1/10000 dilutions. Day 5, 8, 16 and 33 samples were analysed undiluted and at 1/10, 1/100 and 1/1000 dilutions. Only ELISA results falling within the range of the standard curve were used for further analysis (OD 0.1 to 1.5) (Figure4-4).

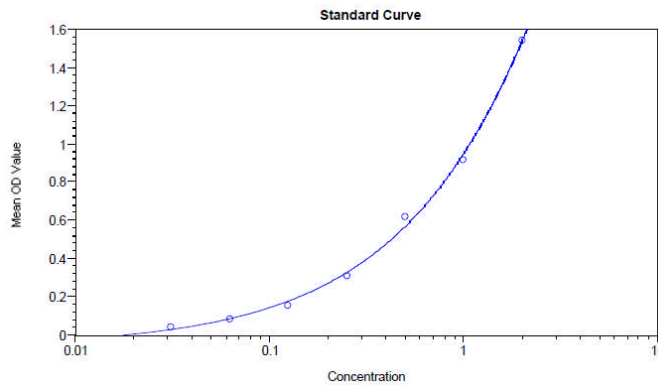


Figure 4-4 Standard curve from ELISA experiment to determine concentration of GDNF in wild type mouse eyes. Known concentrations of recombinant GDNF were run alongside samples to be evaluated in order to correlate optical density (OD, y-axis) with GDNF concentration (x-axis). A 4 parameter sigmoidal best fit line is used with the ELISA because of plateaus at high and low concentrations. This fits the data with a high correlation coefficient ($r^2=0.997$).

Mean values of GDNF concentration at the selected timepoints are shown in Figure 4-5. On a logarithmic scale the decrease between day 1 and day 8 is approximately linear which is suggestive of GDNF elimination following 1st order kinetics. This would indicate that drug elimination is proportional to drug concentration, which is the case for most pharmaceutical agents within the body. The levels from day 8 onwards were at the detection limit of the assay.

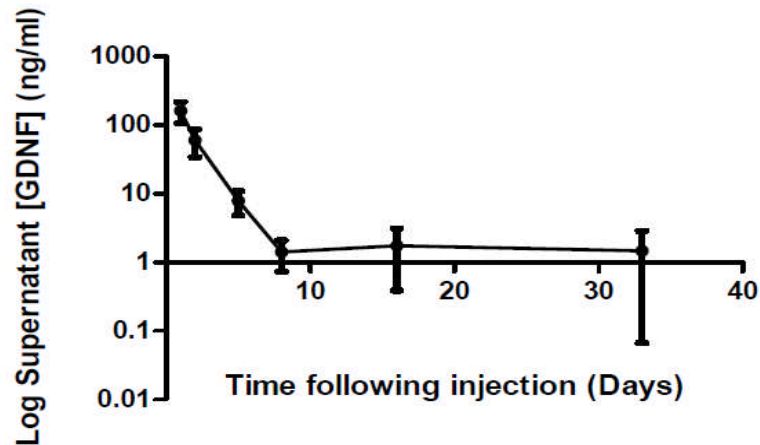


Figure 4-5 The decrease in GDNF levels following intravitreal injection in the mouse eye. Mean \pm sd. Single eyes of 18 wild type mice were injected intravitreally with 500ng of recombinant murine GDNF. At days 1, 2, 5, 8, 16 and 33 three mice were culled to establish intra-ocular GDNF levels.

To calculate the half life of GDNF in the mouse eye it was assumed that the drug does indeed follow first order decay, and an exponential best fit line was applied to the results of the first 4 timepoints (Figure 4-6). The curve fits with a correlation coefficient of 0.84 and has a half-life of 0.68 days (95% confidence intervals 0.40 to 2.44). The half-life of GDNF in the murine vitreous cavity is therefore calculated to be 16 hours. This is shorter than the half-life of 37 hours that has been reported in pig eyes³¹⁹, which may relate to the substantial differences in vitreous volume or the relationship of metabolic rate to animal size. The adult mouse eye has a relatively small vitreous cavity, which is estimated to be $\sim 7\mu\text{l}$. In contrast the volume of the vitreous cavity in the pig eye is closer to that in a human, $4000\mu\text{l}$. In adult eyes the vitreous body is avascular, and so drug elimination will occur primarily at the outer surface by diffusion. A smaller surface area to volume ratio, as is the case in the porcine eye^a will therefore be

^a The equations for the surface area and volume of a sphere are $S=4\pi r^2$ and $V=(4\pi r^3)/3$ respectively. With volume being proportional to radius to the power of 3, but surface area being proportional to radius to the power of 2, the surface area to volume ratio will decrease with an increase in radius (r).

associated with a lower rate of drug elimination. In addition Kleiber's Law refers to the finding that metabolic rate of organisms is proportional to body mass to the power of $\frac{3}{4}$.³²⁰ The higher metabolic rate in the mouse than the pig could also explain the difference in half life, if the higher metabolic rate corresponds to a steeper concentration gradient.

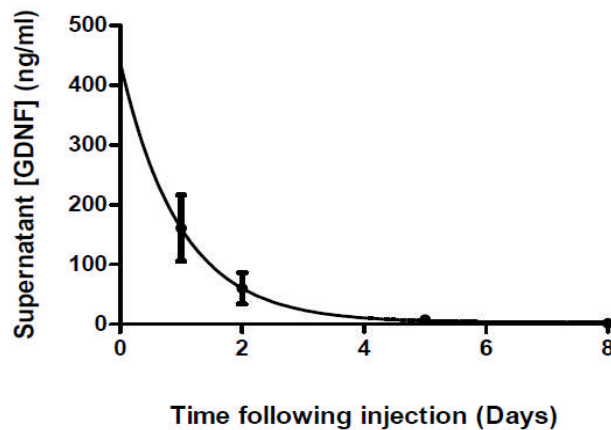


Figure 4-6 Application of an exponential best fit line to the GDNF level results from day 1 to 8. $R^2=0.84$. (Mean \pm sd).

Conversion to absolute values

For all the GDNF ELISA experiments each harvested eye was diluted in 120 μ l of reagent diluent. Harvested eyes were approximately 3mm in diameter, giving an ocular volume of 14 μ l, in keeping with published estimates. The ELISA measured values therefore reflect an approximate 10-fold dilution of absolute concentrations within the eye.

4.3.3 Evaluation of single bolus

LaVail previously evaluated a large number of neurotrophic factors by performing intra-vitreous injections, at a single timepoint, into 1 eye of mice with various retinal degenerations.³⁰¹ GDNF was not one of the neurotrophic factors

evaluated. The value of these experiments was that for CNTF, and to a lesser extent BDNF, a single injection was sufficient to produce a protective effect in some of the mouse models. The CNTF mediated neuroprotective effects were seen in the rd, nervous and Q344ter models of retinal degeneration. Similar experiments have demonstrated neuroprotective effects for FGF-2 in the RCS rat and, the TgnS344ter-4 rat, and in albino rats with light-induced photoreceptor degeneration.^{143;149;150;321}

Of note, whilst the half-life of GDNF in the mouse vitreous eye is relatively short at 16 hours, that is not to say the biological effect is not considerably longer. Within the nigrostriatal dopaminergic system of parkinsonian rats a single injection of GDNF exerts a biological effect lasting over 8 weeks.³²² It is important to identify whether GDNF has a prolonged biological effect in retinal degenerations as repeat intravitreal injections are feasible clinically, as seen with the treatment of AMD with antivegf agents.

Dose

The effect of a single intra-vitreous injection of 500ng of GDNF was evaluated in 11 *Rho-/-Opn.gfp* mice. Whilst the exact effective dose (ED50) of GDNF for outer retinal degeneration is unknown, Frasson et al. demonstrated a neuroprotective effect in the rd mouse with 330ng of GDNF, in an injection volume of 1µl, when delivered directly into the sub-retinal space. This is a similar dose as used for other growth factors with intra-vitreous injections in mice.^{143;301} It is a considerably higher concentration of GDNF than has been found to be effective in neural tissues²⁷³, but is supported by the short-term *in vitro* studies of rat rod photoreceptor morphology by Carwile et al., where 1ng/µl of GDNF, but not 0.1ng/µl was found to enhance rod outer segment survival.²⁸³

330-500ng/µl is also a considerably higher dose than that found to be effective in preventing retinal ganglion cell apoptosis in rat models of glaucoma when one takes into account the vitreous volume. In a dosing study in rats by Klocker et al. 500 ng intra-vitreally was found to have an optimal effect, and 2µg had no

additional benefit.³⁰⁵ The vitreous volume in the adult rat is approximately 56µl³²³, and so the approximately 10 times greater than the vitreous volume in the mouse eye.

An intravitreal dose of 500ng is therefore likely to be suprathreshold for GDNF receptors in the inner retina, and in the same order as used previously for sub-retinal injections in mice. Furthermore a concentration of 500ng in 1µl (an appropriate volume for the intra-vitreous injections in mice) has been reported as showing no signs of toxicity in cell culture.³¹⁹ The following experiments were therefore performed with a GDNF dose of 500ng in 1µl injected intra-vitreally.

Intra-vitreous Injections

Injections were administered at day 38 of age so as to treat before the ONL was lost by over 50%, and before cone function had already started to deteriorate. A single eye of each of the 11 animals was treated, with the side randomised to control for any bias in subsequent ERG analysis. To control for the effects of sub-retinal injection a further 4 mice were treated at the same timepoints with unilateral injections of 1µl of PBS. All injections were performed under direct visualisation with an operating microscope; with the needle tip held in close proximity to the optic nerve head an assistant depressed the plunger with a slow motion so as to ensure delivery to the inner retina, whilst minimising the potential for direct mechanical trauma from the infusion.

Results

Cone function in GDNF, PBS and untreated eyes was evaluated with ERG assessments under photopic conditions. Assessments were performed at days 45, 52, 60 and 73 for pre-, early-, mid- and late-degeneration time-points respectively.

The assessment at day 45 was performed to look for functional consequences following the intra-vitreous injection procedure 7 days previously. As this

timepoint is pre-degeneration, a neuroprotective effect is unlikely to be detectable but lasting iatrogenic damage will be. Neither intra-intravitreal injections of PBS or rGDNF had an effect on baseline cone function, as compared to fellow untreated eyes (paired t-test, $p=0.87$ and $p=0.38$ respectively).

To detect an effect on cone function degeneration rGDNF, PBS and untreated eyes were assessed at 3 timepoints spanning the degeneration, and analysed with analysis of variance (ANOVA) and post test Bonferroni tests. Time point, but not treatment group, was a significant determinant of cone function. There was no evidence that a single bolus of rGDNF at day 38 improved cone function at subsequent timepoints, or led to a delay in the cone degeneration. The rate and time course of cone function degeneration was not altered, as shown in Figure 4-7. Comparison of treated and untreated eyes in individual mice revealed that in only 1 of the 11 treated with GDNF was function greater in the treated eye than in the untreated eye at all timepoints. In 2 of the 11 cone function was greatest in the untreated eye at all timepoints, and for the rest the eye with greatest function varied over time. There was therefore no evidence of a sub-group of responders that should be analysed separately to non-responders.

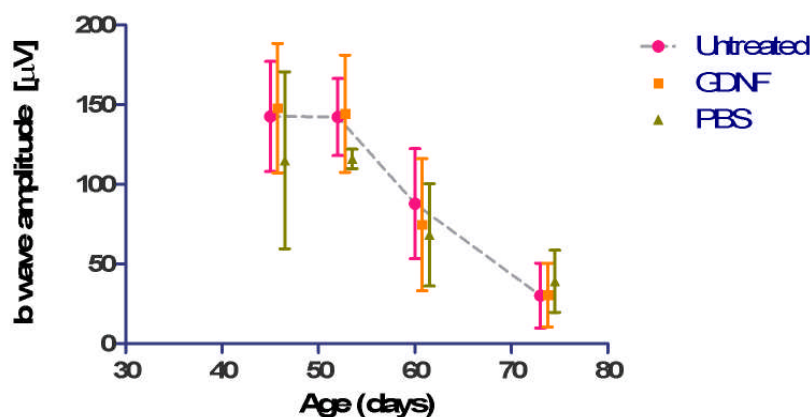


Figure 4-7 The effect of single intravitreal rGDNF or PBS injections in the *Rho*^{-/-} *Opn.gfp* mouse. All eyes were treated with 500ng of intravitreal GDNF at day 38 of age. Mean b-wave amplitude (± 1 sd) to a photopic flash of 10 cds.m⁻² is shown at each timepoint. The interconnecting line is shown for the untreated eyes to show the normal course of degeneration.

Discussion

Injections into the mouse vitreous cavity are potentially complicated by the small vitreous cavity and relatively large intraocular lens. Compromised retinal function could result from direct damage to ocular tissues, or from consequent variations in intraocular pressure in particular. Conversely however, studies of intra-ocular injections in the rat have also demonstrated that the procedure itself can induce neuroprotection.^{143;321} This is most pronounced with sub-retinal injections in the RCS rat, probably due a combination of clearance of sub-retinal toxins and the release of endogenous growth factors in response to the injury. However in their initial study of FGF in the RCS rat, Faktovich et al. found histological evidence of photoreceptor rescue in eyes which had undergone a single intra-vitreous injection of PBS.¹⁴³ Their intra-vitreous injections were performed through the retina whereas in these experiments the aim was to inject through the pars plana and thus avoid direct injury to the retina. None the less it was important to evaluate whether the procedure itself compromised cone function in this animal model, or resulted in a subsequent neuroprotective effect. This was achieved by pre-degeneration (p45) assessments and following PBS-treated controls during the course of the degeneration. These evaluations were consistent in showing no procedure-related effects on cone function.

GDNF has a prolonged biological effect on dopaminergic neurons,³²² but an analogous effect on cone photoreceptor function was not demonstrated in these experimental conditions. This was despite using a supra-threshold dose, and a timepoint chosen to aid the chances of detecting any effect. At p38 cone numbers are still approximately maximal, and most rod photoreceptors are still present so there was the potential for both a direct action on cone photoreceptors, and an indirect effect by augmenting rod photoreceptor survival. No effect was evident however.

A negative result following such experiments with a single intra-vitreous injection is open to a far greater number of interpretations than a positive result. In particular methodological factors such as the timing of injection, or dose used may lead to a potential therapeutic effect being undetected. Furthermore the

response to intra-ocular survival factors has been found to vary considerably with the animal model in which it is tested.^{301;324}

LaVail noted that the variability of results was far greater with intravitreal injections into mouse as opposed to rat eyes, and suggested that the small size of the mouse eye presents particular challenges to achieving consistent delivery of proteins with intravitreal injections.³⁰¹ The authors therefore expressed reservations regarding negative interpretations from such studies evaluated in the small mouse eye only. In order to try and minimise variability of delivery in the experiments presented here, intravitreal injections were performed under direct visualisation with the needle tip maintained directly above, and in close proximity, to the optic disc. This is in contrast to the technique used in humans where the needle is kept in the centre of the vitreous cavity, and direct visualisation is not necessary.³²⁵ The pharmacokinetics evaluation on page 169 validated this technique of intra-ocular protein delivery and did not support LaVail's concerns of inconsistent protein delivery in the mouse eye.

4.3.4 Evaluation of repeated bolus

Given the short half-life of GDNF within the murine vitreous, further experiments were performed to reduce the risk of a positive treatment effect in this model being missed due solely to timing of injection.

Rho-/-Opn.gfp mice (n=7) were treated with 500ng of GDNF, delivered by intravitreal injection to a single eye, at days 36, 42, 50, 57 and 64. Fellow eyes were treated with 1µl of PBS to act as a control for the effect repeated injections might have on function, and media clarity for subsequent SLO imaging. Functional analysis was performed at days 45, 60 and 73 to leave adequate intervals between anaesthetics, and SLO imaging was performed at day 77.

Results

1 of the 7 mice failed to recover fully from the first anaesthetic a further 2 developed corneal scars during the course of the experiment preventing inclusion

in the day 73 and day 77 assessments. Functional assessments are presented across the full range of flash intensities examined and reveal no difference between the GDNF and PBS treated eyes (Figure 4-8). There was no evidence of either a protective or toxic effect from the repeated GDNF injections on cone function.

In order to confirm that cone survival was similar in GDNF-treated animals compared to controls, SLO imaging was also performed at day 77. This was the 9th anaesthetic and procedure for the remaining cohort of animals, and by this time the ocular media were sufficiently clear for good quality SLO imaging in only 3 of the initial cohort of 7 animals. Mean central cone counts were 838 ± 212 and 580 ± 189 for the GDNF and PBS treated eyes respectively.

Comparison of GDNF and PBS treated eyes in individual animals, to limit the effect of inter-animal variation, revealed no statistically significant difference between the two groups ($p=0.22$, paired t test, $n=3$).

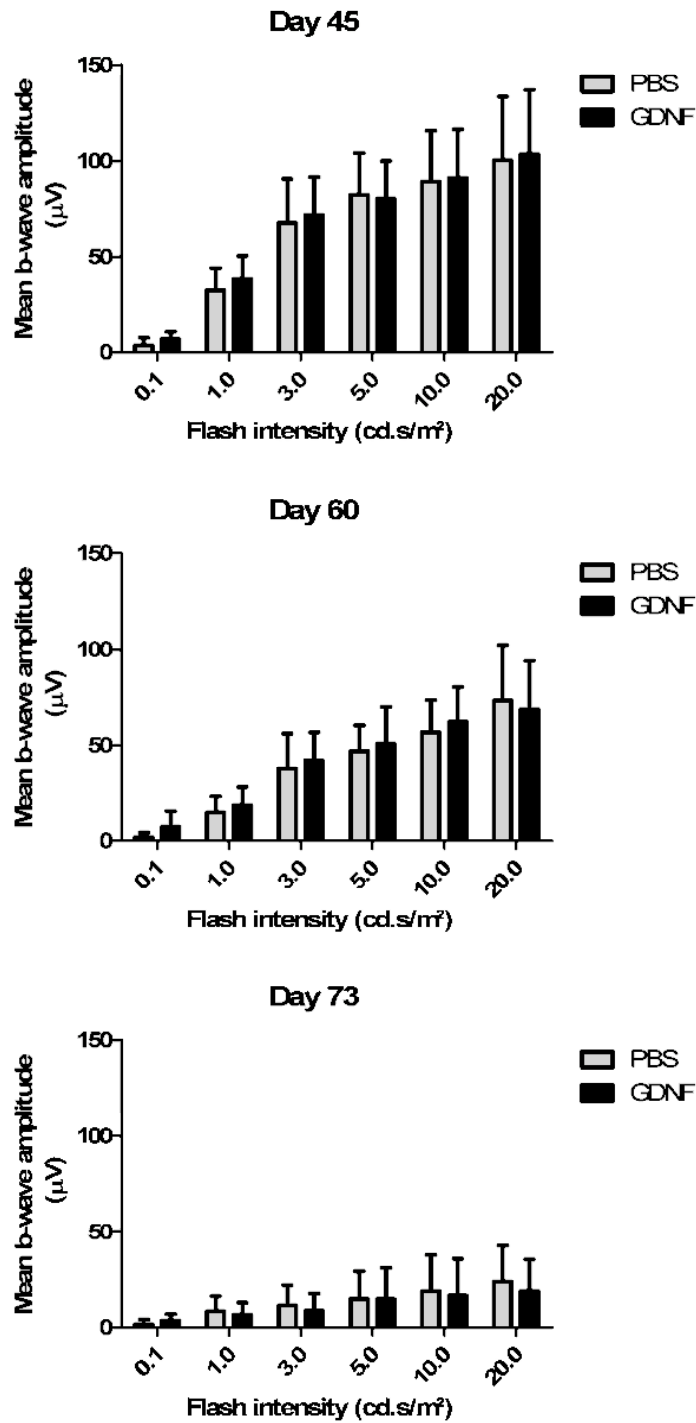


Figure 4-8 The effect of repeated GDNF bolus injections on cone function. Mean b-wave amplitudes to a range of photopic stimuli are shown, with standard deviations indicated by error bars. At each of the timepoints there is no significant difference in cone function between the GDNF treated and PBS treated eyes. The rate of functional cone degeneration over time is the same in both groups of eyes.

4.3.5 Conclusions

GDNF has been reported as a potential neuroprotective agent for inherited retinal degenerations. Histological and functional efficacy has been demonstrated in selected animal models of retinitis pigmentosa, and of the photoreceptor-toxic and angiogenic side-effects that have been found with other growth factors when administered within the eye have not been found with GDNF.^{150;152-155}

The experiments here, identifying GFR α 1 and α 2 expression in the degenerating *Rho*^{-/-}*Opn.gfp* retina, are supportive of further work to evaluate GDNF as a potential therapeutic agent. The pharmacokinetics of a single dose of GDNF to the mouse vitreous cavity was investigated, and the half-life determined.

The combination of a single bolus, and then repeated bolus, injection regime was used to look for a treatment effect at multiple timepoints. Previously McGee Sanftner et al. have demonstrated rod photoreceptor neuroprotection in transgenic rats with a rhodopsin mutation.¹⁶⁰ It was therefore of interest to examine the effects of GDNF supplementation both at early timepoints which were favourable for rod neuroprotection, as well as at later timepoints when the rods have largely degenerated and any treatment effect would have been likely to be independent of rods. Recombinant protein injections were used for these experiments as a means of delivering precisely known doses at exact timepoints. The experiments demonstrated that with these intravitreal boluses of GDNF protein there was no effect on cone photoreceptor function in this animal model of rod-cone degeneration. There was also no evidence or repeated GDNF boluses having an effect on the numbers of surviving non-functional cone photoreceptors in the latter stages of the degeneration.

If substantiated these results would preclude a valuable role for GDNF, at least as a sole therapeutic agent, in the clinical setting. It could be that the pro-degeneration stimuli in this model are too strong for the neuroprotective effects of GDNF found in other models of RP. Alternatively, it remains possible that

GDNF does not have a neuroprotective effect on cone photoreceptors. However, experimental limitations could also lead to a neuroprotective effect remaining undetected with these experiments. In particular, with this mode of GDNF delivery the intra-ocular levels will have been highly fluctuant, as shown by the pharmacokinetics data. The most convincing evidence for a neuroprotective effect from GDNF in other models has been with sustained expression of the protein, using gene therapy for example. It could therefore be that a neuroprotective effect of GDNF is dependent on consistently high intra-ocular levels of the protein. Furthermore, the timing of GDNF administration in these experiments was targeted to preserve the cone photoreceptors directly. It could instead be that GDNF has an indirect effect on cones, and that by preserving rod survival even transiently to preserve oxygen consumption or trophic factor release, it indirectly preserves cone function and survival. To detect such an effect GDNF should be administered early on during the rod phase of the rod-cone degeneration. In addition, the power of these experiments to detect a therapeutic effect was compromised by exclusions during the course of the repeated bolus experiments. Corneal and lens clarity in the mouse eye is readily compromised with repeated anaesthetics and procedures which entail a risk of corneal desiccation or abrasions. In the repeated bolus experiments the protocol included 9 anaesthetics and procedures, and the outcome measures were highly dependent on corneal clarity. Over 50% of the experimental animals were excluded by the completion of the experiment, such that numbers of cone photoreceptors at p77 were assessed in only 3 animals.

The findings therefore provide no evidence of a neuroprotective effect of GDNF on cone photoreceptors in this RP model. This could however be due to the need for sustained GDNF expression and it might be that weekly injections were simply not regular enough to maintain sustained levels of intraocular protein. To determine whether these findings reflect the true potential of GDNF further experiments were performed using gene therapy to achieve sustained and long-lasting elevation of intra-ocular GDNF levels.

Chapter 5 Inner-retinal GDNF gene therapy

5.1 Introduction

Following the isolation and sequencing of GDNF,²⁷³ the principle challenge to studying its efficacy as a neuroprotective agent *in vivo* has been how to deliver the protein to the neuronal tissue of interest at sustained and high levels without repeated invasive procedures. Systemic delivery has proved ineffective given the inability of therapeutic amounts to penetrate the blood–brain barrier. In an early trial of GDNF for Parkinson’s disease a cannula was implanted intra-cranially with the tip within the right front ventricle, and a distal access port lying under the scalp skin into which repeated injections could be administered.³²⁶ There was however no improvement in parkinsonism in this trial, and there were significant side effects related to the implanted cannula and central actions of GDNF. Furthermore, examination of the brain of a trial subject who died of unrelated causes provided no evidence of significant diffusion of the intracerebroventricular GDNF to the relevant brain regions, the putamen and substantia nigra.³²⁷

Implantable devices from which GDNF is secreted have also been developed for use within the eyes of animal models.¹⁵⁹ These however retain the disadvantage of releasing the GDNF distal to its site of action and relying on diffusion down a concentration gradient. Injections of GDNF-secreting mouse embryonic stem cells into the vitreous cavity of rat eyes were reported to result in significant elevations of plasma GDNF.¹⁵⁷ The explanation for this finding is unclear as the plasma levels were higher than the vitreous levels in treated animals. None the less the finding at least raises the concern that high intra-vitreous levels could

result in systemic side-effects, particularly in the context of retinal dystrophies and disruption to the normal blood-retinal barrier.³²⁸

Gene therapy, using viral vectors, has the advantage of being an effective and safe means of inducing sustained expression of proteins close to their site of action.¹⁹⁷ Intra-retinal transgene expression and functional effects have been observed for at least 3 years after a single administration of viral vector.^{198;329} These are likely to persist considerably longer given that the transduced cells are typically non-dividing.^{197;198}

For retinal gene therapy the viral vector, containing the transgene sequence, is delivered into the eye by means of a single intra-vitreous or sub-retinal injection, with the former being the less invasive option. Recombinant adeno-associated virus serotype 2 (rAAV2/2), injected intra-vitreally, leads to effective transduction of predominantly ganglion cells in the inner retina.^{330;331} It is therefore well suited to the delivery of GDNF which is a diffusible extracellular protein, for which the majority of the receptors are ordinarily found in the inner retina.

5.2 Gene Therapy to express GDNF in the inner retina

5.2.1 The *cmv.gdnf* plasmid and in vitro testing

The cytomegalovirus (CMV) promoter sequence is derived from the major immediate-early promoter of the human cytomegalovirus. It is one of the first viral promoters to be activated following viral infection, and has proved to be an effective promoter in cell types that are naturally infected by the CMV virus in a human host, which includes photoreceptors, RPE and ganglion cells within the retina.^{331;332} It is a constitutive promoter, that is largely unregulated allowing for continual transcription of its downstream gene (although in certain circumstances activity may be down-regulated by methylation).³³³ It was therefore chosen as the promoter to drive *Gdnf* production in the following experiments.

The murine *Gdnf* coding sequence was cloned into the pd10 plasmid downstream of the CMV promoter (shown schematically in Figure 5-1 with the full plasmid

map in the supplementary data chapter). Following an initial ATG start codon the sequence encodes a highly conserved secretion signal enabling extracellular secretion of the mature GDNF protein by transduced cells.³¹⁸

The pd10 plasmid into which *Gdnf* was cloned contains the 2 inverted terminal repeat (ITR) regions (of 145 nucleotides each) that are required for viral vector formation (specifically for encapsidation of the nucleic acid genome).³³⁴ At the 3' end there is also the SV40 polyadenylation (SV40pA) sequence. The polyadenylation signal, in this case derived from the simian 40 virus, allows for efficient transcription termination, and polyadenylation of the mRNA formed (an essential processing event for most eukaryotic mRNAs). Multiple restriction enzyme sites within the plasmid facilitate the inclusion of transgene and promoter DNA. The sequence of the CMV.*Gdnf* pd10 plasmid generated was confirmed with restriction enzyme digests and sequencing of the region containing the CMV and *Gdnf* sequences.

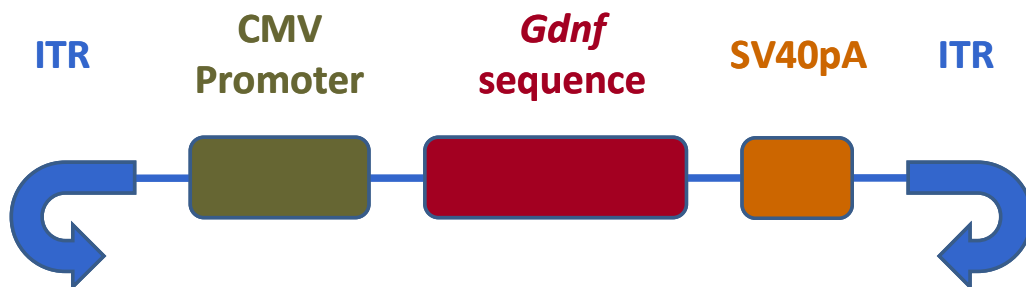


Figure 5-1 The pd10 plasmid following ligation with the CMV promoter and murine *Gdnf* transgene. The pd10 plasmid includes a polyadenylation site derived from simian virus 40 (SV40pA) and two inverted terminal repeats (ITR).

To test whether the plasmid could successfully induce *Gdnf* production in transfected cells 3 wells of 293T cells (75 000 cells/well) were transfected with CMV.GFP (as a negative control) and 3 wells were transfected with the CMV.GDNF plasmid. Supernatant was collected after 48 hours and tested for

evidence of Gdnf protein using an enzyme-linked immunosorbent assay (ELISA). Gdnf protein was detected in the supernatant from CMV.GDNF transfected cells at a concentration of 41 ± 1.97 pg/ml where as in the supernatant from CMV.GFP transfected cells and untransfected cells the recorded concentrations were 0.05 ± 0.01 pg/ml and 0.01 ± 0.00 pg/ml respectively (Figure 5-2). The plasmid was therefore confirmed to be a successful means of inducing cellular Gdnf production.

5.2.2 AAV 2/2 production and *in vitro* testing

Recombinant AAV serotype 2 carrying the CMV.GDNF construct was produced using published methods and purified using a heparin column.^{131;230} The viral vector titre was determined with a dot-blot and found to be 1.3×10^{13} genome particles/ml, as shown in Figure 5-3.

Vector efficacy was tested *in vitro* prior to *in vivo* use. This was performed by infecting 3 wells of 293-T cells with and without co-infection with adenovirus which increases the speed and efficiency of infection by AAV2/2. After 3 days the concentration of Gdnf in the supernatant was determined. The results shown in Figure 5-2 confirm Gdnf production in AAV2/2 infected cells.

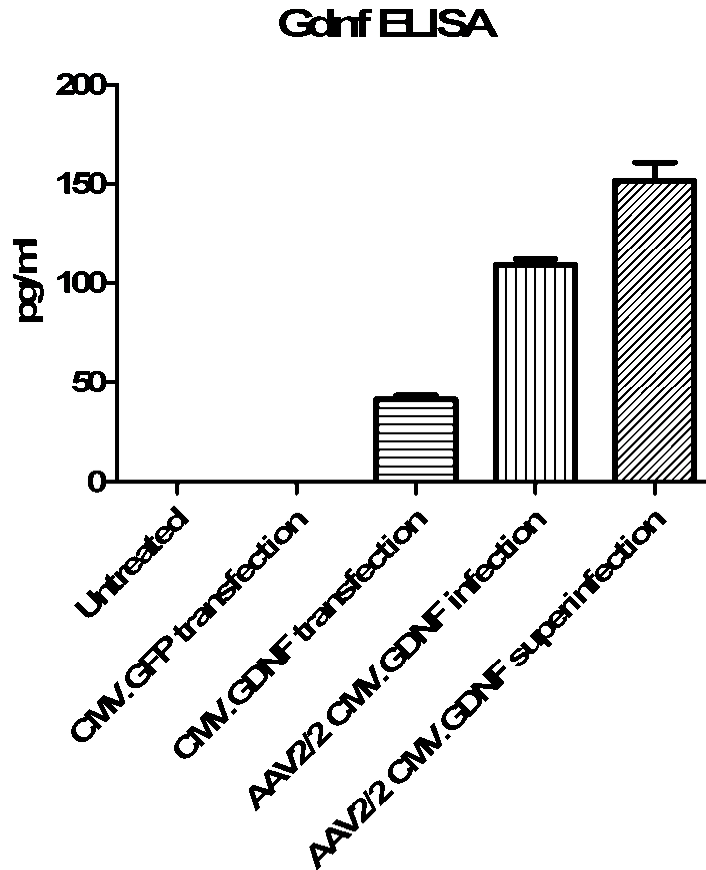


Figure 5-2 In vitro testing of the CMV.GDNF plasmid and rAAV2/2. Supernatant from 293 T cells transfected CMV.GFP or CMV.GDNF plasmids, or infected with rAAV2/2 CMV.GDNF was collected, and the Gdnf concentration determined by ELISA. Viral infection was performed with and without concomitant adenovirus infection to improve infection efficiency (superinfection). Supernatant from untreated cells was analysed alongside. Concentrations were determined with ELISA.

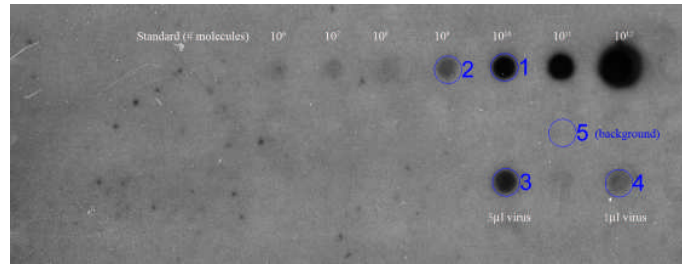


Figure 5-3 Measurement of AAV2/2 CMV.GDNF titre by dot-blot analysis. Blue circles and text indicate sample points for the densitometric analysis, indicating a titre of 1.3×10^{12} vg/ml.

5.2.3 *In vivo* quantification of Gdnf after intra-vitreous rAAV2/2

At day 11 of age, 4 *Rho*^{-/-}*Opn.gfp* mice were treated with a single intravitreal injection of AAV2/2 CMV.GDNF to the right eye (1 μ l) and the left eye was untreated. These 4 mice were used for functional assessments (ERG analysis at 3 timepoints) and then culled at day 73 of age. Gdnf concentrations in both eyes from each animal were assayed by ELISA, and the results are shown in Figure 5-4. Levels of protein are shown per eye, which were calculated from measured levels assuming that the volume of each eye was approximately 14 μ l. Mean Gdnf concentration in treated eyes was 5 times as high as in untreated fellow eyes.

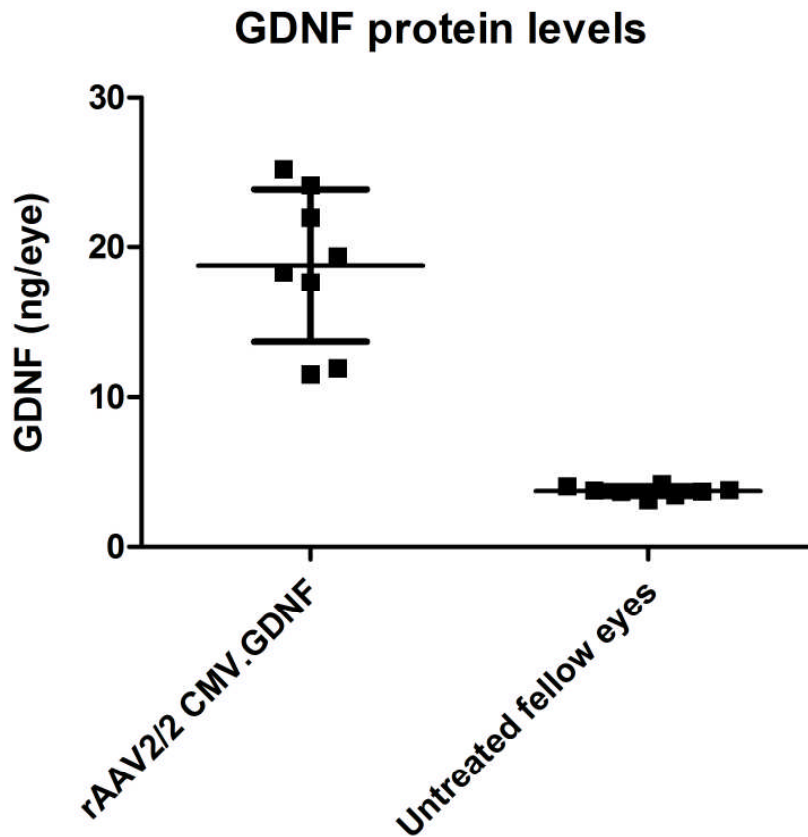


Figure 5-4 GDNF protein assays (ELISA) in AAV2/2 CMV.GDNF treated and untreated fellow eyes of 4 *Rho*^{-/-}*Opn.gfp* mice. Each eye was analysed in duplicate. There was a 5 fold difference between treated and untreated fellow eyes.

5.3 In vivo examination of the effect of inner retinal GDNF production on cone photoreceptor loss.

The aim of the following experiments was to determine whether increased inner retinal Gdnf expression in the *Rho*^{-/-}*Opn.gfp* mouse has an effect on the degeneration of cone function. rAAV2/2 CMV.GDNF treated eyes were compared with untreated fellow eyes. However, it is also important to control for potential effects of the intravitreal injection procedure, and the effect of viral-vector mediated transduction on inner retinal cells.

The importance of such controls is well illustrated by related experiments in other rodent models of retinal degeneration. In the RCS rat injections of saline alone into the sub-retinal space result in beneficial, albeit transitory, effects on photoreceptor survival.^{143;335;336} This is likely to be due to the combination of the injection reducing the local concentration of accumulated toxins and an injury effect stimulating endogenous growth factor release. Working in the mouse, Cao et al. likewise found that a trans-scleral 1mm stab incision into the outer retina led to upregulation of bFGF and CNTF expression, which persisted for 16 days following the injury.³³⁷ To isolate the specific effects of Gdnf, experiments were first performed with a related viral construct expressing an alternative reporter gene.

5.3.1 The effect of intra-vitreous injection and inner retinal cell transduction on cone photoreceptor mediated retinal function.

AAV2/2 was prepared using an existing 'CBA.RFP' plasmid (for map see appendix). The chicken β -actin promoter (variously abbreviated to CBA or CAG) consists of the chicken β -actin promoter cloned downstream of the CMV enhancer. Like the CMV promoter is it a strong constitutive promoter, and is therefore an appropriate promoter to use to control for the effect of inner retinal cell transduction. A plasmid with the red fluorescent protein (RFP) reporter gene was chosen to facilitate confirmation of expression in the rhodopsin knockout-gfp mouse, where there is already strong gfp expression in the outer retina.

6 mice were treated with AAV2/2 CBA.RFP (1 μ l intra-vitreous at p11) to a single eye, with the fellow eye untreated as a control. Virus was approximately titre-matched to the concentration of AAV2/2 CMV.GDNF used elsewhere (to within 0.5 of a log unit). Functional ERG assessments were performed at days 52, 60, 66 and 73 of age (Figure 5-5).

Analysis of variance (ANOVA) with Bonferroni post-hoc tests revealed no difference between cone function in the rAAV2/2 CBA.RFP treated eyes, and fellow untreated eyes. Following the day 73 assessments eyes were prepared for histological analysis which confirmed transduction and RFP expression in inner retinal cells of the treated eyes (Figure 5-6).

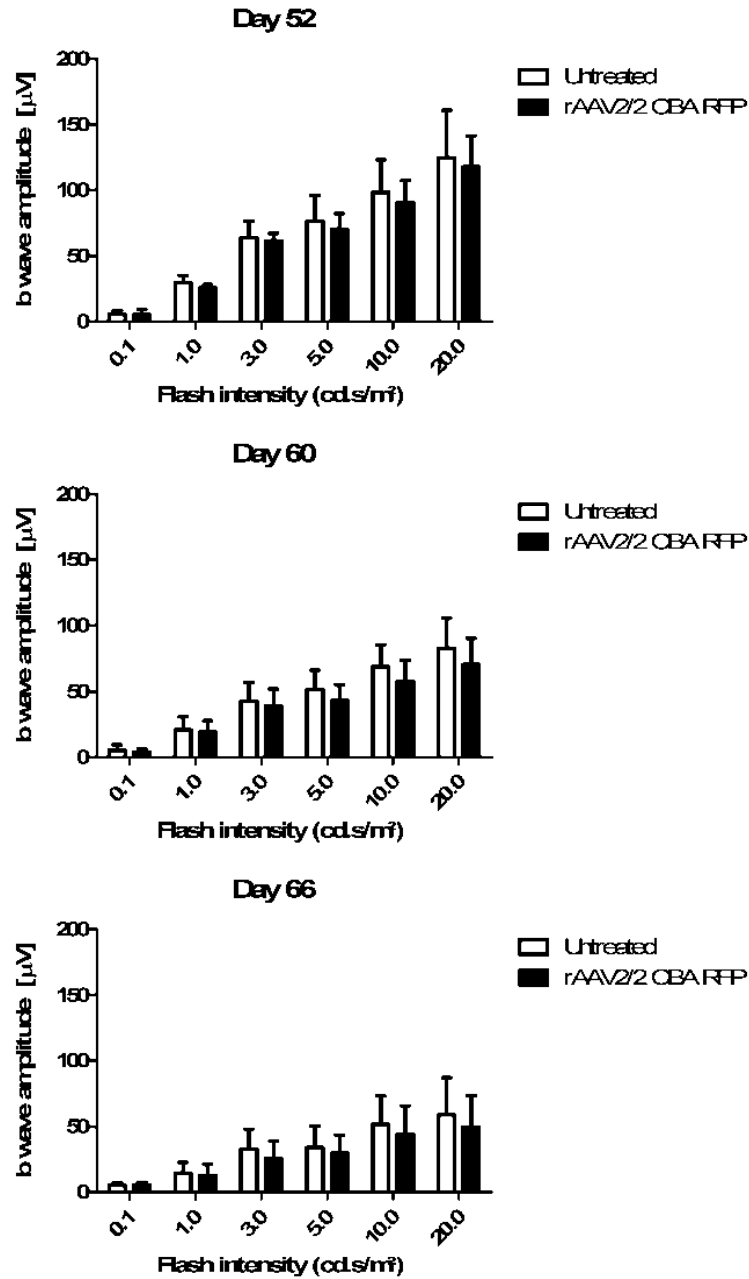


Figure 5-5 The effect of AAV2/2 CBA.RFP on cone function in the rhodopsin knockout cone-GFP mouse. ERG b-wave amplitudes, to a range of flash intensities, are shown in treated and fellow untreated eyes, for 3 timepoints during the degeneration. By day 73 the cone functional degeneration was complete in both eyes of this litter.

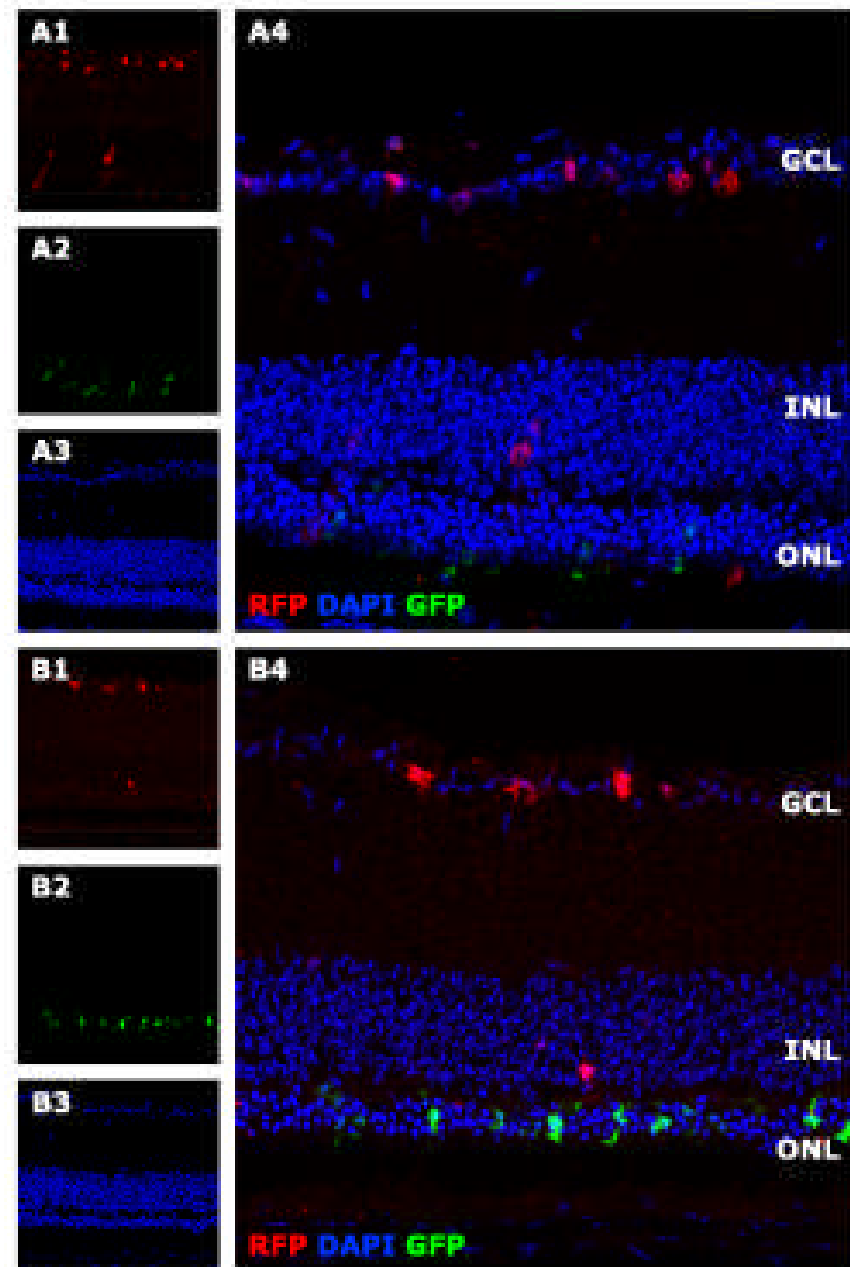


Figure 5-6 RFP expression in AV2/2 CBA.RFP treated eyes of the rhodopsin knockout cone-GFP mouse. Image sets A and B are from separate mice, sacrificed at day 73 of age. At this timepoint the retinal degeneration is well established such that ONL thickness is reduced and cone photoreceptors expressing GFP are dysmorphic. As shown in both image sets, the RFP is predominantly expressed in the ganglion cells. Less frequently cellular RFP expression is also seen within the INL. For each animal panels 1-3 show RFP, GFP and DAPI separately, and then panel 4 is a combined image.

5.3.2 Inner retinal GDNF expression and cone photoreceptor degeneration

To evaluate the effect of intra-vitreous rAAV2/2 cmv.gdnf, eyes were injected with GDNF or PBS at p10-p14, and compared to untreated fellow eyes. The volume of all injections was 1 μ l. Pooled b-wave amplitudes to a single flash intensity (10 cd.s/m²) in GDNF-, PBS- and un-treated eyes are shown in Figure 5-7. Analysis of variance with post-hoc bonferroni tests revealed cone function was dependent on time, but was not different in the GDNF-, PBS- and untreated groups. The course of functional degeneration was not altered in the GDNF treated eyes.

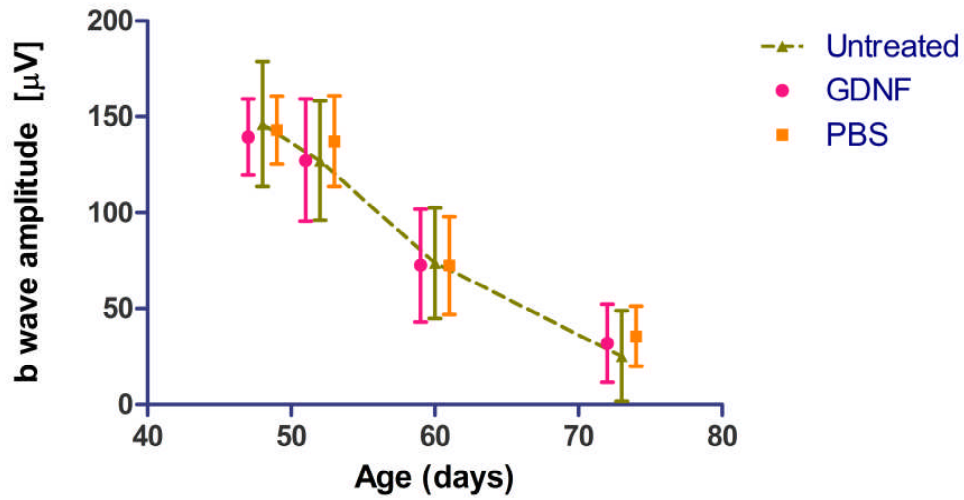


Figure 5-7 Cone function over time in treated and untreated eyes of the rhodopsin knockout cone-GFP mouse. Means \pm sd are shown for GDNF (n=20), PBS (n=12) and untreated (n=14) eyes.

To establish whether inner retinal Gdnf expression resulted in a relative preservation of cone cell bodies SLO imaging was used to quantify cones in GDNF-, PBS- and untreated eyes at weeks 11 and 17 of age (Figure 5-8).

As for the functional analysis analysis of variance (ANOVA) with post-hoc bonferroni tests revealed that cone numbers were dependent on the week of analysis ($p < 0.0001$) but not the intervention group ($p = 0.75$).

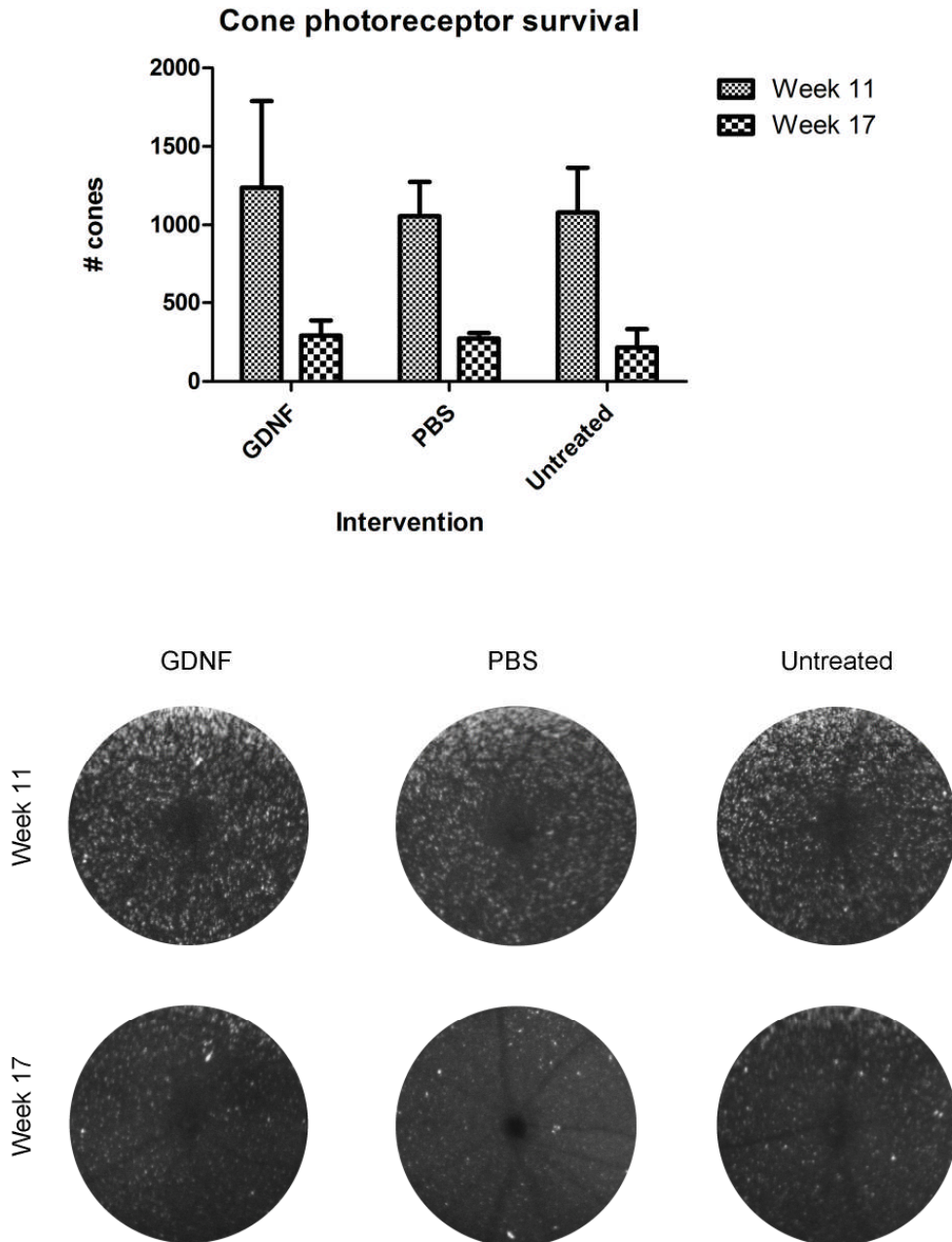


Figure 5-8 *In vivo* cone photoreceptor quantification in the rhodopsin knockout cone-GFP mouse. Mean counts (\pm sd) at weeks 11 and 17 are shown for GDNF (n=4), PBS (n=3) and untreated (n=3) eyes. Example SLO images are shown in the lower panel.

5.4 Discussion

These results show, with larger numbers of mice, that inner retinal expression of *Gdnf* had no effect on cone functional deterioration in the rhodopsin knockout cone-GFP mouse. This was demonstrated at 4 timepoints spanning the full timecourse of cone degeneration, and there was no evidence of either a transient or long-lasting effect. Analysis of cone numbers in the posterior pole of the eye, also at timepoints spanning the period of maximal cone photoreceptor loss, likewise demonstrated no treatment effect with inner-retinal *Gdnf* expression.

Previously an improvement in cone function has been reported following GDNF supplementation in the *rd* mouse.¹⁵⁹ In this study biodegradable microspheres that release approximately 10ng of GDNF per day were injected into the vitreous cavity of mice at PN11 of age. An improvement in averaged b-wave amplitude to 10 cds/m² stimuli under photopic conditions was reported at PN23. This time point is at the completion of the majority of rod photoreceptor death, but prior to the point of maximal cone photoreceptor loss.^{75;213} The b-wave amplitude in the GDNF loaded spheres was found to be approximately 30% higher than that in eyes treated with blank spheres, though background levels of noise in the example traces shown are also high. It was also found that function in the eyes treated with blank microspheres was approximately 40% higher than that in untreated eyes. The substantial ‘sham’ effect is likely to be due to the observed inflammatory response, and endogenous growth factor release, following the treatment intervention.³³⁷ The effect of GDNF on top of the sham effect was limited, and only demonstrated at a single timepoint. Furthermore, there was no corresponding cone-specific histological outcome measure to corroborate functional findings.

Repeated functional and histological assessments in the rhodopsin knockout cone-GFP mouse allow for a more robust assessment of cone neuroprotection. In this model, the functional and histological outcome measures were consistent in showing no cone neuroprotection mediated by GDNF expression in the inner retina, under the experimental conditions used.

The levels of GDNF protein expressed in these experiments in the rhodopsin knockout cone-GFP mouse were comparable to those achieved with the slow-release intra-vitreous microspheres used by Andieu-Soler in the rd mouse.¹⁵⁹ They are however likely to be lower than the levels of GDNF which were used to demonstrate rod photoreceptor neuroprotection in the TgN S334ter-4 rat model of retinal degeneration.¹⁶⁰ In these latter experiments photoreceptors and RPE cells were transduced following sub-retinal injection of an rAAV2/2.CBA.GDNF vector. Although absolute levels of the human GDNF transgene were not determined, it has been demonstrated previously that sub-retinal delivery of an rAAV2/2 vector leads to higher levels of transgene expression than is seen following intra-vitreous delivery of the same vector.³³¹ Further experiments were therefore performed to evaluate whether cone neuroprotection is achieved with GDNF expression at higher levels and in the outer retina.

Chapter 6 Outer-retinal GDNF gene therapy

6.1 Introduction

To study the effects of sustained and high levels of GDNF expression in the outer retina rAAV serotype 8 (rAAV2/8) was delivered to the sub-retinal space through trans-scleral sub-retinal injections.

The rAAV2/8 vector has a wide range of tissue tropisms, and exceptionally high rates of gene transfer.³³⁸⁻³⁴¹ In addition, the onset of transgene expression is particularly fast. Following sub-retinal injection of the vector into the mouse eye, Natkunarajah *et al.* demonstrated RPE cell transduction after just 24 hours and photoreceptor transduction by day 5.¹⁹⁴ By 7 weeks stable levels of transgene expression had been achieved that were higher than maximal levels achieved with either rAAV2/2 or rAAV2/5. rAAV2/2 and 2/5 were found to have higher tropism for RPE cells than for photoreceptors. In contrast, the rAAV2/8 transduced both cell types approximately equally. Sub-retinal injections of rAAV2/8.CMV.GDNF were therefore used to achieve much higher levels of transgene expression in the outer retina than would be achieved following intravitreal or subretinal delivery of the rAAV2/2.CMV.GDNF used in the previous chapter.^{194;330;331}

The disadvantage however with sub-retinal injections of viral vector is that there is inevitably iatrogenic damage to the retina. This was evident for example in the recent study showing successful treatment of *Aip1l*^{h/h} mice, where at the initial timepoint following sub-retinal injection ERG function was significantly worse in the treated eyes than in the untreated eyes.¹³³ This pattern reversed in time as the effects of photoreceptor rescue overcame the initial effects of trauma. Any

potential treatment must have benefits that not only outweigh negative effects induced by its delivery, but also result in an improvement over the natural history. In the following experiments sub-retinal rAAV2/8.CMV.GDNF is therefore compared with untreated fellow eyes, and control vector and PBS are used to control for the effects of sub-retinal injections in this murine model.

6.2 AAV2/8 mediated delivery of GDNF to the outer retina

6.2.1 Viral vector production and testing

rAAV2/8 was prepared using the pd10 CMV.GDNF plasmid tested previously *in vitro* and in the *in vivo* AAV2/2 experiments. Batch #1 was purified using the standard ion exchange technique discussed in the methods section, and a dot-blot examination determined the vector titre to be 5×10^{13} vg/ml (see supplementary data).

GDNF expression in eyes treated with the vector was confirmed with ELISA. Total protein and GDNF concentrations were measured in the treated and untreated eyes of 6 *Rho*^{-/-}*Opn.gfp* mice. Treated eyes were injected at p14 of age with superior and inferior injections of 1.5 µl of viral vector. Eyes were analysed in the late stages of degeneration (weeks 15-17 of age). GDNF levels were expressed relative to total protein to facilitate comparison between eyes, and between different studies.

As shown in Figure 6-1, for 5 of the 6 animals GDNF concentration in treated eyes was 2 log units higher than in untreated fellow eyes. In one animal (2654=4) there was no detectable GDNF in the treated eye despite total protein being approximately normal (data in supplementary data chapter). The absence of any detectable GDNF in this sample, in contrast to the untreated fellow eye, is indicative of an experimental error in the ELISA for this sample. Results from this eye have therefore been excluded from further analysis. Results from

animals culled at week 15 and week 17 of age are not significantly different to one another and have been pooled together for further analysis.

The mean GDNF concentration in uninjected eyes was 5.3 ± 5.2 pg/ μ g protein. The GDNF concentration in eyes transfected with rAAV2/8 CMV.GDNF was 1236.4 ± 546.9 pg/ μ g protein. This was over 232-fold higher than levels in untreated fellow eyes, and the difference is significantly different (unpaired t test, $p=0.0003$). At weeks 15 and 17 rod photoreceptor degeneration is largely complete and cone numbers are reduced. GDNF expression at these timepoints will therefore have been from RPE cells and residual cones, and is likely to have been considerably higher prior to rod photoreceptor degeneration. Nonetheless the 232-fold difference between treated and untreated fellow eyes in these AAV2/8 CMV.GDNF experiments can be compared to the results obtained following AAV2/2 CMV.GDNF where there was a 5 fold difference between treated and untreated eyes (Figure 5-4).

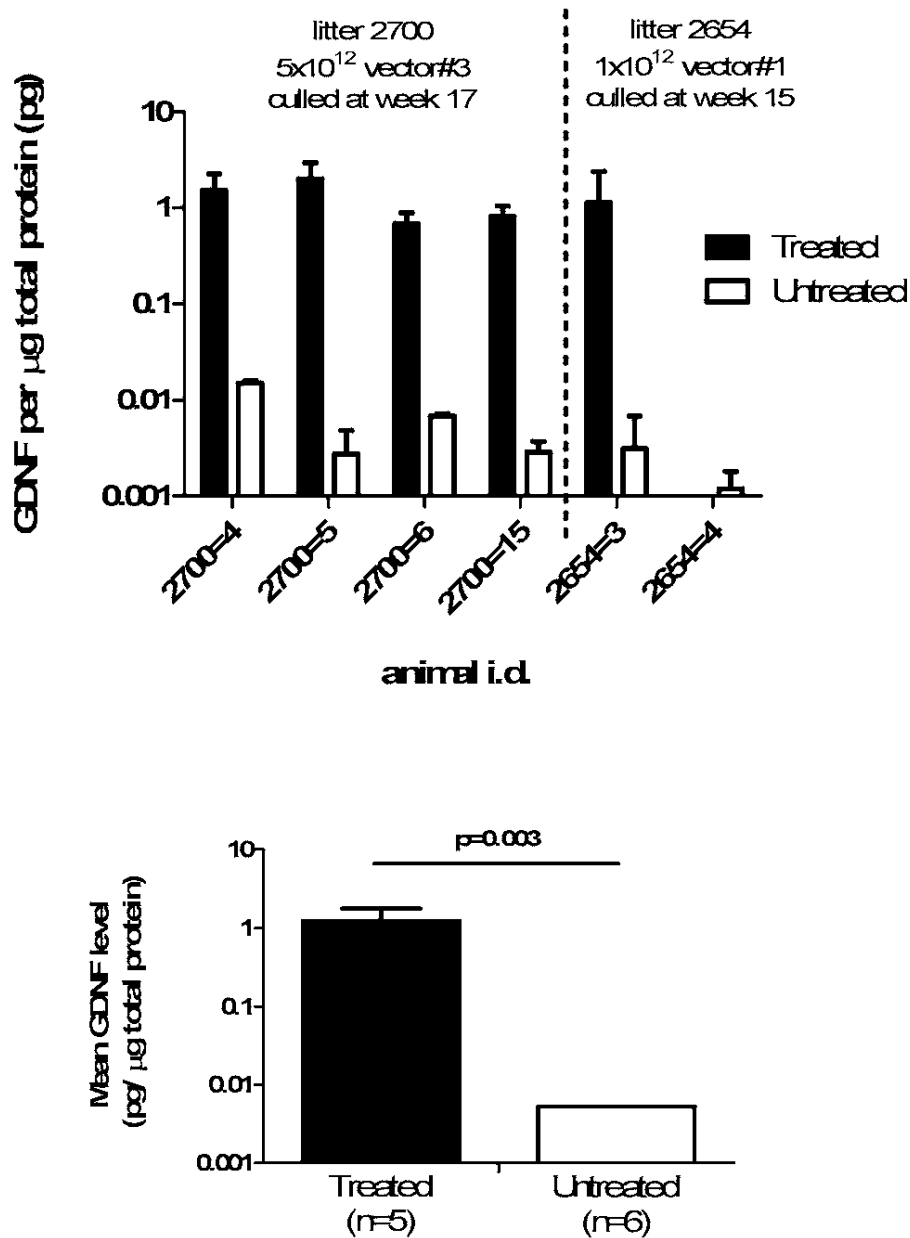


Figure 6-1 ELISA identifying [GDNF] after rAAV2/8 CMV.GDNF injection. Single eyes of *Rho^{-/-}Opn.gfp* mice were injected at p14 and eyes were enucleated at late stages of retinal degeneration. The results from two different treatment cohorts (using different vectors, doses and timepoints) are shown. Treated eyes are compared with untreated fellow eyes. Each eye was tested in triplicate at two different dilutions. The upper graph shows [GDNF] in treated and untreated eyes of 6 different animals. Means are shown in the lowermost graph. Error bars represent the standard deviation .

6.2.2 The effect of rAAV2/8.CMV.GDNF (batch#1) on cone degeneration.

Four *Rho*^{-/-}*Opn.gfp* mice were treated with superior and inferior injections of rAAV2/8.CMV.GDNF (batch#1) at P14. Evaluation of cone function at P52 and P60 demonstrated a marked reduction in function in the treated eyes. Pooled data, and inter-eye differences for individual animals, are shown in Figure 6-2. The mean reduction in cone function to a 10 cd.s/m² flash was 64% of the untreated value at day 52, increasing to 78% at day 60. In each of the 4 animals cone function was substantially diminished in the treated eyes, as compared to untreated fellow eyes.

rAAV2/8.CMV.GDNF treated eyes, and fellow untreated eyes, were enucleated at day 60. Eyes from two animals were used for confirmation of GDNF expression, whilst the remaining two pairs of eyes were used for histological analysis. ELISA confirmed high concentrations of GDNF protein (>30 ng/ml) in duplicate samples of both treated eyes, whilst levels in untreated fellow eyes were 5.4ng/ml (sd=0.6ng/ml). Cryosections revealed ONL thinning in treated eyes, as compared to the untreated fellow eyes (Figure 6-3). ONL thinning was apparent across the entire retinal cross-section, and not confined to the point at which the injection needle had entered the sub-retinal space. In addition in the treated eyes the gfp-labelled cones were dysmorphic with evidence of mis-localisation of the cone photoreceptor bodies within the ONL. There were also sub-retinal deposits of GFP protein, which may be due to degenerating cones being phagocytosed by inflammatory or RPE cells in the subretinal space. In contrast, in the untreated eye at day 60 the normal cone photoreceptor morphology is still evident and the ONL is thicker. These changes indicate that retinal degeneration was more advanced in the treated eyes, which is in keeping with the ERG data. To help elucidate the cause of this negative and presumed toxic response further experiments were performed with sub-retinal injection of control vector and PBS, in addition to a titration series of the vector used and an evaluation of vector purity.

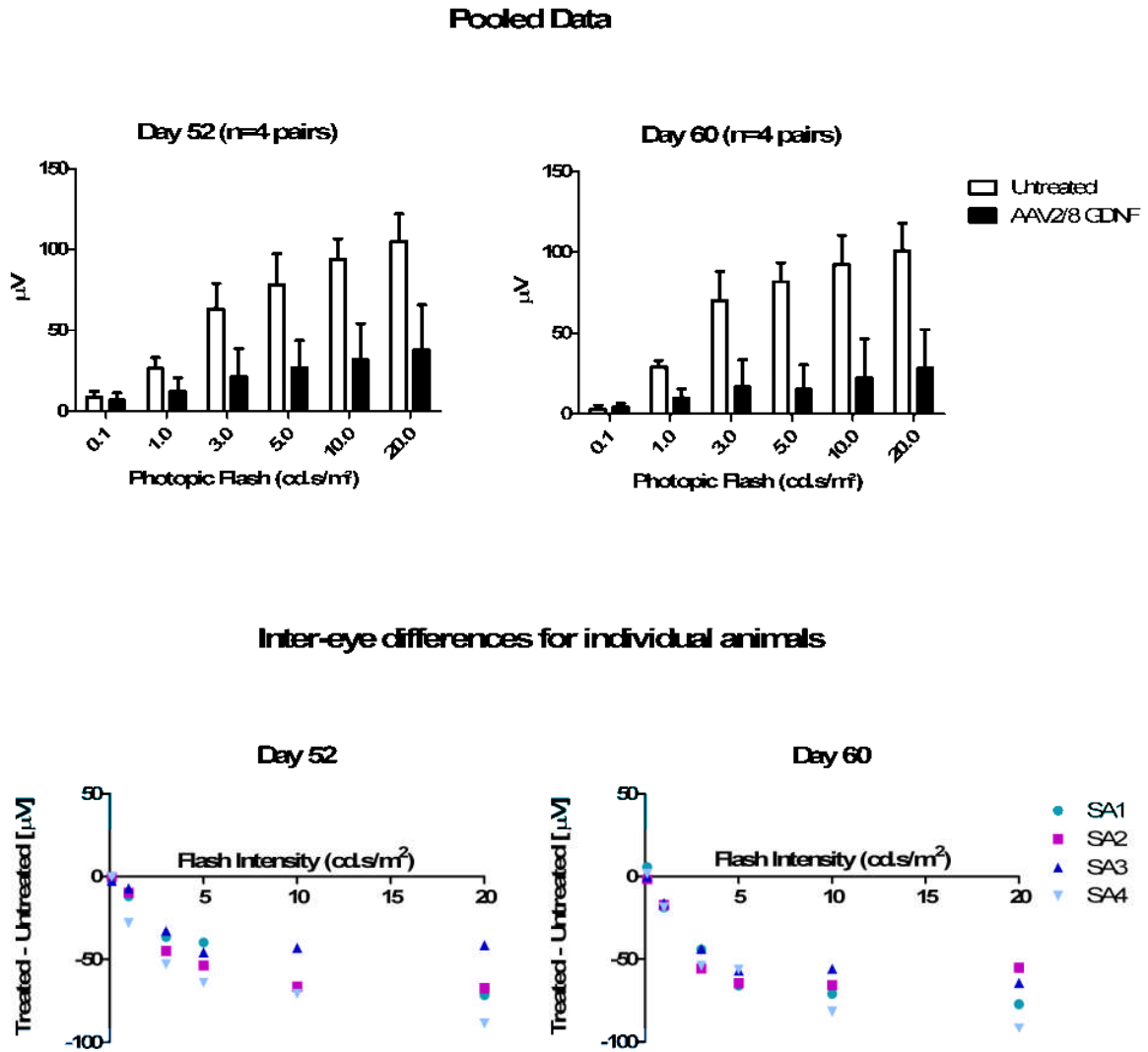


Figure 6-2 Assessment of cone function following treatment with rAAV2/8.CMV.GDNF (batch#1). ERG assessments were performed at day 52 and day 60 of age. b-wave amplitudes to a series of flash intensities in photopic conditions are presented. In the upper row mean values in the treated and fellow untreated eyes are shown for the 2 time-points, and for each flash intensity examined. In the lower row the difference between treated and untreated eyes is shown for individual mice (labelled SA1-4) at day 52 and day 60.

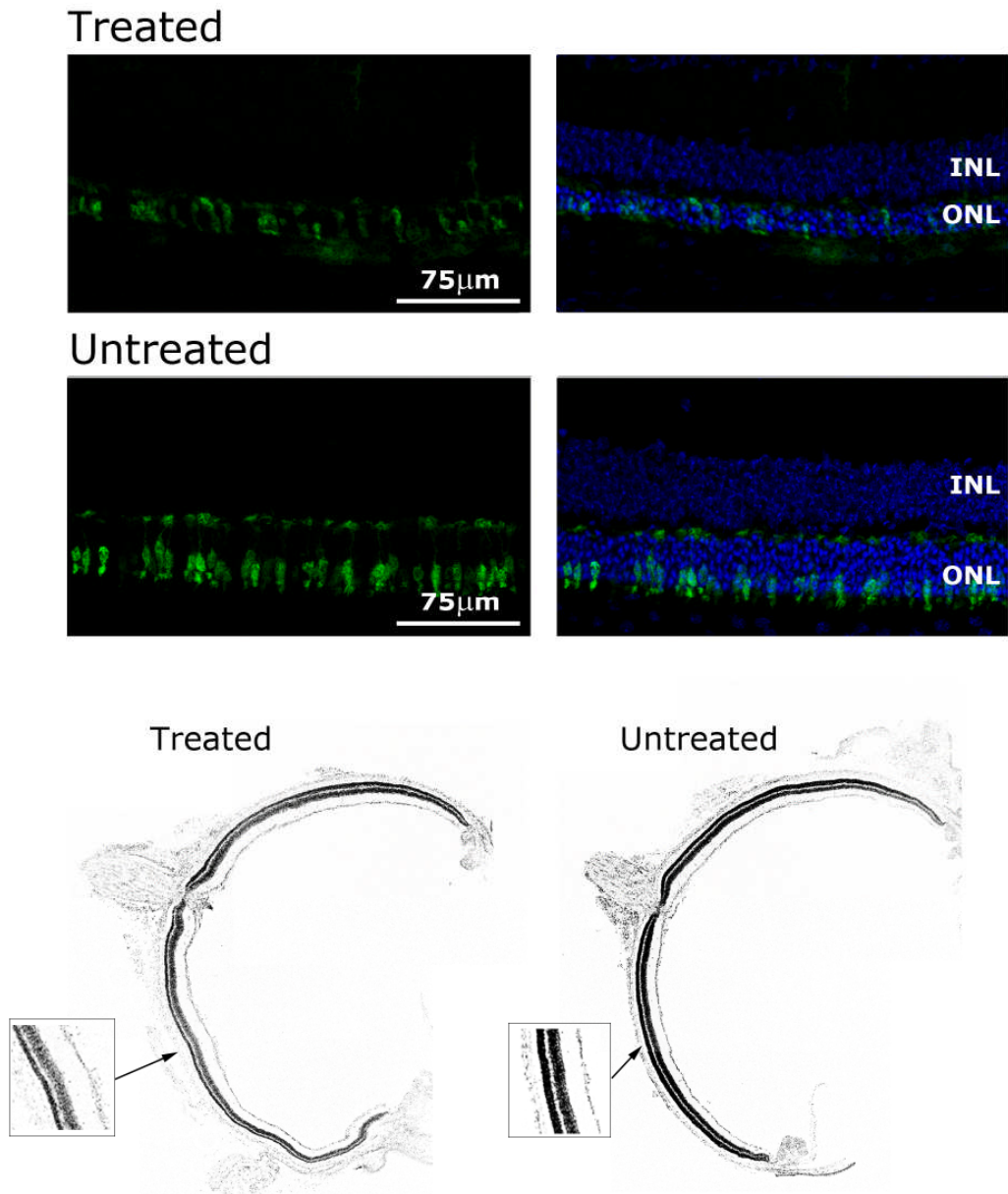


Figure 6-3 Retinal morphology in the eyes of *Rho*^{-/-}*Opn.gfp* treated with AAV2/8.CMV.GDNF (batch#1) compared to untreated fellow eyes. Eyes were harvested at day 60. The GFP labelled cones are dysmorphic in the treated eyes as compared to in the untreated fellow eyes. In addition the ONL is reduced in thickness in the treated eyes as compared to a corresponding section from the untreated fellow eye.

6.2.3 Sub-retinal injection in degenerating retina

Sub-retinal injections in patients undergoing gene therapy are generally performed following a vitrectomy and via a fine (41 gauge) trans-retinal needle, the tip of which is passed from the vitreous cavity through the retinal layers and into the sub-retinal space. With gentle fluid pressure the retina separates from neighbouring RPE cells. The procedure used here in mice, described in detail in the methods section, instead uses the trans-scleral approach to access the sub-retinal space. A 34 gauge needle is passed tangentially through the tough sclera, and once the needle tip is seen to be penetrating the RPE it is advanced further with gentle injection of fluid to form a bullous retinal detachment. In patients treated with *RPE65* gene therapy the sub-retinal fluid is seen to be absorbed rapidly in the first 2-3 days following surgery.¹⁹⁹ The detachments induced here in mice affect a larger portion of the retina, but the retina reattaches relatively readily and more quickly in mice which has been one of the major challenges for researchers using murine models of retinal detachment.³⁴² Observed differences in speed with which the retina reattaches in human and mouse eyes may relate to differences in the relative size of the vitreous body. The vitreous in humans is important in the pathophysiology of retinal detachments and makes up a large portion of the ocular volume; in mouse eyes the solid crystalline lens occupies a much larger portion of the eye, and the vitreous cavity is a relatively small.

In these GDNF experiments large retinal detachments are formed in young mice with an inherited retinal degeneration. Cone photoreceptor outcome measures are then assessed, which is of note in view of studies indicating that cone photoreceptors are particularly vulnerable to the effects of retinal detachment.³⁴³⁻³⁴⁶ Experiments were therefore performed to control for the effect of sub-retinal injections of vector into this mouse model.

An rAAV2/8 control vector was prepared using the same protocols and in the same laboratory as the GDNF vector, but using a similarly-sized pd10 null plasmid which lacked a start codon (Figure 6-4). The titre of the control vector

was 4.2×10^{12} vg/ml. A western blot performed on transfected cells and animals treated with the control vector confirmed no transgene expression (data in supplementary data chapter).

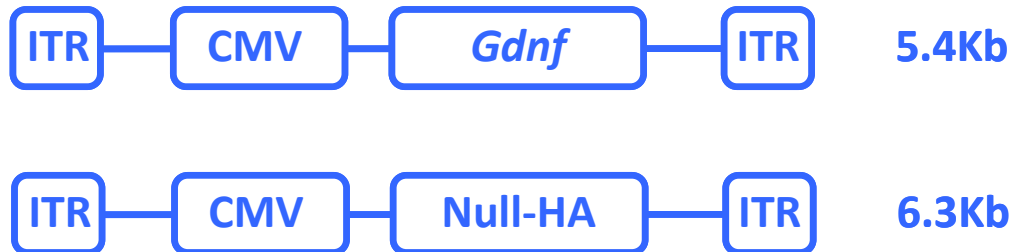


Figure 6-4 GDNF and null plasmids. Both plasmids contained a CMV promoter. The null plasmid lacks an ATG start codon and was non-protein producing. This was confirmed by western blots to look for expression of a haemagglutinin (HA) tag fused with the null sequence (see supplementary data).

The advantage of using this control vector rather than just PBS is that it, like the *Gdnf* vector, will transfect the photoreceptors and RPE cells, be transported to the nucleus, and will initiate mRNA transcription. There will however be no transgene translation in control vector transfected cells. The control vector was produced and purified using the same standardised protocols as the GDNF vector, and so they will both have broadly the same chemical properties. To examine whether injections of viral vectors have an impact over and above the mechanical effects of forming a retinal detachment, control vector injections were compared to PBS injections.

In order to determine the effects of sub-retinal rAAV2/8 injections 6 *Rho*^{-/-} *Opn.gfp* mice were injected with control vector to one eye; fellow eyes were used as untreated controls for comparison. A further 4 animals received bilateral injections with control vector to one eye and PBS to the other. All injections were performed at p14 of age, and involved superior and inferior injections with

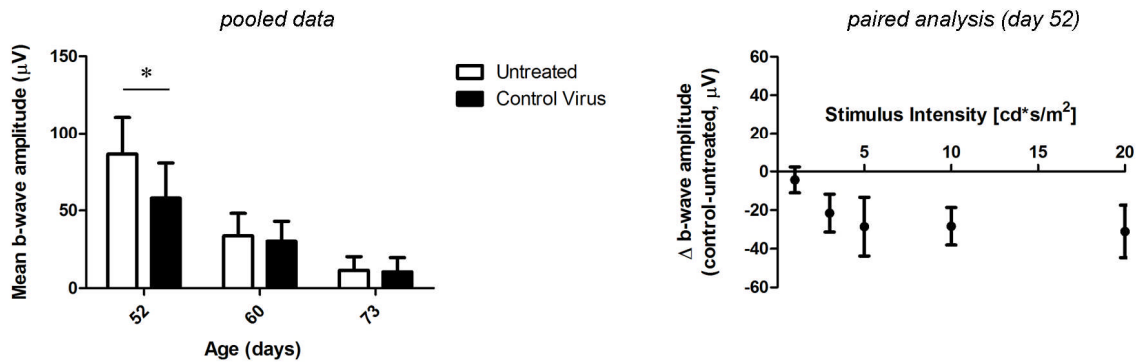
a volume of 1.5 μ l. Statistical analysis was performed using two-way analysis of variance (ANOVA) and post-hoc Bonferroni tests.

Cone function was significantly reduced in the control vector treated eyes, as compared to fellow untreated eyes at day 52 ($p < 0.05$) (Figure 6-5). This was evident at all flash intensities tested, except for with the 1cd.s/m² flash to which the responses were small in either eye. At days 60 and 73 inter-eye differences were not significant. The reduction in function to a 10cd.s/m² flash at day 52 was 33.8% of the untreated value (sd=9.8%).

The finding that the 33.8% reduction in cone function was not sustained at the day 60 and day 73 examinations indicates that the degeneration was not accelerated in the treated eyes, but rather there is likely to have been some recovery such that responses in treated and untreated eyes were no longer significantly different at later timepoints. The caveat however is that these mice have a relatively fast degeneration and the reduction in response amplitude with time makes it progressively less likely that inter-eye differences will be detected.

Likewise, in the mice treated with control vector in one eye and PBS in the other, there was an inter-eye difference evident at day 52 only. The reduction in function with control vector at this timepoint was 31.5% (sd 21.1%). This could be due to chemical constituents of the vector preparation compromising retinal function, or a consequence of vector transduction in stressed and degenerating cone photoreceptors.

Sub-retinal control virus vs untreated (n=6)



Sub-retinal control virus vs PBS (n=4)

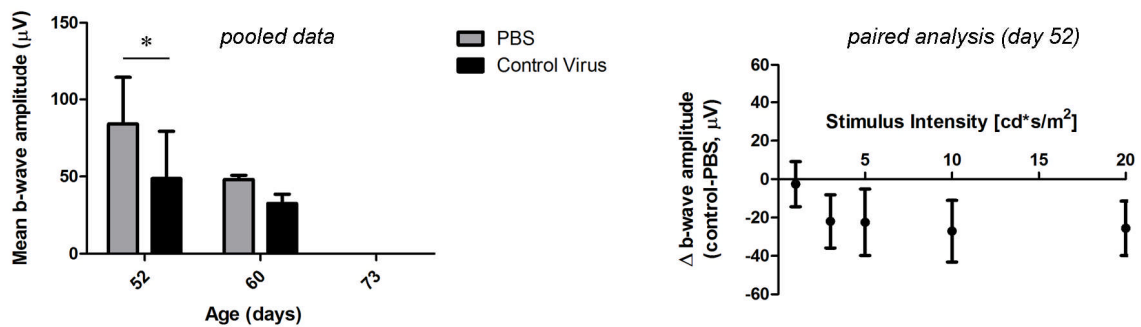


Figure 6-5 A comparison of cone function in control vector or PBS treated and untreated eyes. In the graphs to the left pooled data is presented for b-wave amplitudes in response to a $10\text{cd}\cdot\text{s}/\text{m}^2$ flash stimulus. Statistical analysis was performed using 2 way ANOVA and Bonferroni post-hoc tests. Significance ($p < 0.05$) is highlighted an asterix (*). In the graphs to the right the mean and standard deviation of inter-eye differences are presented across the range of stimuli used, at the day 52 timepoint. These graphs show that although the pooled data is presented for 1 stimulus intensity only, similar differences were found for the 4 brightest flash intensities tested. At the 4 brightest flash intensities examined cone function was worse in control vector treated eyes than in either untreated or PBS treated fellow eyes.

6.2.4 Sub-retinal injection in wild-type retina

To test whether these substantial detrimental effects of the control vector were specific to the *Rho^{-/-}Opn.gfp* mouse and degenerating cones, subretinal injections were also performed in wild type mice. Wild type mice were assigned to one of three treatment groups in order to compare PBS injections in one eye to the untreated fellow eye, control vector injections in one eye to the untreated fellow eye, or PBS injections in one eye to control vector injections in the fellow eye. In each group injections were performed in wild type mice at p14 of age, and consisted of superior and inferior injections of 1.5 μ l each. Functional ERG assessments were performed at day 52 of age.

As indicated by the photopic traces in Figure 6-6 cone function was similarly diminished in the PBS and control vector treated eyes in comparison with contralateral untreated eyes. The reduction in cone function with PBS and control vector injections to a 10cd.s/m² flash was 28.1% (sd 9.9) and 23.3 % (sd 4.6) respectively. Comparison of the percentage reductions revealed that the effect of control vector injections was the same for cones in wild type retina as in degenerating retina ($p(\text{difference})=0.37$, $n=6$ degenerating; $n=5$ wildtypes). The effect of control vector over and above that of PBS in degenerating retina, was not seen in wild type mice. In wild type mice there was no difference between control vector and contralateral PBS treated eyes.

Stimuli of low flash intensity in scotopic conditions elicit a rod-specific response, but at higher flash intensities the response is mediated by both rods and cones. In the dark adapted rhodopsin knockout mouse the flash intensity threshold to induce cone function (as defined by a 5 μ V b-wave) is 0.085 cd.sec/m².²⁴² If one assumes the cone threshold is the same in the wild type as in the rhodopsin knockout then the first 4 flash intensities in the scotopic series in Figure 6-6 (0.0005, 0.003, 0.007 and 0.03 cd.s/m²) are rod specific. At the 0.007 and 0.03 cd.s/m² intensities the mean b-wave amplitude is lower in the PBS or control vector treated eyes than in untreated fellow eyes. There is no significant

difference in rod function between PBS and control vector treated eyes of the same animal.

The greatest reduction in rod function following control vector injections was at 0.007 cd.s/m², and in this cohort of 5 animals was a reduction of 31.7% (sd 28.4) of b-wave amplitude in the untreated eye. There is no evidence of sub-retinal injections having a significantly different effect on rods or cones in these results.

These experiments therefore determined that sub-retinal injections cause a decrease in rod and cone function at 5 weeks following injection. No difference in magnitude of effect was found between rod or cone photoreceptors, or between injections of control vector or PBS in wild type eyes. In the *Rho*^{-/-} *Opn.gfp* eyes there was evidence of the control vector having a greater detrimental effect than PBS alone in 4 animals. This has not been repeated or investigated further. However, in both wild types and rhodopsin knockout cone-GFP eyes sub-retinal injections resulted in approximately a 30% reduction in cone function, as compared to fellow untreated eyes at 5 weeks post injection. This provides a baseline for comparison with other vector preparations, and suggests that the cones in the degenerating rhodopsin knockout cone-GFP retina are not significantly more sensitive to the effects of retinal detachment, than those in age-matched wild type mice.

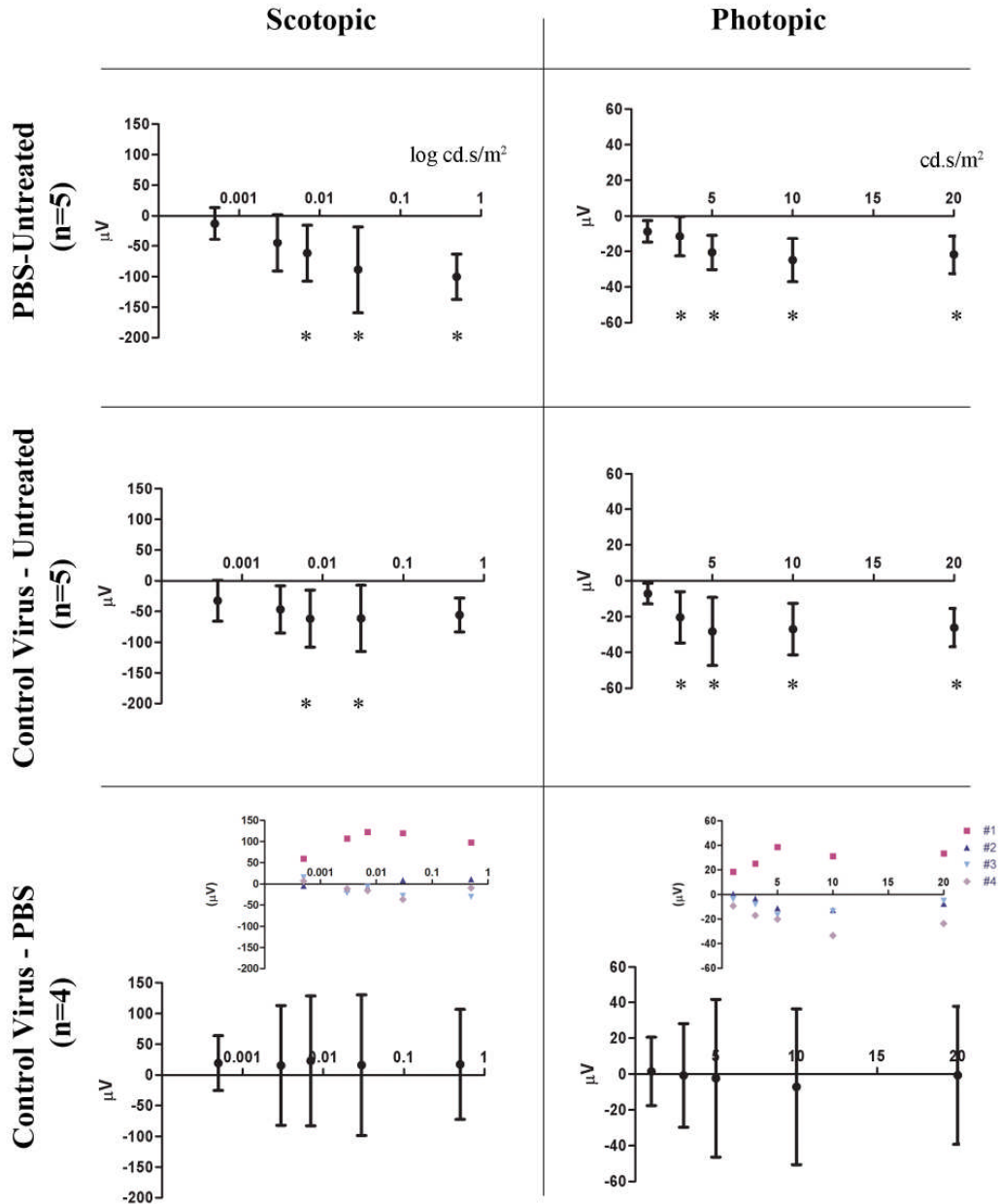


Figure 6-6 The effect of sub-retinal injections on rod and cone function in the wild type mouse. Mice were treated with PBS to 1 eye only, control vector to 1 eye only or control vector to 1 eye and PBS to the other. Mean inter-eye differences in b-wave amplitudes to scotopic and photopic ERG protocols are shown in each graph. 95% confidence intervals are shown by the error bars. Significance ($p < 0.05$) is indicated with an asterisk (*) and was tested for using ANOVA analysis with the Bonferroni correction for multiple analyses. Individual responses for the 4 animals in the control vector-PBS groups are shown in the inset graphs, with coloured symbols for each animal.

6.2.5 Titration series of rAAV2/8.CMV.GDNF (batch#1)

Sub-retinal injections of a dilution series of the rAAV2/8 CMV.GDNF (batch#1) were performed in *Rho-/-Opn.gfp* mice. These experiments were carried out in order to determine whether the toxic effect was dependent on the concentration of the vector administered into the sub-retinal space, and to enable comparison with the control vector in the same animal model.

Viral dilutions were performed in ultrapure PBS-MK, which is the same solution as is used to elute purified rAAV2/8 in the standard production protocols. The volume of sub-retinal injections was identical in all groups (superior and inferior injections of 1.5 μ l of viral vector). All injections were performed at p14 of age, and for comparisons between groups cone function was assessed to a 10 cds/m² flash at p52.

At each viral vector concentration used treatment had a negative effect on cone function (Figure 6-7). The toxic effect was diminished with dilution of the vector. Injections of 1x10¹² and 5x10¹² viral vector lead to a smaller toxic effect on cone function than injections of the undiluted 5x10¹³ preparation (p=0.019 and p=0.021 respectively, unpaired t-test). Differences between the 1x10¹² and 5x10¹² preparations were not significant.

The 5x10¹² CMV.GDNF (batch#1) and control viral vector preparations were effectively titre matched given the sensitivity of the dot-blot assay used. Comparison of the effect of these two preparations on cone function revealed no difference (p=0.37, unpaired t-test) (Figure 6-8)

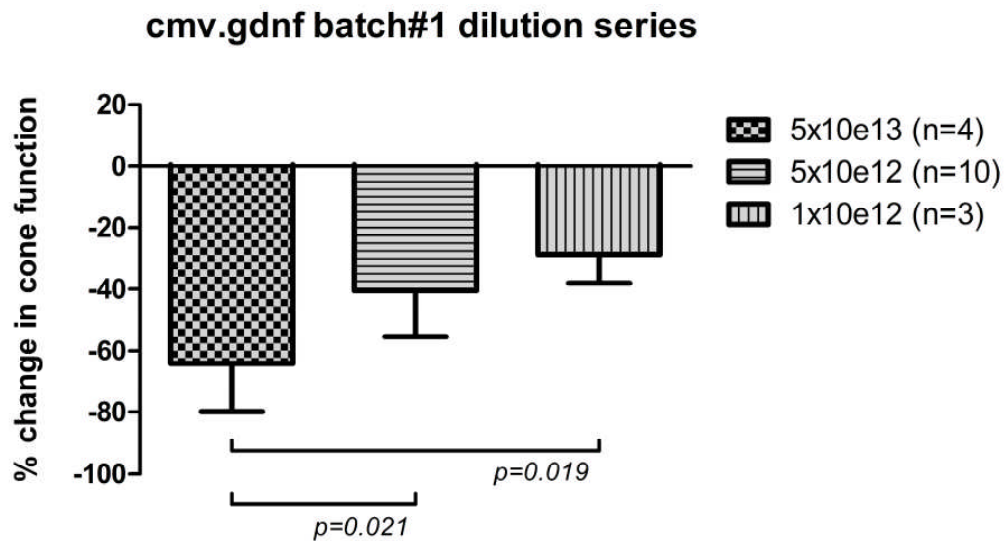


Figure 6-7 Dilution series of rAAV2/8 CMV.GDNF (batch#1). The difference in b-wave amplitudes, to a photopic 10 cd.s/m² flash stimulus, between the treated and untreated eyes of individual animals was calculated, and expressed as a percentage of the untreated value; positive values indicate a positive treatment effect, whilst conversely a negative difference indicates that function was greater in the untreated eye. Means for each treatment group are shown, with the error bar showing standard deviation.

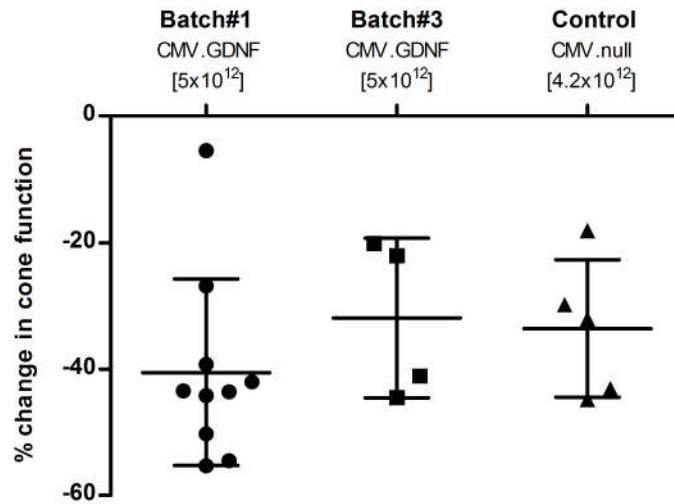


Figure 6-8 Comparison of the effects of titre matched rAAV.CMV.GDNF and control vector preparations on cone function. Percentage differences in cone function (b-wave amplitude to a 10 cd.s/m² flash at P52) between treated and untreated eyes of individual mice are shown for CMV.GDNF-batch#1 (n=10), CMV.GDNF-batch#3 (n=4) and control vector treated (n=5) mice. Means for each treatment group are shown with horizontal lines, and the error bars indicated the standard deviations.

6.2.6 Modified Vector Purification Protocol: Phase Separation

The finding that vector titre correlated with the magnitude of the functional deficit following sub-retinal injection could be explained by a dilutable constituent of the vector preparation having a toxic effect. The rAAV2/8 production method used for the rAAV.CMV.GDNF (batch#1) and control vector has been used previously to successfully rescue rod photoreceptors in the *Aipl1* hypomorphic and knockout mice using gene replacement therapy.¹³³ Any toxic effects in those preparations was rapidly outweighed by beneficial effects of the gene replacement constructs used, and so potentially the fact that toxicity was evident with the CMV.GDNF vector may reflect the absence of a strong therapeutic effect in the *Rho-/-Opn.gfp* mouse. Alternatively, iatrogenic damage to cone photoreceptors may be much more demanding to overcome. Ongoing work by Dr. Carvalho and Professor Ali has however demonstrated cone photoreceptor rescue in the CNGB3 mouse model of retinal degeneration (personal communication) using the same rAAV2/8 preparation protocols and agents; this has been achieved with a gene replacement construct. Some treated animals have been found to gain a substantial improvement in cone function but of note in others the effect was not seen and there was evidence of significant damage following the sub-retinal injections.

With the anion exchange column method of vector purification used here for rAAV2/8 purification there is the potential for contaminant proteins in the 293T cell lysate to have a similar affinity to the ion exchange column, and so to be co-eluted along with the rAAV; this potential source of toxicity has been reported previously with heparin-based affinity chromatography columns.³⁴⁷ A further vector purification step was therefore introduced in an attempt to separate vector from co-eluted components of the cell culture medium.

Chahal et al. used a two-phase extraction technique to demonstrate that purified rAAV2/2 could be selectively partitioned into the aqueous phase when added to a mixture of the high molecular weight polymer polyethylene glycol (PEG-4000) with ammonium sulphate.³⁴⁸ Analogous techniques have been used previously to

separate other types of viral vector (including adenoviral and retroviral vectors) from cellular and protein contaminants. With time the mixture separates into 2 phases with a lowermost aqueous phase, and an uppermost polymer based phase. Chahal et al. demonstrated that 100% of added AAV could be recovered from the aqueous phase, whilst many cell or medium components appeared to be partitioned to the hydrophobic supernatant. Their production and purification protocol for AAV2 produced in insect cells resulted in high purity vector (as examined with SDS-PAGE and silver stains). However, this technique had not been used previously in combination with the AAV2/8 purification protocols, and for rAAV produced using co-infection of 293T cell cultures.

To investigate whether addition of a two-phase extraction step improved rAAV2/8 purity in combination with existing 2/8 purification protocols¹³³, a 40 plate preparation of 293T cells was transfected with the CMV.GDNF plasmid. Harvested cells were sub-divided into 2 equally sized aliquots. One aliquot was purified using the standard protocol (batch#2), and the other was prepared in parallel incorporating the two-phase separation step (batch#3) (Figure 6-9). The latter step involved cell lysate being added to a mixture of ammonium sulphate and 20% PEG, after repeated centrifugation and passage through a 0.22 μm filter. The mixture was left to partition into aqueous and hydrophobic phases before the vector-containing aqueous phase was used for further purification. The hydrophobic phase was discarded.

The titre of both vector preparations was examined on the same dot-blot to facilitate comparison. Both preparations were of high titre. Vector purified with the two phase separation had a genomic titre of 1.5×10^{13} vg/ml. The identical aliquot of harvested cells purified using the standard protocol produced vector with a titre of 1.1×10^{13} vg/ml. This equates to a titre difference of approximately 30%. A difference of this relatively small magnitude is unlikely to be of functional significance.

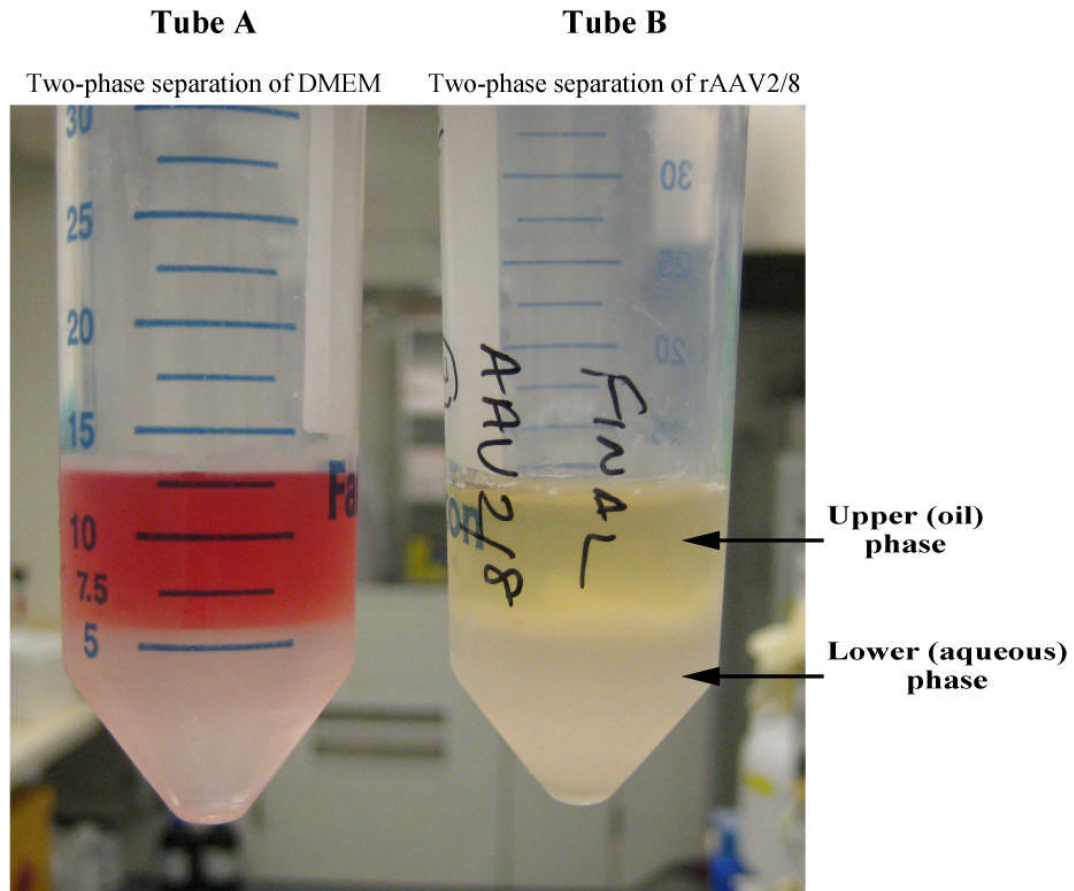


Figure 6-9 Two-phase separation. 5 mls of a 1M ammonium sulphate and 20% PEG4000 mix have been used to form a hydrophobic upper phase, and a hydrophilic lower phase in each of the 2 falcon tubes shown. In tube A 5mls of DMEM medium has been added to this mix to aid illustration of the 2 phases. An equal volume of lysate from transfected 293T cells, from which cell debris had been removed by repeated centrifugation and passage through fine filters, was added to tube B. The upper phase, supernatant, is hydrophobic and contains proteins and cellular contaminants. The vector is partitioned in the lower aqueous phase.

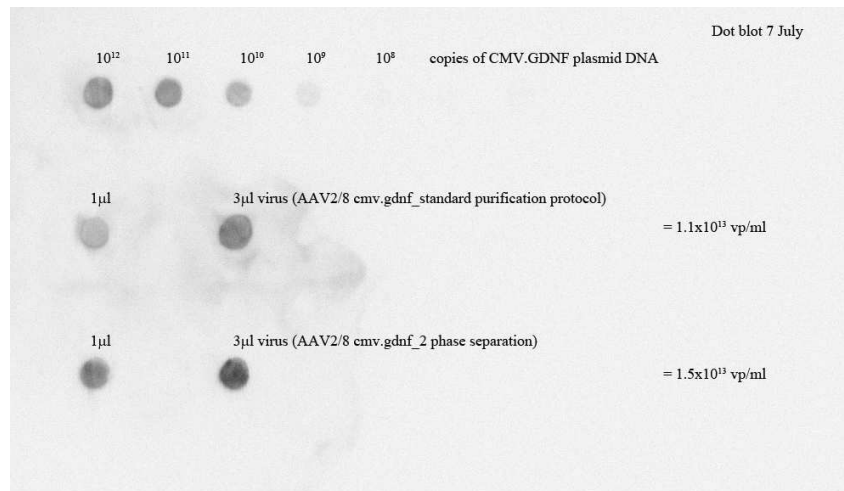


Figure 6-10 Genomic titres of the CMV.GDNF vector made with and without two phase separation. Vector purified with and without the two phase separation is of a similar high genomic titre (1.5×10^{13} and 1.1×10^{13} respectively).

To examine the protein content of each vector the constituent proteins were separated with sodium dodecyl sulphate-polyacrylamide gel electrophoresis (SDS-PAGE), and then visualised with a fluorescent protein stain (Spyro Ruby protein stain, Invitrogen). 1 and 3 µl samples of each vector (batch #2 and #3 of CMV.GDNF) were titre-matched and run in parallel. The results are shown in (Figure 6-11). As expected the 3 µl sample of each vector has identical but stronger protein bands than the corresponding 1 µl sample. In each lane there are 3 protein bands that are considerably stronger than any of the others. These are seen at 87, 72 and 62 KD in all the samples and correspond to the 3 protein bands of the AAV-2 capsid, VP1, VP2 and VP3 respectively.^{230;349} Furthermore the relative densities of the VP1, VP2 and VP3 bands are in keeping with the expected ratio of 1:1:10.

In the vector sample purified without phase separation there are multiple additional protein bands, that are either not evident at all, or only to a lesser extent, in the sample purified with phase separation. Those smaller than the VP1-3 bands may be due to degraded capsid proteins. In the standard purification sample there is also evidence of protein of greater than 90 KD; this is

a contaminant that is not normally seen in the preparation of rAAV2 based vectors; it is not in keeping with any of the capsid proteins. The VP1-3 bands are themselves also stronger in the vector sample purified without phase separation, despite the titre-matching. This could be due to incomplete or damaged capsids or loose hydrophobic proteins being removed in the partitioning procedure.

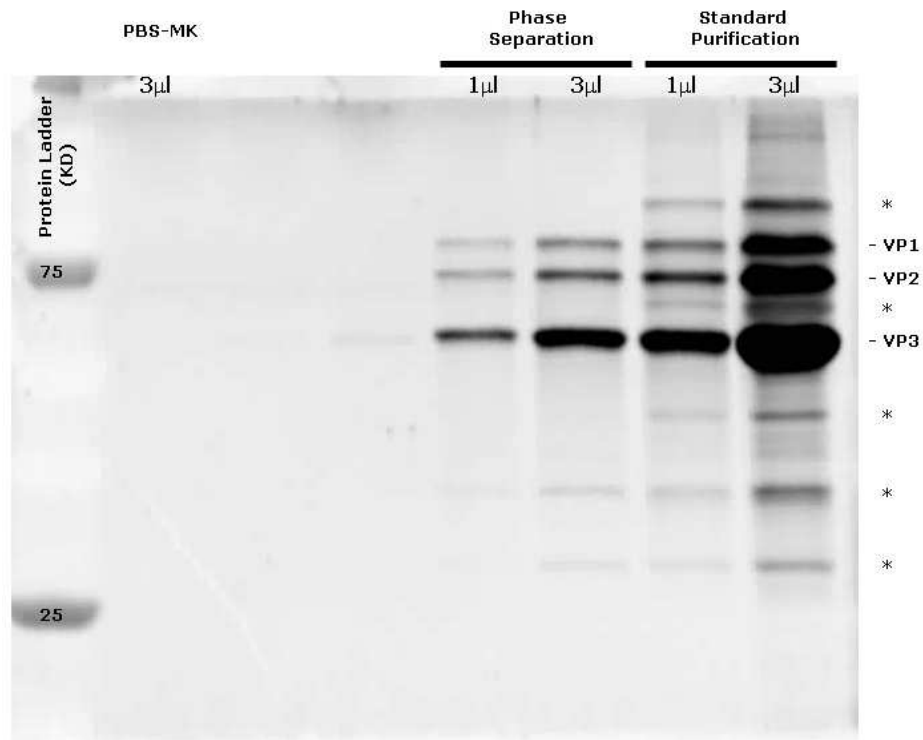


Figure 6-11 SDS-PAGE separation and protein staining of vector samples. Identical aliquots of rAAV2/8.CMV.GDNF were purified with and without an additional phase separation step. 1 and 3µl titre-matched samples of each vector are analysed here, alongside a sample of the buffer in which the vectors were eluted, PBS-MK. A commercial protein ladder was also run in conjunction to allow sizing of the protein bands. The AAV-2 capsid proteins VP1, VP2 and VP3 are seen in each of the vector samples, but not in the PBS-MK. These bands are stronger in the 3µl than in the corresponding 1µl samples for each vector preparation. Additional protein bands (*) are particularly evident in the vector sample prepared without phase separation. Some of the same contaminant bands are also evident in the phase separation sample, but to a lesser extent.

Electron microscopy (EM) was performed using the negative stain uranyl acetate to enhance contrast. This stain binds to the edge of protein matter but is excluded from the space occupied by it. Low protein content areas appear dark on the EM image due to the presence of stain which scatters incident electrons. In contrast electrons pass relatively unimpeded through areas of high protein content resulting in bright areas on the image formed.

The electron micrographs of both samples show non-enveloped icosahedral particles with a diameter of approximately 20-25 nm (Figure 6-12). This is as expected for a vector derived from *Parvoviridae* family virions.^{232;350} In both samples a mixture of clear and dark centred particles are seen, which correspond to full and empty capsids respectively. These are shown in the enlargement within Figure 6-12 and counted in Figure 6-13. Between 83 and 86% of vector capsids in these two samples were devoid of genome and hence non-functional. These figures are as expected for experimentally produced viral vectors.³⁵¹

Comparison of the electron micrographs from the two vector samples reveals less background staining in the phase separation sample and a relative increase in the contrast between vector particles and the background medium rendering the particles more defined. These are markers of a lower protein content in the vector carrier solution.

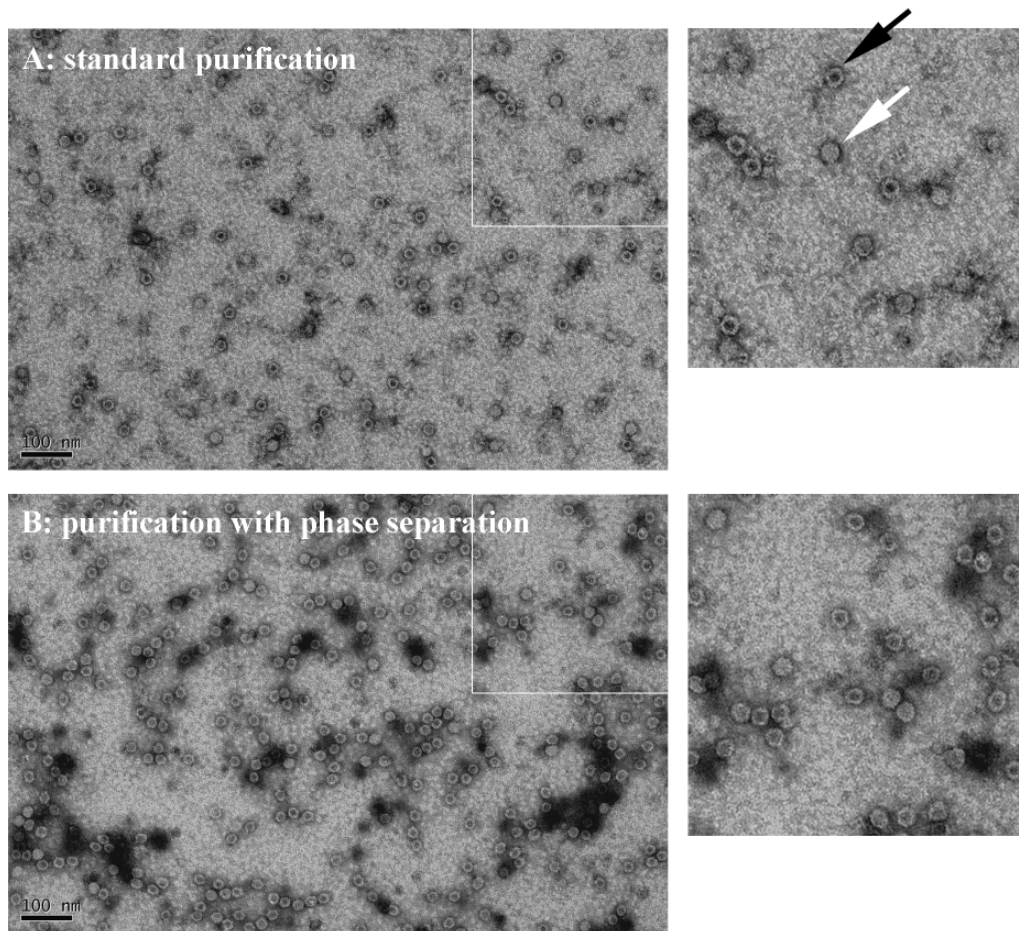
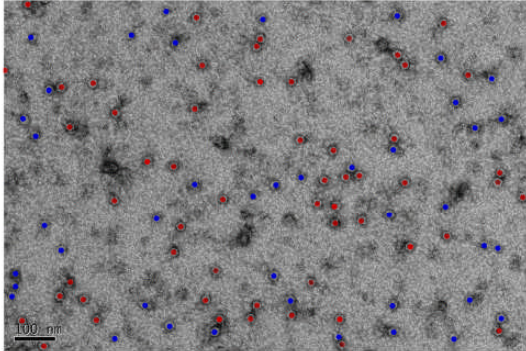


Figure 6-12 Transmission electron micrographs of rAAV2/8 purified with and without two-phase separation. Titre-matched samples of each vector were negatively stained with 4% uranyl acetate solution prior to imaging. Digital enlargements (1.7X) are shown alongside the main images to show morphological detail. In both samples a mixture of full and empty vector particles are seen (as indicated by white and black arrows respectively). Vector particles containing genome DNA have a homogenous grey centre, whilst empty particles have a black centre. The black patches in both images, which overlie some of the vector particles, are artefacts.

Standard purification



Phase separation

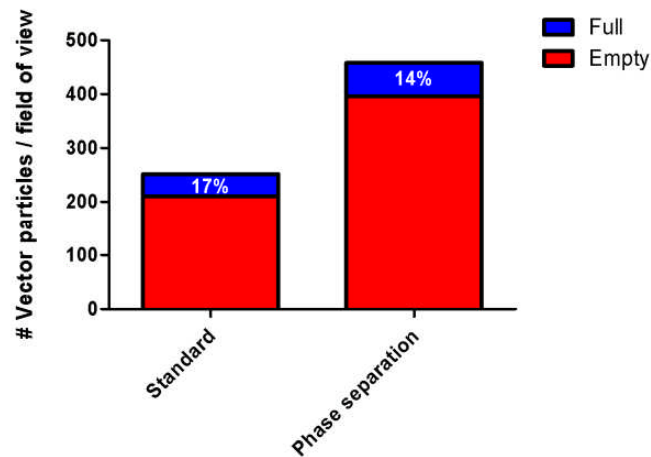
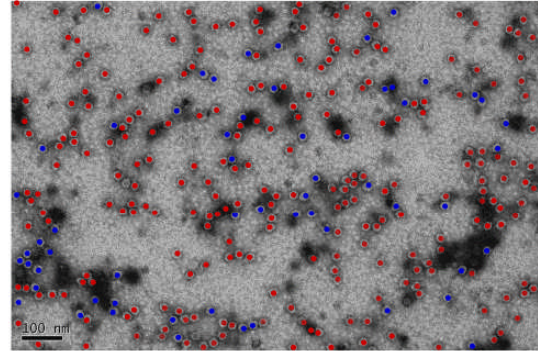


Figure 6-13 Genome packaging in vectors sample purified with and without phase separation. 2 μ l samples of each vector preparation were prepared for EM. The sample prepared with phase separation had a higher titre (1.5×10^{13} vg/ml) than the standard purification sample (1.1×10^{13} vg/ml). The greater number of vector particles in the phase separation sample is therefore as expected. Single images from each sample were counted. Full (blue) and empty (red) capsids were marked on the EM images and counted using Image Pro-Plus software.

6.2.7 The effect of AAV2/8 CMV.GDNF on cone degeneration

4 *Rho*^{-/-}*Opn.gfp* mice were treated with rAAV2/8.CMV.GDNF (batch #3 – purified with two-phase separation) to 1 eye only. Fellow eyes were left untreated for comparison. Mice were treated at p14 of age with vector diluted in PBS-MK to 5×10^{12} vg/ml. Superior and inferior injections of 1.5 μ l of vector were delivered by sub-retinal injections as described previously.

Treated animals were evaluated with ERG assessments at p52, p60 and p73. Cone function was diminished in treated eyes by 31, 48 and 63% of the untreated value at days 52, 60 and 73 respectively. The effect of ultra-pure CMV.GDNF (batch#3) preparation on cone function at P52 was no different from that seen with CMV.GDNF (batch#1) or with the control vector ($p=0.33$ and $p=0.84$ respectively, unpaired t-test) (Figure 6-8).

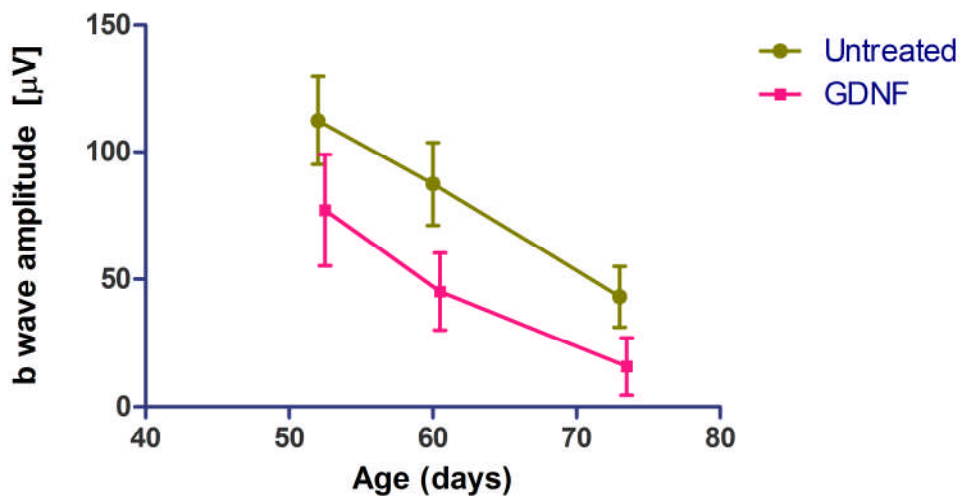


Figure 6-14 Cone function in rAAV2/8 CMV.GDNF treated and untreated eyes (n=4). Mean b-wave +amplitudes to a 10 cds.m⁻² flash are presented at 3 timepoints (p52, p60 and p73) +/- standard deviation as shown by the error bars.

A repeat cohort of *Rho*^{-/-}*Opn.gfp* mice (n=6) were treated with rAAV2/8.CMV.GDNF and central cone counts performed at weeks 12 and 17. Analysis of these counts and the raw images are shown in Figure 6-15 and Figure 6-16 respectively. Single eyes were treated and fellow eyes were used as untreated controls. Two-way ANOVA with Bonferroni post tests confirmed that counts were lower in the treated eyes (p=0.0285). The cone degeneration was therefore more advanced in eyes treated with rAAV.CMV.GDNF which is in keeping with the functional assessments.

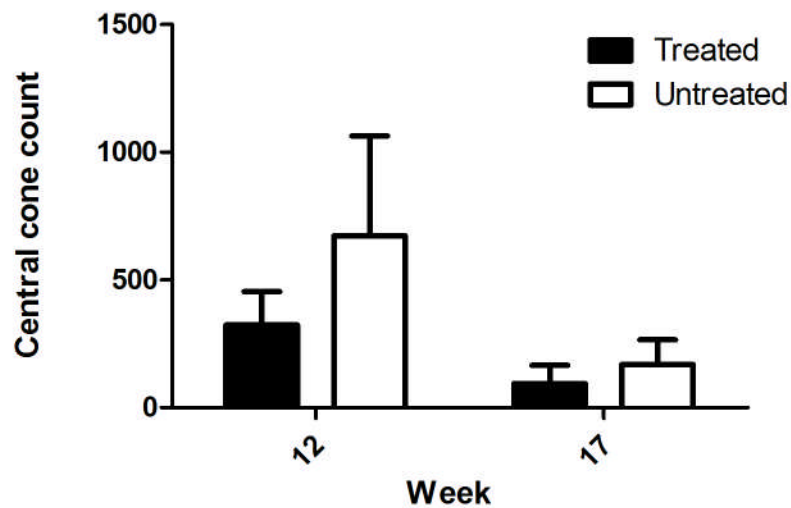


Figure 6-15 Central cone counts in GDNF and untreated eyes. *Rho*^{-/-}*Opn.gfp* mice (n=6) were treated to one eye only with rAAV2/8.CMV.GDNF (batch#3). Fellow eyes served as untreated controls. Cone counts at weeks 12 and 17 revealed that cone degeneration was more advanced in treated eyes (p=0.03).

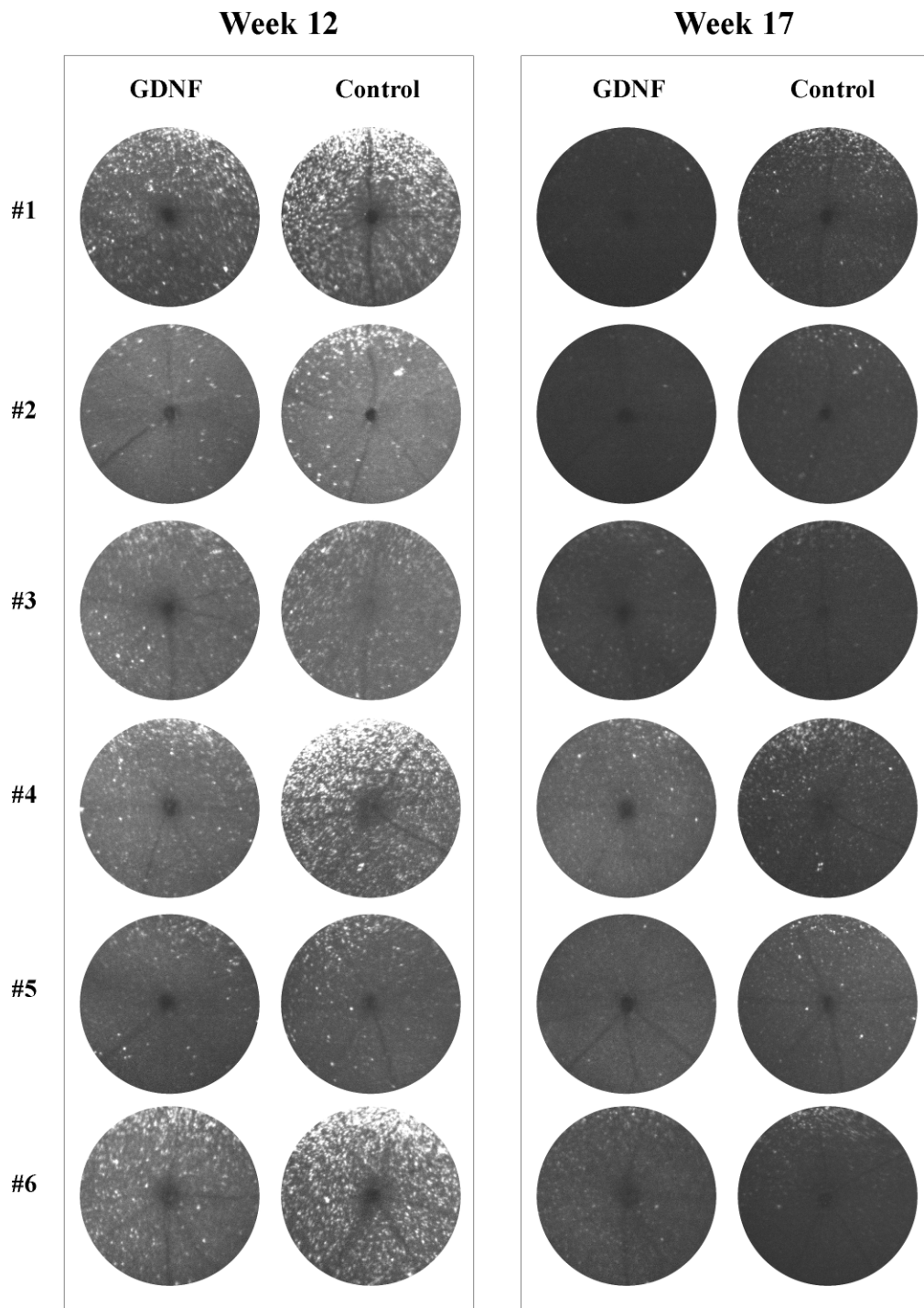


Figure 6-16 *In vivo* imaging of cone photoreceptors in GDNF treated and untreated eyes of degenerating retina. *Rho*^{-/-}*Opn.gfp* mice (n=6) were treated to one eye only and fellow eyes served as untreated controls. All images have been equally brightened and enhanced to aid printing.

6.3 Discussion

In these experiments rAAV2/8 has been used to induce expression of GDNF in the outer retina. There was no difference in cone function between CMV.GDNF treated and null vector treated eyes, and in all animals cone function in treated eyes was diminished as compared to that in untreated fellow eyes. There was no evidence of a neuroprotective effect from GDNF.

Previous experiments with rAAV2/2 revealed no histological or functional evidence of toxicity after 1 year of inner-retinal GDNF expression in Sprague-Dawley rats.³⁰⁸ Similarly in a separate study no functional evidence of toxicity was found in wild type mice 8 weeks following sub-retinal injection of rAAV2/2.CBA.GDNF.¹⁵⁴ However, sub-retinal rAAV2/8 leads to substantially higher levels of transgene expression than is achieved with rAAV2/2.¹⁹⁴ In the experiment by Wu et al. with intravitreal rAAV2/2 in Sprague-Dawley rats, the background levels of GDNF in untreated eyes was 8.0 ± 5.4 pg/ μ g protein. This is very similar to the level found in untreated mouse eyes in these experiments, 5.3 ± 5.2 pg/ μ g protein. However, in the experiments by Wu *et al.* treatment with rAAV2/2 lead to a five fold increase, where as here with rAAV2/8 CMV.GDNF there was a 232 fold increase evident in the end stages of the retinal degeneration. The CMV.GDNF plasmid, delivered into the subretinal space packaged in rAAV2/8, will have initially lead to approximately equal levels of GDNF expression in RPE cells, rod photoreceptors and cone photoreceptors.¹⁹⁴ GDNF levels in the treated eyes are therefore likely to have been even higher prior to rod photoreceptor and cone photoreceptor degeneration. It was therefore of interest to identify why cone function was impaired in the treated eyes in these experiments, and include experiments to identify whether high levels of GDNF could themselves be the cause of the toxicity.

There was no difference in cone function between eyes treated with titre matched preparations of rAAV2/8.CMV.GDNF (batches #1 and #3) and control vector containing a null plasmid. Sub-retinal injection of each of these three preparations lead to a similar effect on cone function at 5 weeks post injection.

There was therefore no evidence that GDNF expression, from vector at this titre, augmented the negative effects of a sub-retinal injection. However, isovolumetric sub-retinal injections of higher titre CMV.GDNF (5×10^{13} vg/ml, batch #1) vector did increase the magnitude of the negative effect on cone function. This could be explained either by a constituent of the vector preparation having a toxic effect, or by there being increased GDNF expression induced by high-titre vector injections and at this level GDNF itself exerted a toxic effect. It has however not been established that CMV.GDNF batch#1 injected at 5×10^{13} vg/ml does indeed induce significantly higher levels of GDNF expression than is seen with isovolumetric injections of 5×10^{12} vg/ml. Although the repeated injections of 500ng of recombinant protein in chapter 4 produced no functional toxicity, this are not directly comparable with the rAAV2/8 experiments as gene-therapy mediated expression leads to much more sustained levels of transgene expression, and the gene therapy was performed at far earlier timepoints (p14 as opposed to the first injection of recombinant protein at p36).

The detrimental effect of subretinal rAAV2/8 at 5×10^{12} on cone function was not due to GDNF expression. It was also not significantly reduced by a dilution of the vector to 1×10^{12} vg/ml, or by altered purification methods to reduce protein contaminants. This would be in keeping with the detrimental effects of viral vector at this titre being dominated by mechanical effects of the retinal detachment induced, as opposed to a dose-related toxic effect due to a viral vector constituent. This conclusion is supported by the experiments comparing control vector (at 5×10^{12} vg/ml) and PBS in wildtype mice, where there was no difference in detrimental effect. The related comparison of control vector and PBS in rhodopsin knockout cone-GFP mice was however at odds with this conclusion as a greater effect was seen with control vector than with PBS. The latter result was obtained with just 4 mice and would need to be repeated in much larger numbers were it necessary to investigate this negative effect further.

The damage to photoreceptors that follows a retinal detachment is likely to result primarily from physical disruption of normal cellular structures and interactions, and reduced oxygen tensions whilst the retina remains separated from the RPE.

Ordinarily photoreceptors are embedded in an inter-photoreceptor matrix (IPM) and closely surrounded by RPE cell microvilli. Cone photoreceptors, in addition, are surrounded by a specialized area of IPM known as the cone sheath,³⁵² which is of particular importance in maintaining retinal adhesion through interactions with both the neural retina and the RPE.³⁵³ Separating the retina from the RPE leads to disruption of these physical interactions, with damage to the morphology of photoreceptors and RPE monolayer in the area of detachment.^{344;354;355}

Whilst the inner retina is dependent on the retinal blood vessels, the photoreceptors of the outer retina are reliant on the deep choroidal vasculature. A retinal detachment therefore causes physical separation of the photoreceptors from their normal blood supply, affecting diffusion gradients and active transport through the RPE. In experimental models of retinal detachment oxygen supplementation has been found to reduce photoreceptor death, suggesting that oxygen-deficiency is at least one of the causes of detachment-associated photoreceptor loss.^{345;356;357} In addition the detachment stimulates a reactive gliosis which itself impairs neuronal survival, and augments photoreceptor degeneration. Evidence for this comes from glial fibrillary acidic protein (GFAP) and vimentin deficient mice in which there are attenuated glial cell responses, and reduced rates of photoreceptor degeneration following detachment.³⁵⁸ It may be that the damaging reactive gliosis is itself initiated by the relative oxygen deficiency, and hence secondary to it.

With a long-standing retinal detachment there is substantial photoreceptor loss in the area of detachment, and this is through apoptosis.³⁵⁹⁻³⁶¹ However, even with early and successful reattachment surgery in previously healthy eyes (and hence grossly normal retinal and RPE cells), the restoration in vision following surgery is usually incomplete.^{344;362} Yang et al., working in a mouse model of retinal detachment, found that the peak of photoreceptor death was within the first 3 days of the detachment.³⁴² This is in keeping with other studies in humans and ground squirrels (which have a cone rich retina) showing apoptosis as early as 8 hours following detachment, and diminishing rapidly after one week.^{343;363} Cone photoreceptor outer segments are also extensively disrupted following just 1 day of retinal detachment.³⁴⁴

Re-attachment of the retina does however stop further apoptosis and is followed by reversal of IPM disruption and a gradual improvement in photoreceptor morphology.³⁴⁴ Sakai found photoreceptor length and ERG function to continue to improve for up to 96 days following a 1 day experimental detachment;³⁴⁴ this is in keeping with clinical studies reporting slow improvements over the long term.^{364;365} At the 96 day timepoint in Sakai's study cone outer segment length was approximately 70% of normal.

Studies of experimental detachments in both cat and squirrel models have found retinal detachment to have a greater impact on cone photoreceptors than on rods, both in terms of morphology and cell death.³⁴⁴⁻³⁴⁶ Yang et al., working in the mouse model of detachment which differs in being more rod-dominated, did not detect a difference in levels of apoptosis but did find a greater loss of opsin expression in the cones than in the rods.³⁴² Other studies too have found early down-regulation of opsin and calbindin proteins in cone photoreceptors, but not rods, following experimental retinal detachments.^{343;366} Based on the numbers of mitochondria found in these cell types it is estimated that cones have a faster metabolic rate than rods,³⁶⁷ and potentially the down-regulation of protein expression in cones could be a survival mechanism to conserve energy in the hypoxic conditions induced by a detachment.³⁶⁶

The absence of a neuro-protective effect of GDNF on cone photoreceptors in the *Rho-/-Opn.gfp* mouse is a novel finding. In selected rodent models GDNF supplementation has been demonstrated to preserve rod-dominated outcome measures in the short-term.^{80;159;160} The absence of a significant neuroprotective effect on cone photoreceptors would preclude these positive experimental findings translating into substantial benefits for patients with rod-cone dystrophies.

Chapter 7 Inhibition of apoptosis

7.1 Introduction

7.1.1 Apoptosis pathways and the caspase enzymes

Controlled cell death, and specifically apoptosis, is a highly conserved feature of multi-cellular organisms and is prominent during both development and adult life. The apoptosis pathway is also central to many pathologies. For example, in inherited retinal degenerations the increased loss of neuronal cells is through the apoptosis pathway.^{44;102;113} Conversely reduced rates of apoptosis are found within malignant tumours, where specific inhibitors of apoptosis are associated with malignant transformation and resistance to chemotherapy agents, which themselves act through promotion of apoptosis.^{368;369}

Central to the process of apoptosis are the caspases, a family of cysteine protease enzymes. These enzymes are constitutively expressed as very low-activity pro-enzymes. Activation of the apoptosis pathway leads to ‘initiator’ caspases (eg -6, -8, and -9) cleaving and hence activating one another in a hierarchical order, thus generating a self-amplifying initiation cascade. Downstream caspases, known as ‘effector’ or ‘executioner’ caspases (eg -2, -3 and -7) will then, once activated, effect the molecular steps of cell death and organised destruction of cellular structures.

Activation of the caspase cascade occurs through either extrinsic or intrinsic pathways (Figure 1). The extrinsic pathway originates from activation of a cell surface receptor (eg Fas) whereas the intrinsic pathway is triggered by cytoplasmic stimuli, such as cytochrome *c* release from mitochondria. The pro-apoptotic potential of these caspase pathways is balanced by the anti-apoptotic effect of the Bcl-2 and inhibitor of apoptosis regulatory proteins.

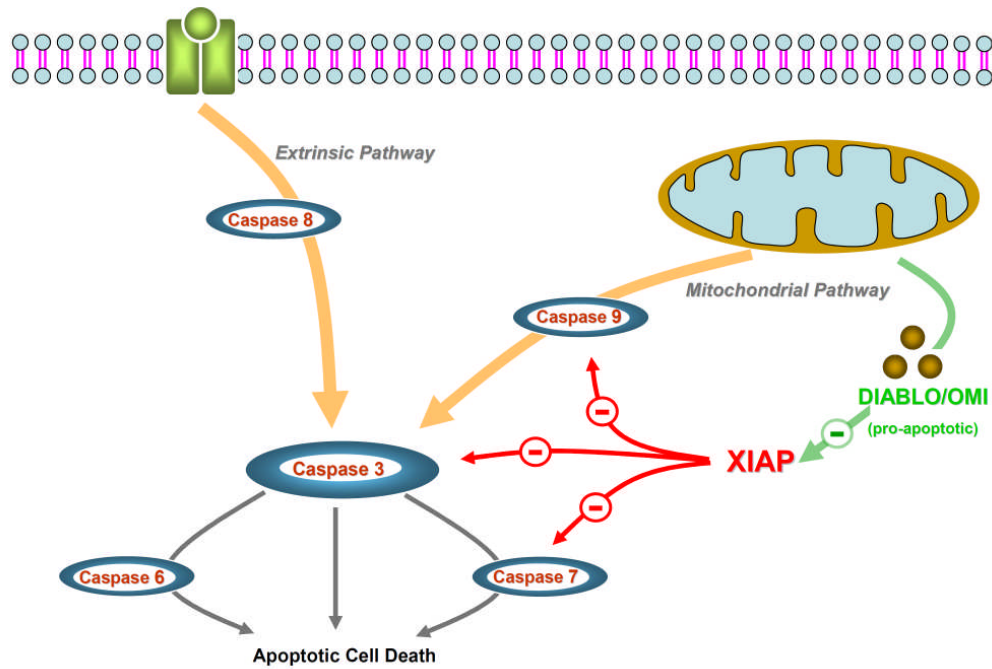


Figure 7-1 The Intrinsic and Extrinsic pathways of Apoptosis. The caspase enzymes are involved in the initiation of the apoptosis pathway, as well as effecting the steps of organised destruction of the cell. There are 2 principle pathways of activation. The ‘extrinsic’ pathway is activated by binding of extra-cellular signals (typically emitted by immune effector cells including cytolytic T lymphocytes (CTLs) or natural killer (NK) cells) to membrane bound death receptors (members of the tumor necrosis factor membrane-receptor (TNF-R) family). Ligand binding to the receptors leads to formation of death-inducing signalling complexes (DISC) or exocytosis of granules containing perforin and granzymes, and subsequent caspase-8 activation. The ‘mitochondrial’ (also known as ‘intrinsic’) pathway is initiated by the release of mitochondrial pro-apoptotic factors such as cytochrome *c* in response to intracellular stress responses; this in turn activates caspase-9. The activated initiator caspases (-8 and -9) in turn lead to activation of effector (also know as ‘executioner’) caspases such as caspase 3. The X-linked inhibitor of apoptosis (XIAP) protein is however a potent inhibitor of the apoptosis pathway through its binding to both initiator and effector caspases; therefore to allow apoptosis to proceed the release of additional pro-apoptotic factors is required from the mitochondria (eg DIABLO or OMI) to displace XIAP from the required caspases.

7.1.2 Bcl-2 regulatory proteins.

Members of the Bcl-2 protein family have an inhibitory effect on the apoptosis-activation pathway by impeding release of cytochrome *c* from the inter-membrane space of mitochondria.^{370;371} *In vitro* supplementation of *bcl-2* has a neuroprotective effect on neurons dying through apoptotic mechanisms,^{372;373} but *in-vivo* the effect on photoreceptors has been limited and transient.^{115;116;118} In the study by Bennett *et al.* recombinant adenoviral mediated expression of *bcl-2* was reported to result in histological evidence of photoreceptor neuroprotection for approximately 6 weeks in the rd mouse.¹¹⁶ This viral vector is not an effective means of transducing photoreceptors however, and so the limited histological effects may not have been directly due to transgene expression in specifically photoreceptors. Studies of transgenic mice with genomically delivered *bcl-2* and an inherited photoreceptor degeneration have demonstrated either no effect³⁷⁴ or limited and short-lived effects.^{115;118} Furthermore, Chen *et al.* found that expression of high levels of *bcl-2* expression resulted in loss of wild-type photoreceptors. This occurred in a dose-dependent manner but further underlines the case that *bcl-2* is not a favourable therapeutic target.¹¹⁵ The mechanism of cell loss with increased levels of *bcl-2* is not established.

7.1.3 Inhibitor of apoptosis (IAP) proteins and their regulation

In contrast to the *bcl-2* proteins, the inhibitor of apoptosis proteins (IAPs) bind directly to specific initiator and effector caspases. This contributes to their being the most powerful intrinsic inhibitors of cell death when over-expressed. The X-linked inhibitor of apoptosis (XIAP) binds to both initiator and effector caspases³⁷⁵⁻³⁷⁷ and is the most potent of the IAPs.^{378,379} (Figure 7-1).

Structurally the IAPs are defined by the presence of an amino-acid-zinc-finger motif, known as the baculoviral IAP repeat (BIR). The number of BIRs in each IAP varies between 1 and 3, but they are highly conserved regions and mediate the protein interaction with caspase enzymes (Figure 7-2).³⁸⁰

IAPs, and specifically XIAP, are highly expressed in a variety of cancers, and there is evidence that they are central to the means by which cancer cells acquire resistance to apoptosis.^{379;381;382} Reducing IAP expression or activity has therefore been a focus for anti-malignancy treatments. Antisense oligonucleotides to knockdown XIAP mRNA were found to exert potent antitumor activity in preclinical solid tumour models,³⁸³ and this approach has now entered the clinical domain. A phase I/II trials found a XIAP antisense oligonucleotide, in combination with chemotherapy, to be highly effective in cases of refractory acute myeloid leukaemia,³⁸⁴ and further clinical trials are ongoing (www.clinicaltrials.gov).

Conversely increasing expression of IAPs could be a potent means of inhibiting or slowing apoptotic cell death in neurodegenerative disorders, and notably RP where there is a secondary mutation-independent loss of cone photoreceptors. This hypothesis is supported by a number of studies in which over-expression of XIAP has been demonstrated to reduce cell death in response to cyto-toxic stimuli including ischemia,^{385;386} neurotoxin,³⁸⁷ and in motoneurons following axotomy and in the SOD1 transgenic mouse mouse of amyotrophic lateral sclerosis.^{293,488} Transgenic over-expression of XIAP in mice has also been associated with reduced age-related cochlea hair cell loss within the ear, as compared to wild type littermates.³⁸⁸

However, unsurprisingly it is also apparent that the role of IAPs is more complex than a simple correlation between levels of IAPs and rates of apoptosis.³⁷⁹ These proteins are highly regulated, and exist in equilibrium with endogenous regulators. Their binding to caspase enzymes, through the BIR domains, is reversible, and hence a dynamic process subject to regulation.

Means of IAP regulation can be considered in terms of ‘autologous’ features of the proteins themselves, and then external influences whereby the action of IAPs are modulated by other proteins.

With regard to the ‘autologous’ control, selected IAPs contain a carboxy-terminal RING (really interesting new gene) zinc finger which allows for auto-

ubiquitination, the process by which proteins can be labelled for proteasomal degradation.³⁸⁹ Through this domain certain IAPs including XIAP inhibit apoptosis under normal conditions but in response to more severe apoptotic stimuli they promote their own degradation.^{389;390} Their inhibition of specific caspases is therefore a measured and variable response to cellular stresses.

The IAP antagonistic proteins that block anti-apoptotic activity of IAPs include the 'direct IAP binding protein with low pI' (DIABLO),^{391 392;393} which was previously known as 'second mitochondria-derived activator of caspase (Smac)'.³⁹⁴ This protein is itself activated in mitochondria and the released form can then bind directly to IAPs to inhibit their caspase-inhibitory binding. Others include Omi/HtrA2 and GSPT1/eRF3, all of which share the presence of an IAP-binding motif (IBM) at the amino terminus of the mature protein to directly interfere with IAP binding to caspase enzymes.³⁹⁵⁻³⁹⁷

More recently the protein XAF1 (XIAP-associated factor 1) has been identified as a negative regulator of the caspase-inhibiting activity of XIAP and interestingly it is found to be down-regulated in many proliferating tumours.^{398;399} Thus, whilst looking at IAP levels alone is too simplistic a means of anticipating rates of cellular apoptosis, the ratio between XAF1 and XIAP has been found to correlate with rates of apoptotic cell death in at least two types of tumour.^{400;401}

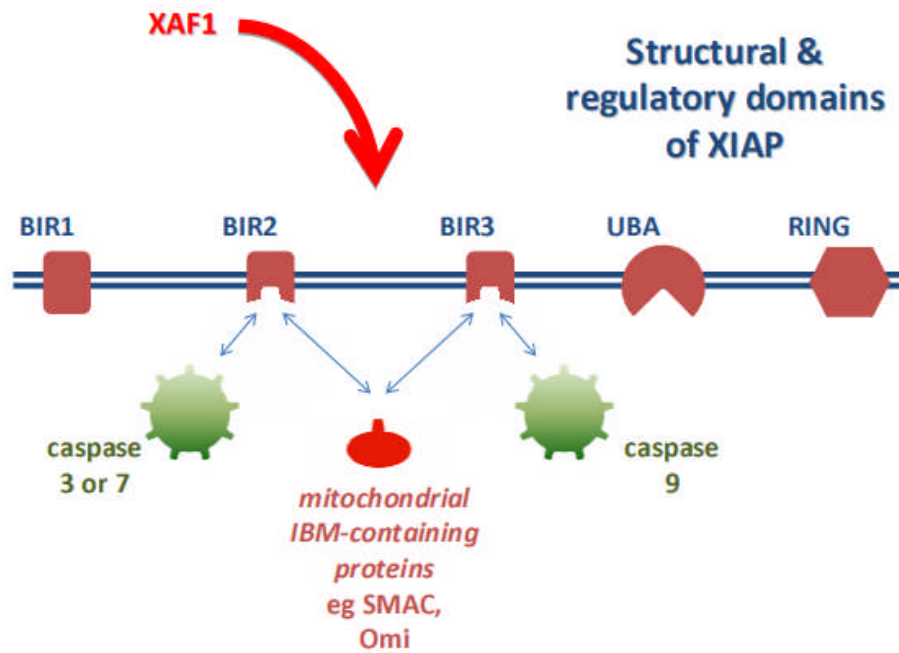


Figure 7-2: The structural and regulatory domains of XIAP. The xiap protein contains 3 baculoviral IAP repeats (BIR). BIR 2 & 3 each contain a conserved surface groove, which mediates direct binding to specific caspase enzymes. However, mitochondrial IAP-binding motif (IBM)-containing proteins bind at these same sites and so inhibit the caspase related activity of XIAP. XIAP also contains a ubiquitin-binding (UBA) domain and a RING-finger domain conferring ubiquitin protein ligase (E3) activity which mediates auto-ubiquitination in times of severe apoptotic stress.

7.1.4 Physiological roles of XIAP

The anti-apoptotic effects of IAPs and XIAP, when found at increased levels in tumours or when expressed artificially, have obvious clinical implications and have been the focus for much of the early work relating to these proteins.

However these proteins are also involved in copper homeostasis, intracellular signalling, cell division and cellular morphogenesis (reviewed by Srinivasula and Ashwell).³⁶⁹ The “inhibitor of apoptosis” description may even be considered as misleading with regards to the physiological roles of these proteins, as under normal conditions (in contrast to when over-expressed) they provide only limited resistance to apoptosis.^{369;402} In part this may be due to the RING-domain that for many of the IAPs catalyses degradation in response to proapoptotic stimuli under normal conditions.^{389;403} An alternative nomenclature that names the proteins after their distinctive structural motif, the BIR, rather than implying function has therefore been proposed, though is not so widely used.⁴⁰⁴

In humans, congenital absence of XIAP expression causes an X-linked lymphoproliferative disorder.⁴⁰⁵ Lymphocytes from affected patients show enhanced rates of apoptosis in response to stimulation with the TNF-associated apoptosis-inducing ligand receptor, the death receptor CD95 (also termed Fas or Apo-1) and the T-cell antigen receptor (TCR)-CD3 complex. XIAP-deficient patients also have low numbers of natural killer T-lymphocytes, which could be explained by reduced survival or reduced differentiation of this cell type. In mice lack of XIAP, or any of the common RING-containing IAPs, still permits grossly normal development and survival.^{369;406} Absence of XIAP does lead to delayed lobuloalveolar development in the mammary gland,⁴⁰⁷ but it is somewhat surprising that the phenotype is not more severe given the number of functions with which the IAPs are implicated. It is also evident that there are differences in the apparent physiological roles of XIAP between mice and humans. The limited phenotypes may be explained by compensatory up-regulation of agonists and/or down-regulation of antagonists and redundancy in the pathways in which XIAP is involved.

7.1.5 Over-expression of XIAP

Whilst the exact role of XIAP at physiological levels is complex, and apparently non-essential for most cell types, the question remains as to whether manipulation of levels is of potential therapeutic benefit. In particular it is of clear clinical importance to identify if increased expression, to supra-physiological levels, is effective at slowing cell death and achieving sustained neuroprotection. Likewise down-regulation in tumours may be a means of slowing tumour growth, or increasing susceptibility to adjunctive chemo- or radiotherapy. Seeger *et al.* generated cell lines stably expressing XIAP at approximately two to five times the normal physiological levels, which is approximately comparable to levels found in tumour cells. At this level of expression XIAP levels alone were not predictive of cellular fate when exposed to chemotherapy agents, but instead the outcome was also dependent on levels of its physiological inhibitor DIABLO.⁴⁰⁸ In these experiments the absence of a single inhibitory protein rendered XIAP over-expressing cells severely resistant to cytostatic agents. This is in keeping with clinical studies showing that XIAP levels alone are not predictive of clinical outcome, and that levels of its inhibitors are also of relevance.^{400;401;409}

7.1.6 XIAP mediated resistance to photoreceptor apoptosis

As with GDNF, the initial studies demonstrating a neuroprotective effect for XIAP within the retina were with acute models of apoptosis.⁴¹⁰⁻⁴¹² Petrin *et al.* treated rats with a DNA methylating agent, *N*-methyl-*N*-nitrosourea (MNU), which causes a peak of photoreceptor apoptosis at 24 hours following intra-peritoneal (IP) injection. XIAP expression was induced in photoreceptors using a rAAV2 vector injected in to the sub-retinal space, and a photoreceptor specific promoter (MOP500). rAAV2 vector was injected 6 weeks prior to the MNU administration to allow time for high levels of expression to develop. At 48 hours, 72 hours and 1 week following the IP injection of MNU there was evidence of histological protection in four of the six XIAP treated eyes. This was judged by comparison to untreated and rAAV2.GFP treated eyes. In two of the four XIAP treated eyes with morphological protection there was still

evidence of ERG function at 1 week post IP injection, where as in untreated and GFP treated eyes there was none. Each animal was treated with only a single sub-retinal injection of vector and so the area of optimally treated retina was limited, as was evident from the histological analysis where the greatest protective effect was seen close to the injection site. The ERG outcome measures may have been improved with double sub-retinal injections to maximally treat a larger area of retina.

The loss of photoreceptors in RP is also through apoptosis, although this is in the context of chronic cellular stress rather than an acute chemical insult as with MNU. Potentially a chronic and persistent source of cellular stress could be harder to treat than an acute and transient insult. Leonard *et al.* evaluated gene therapy mediated expression of XIAP in the P23H and S334ter transgenic rat models of RP, in which rhodopsin mutations lead to a rod cone degeneration which was followed over approximately 7 months.¹¹⁹ rAAV2/5 was used with the chicken β -actin promoter to achieve expression in photoreceptors, and sub-retinal injections were performed at P14-17. At 28 weeks following injection there was histological evidence of neuroprotection in the treated eyes of both rat models. The ONL was thicker in XIAP treated eyes than in untreated and GFP-treated controls. However, in the S334ter rat there was no functional benefit from XIAP treatment, and the ERGs were no different to those in GFP treated eyes. There was a tendency for b-wave amplitude in GFP treated eyes to be worse than that in untreated fellow eyes. This was not tested for significance but is likely to relate to the effects of sub-retinal injection. Likewise, in the P23H rat mean a- and b-wave amplitude was lower in GFP treated eyes than in untreated fellow eyes at all timepoints, although again this was not tested for significance. ANOVA analysis with Bonferroni-Dunn correction revealed a significant difference between the XIAP and GFP treated groups. However it was only at the latter stages of the degeneration that XIAP treated eyes were better than untreated fellow eyes, and by this stage the levels of function are substantially reduced relative to pre-degeneration. The statistical analysis presented by the authors only confirmed that XIAP treated eyes were different from GFP treated controls, and not untreated fellow eyes. Subretinal injections induce retinal

damage, and photoreceptor death which is also through apoptosis.³⁵⁹⁻³⁶¹ It thus appears that in these models, and following a subretinal injection, the ability of XIAP expression to prevent apoptosis and maintain photoreceptors in a functional state is limited. The authors caution that the magnitude of the functional effects in their study could be an underestimate because of single injections only treating approximately 20% of the retina. Furthermore the sub-retinal injection procedure used (which was trans-corneal) may have caused confounding variables including corneal opacities that were not controlled for. Similar results were found with XIAP overexpression in the rd10 model of retinal degeneration.⁴¹³ This murine model has a relatively slow retinal degeneration caused by a loss-of-function mutation in the β -subunit of rod cGMP phosphodiesterase gene (Pde6b). rAAV2/5 mediated photoreceptor expression of XIAP in these animals likewise resulted in transient histological evidence of neuroprotection, but no evidence of a functional benefit.

7.2 Aims

To test whether XIAP over-expression leads to cone neuroprotection in the *Rho-/-Opn.gfp* mouse XIAP was first expressed in both rods and cones using gene therapy and the CMV promoter. With this approach cone neuroprotection could be mediated indirectly by augmenting rod survival and slowing rod-cone degeneration, or directly through an effect within degenerating cones. To separate these potential mechanisms of action in the event of a therapeutic effect a cone-specific promoter was also prepared and tested.

In the evaluation of XIAP in the P23H and S224ter transgenic rats the authors noted limiting factors that could have led to functional effects being underestimated.¹¹⁹ In the experiments here double sub-retinal injections were performed with high titre virus; this approach can lead to transduction of high percentages of photoreceptors across the entire retinal surface. In ongoing work fluorescence-activated cell sorting of rAAV2/8.CMV.GFP treated eyes (double sub-retinal injections at P10 of age) resulted in over 80% of photoreceptors expressing GFP (personal communication Dr Livia Carvalho). In addition in the following experiments sub-retinal injections were performed through the trans-

scleral route, instead of via the trans-corneal approach that was used previously to evaluate XIAP expression in photoreceptors.¹¹⁹ Animals were also examined for corneal opacities prior to ERG and SLO procedures, and so corneal opacities are less likely to have affected the experimental results.

7.3 The cone arrestin promoter

The human arrestin 4 promoter was investigated as a cone-specific promoter. The arrestin proteins block the activity of G protein-coupled receptors that have been phosphorylated by G protein receptor kinases. Within photoreceptors they participate in a gateway controlling G protein-mediated signalling and hence leading to deactivation of the phototransduction cascade. Absence of arrestin proteins in deficient mice leads to prolonged activation of the signalling pathways rendering photoreceptors more susceptible to saturation.^{414;415}

There are 4 arrestin subtypes; arrestin-1 is expressed in high levels in both rods and cones. Arrestins 2 and 3 are the ‘non-visual’ forms, and the more recently discovered arrestin 4 is found in cones and a subset of pinealocytes.^{415;416} Arrestin 4 (ARR4), also known as ‘cone arrestin’, is found in mouse cones driven by either the S or M opsins (Nikonov *et al.*, 2008). Due to the specificity of its expression within the retina the promoter for this protein was chosen for further investigation. The human ARR4 promoter was cloned by Dr Livia Carvalho, and subcloned into the pd10 plasmid with a downstream hrGFP reporter gene.

To establish specificity and transduction efficiency of the promoter rAAV 2/8 virus was prepared with the hARR4.hrGFP plasmid. The virus was titred by dot-blot analysis at 1×10^{12} virus particles/ml. 2 μ l of this virus was injected into the sub-retinal space in each eye of 4 rhodopsin knockout mice. The mice were 3 weeks of age at the time of injection, and were imaged with the scanning laser ophthalmoscope 3 weeks later (Figure 7-3). The retina shown had been treated with a single sub-retinal injection in the superior retina. This image shows that with sub-retinal injections it is possible to treat cells in the posterior pole of the eye that can then be imaged with the SLO *in vivo*.

Following imaging the mice were sacrificed and dissected eyes were fixed in 4% PFA for 1 hour. 10µm thick sections were prepared following cryopreservation in OCT, and stained with primary antibodies to cone transducin, S opsin or ML opsin. The GFP expressing transduced cells were found to almost exclusively co-localise with the cone-specific markers, as shown in Figure 7-4. Occasional expression was evident in rod photoreceptors indicating expression was not 100% cone specific, but this was rare. Of note the hrGFP expression was confined to cone outer segments, which is in contrast to eGFP expression in the *Rho*^{-/-}*Opn.gfp* mice.

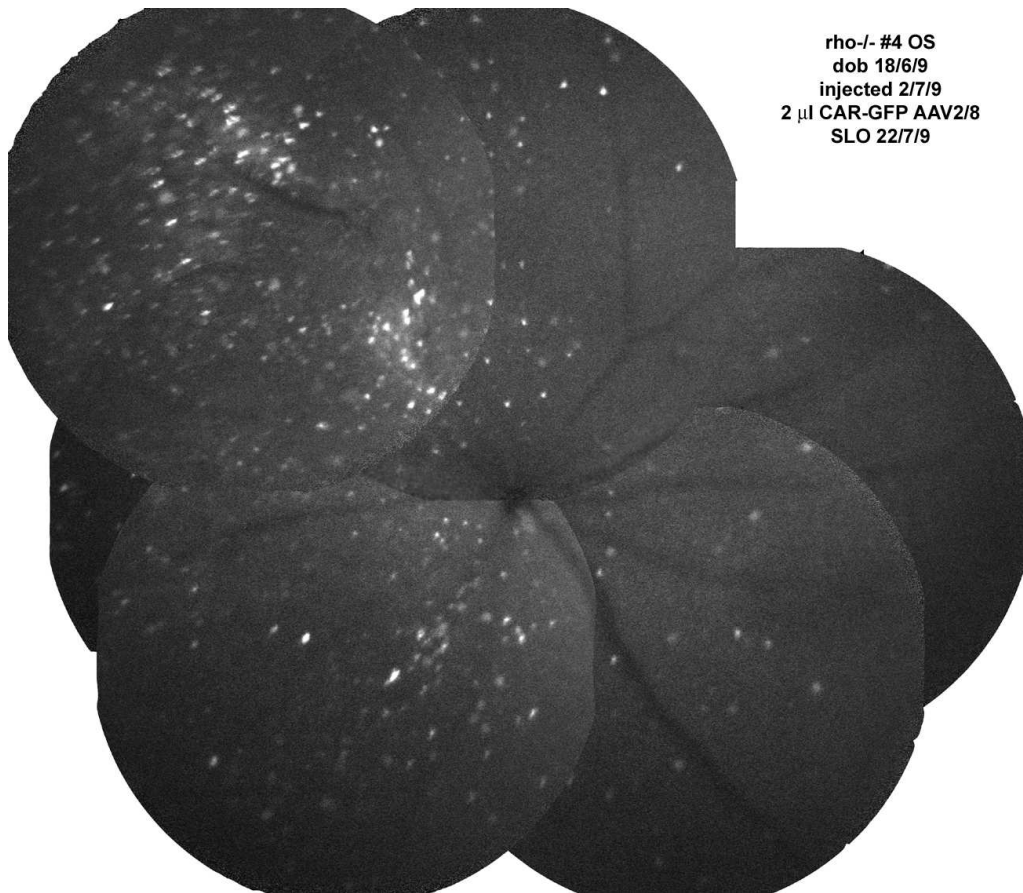


Figure 7-3 Collage of SLO images from ARR4-GFP injected eye. A rhodopsin knockout mouse was injected with 2 μ l of rAAV2/8 containing the ARR4-gfp cassette, as a subretinal injection. These SLO images were taken from the left eye 3 weeks following injection showing transduced cells expressing GFP. The single injection was performed under the superior retina.

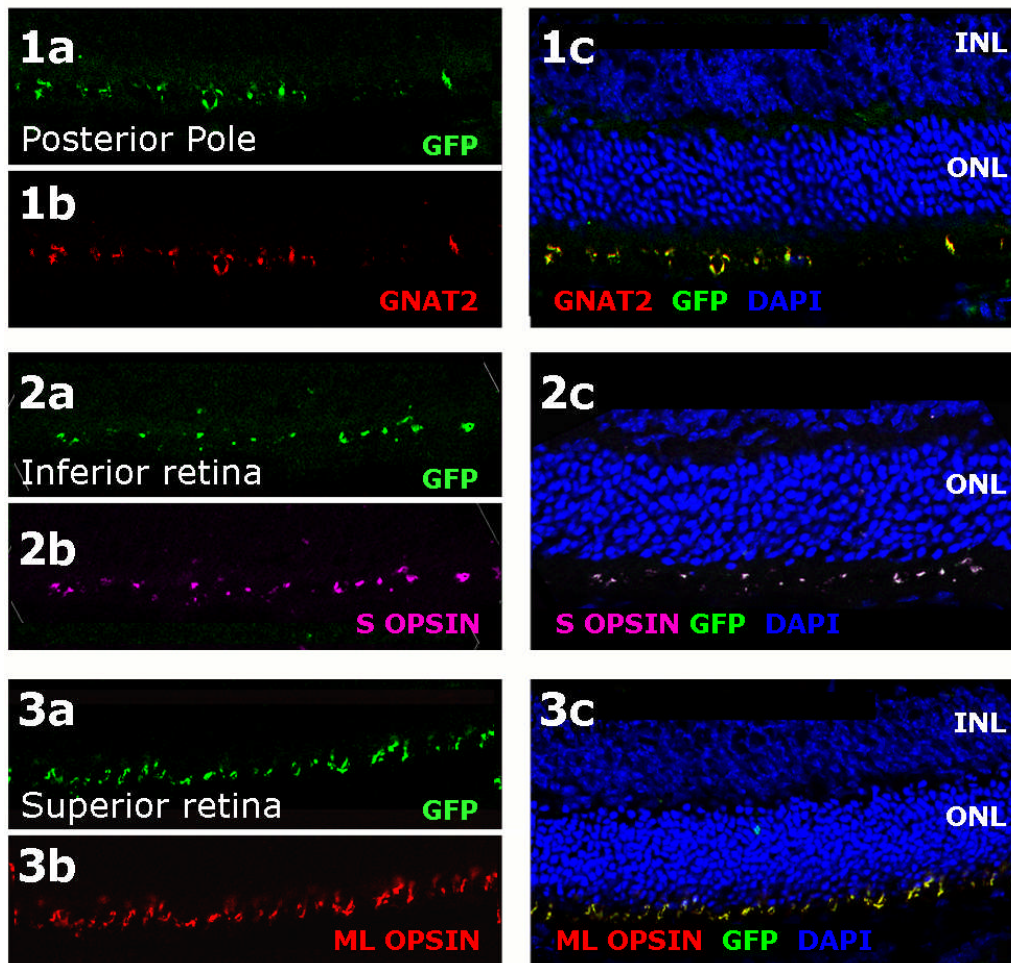


Figure 7-4 Immunohistochemistry of retina treated with rAAV2/8.ARR4.hrGFP. GFP expression is seen to co-localise with cone transducin (GNAT2, 1a-c), s-opsin (2a-c) and M/L opsin expression (3a-c). In 3c GFP expression is seen within a single rod nucleus. hrGFP expression within cones was seen in the outer segments. The images shown are not from the same eye as shown in Figure 7-3.

7.4 Testing of CMV.XIAP in vitro

PCR reactions were used to generate XIAP cDNA with appropriate restriction enzyme sites (Apa I and BsrG I) to allow cloning into a pd10 plasmid. The CMV promoter was used in order to drive high levels of transgene expression in both rod and cone photoreceptors.³³¹ The sequence of the entire CMV, XIAP and intervening linkage region was checked following cloning.

7.4.1 Species-specific primers

The XIAP sequence is highly conserved between species. However there are subtle differences in the coding sequence of human and murine XIAP that can be used to distinguish between the two. Primers, shown in Table 7-1, were designed to exploit the limited differences between murine and human XIAP. The binding efficacy and specificity of these primer pairs was tested by running PCR reactions, for each primer pair, with cDNA prepared from adult wild type mouse retina and linearised plasmid DNA containing the human XIAP sequence. Linearisation of the plasmid was performed to aid primer binding, and was achieved by incubation of the circular DNA with the SpeI restriction enzyme for 2 hours. The PCR reactions were run at a range of temperatures between 55 and 62°C, and the products were examined on a 2% agarose gel (Figure 7-5).

	Sequence (5'-3')	Amplicon Size (bp)
Mouse Xiap Left	GAATTCAGATCCCCAGAACG	120
Mouse Xiap Right	GCTGGCTTCAAACCCAGATA	
Human XIAP Left	ACTGGTGAAGGAGATACCGTGCG	445
Human XIAP Right	CAACAAAAGCACTGCACTTGGTCAC	

Table 7-1 Species specific XIAP PCR primers

The murine and human primer sets were found to be specific for the mouse and human XIAP sequences respectively. The absence of a PCR product with

murine primers and murine DNA at 57.5°C is likely to be an experimental artefact.

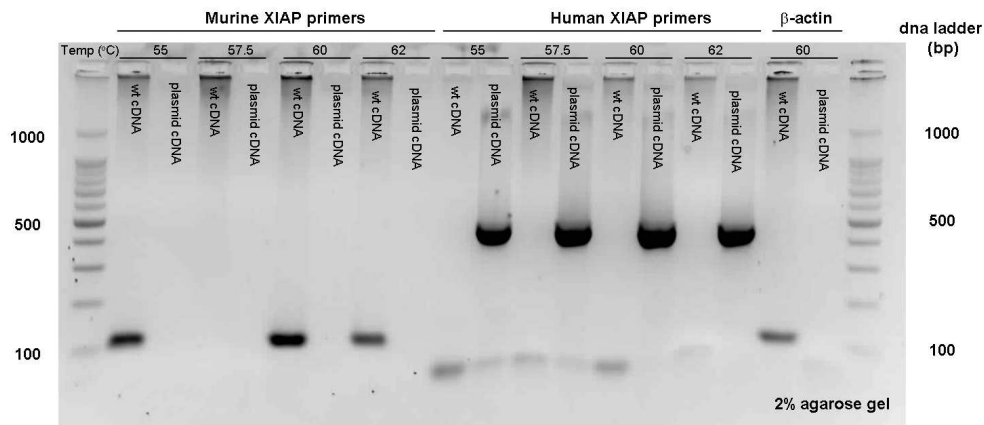


Figure 7-5 Determination of primer efficacy and specificity. 40 cycle PCR reactions were run with each of human and mouse primers and human and mouse XIAP sequences, at a range of temperatures. To test for murine Xiap DNA mRNA from wild type retinas was isolated and cDNA generated. These samples are labelled “wt cDNA”. To test for human XIAP cDNA linearised pd10 plasmid contain human XIAP cDNA was used, and is labelled “plasmid cDNA”. Murine β -actin primers were run alongside to act as a positive control (using the murine cDNA) and as a negative control (using the sequenced plasmid DNA which is known not to contain the β -actin sequence).

7.4.2 *In vitro* testing of plasmid expression

The CMV.XIAP plasmid was assessed *in vitro* for its ability to produce XIAP mRNA. BHK cells are were used in the first instance, because of the relative reliability with which they can be transfected.

BHK cell transfection

BHK cells were seeded in a 24 well plate to give 75 000 cells per well. 8 wells were transfected with the CMV.XIAP plasmid, 8 with a CMV.GFP plasmid and the remaining 8 wells were left untransfected. Transfections were performed using a lipofectin protocol; after 48 hours the success of transfection was confirmed by examining for GFP expression, and the CMV.XIAP transfected and un-transfected cells were collected for mRNA isolation.

mRNA samples from the collected cells were treated with DNase to remove any residual plasmid DNA. To determine whether this process was complete, and hence that any XIAP detected with the hXIAP primers was from the transfected cells and not a false positive from residual plasmid DNA, the cDNA preparation steps were performed in duplicate with one sample being treated with water rather than reverse transcriptase (termed “no-RT controls”).

PCR reactions with the hXIAP primers (Figure 7-6) were positive with samples from both the transfected and un-transfected BHK cells, but not in the no-RT controls, indicating that the xiap naturally produced by this hamster cell line is itself detected by the human xiap primers. The possibility of contamination was also considered and so an additional plate of un-transfected bhk cells was prepared, and analysed, again confirming the PCR product from untransfected cells. These results indicate that at the sites of primer binding hamster XIAP has high congruity with human XIAP, and differs from mouse Xiap. Further testing for specifically plasmid expression was therefore performed in murine cell lines as the murine Xiap sequence is known, and cross-reaction of murine Xiap with these hXIAP primers should be avoided.

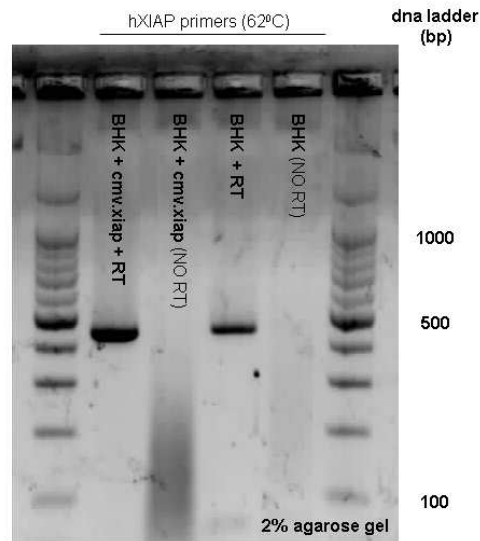


Figure 7-6 Testing for hXIAP in transfected BHK cells. PCR reaction products have been run on a 2% agarose gel. PCR reactions were run with hXIAP primers, shown previously to detect specifically human XIAP cDNA with the formation of a 445bp product. Samples were used from BHK cells transfected with CMV.XIAP and untransfected cells. Each sample was run in duplicate, with and without reverse transcriptase (RT). If the treated samples contained residual plasmid cDNA a positive band would have been seen with the “NO RT” samples. Positive bands were seen with both the transfected and untransfected BHK samples.

Mouse Fibroblast transfection.

Lipofectin and PEI transfections using a CMV.GFP were first attempted in the NSL mouse fibroblast line, but without success. The NIH-3T3 cell line was therefore used instead, which is a line of mouse fibroblast cells, originally derived from the NIH Swiss mouse. Lipofectin and PEI transfections were performed in parallel.

Two 24 well plates were seeded with 80 000 NIH-3T3 cells per well. 8 wells of one plate were transfected with a 50:50 mix of CMV.XIAP and CMV.GFP plasmids using lipofectin. 8 wells of the other plate were similarly transfected using a PEI protocol. The other wells in each plate were left untransfected to serve as controls.

72 hours following transfection the cells were examined for GFP expression. This was evident in PEI transfected cells (Figure 7-7: PEI transfected 3T3 cells expressing GFP (shown in black and white), but not in the lipofectin infected cells.

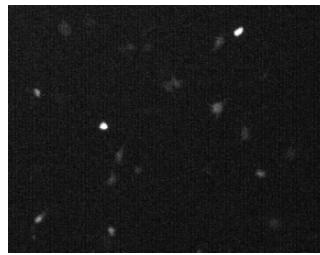


Figure 7-7: PEI transfected 3T3 cells expressing GFP (shown in black and white).

mRNA from the PEI transfected cells, and associated un-transfected controls, was isolated. To enhance mRNA yield the cells from groups of 4 wells were pooled prior to mRNA isolation. The 2 resultant samples of mRNA from transfected cells, and 2 samples from untransfected cells, were used for cDNA generation using the reverse transcriptase protocol (with and without the reverse transcriptase enzyme). Samples were then used for PCR reactions using the hXIAP primers.

As shown in Figure 7-8 human XIAP expression was detected in both samples from the CMV.XIAP transfected cells, but not in the un-transfected cells nor no-RT controls. These experiments confirm that the CMV.XIAP plasmid produced XIAP mRNA in murine cells.

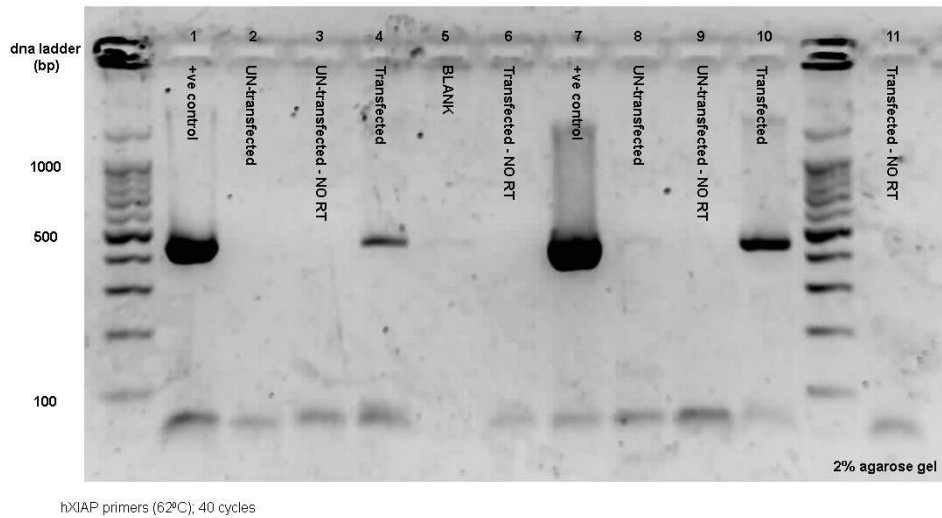


Figure 7-8: PCR detection of XIAP expression. PCR reactions using 100 ng of linearised CMV.XIAP DNA were run as positive controls in lanes 1 and 7; these show the expected PCR product of 445bp. The XIAP PCR product is not seen in lanes 2&3 or 8&9 from untransfected NIH-3T3 cells. However, in lanes 4 and 10 from cells transfected with CMV.XIAP the 455bp PCR product is seen confirming expression. Lanes 6 and 11 serve as negative “no-RT” controls, confirming that the XIAP product seen in lanes 4 and 10 results from cellular expression of the plasmid, and not from residual plasmid DNA in the collected samples.

7.5 Confirmation of transgene expression *in vivo*.

rAAV2/8 CMV.XIAP was prepared with a genomic titre of 1×10^{13} vg/ml. In order to confirm virus function *in vivo*, one of a litter of treated mice was culled to look for transgene-specific mRNA expression in the treated eye. The mouse in question had been treated with inferior and superior injections of $1.5 \mu\text{l}$ of CMV.XIAP virus (1×10^{13} vg/ml) to the right eye, at 19 days of age; the left eye was untreated. Four weeks following injection mRNA was isolated from the retinas of each eye, and cDNA generated. Transgene expression was confirmed using primers to distinguish between endogenous and human (transgene) XIAP mRNA.

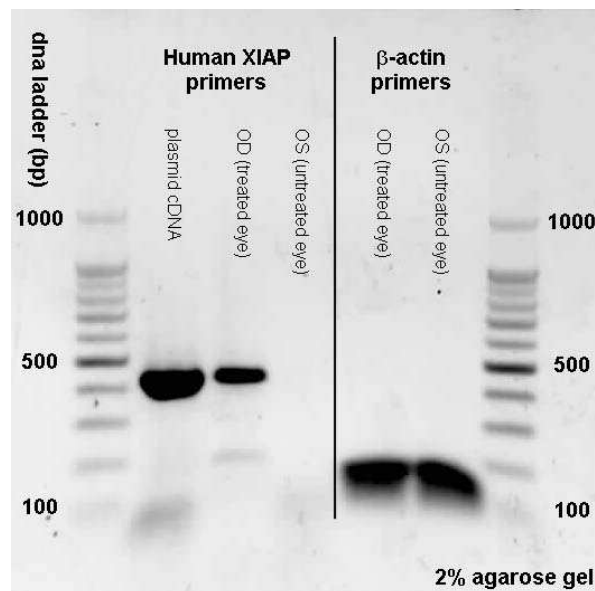
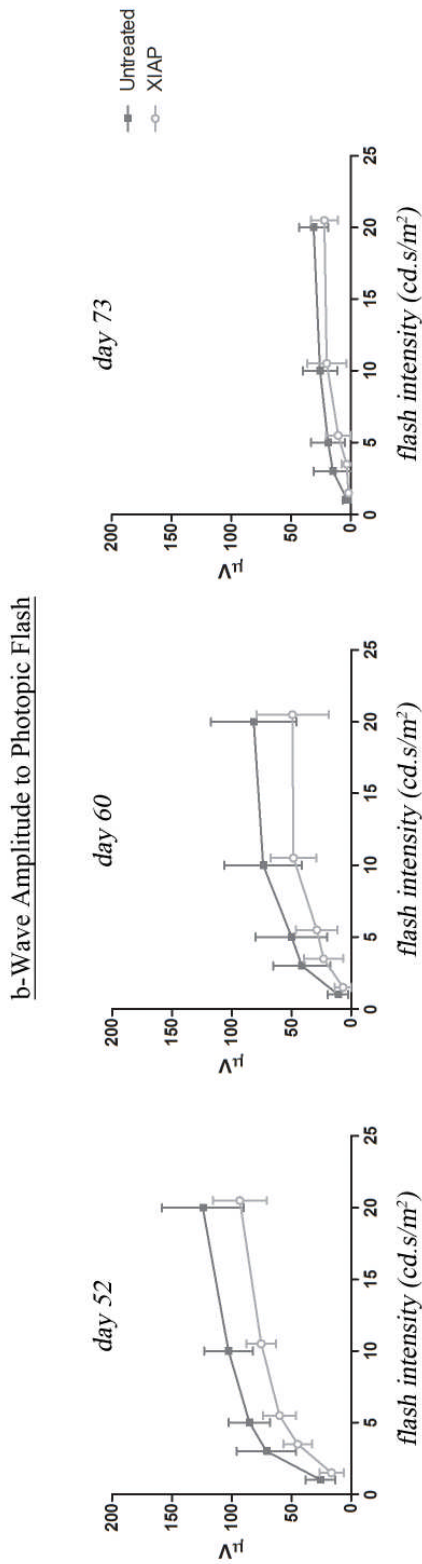


Figure 7-9 Confirmation of hXIAP transgene expression. cDNA was generated from the CMV.XIAP virus treated, and untreated, eyes of a *Rho^{-/-}Opn.gfp* mouse. This cDNA was run in a PCR reaction with β -actin and human XIAP (transgene) specific primers. A PCR reaction with the linearised CMV.XIAP plasmid was run alongside as a positive control. The human XIAP amplicon (445 bp) is seen in the treated eye, and positive control, only. Murine β -actin amplicons were seen for both the treated and untreated eyes, confirming successful cDNA generation.

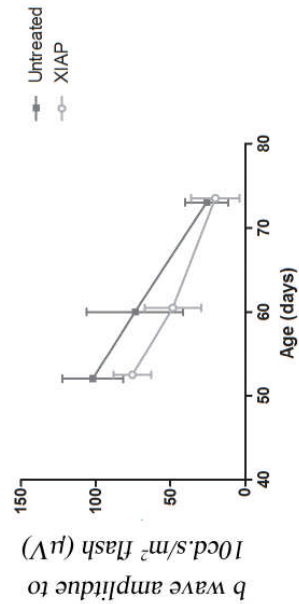
7.6 XIAP expression and degeneration of cone function

To examine the effect of XIAP expression on cone photoreceptor degeneration 5 *Rho*^{-/-}*Opn.gfp* mice were treated with rAAV2/8.CMV.XIAP and evaluated with photopic ERGs at days 52, 60 and 73 of age (pre-, mid- and terminal stages of the cone functional degeneration). Mice were treated with double sub-retinal injections of the viral vector, each of 1.5µl, at day 11 of age. ERG function results are presented in Figure 7-10. At each flash intensity, and at each timepoint, mean cone function was lower in the treated eyes than in untreated fellow eyes. At days 52 and days 60 cone function, in response to a 10 cd.s/m² flash, was worse in the treated eye than untreated eye in every one of the animals.

The effect of subretinal rAAV2/8.CMV.XIAP on cone function was compared with that of control vector. There were minor differences in the timing of injection and vector titre to take into account with this comparison. rAAV2/8.CMV.XIAP was injected at P11 and at a titre of 1×10^{13} , giving 3×10^{10} genome particles per eye. Control rAAV2/8 was injected at P14 instead, and at a titre of 4.2×10^{12} , giving 1.3×10^{10} particles per eye. The percentage reduction in cone function for each animal, and at each timepoint, was calculated for the b-wave amplitude in response to a 10 cd.s/m² flash [(untreated eye-treated eye)/untreated eye]x100]. Despite the greater number of vector particles injected with the CMV.XIAP preparation the effect on cone function was the same as that seen with the control vector (Figure 7-11). T-tests revealed no difference between the reduction in response seen with CMV.XIAP with that seen with control vector (p=0.68, 0.13 and 0.39 for day 52, 60 and 73 respectively). There was therefore no evidence that CMV.XIAP had a detrimental effect over and above that from a sub-retinal injection of control vector.



Cone Function over Time



5 *Rho*^{-/-}*Opn.gfp* mice were treated with rAAV2/8 CMV.XIAP to the right eye at p11. The left eye was untreated. The top row of graphs show cone function, in response to a range of flash intensities, at 3 different timepoints; at each cone function in the treated eye is lower than that in the untreated eye. The lower graph shows the course of cone function degeneration over time. The time course of cone degeneration was not slowed by gene therapy mediated XIAP expression.

Figure 7-10 The effect of rAAV2/8 on cone function in the *Rho*^{-/-}*Opn.gfp* mouse.

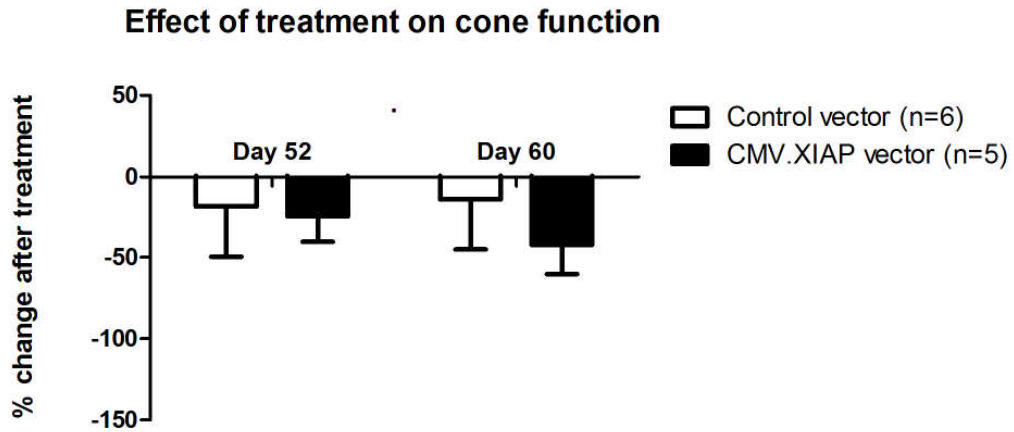


Figure 7-11 For each animal the difference in cone function between treated and untreated fellow eyes was calculated and expressed as a percentage of function in the untreated eye. Cone function was examined using a photopic flash ERG sequence in light-adapted animals; b-wave amplitudes to flash stimuli of an intensity of 10 cd.s/m^2 were used for analysis. Means of the % change are plotted for each treatment cohort and compared using the t-test.

7.7 XAF1 expression

XAF1 is one of the principal inhibitors of XIAP. If increased XIAP expression leads to a secondary up-regulation of XAF1 the anti-apoptotic effect of XIAP could be negated. *In vivo* the ratio of XIAP and XAF1 expression is a more informative predictor of outcome than levels of XIAP expression alone.^{400;401} Therefore in three animals, all of which had shown no treatment effect with rAAV2/8.CMV.XIAP eyes were enucleated for determination of XAF1 expression levels.

Animals were culled at week 17 following functional (ERG) and anatomical (SLO) assessments, and so were in the late stages of retinal degeneration. mRNA was isolated, and cDNA generated, from the treated and untreated eyes in each animal. XAF1 expression was quantified using quantitative real-time PCR, and determined relative to β -actin expression. A range of cDNA, probe and primer concentrations were first evaluated to optimise the reaction conditions. Optimised reaction curves along with the primers and conditions used, are shown in the supplementary data chapter. Each sample was analysed in triplicate at two dilutions.

β -actin (gene name ACTB) is a cytoskeletal protein expressed at approximately stable levels in all cells. Levels of expression are likely to have been equal in treated and untreated eyes, and so in each eye the number of copies of XAF1 cDNA were first normalised to number of copies of β -actin cDNA to allow comparison between samples. In 2 of the 3 animals XAF1 expression was greater in the treated eye than in the untreated eye (Figure 7-12). There was however no experimental reason to exclude the animal (#1) with no difference between treated and untreated eyes; the sub-retinal injections had been satisfactory in this animal, and ERG and SLO data was in keeping with the rest of the cohort. Analysis including all 3 animals revealed no overall difference in XAF1 expression between treated and untreated eyes ($p=0.18$, paired t-test). Increasing the numbers of eyes examined would increase the probability of detecting a small difference between treated and untreated eyes. However, even

in animals #2 and #3 the levels in the treated eye were only between 3 and 5 fold those in the respective untreated fellow eyes. In the previous chapter it was identified that rAAV2/8 mediated expression of GDNF, using the same promoter, lead to a 232 fold increase in expression. The relative increase in XIAP expression achieved with rAAV2/8 will also depend on the endogenous expression levels, but is likely to have been orders of magnitude greater than a 3-5 fold difference. A 3 to 5 fold change in XAF1 expression is therefore unlikely to be of biological significance and so no further animals were injected.

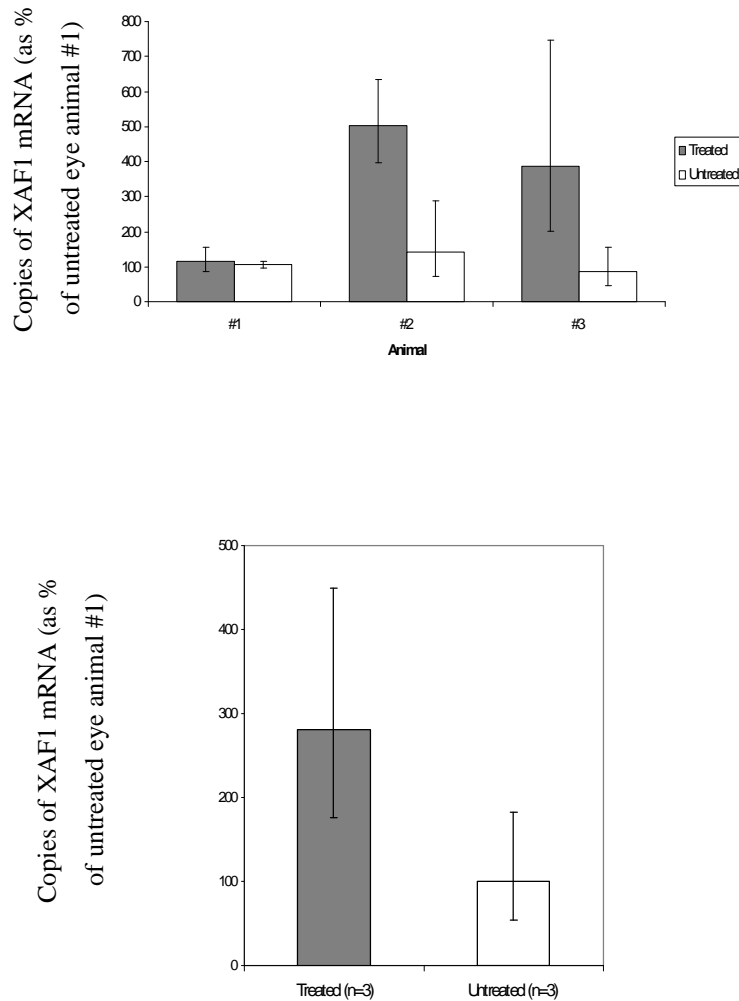


Figure 7-12 XAF1 expression levels in CMV.XIAP treated and untreated eyes of the *Rho-/-Opn.gfp* mouse. In the uppermost graph XAF1 expression levels are compared between eyes of individual animals. Levels are expressed as a percentage of those in the untreated eye of animal #1. Mean levels, in treated and untreated eyes, are shown in the lowermost graph. A paired t-test including the data from all 3 animals revealed no significant difference between treated and untreated eyes.

7.8 Discussion

7.8.1 rAAV2/8.CMV.XIAP in the *Rho*^{-/-}*Opn.gfp* mouse

The aim of these experiments was to slow cone photoreceptor loss in the *Rho*^{-/-}*Opn.gfp* mouse through the expression of XIAP. A plasmid containing XIAP cDNA was validated *in vitro*, and used *in vivo* with the same promoter and vector that had previously expressed GDNF at over 200 times the levels found in fellow untreated eyes. One of the treated mice was culled for mRNA analysis and this confirmed expression of the human transgene in the mouse eye.

There was however no evidence of cone neuroprotection in mice treated with the rAAV2/8.CMV.XIAP vector. Cone function in treated eyes was no different to that in control vector injected eyes. In CMV.XIAP and control vector injected eyes cone function was worse than in untreated fellow eyes due to effects of the sub-retinal injection.

Despite the evidence for transgene mRNA in a treated eye attempts to quantify protein levels in 4 other treated mice have been unsuccessful. Related *in vivo* experiments with XIAP constructs have used a haemagglutinin (HA) tag fused to the XIAP protein in order to detect and quantify transgene expression.^{119;412}

Despite the possible impact on XIAP protein function this was done specifically because of difficulties with available antibodies to the XIAP protein when used with *in vivo* samples (personal communication, Dr Wai Gin Fong). There was no reporter gene or HA tag with the construct evaluated here. The *in vitro* data confirming a functional plasmid, and the *in vivo* result confirming human XIAP mRNA show the plasmid and vector to be functional. It remains possible however that the expression of the transgene mRNA did not lead to adequate expression of transgene protein. This could have been due to inhibition of translation for example.

Alternatively it is possible that the human XIAP protein is not effective in mouse. Human XIAP has previously been evaluated in rats.^{119;410;412;417} Rat and mouse XIAP coding sequences both have 89% homology to the human XIAP coding

sequence, and have 90% homology to one another, as determined from the National Institute of Health databases, and comparison of the sequences (www.ncbi.nlm.nih.gov). A difference in human XIAP efficacy between rats and mice is therefore relatively unlikely.

Leonard *et al.* demonstrated evidence of rod photoreceptor preservation in rAAV-XIAP treated eyes in two rat models of retinal degeneration.¹¹⁹ In both the P23H and S344ter models XIAP treated eyes had a relative preservation of ONL morphology and thickness; this indicates a difference in the numbers of rod photoreceptor nuclei but gives no indication as to the number of cone photoreceptors in view of the relative abundances of these two types of photoreceptor. In the P23H rat rAAV-XIAP was associated with improved ERG in late stages of degeneration. The effect was small but significant. However by the time the effect was seen the majority of pre-degeneration ERG function had already been lost. The data shown is for responses to a relatively dim flash (0.63 cd.s/m²) without prior light adaptation to bleach rod responses. The functional data in this study is therefore also predominantly, if not exclusively, a measure of rod-specific outcomes and provides no evidence of cone neuroprotection. Likewise Yao *et al.* demonstrated that increasing XIAP expression in rod photoreceptors, subsequently transplanted into the rd9 mouse, enhanced their survival.⁴¹⁸ Rod numbers were increased at both early and late timepoints in the XIAP treated group as compared to cells transplanted without XIAP treatment. The absolute numbers of XIAP treated cells still declined in time though. There are likely to have been multiple stimuli for cell death during this time course, and differing molecular mechanisms involved. These are not characterised but the results do provide further support that XIAP overexpression has the potential to partially reduce rates of rod photoreceptor death. The experiments here in the *Rho-/-Opn.gfp* mouse in contrast used exclusively cone specific outcome measures. A positive treatment result with the CMV.XIAP construct would have given evidence of cone neuroprotection, and the mechanism could have been investigated with means of a cone-specific promoter to distinguish between a direct effect on cones or enhanced cone survival secondary to rod photoreceptor survival. However, the negative results reported here are open to multiple interpretations as discussed. It can be more challenging to prove a negative

treatment effect, and in this situation evidence of protein expression *in vivo* would be required. It therefore remains to be demonstrated therefore whether overexpression of XIAP does or does not mediate cone photoreceptor neuroprotection in the context of a rod-cone degeneration.

The study of XIAP overexpression in the P23H and S344ter rats indicates that even in rods the effect of XIAP over-expression is limited.¹¹⁹ These are two relatively slow retinal degenerations. In the S344ter model there was no functional benefit over untreated eyes. In the P23H rat there was only a benefit at late stages of the degeneration, and this was limited in magnitude. Further studies in the *Rho^{-/-}Opn.gfp* mouse, which has a much faster retinal degeneration and more severe phenotype, may be better placed using mutant XIAP that is resistant to autoubiquitination and so potentially of greater efficacy.³⁸⁹

7.8.2 The ARR4 promoter

In the absence of a positive treatment effect with the ubiquitous CMV promoter XIAP expression was not investigated with a cone-specific promoter. The evaluations of this novel promoter (cloned by Dr Carvalho) and not previously used therapeutically *in vivo*, confirmed predominantly cone-specific expression. In the 6 week old rhodopsin knockout mouse GFP expression driven by the promoter was seen in cone photoreceptors. None of the injected mice were evaluated at later timepoints, but the previous investigations in the *Rho^{-/-}Opn.gfp* mouse identified that arrestin expression in cones was down-regulated prior to cell death, and indeed whilst eGFP was still evident when driven by a derivative of the human long wavelength sensitive cone promoter (OPN1LW-human). It is not known whether the reduced arrestin protein expression in the non-functional cones was due to reduced transcription or post-transcriptional regulation of the protein, but the former in particular could limit effectiveness of the promoter in treating degenerating cones. Komaromy *et al.* have confirmed that derivatives of the OPN1LW-human promoter are effective in non-functional cones of the dog CNGB3^{-/-} achromatopsia model as well.⁴¹⁹ The ARR4 promoter was not used

further here but it would be of interest to study whether it too leads to transgene expression in non-functional cones.

Chapter 8 Rhodopsin gene replacement

8.1 Introduction

Mutations in the rhodopsin gene account for approximately 25% of cases of autosomal dominant RP,⁴⁸ and are less commonly causative of autosomal recessive and sporadic cases as well.⁴⁹⁻⁵¹ Some of these mutations may be best treated by expression of wild type rhodopsin to effectively dilute out a negative effect of the mutant protein. “Block and replace” approaches are also under investigation experimentally where by all endogenous rhodopsin expression (mutant and wild type) is suppressed and gene replacement therapy is used to express replacement rhodopsin. The former approach in particular, like the use of neuroprotective factors, could be applicable to large numbers of patients regardless of the exact nature of the underlying mutation. Either strategy is however reliant on the expression of wild type rhodopsin. This presents particular challenges because the rhodopsin protein is highly expressed but overexpression has toxic sequences. If however rhodopsin gene replacement is effective at slowing secondary cone photoreceptor loss it could be of benefit to large numbers of adRP patients.

8.1.1 Strategies for adRP

Dominant phenotypes are caused by loss of function, gain of function or dominant negative mechanisms, or due to a combination of these.⁴²⁰ Loss of function mutations are most commonly associated with recessive inheritance, but are also seen in dominant disease when the expression of one functional allele is not sufficient to maintain the normal phenotype. In this situation a loss of function mutation in a single allele results in a pathological phenotype, and this is known as haploinsufficiency. Haploinsufficiency is not a common cause of RP, but has been described in association the *PRPF31* gene which encodes an mRNA splicing factor.^{421;422} Gain of function mechanisms have been associated with the P23H mutation seen in approximately 12% of AdRP patients.²⁶ The mutant protein is misfolded and aggregates into intracellular inclusions with a detrimental effect on cell function.²²⁶ Dominant negative mechanisms, where by the expression of mutated gene compromises the role of the normal allele, are also implicated with the P23H mutation however, as wild type proteins were found to be co-sequestered within the inclusions. Dominant negative mechanisms are sometimes considered as a form of gain of function mutations.

Selected dominant mutations may be treated by increasing expression levels of the wild type protein. Mao and colleagues expressed wild type rhodopsin in the P23H transgenic mouse using rAAV2/5.⁴²³ Increasing the levels of wild type rhodopsin was found to slow the retinal degeneration suggesting that the effect of the dominant mutation could, at least to an extent, be competed out. It will be of interest to see if similar effects are seen in models with related rhodopsin mutations, and to determine the effect of varying expression levels.

Overexpression of rhodopsin in wild type mice leads to photoreceptor degeneration. The rhodopsin expression level to be therapeutic in the presence of a mutation, but avoid toxicity, could therefore be variable depending on the strength of the dominant negative mechanisms in play.

An alternative approach being developed is to suppress expression of the mutated gene, and concurrently express replacement wild type protein. Suppression of

specific genes may be achieved with antisense nucleotides, ribozyme technology or RNA interference, of which it is the latter that has shown the greatest promise for chronic conditions such as inherited retinal degenerations. Antisense oligonucleotides bind to specific mRNAs, and inhibit expression through structural changes that block translation or by inducing degradation. They have a short half-life within the cell however, and so structural modifications are required to potentiate the silencing effect. Antisense oligodeoxynucleotides, which incorporate a deoxyribose sugar, have proved effective at targeting VEGF expression and reducing laser-induced neovascularisation in primate eyes.⁴²⁴ This treatment effect was demonstrated in the short-term at 3 days following laser. The fast degradation of oligonucleotides and oligodeoxynucleotides renders this approach less suited to the long-term silencing of a mutated gene. Ribozymes have a structure more resistant to degradation. Sub-types can be designed to cleave specific mRNA molecules, and thus effectively silence a particular transcript. Specificity to single point-mutations has been demonstrated *in vitro*,⁴²⁵ and limited efficacy has been demonstrated *in vivo* in the P23H rat model of dominant RP.^{134;135;426} Treatment effects have been demonstrated for up to 3 months following treatment. However the use of double stranded RNA (dsRNA) molecules and the RNA interference approach, has largely superseded the previous knockdown results achieved with ribozymes. Through eukaryotic cellular pathways low numbers of dsRNA molecules are able to achieve almost total cellular knockdown of a particular mRNA transcript.⁴²⁷ It is likely that this powerful system evolved as a line of defence against transposons and viral infections. In mammalian cells short dsRNA molecules, 19-21 bp long, are incorporated into the RNA induced silencing complex (RISC).^{428;429} The short-interfering dsRNA (siRNA) then guides the RISC to the complementary mRNA which is catalytically cleaved. *In vitro* and *in vivo* studies have now demonstrated that expression of short hairpin RNA (shRNA) molecules, which are cleaved within the cell to generate siRNA, can be used to silence dominant rhodopsin mutations. O'Reilly et al. demonstrated approximately 90% silencing of the rhodopsin gene in retinal explants using shRNAs.¹³⁸ Rhodopsin cDNA was also generated that was resistant to the shRNA used. Rhodopsin targeting shRNA and resistant rhodopsin cDNA, were then expressed using rAAV2/5 in transgenic mice carrying the P23H allele on a *rho*^{+/-} background. This resulted

in morphological preservation of photoreceptors in the treated eyes, as compared to control eGFP injected eyes. ONL thickness was approximately 33% thicker in the treated eyes at 2 months of age following injections at P10. It would of course be interesting to compare function in treated eyes to that in uninjected controls and evaluate whether this preservation is maintained at later timepoints, but none the less this study showed proof of principle for the “block and replace approach” to dominant mutations.

8.1.2 The challenges of rhodopsin gene replacement

Rhodopsin is one of the most prevalent proteins within the retina and constitutes over 90% of the protein content of rod outer segments.⁴³⁰ Furthermore rod outer segments are replaced at a rate of approximately 10% per day^{430;431} and continued high levels of rhodopsin expression are required to compensate for this turnover. In addition to being highly expressed, rhodopsin protein is also essential for normal rod cell development and survival. This is evident from the rhodopsin knockout models where the rod photoreceptors fail to develop outer segments or detectable function, and rapidly degenerate.^{90;242} These factors render the rhodopsin gene a challenging target for gene replacement therapy. It is also evident that overexpression of rhodopsin has a toxic effect on rod photoreceptor survival. This was first demonstrated in transgenic models where congenital overexpression of rhodopsin resulted in retinal degeneration. Subsequently Mao and colleagues demonstrated that mature photoreceptors are also susceptible.⁴²³ rAAV5 mediated rhodopsin expression in wild type mice lead to reduced ERG function in treated eyes, as compared to untreated controls. There was no comparison made to control vector injected controls or histological analysis of these eyes, but injection of the same vector into the P23H transgenic mice had a positive treatment effect. The authors hypothesised that in the wild type retina the relative excess lead to rhodopsin protein being mis-folded and aggregating.

Palfi *et al.* demonstrated rAAV2/5-mediated rhodopsin replacement, to approximately 40% of physiological levels in rhodopsin-knockout mice.⁴³² This

was sufficient to generate a rod-derived ERG where there is normally none. However cone function was significantly compromised, probably relating to the timing of sub-retinal injections at P0 as similar reductions in cone function were seen in control vector and PBS-injected eyes. Injections at later timepoints, with the construct and vector used, were less effective at restoring rod function. There was therefore no evidence of cone photoreceptor neuroprotection following rhodopsin gene replacement in this study.

8.1.3 Aims

The aim of the following experiments was to restore rhodopsin expression, in mice homozygous for rhodopsin gene disruption, to approximately physiological levels and study the effect on cone photoreceptor degeneration. Sub-retinal injections were performed at timepoints later than P0 in order to try and limit iatrogenic damage to the cone photoreceptors.

8.2 rAAV-mediated rhodopsin expression *in vivo*

rAAV is the most effective vector for the transduction of photoreceptor cells, and specifically rAAV2/8 has been used to treat a fast rod photoreceptor degeneration in mice.¹³³ AAV2/8 was therefore prepared using the human rhodopsin coding sequence (hRHO) driven by the bovine rhodopsin promoter (bRHO, see supplementary data chapter). This promoter has been used previously to effectively rescue rod photoreceptor function in the rds murine model of retinitis pigmentosa.¹³⁰

Virus was concentrated and purified to a titre of 5×10^{12} vg/ml (supplementary data, Figure 11-8) and injected into the subretinal space of rhodopsin knockout mice at P14 of age. To assess transgene expression *in vivo* the treated and untreated fellow eyes were harvested 4 weeks following injection, fixed in paraformaldehyde and prepared for cryosection. Rhodopsin expression in the treated eye (and not in the untreated eye) was confirmed with immunostaining (Figure 8-1). These results also demonstrate that the technique of superior and

inferior subretinal injections (each of 1.5 μ l of virus) leads to effective transduction of photoreceptors across the retina.

Legend to Figure 8-1 (Following Page)

(A). Superior-inferior section through the optic disc of a treated eye. Superior and inferior injections of viral vector were performed at P14 and the eye harvested at P47. Cryosections were incubated with antibody to rhodopsin protein (red) and counterstained with the DAPI nuclear stain (blue). Rhodopsin protein is evident across the entire superior inferior section of the eye following the double injections. (B). Superior-inferior section through the optic disc of the untreated fellow eye from the same animal as in image A. The fellow eye was prepared and stained with rhodopsin antibody alongside the treated eye in image A. No rhodopsin staining is evident within the retina (C). To control for specificity of the antibody secondary, sections from the treated eye were prepared without applying the primary antibody (to rhodopsin). Weak staining was seen of retinal blood vessels, but there was no cellular staining in the ONL. (D). A high magnification image from the same treated eye shows rhodopsin expression within cell bodies of the ONL and additional expression between the ONL and RPE.

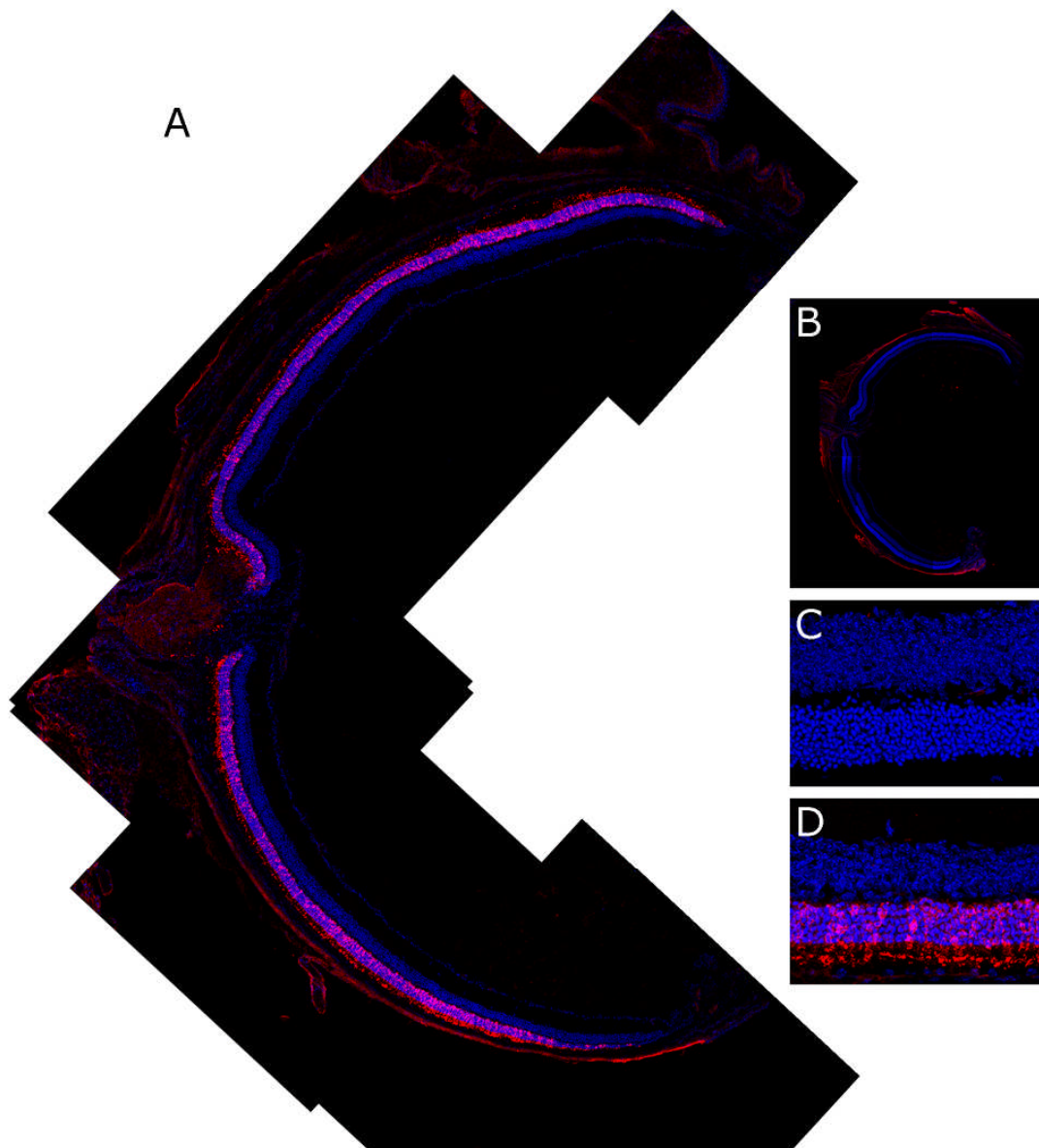


Figure 8-1 Rhodopsin protein in AAV2/8 treated rhodopsin knockout mice. Legend on previous page.

In order to study further the distribution of rhodopsin expression and rod photoreceptor morphology, treated eyes were compared to wild type eyes with immunohistochemistry for the rhodopsin and rod transducin proteins (Figure 8-2). In both treated and wild type rod photoreceptors the rhodopsin protein is primarily located in the outer segments. Protein is also seen within the cell body and inner segments where it is produced and assembled.^{431;433} The outer segments of the treated rods are however considerably reduced in size as compared to those of the wild type mouse. This is of significance as the outer segment is essential for phototransduction. This finding was confirmed by staining for the rod transducin protein which is also located in rod outer segments (Figure 8-2).

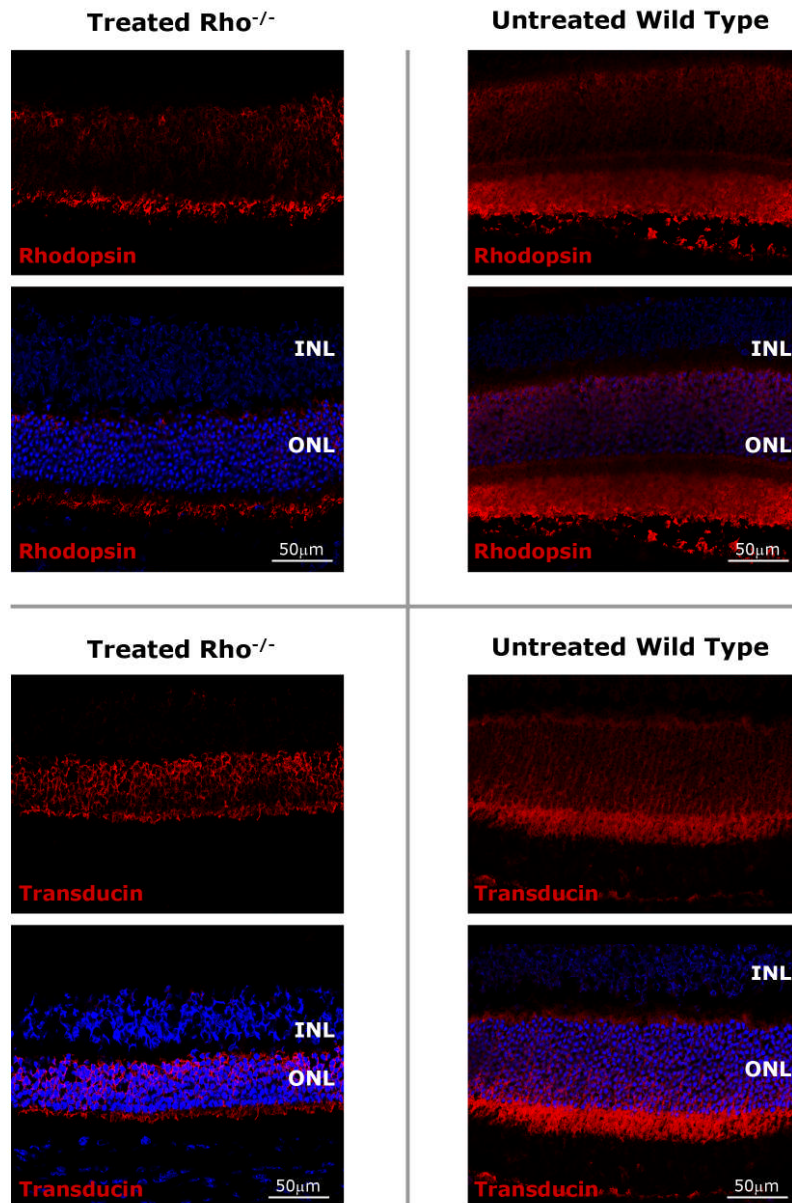


Figure 8-2 Comparison of rhodopsin and transducin expression in treated rhodopsin knockout and untreated wild type retina. All images are single slice confocal sections from mice sacrificed at 7 weeks of age. Rhodopsin and transducin expression in the treated eyes has a similar distribution to that in wild type eyes, but levels are reduced.

8.3 Assessment of the effect of rhodopsin expression on rod function.

To assess whether treatment led to restoration of rod function ERGs were performed at day 40 and 47 of age. In 3 of the 6 rhodopsin knockout mice treated at day 14 b-waves were detected at low light intensities indicative of rod function (Figure 8-3). Although of low amplitude (maximum 30 μ V) these were a consistent feature at both timepoints examined in these 3 animals. Toda *et al.* have previously established that the flash intensity threshold to induce cone function (as defined by a 5 μ V b-wave) in the dark adapted rhodopsin knockout mouse was 0.085 cd.sec/m².²⁴² The responses at the first 3 flash intensities tested (0.003, 0.007 and 0.03 cd.s/m²) are therefore from rod and not cone photoreceptors. This is confirmed by the control traces from the untreated littermates in which no response was detected with a flash intensity below 0.5 cd.s/m².

In all 3 of the successfully treated eyes the dark-adapted 0.5 cd.s/m² flash response was greater in the treated than in the untreated eyes. This is despite the cone function (tested in isolation in the photopic light-adapted protocols) being lower in the treated eye than in the untreated, consistent with the effects of sub-retinal injection on cone function. The increased dark-adapted 0.5 cd.s/m² flash response in the treated eyes can therefore be attributed to rod function in that eye in addition to the compromised cone function.

The 30 μ V rod response is however over 8 fold lower than that detected in age-matched wild types examined with the same ERG protocol (Figure 8-4), indicating only a partial rescue effect. This is in keeping with the histological data indicating reduced rhodopsin expression, transducin expression and outer segment formation in the treated animals as compared to wild types. Reasons for the absence of rescue to wild type levels, despite high titre virus and widespread rod transduction, could relate to the timing of injections or the efficiency of transgene expression with the plasmid used

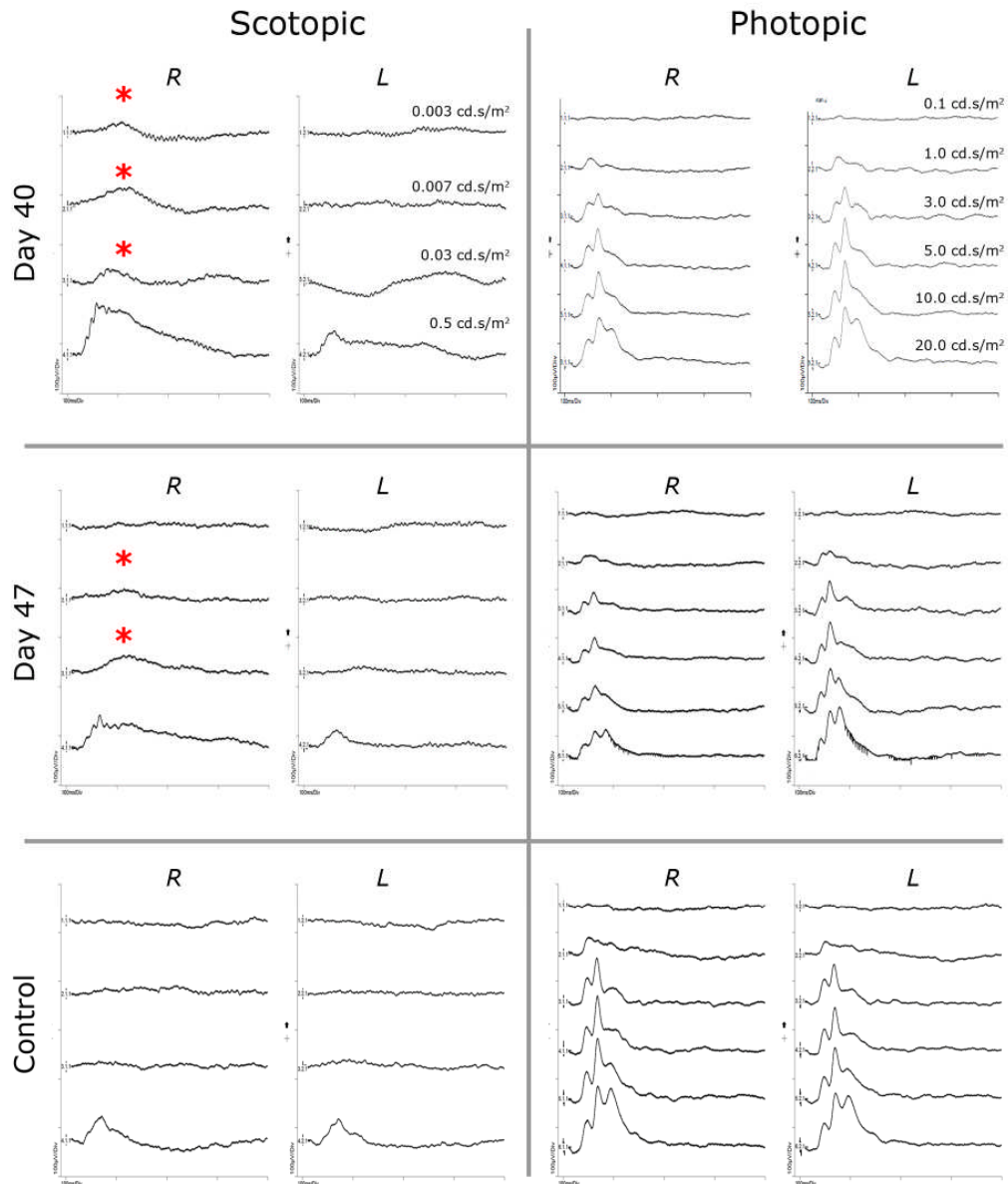


Figure 8-3 Rod and cone function in the rhodopsin knockout mouse treated with rAAV2/8.bRHO.hRHO at P14. The top two rows of traces are from a single mouse treated with AAV2/8 bRHO.hRHO to the right eye only. The third row of traces is from a littermate in which neither eye was treated (analysis performed at day 40). Stimulus intensities are shown on the top row of traces only. As highlighted (*) in the treated eyes only there is evidence of rod function. There is no rod response in the untreated fellow eyes or control littermate. Cone function is reduced in the treated eyes as compared to the untreated fellow eyes.

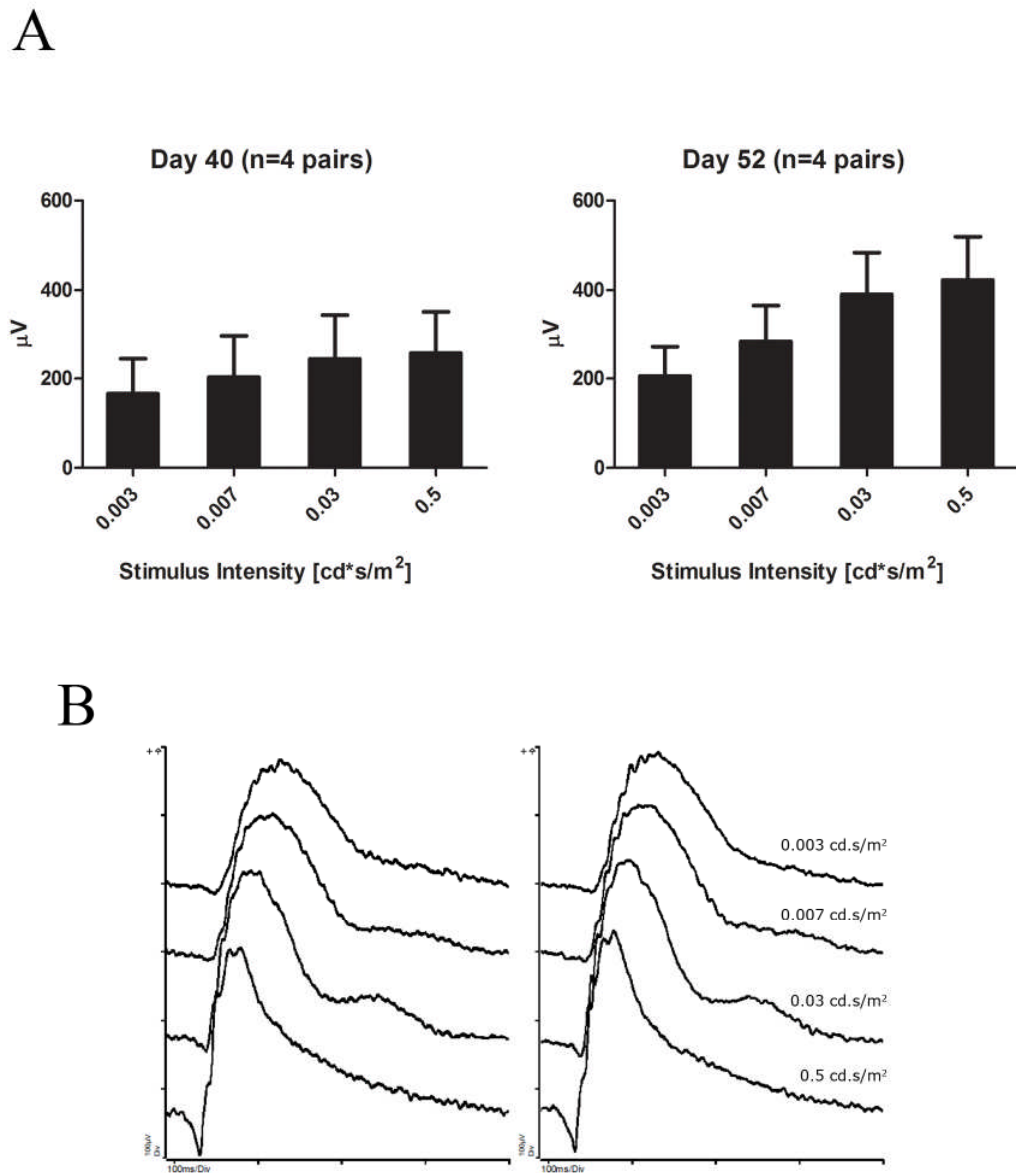


Figure 8-4 Rod function in young wild type mice.

(A) 4 wild-type mice (C57/BL6) were dark adapted overnight and scotopic ERGs performed at day 40 and day 52 of age. B-wave amplitudes are plotted at each of the 4 stimulus intensities examined.

(B) A representative intensity series from one of the mice at 40 days old is shown.

8.4 Timing of rhodopsin expression

In the mouse, rhodopsin expression is well established by P3-5 and increases in levels until after weaning.⁴³⁴⁻⁴³⁶ During this time the number of post-mitotic rod photoreceptors progressively increases, and these mature and develop the outer segments and synapses essential for retinal function (Figure 8-5).⁴³⁷ Early expression of rhodopsin in the *Rho-/-Opn.gfp* mouse is therefore likely to increase the chance of functional rod photoreceptors developing. However, this has to be balanced against disadvantages of performing early subretinal injections. In particular, early sub-retinal injections induce greater levels of cone damage,⁴³² and as the eye is smaller the volume of vector that is well tolerated is smaller too.

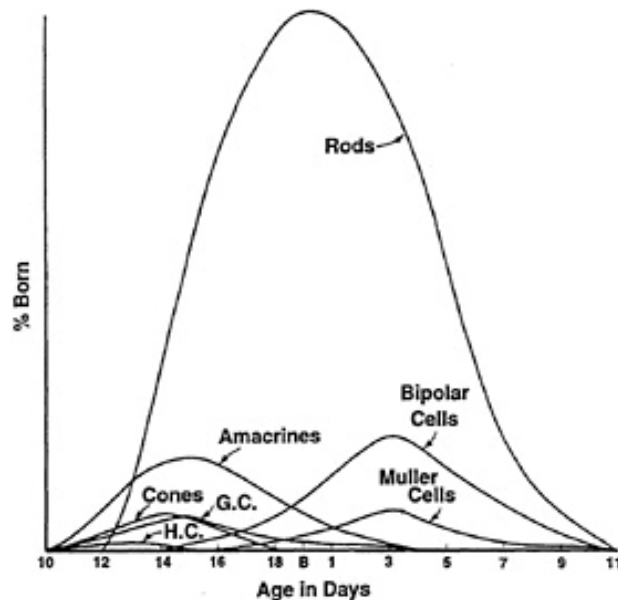


Figure 8-5 Timing of neuronal cell development in murine retina. Developing mice were treated with daily pulses of radioactive thymidine to label cells in S phase at the time of the pulse. With this technique mature cells will retain high levels of the label. However, in cells that undergo subsequent division the label is diluted. By analysing mature retinæ for heavily labelled cells the timing of development of those cells can be determined. This graph from R.W. Young shows the percentage of cells born on a given day is shown for 7 retinal cell types.⁴³⁷ (H.C.-horizontal cell; G.C.-ganglion cell).

To investigate the effect of early injections 4-7 mice were injected at each of days 5, 7 & 8. In view of the small eye at these timepoints a reduced volume of virus was injected (superior and inferior injections of 1 μ l each). None of these early injections resulted in detectable rod function, despite histological evidence of transgene expression (Figure 8-6).

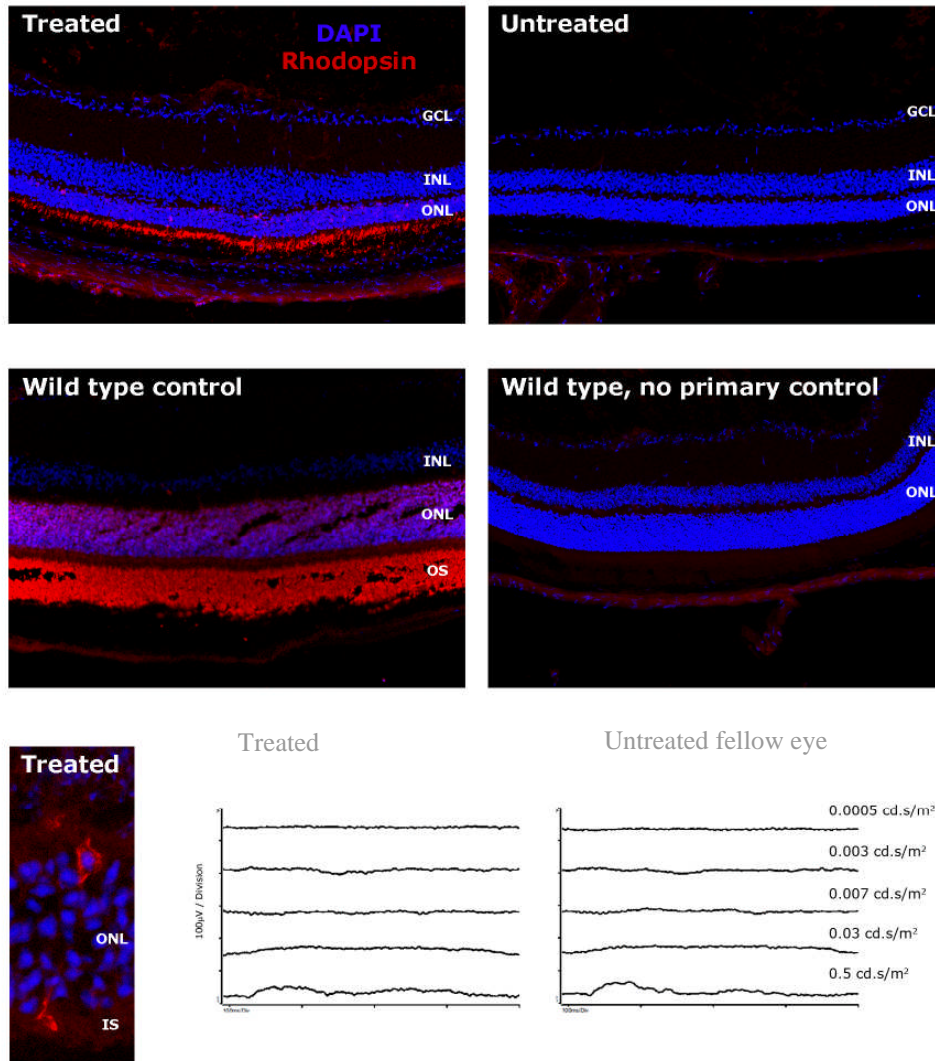


Figure 8-6 Rhodopsin gene replacement in the neonatal rhodopsin knockout mouse. Immunohistochemistry confirms expression in the treated eye following injection at P5 (top row). There is no rhodopsin expression in the fellow untreated eye. However, the extent of expression is reduced as compared to an age-matched wild type eye (middle left). Antibody specificity was confirmed with a no primary control using wild type retina (middle right). A high power image from the treated eye shows rhodopsin expression within the cell body and inner segment of a rod photoreceptor but there is no outer segment staining. Limited outer segment staining is seen in the low power image. Scotopic ERG traces from the same animal, examined at P44 are shown confirming absence of rod function in both eyes, and reduced cone function in the treated eye (as evidenced by the response to a 0.5 cd.s/m^2 flash).

8.5 Combination with GDNF

The efficacy of gene replacement therapy can be augmented through concomitant expression of GDNF. This was demonstrated by Buch *et al.* in the RCS rat and rds mouse, where the combination of *Gdnf* expression and gene replacement improved function and photoreceptor survival as compared to treatment with either construct alone.¹⁵⁴ Eyes receiving gene replacement or growth factor alone were injected with diluted viral vectors such that the number of vector particles for each construct was equal in these eyes as in those receiving combination therapy. In the rds mouse eyes treated with the combination of AAV.CBA.GDNF and AAV.Rho.Prph2 had 51% greater b-wave amplitudes 2 months following injection than eyes treated with AAV.Rho.Prph2 alone. This effect was lost by 4 months following injection. The RCS rat has a null mutation in the RPE-specific gene *Mertk*. Gene replacement was performed using Lentivirus. RCS rat eyes receiving AAV.CBA.GDNF in combination with Lenti.*Mertk* had 50% greater b-wave amplitudes at 6 weeks post injection than eyes receiving gene replacement alone. This effect was not maintained beyond 8 weeks post injection. Thus *Gdnf* had an additive effect, but in the presence of continued cell death the benefit was transient.

Despite earlier results with GDNF alone, *Gdnf* was therefore co-expressed with the rhodopsin replacement construct in the *Rho-/-Opn.gfp* mouse. Single eyes (n=4) were treated with a 50% mixture of rAAV2/8.CMV.GDNF and rAAV2/8.bRHO.hRHO. Vectors were used at maximum titre and eyes were injected at P14 with superior and inferior injections of 1.5µl each. The total number of rAAV2/8.bRHO.hRHO vector particles injected in these eyes was therefore 50% lower than in eyes receiving this construct alone in previous experiments. These eyes were assessed with ERG assessments at weeks 8 and week 10. Week 8 assessments were performed twice (24 hours apart) and there was no repeatable evidence of rod function. Cone function was reduced in all 4 treated eyes as compared to untreated fellow eyes. Immunohistochemistry however showed rhodopsin expression in treated eyes despite the lack of rod function (Figure 8-7). Further experiments were performed to increase levels of rhodopsin expression.

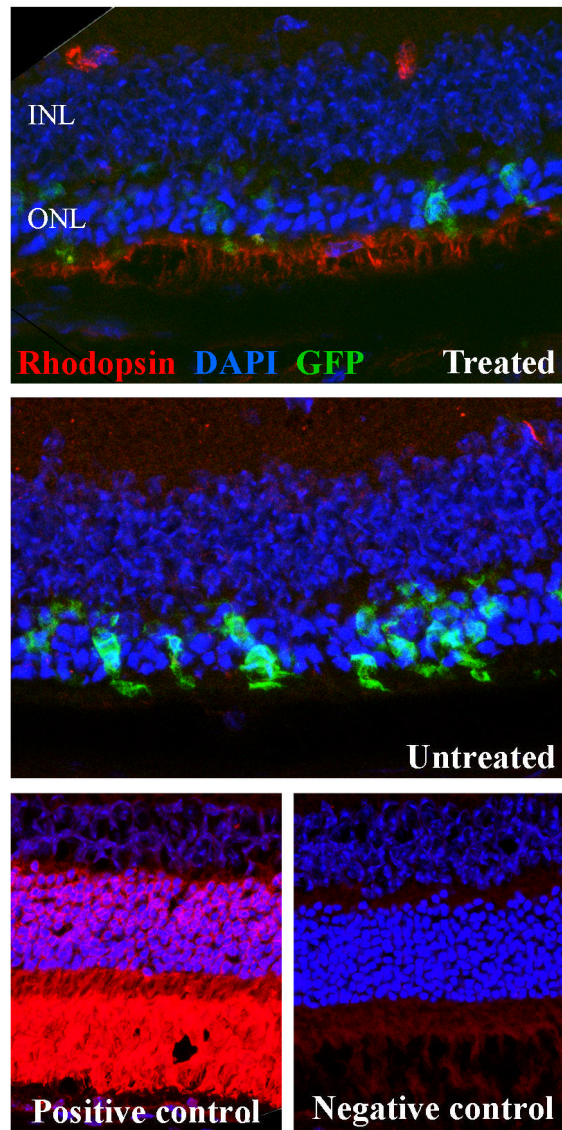


Figure 8-7 Combination treatment with rhodopsin and GDNF in the *Rho^{-/-}Opn.gfp* mouse. Rhodopsin was detected with immunohistochemistry (red) in eyes of 10 week old mice. In the treated eye there is evidence of rhodopsin expression in rod inner segments, whilst there is none in the untreated eye. Sections from a wild type eye were prepared along side and show extensive rhodopsin expression in rod cell bodies, inner and outer segments.

8.6 Optimisation of expression

Gene expression *in vivo* is regulated at multiple levels, including at the level of DNA transcription and mRNA translation. An understanding of the cellular processes through which genes are expressed, and how levels of expression are regulated, allows modification of plasmid sequences to maximise transgene expression. Ultimately this should lead to lower doses of viruses and DNA particles being required to get a therapeutic effect. Significantly, this in turn can be expected to diminish the risks of inflammatory reactions or insertional mutagenesis that have been reported with high titre gene therapy treatments.⁴³⁸ Furthermore maximising transgene expression may facilitate gene therapy treatments in unfavourable cellular environments, such as in the presence of competing mutated proteins or cellular stress responses that act to compromise gene expression; this is of relevance to the treatment of patients with selected missense mutations.⁴³⁹

In the case of the RPE65 plasmid used to demonstrate treatment of LCA first in dogs and then in patients, sequence modifications of the plasmid lead to a four fold increase in protein levels when evaluated in RPE cell culture (personal communication Dr Prateek Buch). This was achieved through intron insertion, optimisation of the Kozak consensus sequence, and codon optimisation. These same approaches were used to optimise the rhodopsin plasmid with the aim of increasing protein expression levels *in vivo*.

8.6.1 Intron insertion

The inclusion of an intron in plasmid DNA can be a highly effective means of increasing transgene expression.⁴⁴⁰ Introns are sequences of non-protein coding DNA that through multiple mechanisms can be associated with increased mRNA levels and increased translational yield from spliced mRNAs (reviewed by Le Hir *et al.* and A.B. Rose).^{441;442} Of note sequences within the intron (enhancers or alternative promoters) can increase levels of transcription, whilst other components can act to aid RNA polyadenylation, stability and transport.^{440;441;443} The process in which intronic sequences are removed from mRNA by the

spliceosome is also associated with increased rates of protein translation. Nott *et al.* found that experimental insertion of a single intron was most effective when the intron was inserted at the 5' end of a transgene, as opposed to the 3' end, with the former leading to a 29 fold increase in *in vitro* gene expression as compared to an intron-less construct.⁴⁴⁰ The effect of intron insertion is however variable, and dependent on the nature of the intron and the point of its insertion.⁴⁴⁴

A short (159bp) intron, originally derived from the SV40 viral genome, was cloned in to the pd10 rhodopsin plasmid (Figure 8-8) and the sequence checked by enzyme digests and plasmid sequencing. This intron has previously been found to increase expression of GFP driven by the human rhodopsin kinase promoter when tested in mice.⁴⁴⁵ It has also been used in concert with codon optimisation and Kozak sequence modifications to increase expression of the *RPE65* gene *in vitro* (Dr Buch, personal communication).



Figure 8-8 The pd10 rhodopsin plasmid optimised for protein expression.

8.6.2 Kozak consensus sequence optimisation

The initiation of mRNA translation by ribosomes is influenced by which bases are found either side of the start codon. At selected positions along the mRNA molecule certain bases can favour ribosomal initiation more than others and so influence levels of protein production.^{446;447} This variability is likely to have evolved as a means of regulating levels of protein translation, and hence the degree to which different genes are expressed. In eukaryotes the -5 to +6 region (with +1 being the first base of the start codon) has the greatest influence and is

referred to as the Kozak consensus sequence.⁴⁴⁶ The nucleotides at the -3 and +4 locations in particular are highly conserved, as shown in Figure 8-9, and changing the sequence to conform with the naturally conserved sites can be a means of increasing gene expression.⁴⁴⁷ Bennicelli *et al.* used this approach when treating the Briard dog model of LCA;⁴⁴⁸ however this was an empirical approach as the effect of the Kozak sequence modifications they made were not determined.

The Kozak consensus sequence of the bovine rhodopsin-rhodopsin plasmid (CA GCC ATG AAC) was compared with data for nucleotide prevalence in mammalian mRNA (as shown in Figure 8-9), and with *in vitro* evidence of the effect of base substitutions in the region of an ATG codon.⁴⁴⁷ The bovine rhodopsin-rhodopsin plasmid has an adenine at +4, which is the second most prevalent nucleotide at that location. A guanine instead could be expected to increase protein production⁴⁴⁷ but is not possible whilst still keeping a codon for asparagine, the first amino acid of the rhodopsin gene. The -5, -2, -1, and +5 nucleotides are all optimal, and the -3, +4 and +6 nucleotides are all of second preference. In the context of a favourable sequence in general the impact of single nucleotide substitutions is diminished. As the existing Kozak sequence was found to be only marginally sub-optimal no substitutions were made.

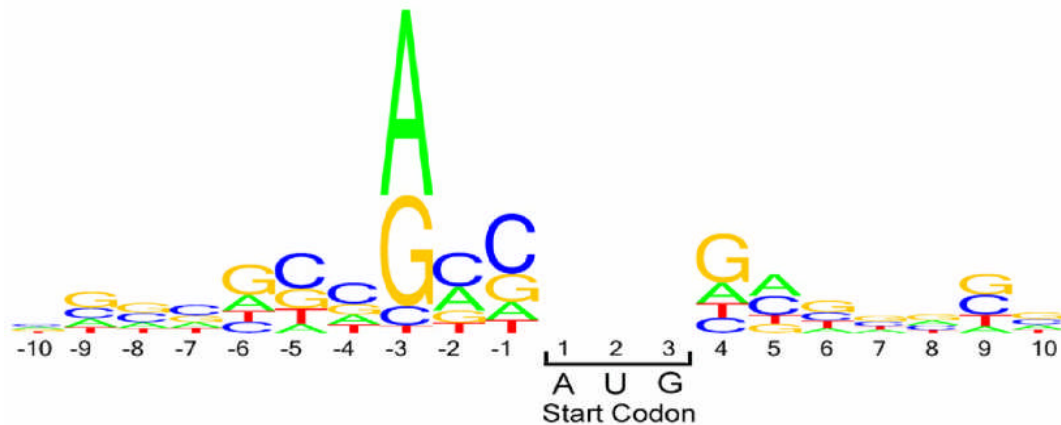


Figure 8-9 Graphical representation of relative nucleotide abundances at locations either side of the AUG translation initiation site in mammalian mRNAs. The overall height of the nucleotide stack indicates the sequence conservation at that position, whilst the height of the nucleotide symbol within the stack indicates the relative frequency of each base at that position. The graphic shows that position -3 is the most conserved site, and that A and to a lesser extent G are commonly found at that location; C or T are uncommon at -3. In contrast the +8 site is not a conserved site, and any of the nucleotides are found at that location with approximately equal prevalence. Adapted from Wegrzyn et al. 2008.⁴⁴⁹

8.6.3 Codon optimisation

Most amino acids can be coded for by multiple different DNA codons. For example, alanine is coded for by GCT, GCC, GCA or GCG. There are therefore typically a very large number of different transgene sequences that can be used to induce expression of the same protein. Which transgene sequence is used can significantly alter the levels of expression through influences on the efficiency of transcription, translation and mRNA stability. In a recent study of lentiviral vector mediated expression of factor VIII (in a study of treatments for haemophilia) codon optimisation increased expression up to 44 fold *in vivo*.⁴⁵⁰ In part this was due to the elimination of transcriptional silencers and inhibitory

sequences in the original cDNA, but may also have been due to effects on the speed of translation and subsequent folding of protein domains. tRNAs associated with less commonly used codons are themselves less prevalent within the cell, and this influences the speed and efficiency of protein translation.^{451;452} Stalling and errors (including terminations, substitutions and frame shifts) in protein translation are all more common with rare codons, and these in turn can lead to alternative protein folding pathways being used with consequences for protein transport and function.^{453;454}

The original rhodopsin transgene sequence was analysed using the OptimumGeneTM algorithm (Genscript, New Jersey, USA; www.genscript.com). This identified that it was possible to use more prevalent codons, and use codon combinations that improve mRNA stability and ribosomal binding, without altering the amino acid sequence of the protein formed. The nucleotide changes made to optimise the rhodopsin transgene are shown in the supplementary data chapter (Figure 11-9), and were performed commercially by Genescript. All changes were made to optimise expression in humans. Although the plasmid is to be tested in mice the largest differences in optimal codons are seen between prokaryotes and eukaryotes. Differences between mammalian species are relatively small. Of note there were no significant cis-acting regulatory elements in the sequence amenable to change. However it was possible to improve the use of more prevalent codons (Figure 11-10, supplementary data), and improve the distribution of more prevalent codons along the length of the transgene sequence (Figure 11-11, supplementary data). The GC content, which is inversely associated with the thermodynamic stability of RNA secondary structure,⁴⁵⁵ was also improved by removing peaks of high GC content in order to prolong the half-life of the mRNA formed (Figure 11-12).

8.6.4 Evaluation of optimised plasmid

Expression of a transgene driven by the rhodopsin promoter can not readily be evaluated in standard cell cultures, and so these optimisation steps were not evaluated in vitro. rAAV2/8 bRHO.hRHO^{Optimised} was prepared using the

optimised plasmid and purified using the standard protocol incorporating phase separation. Vector purity was confirmed using SDS-PAGE and a Spyro Ruby protein stain (supplementary data chapter, Figure 11-14). Unilateral superior and inferior injections of 1.5 μ l of rAAV2/8 bRHO.hRHO at 1×10^{11} vg/ml were performed in 4 *Rho*^{-/-}*Opn.gfp* mice at p10 of age. Treated eyes were compared with untreated fellow eyes.

There was no evidence of rod function with flash intensities below 0.5 cd.s/m² in the treated eyes. However, in 3 of the 4 treated eyes the response to brighter flash intensities under scotopic conditions was greater in the treated eyes than in untreated eyes. In each of these animals photopic ERGs confirmed that cone function was worse in treated eyes than in untreated fellow eyes. The improved response in the treated eyes to bright stimuli under scotopic conditions is therefore likely to be due to rod responses despite the lack of detectable responses to low flash stimuli. Example traces from one of the 3 animals showing this pattern are shown in Figure 8-10. Responses to flashes of 3.0 cd.s/m² were examined under both scotopic and photopic conditions and were compared to one another. The mean difference in b-wave amplitude between treated and untreated eyes under photopic conditions, expressed as a percentage of function in the untreated eye, was a 24.5% reduction (sd 11.4). Cone function was therefore reduced in treated eyes, as compared to untreated fellow eyes, by a similar extent to that seen with injections of control vector. Sub-retinal injections of a control vector lead to a 33.8% reduction in function to a 10.0 cd.s/m² flash (Figure 6-5). In contrast under scotopic conditions the b-wave amplitude to the same flash intensity caused a mean reduction of just 5.2% (24.2). A t-test revealed no significant differences in the percentage reduction in function following treatment seen in scotopic versus photopic conditions (p=0.20). Further experiments are ongoing to determine if increased doses of the optimised plasmid improve the rod responses obtained.

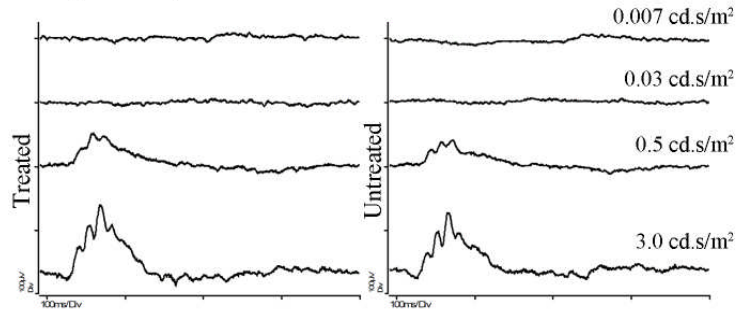
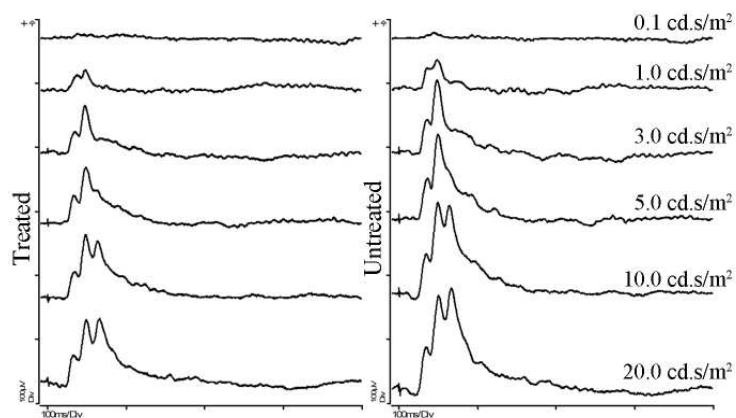
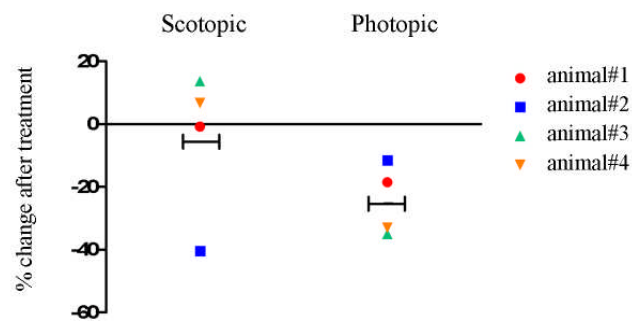
Example scotopic series**Example photopic series****b-wave amplitude to 3 cd.s/m² flash**

Figure 8-10 ERG function in rAAV2/8 bRHO.hRHO^{Optimised} treated eyes. Example ERG traces (animal#4) are shown from scotopic and photopic examinations. Under scotopic conditions function in the treated eye was greater than that in the untreated eye. Under photopic conditions the reverse was true. In the lower most graph the percentage change after treatment is presented for each of the 4 animals (the difference between b-wave amplitude between treated and untreated eyes as a percentage of the untreated value). Mean is shown with horizontal bars.

8.7 Discussion

Gene therapy was used here to induce rhodopsin expression in mice homozygous for rhodopsin gene disruption. Using rAAV2/8, rhodopsin was expressed following injections in mice up to P14. Repeatable ERG responses were seen in a minority of treated animals when exposed to rod-specific stimuli (0.007 and 0.03 cd.s/m² flashes under scotopic conditions). No responses were seen in untreated eyes under these conditions. These responses represent rod function restored by the gene replacement therapy.

Higher flash intensities under scotopic conditions (0.5 and 3.0 cd.s/m²) were used to stimulate a combination of rod and cone photoreceptor mediated responses. These stimuli resulted in greater responses in treated eyes than in untreated fellow eyes in some of the experimental animals. This was despite decreased cone function in the treated eyes as evidenced by ERG recordings under photopic conditions where a bright light was used to suppress rod activity. It is therefore likely that the increased responses to bright flash intensities under scotopic conditions result from rod activity in treated eyes.

Rod function was detected at low light intensities (0.07 and 0.03 cd.s/m²) with b-wave amplitudes reaching up to 13% of wild type levels. Earlier injections, concomitant GDNF gene therapy and modifications of the plasmid with the aim of improving transgene expression all failed to yield rod function at low light intensities, though evidence at higher flash intensities (0.5 and 3.0 cd.s/m²) was variably present. In part this may be due to the lower doses of viral vector used with the latter modifications, and possibly due to increased iatrogenic damage with early sub-retinal injections in neonatal mice. Thus despite rhodopsin expression evident by immunohistochemistry, rod function in the treated eyes was of greatly reduced amplitude and of reduced sensitivity to low intensity stimuli in particular. This is in keeping with the histological images showing that in the treated eyes the rod outer segments were much reduced as compared to age-matched wildtypes, and that there was evidence of abnormal intra-cellular distribution of the rhodopsin protein with increased expression within the cell body.

Similar levels of rod function, in rhodopsin knockout mice following gene replacement therapy, was detected by Palfi *et al.*⁴³² In their study a modified human rhodopsin cDNA sequence (termed “*RHO-BB*”) was used so that the transgene product was resistant to RNAi developed by the same research group.¹³⁸ The altered transgene could therefore be used as part of a block and replace strategy for AdRP. rAAV2/5 containing the construct was injected at P0 resulting in up to 20% of the rod function seen in age-matched controls, at 6 weeks post-injection. Rod function was evaluated by quantifying b-wave amplitudes in scotopic conditions. A different ERG recording apparatus was used by Palfi *et al.* and so the absolute values of b-wave amplitude in treated rhodopsin knockout mice and controls were greater than in the experiments here. At 12 weeks following treatment there were 3-4 rows of rod nuclei in the ONL. This compared favourably to untreated eyes where the ONL was just 1 single row of nuclei thick, but was reduced as compared to treated eyes evaluated at 6 weeks where the ONL was approximately twice as thick. Likewise rod function in treated eyes declined in time. Rod-derived b-wave amplitudes were approximately 85% lower at week 12 than at week 6 ($20.6 \pm 19.3 \mu\text{V}$ versus $135.3 \pm 58.5 \mu\text{V}$).

Palfi *et al.* compared a number of different promoter sequences in order to improve transgene expression. Differing replacement constructs were injected *in vivo* and rhodopsin transgene mRNA levels quantified using qRT-PCR. Maximal expression levels were found with a 1838 bp promoter containing a 1.7Kb fragment of the murine rhodopsin promoter along with two conserved regions containing the CRX (Cone-Rod homeobox-containing transcription factor) and NRL (Neural Retinal basic Leucine zipper factor) sequences. This resulted in approximately 40% of the *RHO* mRNA levels seen in wild type mice. It is possible that further modification of the bovine rhodopsin promoter used in the experiments here, in addition to the inclusion of the SV40 intron, could further increase expression levels. Increased expression levels are likely to be essential in order to significantly slow the rod degeneration, and in turn slow secondary cone photoreceptor loss. O’Reilly *et al.* previously found that expression of rhodopsin to 70% of wild type levels in transgenic mice was

sufficient for a normal phenotype, as evaluated with histological and ERG assessments.⁴⁵⁶

Injections of rAAV2/5 at P0 reduced cone function in treated eyes by approximately 67% (mean photopic b-wave amplitudes in the treated and untreated eyes studied by Palfi et al. were 29 μ V and 89 μ V respectively).⁴³² In the experiments of this thesis sub-retinal injections of rAAV2/8 at P10, also in mice homozygous for disruption of the rhodopsin gene, impaired cone function by approximately 34%. Cone damage was apparently less but still a potential barrier to clinical application of the treatment. For rhodopsin replacement to be a viable treatment option for AdRP high levels of rod function will need to be restored without compromising the existing cone function of central importance to patients and their quality of life.

Chapter 9 Discussion

9.1 Neuroprotection

Clinical trials of memantine for glaucoma,⁴⁵⁷ GDNF for Parkinson's disease,⁴⁵⁸ and CNTF for RP^{7;459} have to date failed to demonstrate in patients the magnitude of neuro-protective treatment effects that have previously been seen in experimental animal models. In part this may be due to the considerable challenges faced by clinical trials in this field. Neurodegenerations typically progress only slowly and so without long studies and large numbers of patients a treatment effect can be hard to detect. This problem is compounded as many clinical assessments are of limited sensitivity and for many neuro-degenerations the major phase of cell death is in pre-symptomatic patients. In Parkinson's disease approximately 70% of substantia nigra dopaminergic neurons have died over a 5-10 year period before patients develop motor symptoms,⁴⁶⁰ and in inherited retinal degenerations over 90% of cones may have ceased functioning before there is a substantial loss in acuity.¹³⁹ Conducting clinical trials in pre-symptomatic patients is only possible if the course of disease can be accurately predicted and the risks of intervention are low. Early phase clinical trials are therefore typically in patients with advanced disease. Nevertheless the apparent differences in treatment outcomes between experimental and clinical studies can serve to highlight the limitations of some of the experimental models used. In particular the timing of disease progression and potential of confounding variables (including ageing, genetic heterogeneity and environmental influences) are often markedly different.

In the field of cone photoreceptor neuroprotection experimental studies are commonly limited by the challenges of longitudinal follow-up and, in rodent models, the difficulty with identifying cone-specific outcome measures. The characterisation and use of the *Rho*^{-/-}*Opn.gfp* model is a step towards addressing

these limitations. Its use in this thesis demonstrated that cone-specific outcome measures can be assessed repeatedly in individual animals to allow the magnitude of any treatment effect to be characterised in time. This allows the identification of potential therapies where the treatment effect soon wanes.

With this model no treatment effect of GDNF was identified, in contrast to previous studies looking at rod-outcome measures at single timepoints.^{80;160} If GDNF were to have a significant and sustained effect on either rods or cones in the *Rho-/-Opn.gfp* mouse one would have expected an effect on the cone photoreceptor outcome measures as cone loss is secondary to rod loss. It is therefore most likely that GDNF does not have an effect on rods or cones in this animal model. The value of the rhodopsin knockout phenotype lies not in a direct similarity to the mutations seen in patients, but in being an experimental model with which to study rod-cone degeneration and to facilitate the study of cone-specific outcome measures. It is a more severe phenotype than that seen in patients and so the absence of an effect in this model does not preclude an effect in others, or indeed in patients. It would therefore now be of interest to study GDNF in the presence of other rod mutations also crossed onto the *OPN.gfp* background.

The use of this model has also illustrated that in many ways it should be easier for us to evaluate neuroprotective agents in inherited retinal degenerations than for researchers studying other neurodegenerations. In contrast to striatal neurons the anatomy and function of photoreceptors can be comprehensively evaluated non-invasively *in vivo*. Furthermore treatments can be delivered to specifically these cells by translatable and well established techniques. This should mean that the problems of systemic side-effects seen with treatments targeting the substantia nigra may be avoidable. The potential clinical impact of even limited neuroprotective effects is massive, and thus despite the negative findings from clinical trials and pre-clinical trials to date the search for neuroprotective agents is highly justified. Improved understanding of the disease mechanisms and potential therapies should drive this research. Studies of inherited retinal degenerations are favourable settings to further the study of CNS neuroprotection

in general and animal models related to the *Rho*^{-/-}*Opn.gfp* mouse are likely to facilitate this.

9.2 Transducing the outer retina

The experiments here in murine models of retinal degeneration and in wild type mice have demonstrated significant iatrogenic damage to cone function following sub-retinal injections. This is in keeping with previous findings in other animal models.^{343-345;354} Investigators therefore sometimes compare eyes injected with potential therapies to eyes injected with control solutions or other vectors.¹¹⁹ The rationale to justify this includes that sub-retinal injections in humans may not be so damaging to retinal function as those induced experimentally in rodents; thus only looking for a treatment effect in rodents sufficient to overcome that damage may be un-necessarily discerning. In addition, in the RCS rat sub-retinal injections of fluid or injury can themselves induce a non-specific therapeutic effect; in this situation control injections are used to quantify these non-specific effects that are not attributable to the therapeutic agent being evaluated. Nonetheless comparison to un-injected fellow eyes gives the clearest indication as to whether the intervention is likely to provide therapeutic benefit.

In the GDNF and XIAP experiments here the outcome measures have been specifically cone photoreceptor related. There was a 30% loss of function with sub-retinal injections of control vector alone in the *Rho*^{-/-}*Opn.gfp* mouse and so only highly effective therapies would lead to an improvement in cone function as compared to untreated fellow eyes. Such an effect was not seen with the GDNF or XIAP constructs used. It may be that in models with slower degenerations the detrimental effect of a sub-retinal injection on cone function is less. In addition, in studies using models with slower degenerations and late outcome measures there will be a longer time period to allow for cone photoreceptor repair. Komaromy et al. studied specifically cone function in *CNGB3*^{-/-} dogs treated with sub-retinal rAAV.⁴¹⁹ Despite a range of transgene expression levels, some of which were possibly supra-physiological in the missense mutant dogs, maximal ERG function was still significantly diminished relative to wild types.

There are multiple potential explanations, including that only a fraction of the retina was treated or that the kinetics and levels of transgene expression are critical for proper assembly of CNGB3 and CNGA3 proteins into functional channels. It is also possible that iatrogenic damage to the cones could be part of the explanation. Alexander *et al.* did however restore light-adapted cone function in the *Gnat2^{cpfl3}* murine model of achromatopsia to wild type levels.⁴⁶¹ These mice were injected at ages of between P23 and P29, and so at later timepoints than those in this thesis, but nonetheless these results illustrate that with highly effective treatments the iatrogenic effects of sub-retinal damage can be overcome.

Intra-vitreous delivery of therapeutic agents is in some cases an alternative. It induces less iatrogenic damage but in general requires diffusion of the therapeutic agent down a concentration gradient to its site of action, with the inherent risk of side-effects. Bejjani *et al.* reported gene expression in RPE cells following the intravitreal delivery of nanoparticles.²⁰¹ This would present a favourable alternative to sub-retinal delivery of viral vectors if expression levels were comparable and sustained. However, in their study expression was only shown for up to 14 days, and there was no indication as to the number of cells expressing the reporter gene. One of the principal problems with nanoparticle technologies such as this is that they contain bacterial DNA, with its characteristic patterns of methylation. Recognition of bacterial DNA by eukaryotic cells can lead to short transgene expression, and this is likely to be one of the contributing factors to the very limited treatment effects obtained to date with nanoparticles as compared to those with viral vectors.^{200;202} Viral vectors are, in contrast, prepared in eukaryotic cells and capable of inducing high levels of transgene expression for many years after retinal cell transduction.^{197;198} They are likely to remain the only clinical means of transducing outer retinal cells *in vivo* for the near future, and are dependent on sub-retinal injections. The recent clinical trials of *RPE65* gene replacement therapy have demonstrated that the procedure itself can be performed safely in young patients, despite strong vitreous attachments and degenerate retina.¹⁻⁶ Patients will have to be carefully counselled about the risks involved but these results open the way for further clinical trials of sub-retinal gene therapy to proceed.

9.3 Dosing and gene therapy

The experiments in this thesis demonstrated no neuroprotective effect of GDNF on cone function following intra-vitreous injection of recombinant protein and following gene therapy that increased endogenous expression between 5 and 232 fold. It is however plausible that there could be a treatment effect with alternative doses of GDNF.

Erythropoietin is a cytokine that like GDNF has been found to reduce rates of neuronal cell apoptosis in *in vitro* and *in vivo* models of relatively acute cell death.^{462;463} As for GDNF, the intracellular PI-3-K/Akt kinase signalling pathway and upregulation of XIAP have been implicated in the cellular mechanisms through which neuroprotective effects are mediated.⁴⁶⁴⁻⁴⁶⁶

Weishaupt characterised the dose-response relationship for EPO supplementation in *in vitro* and *in vivo* models of rat ganglion cell death and found that in both contexts there was a steep bell-shaped dose response curve such that a neuroprotective effect of EPO was identified with only a relatively narrow therapeutic window.⁴⁶⁴

In the experiments discussed in chapters 4-6 GDNF was expressed with the constitutively active CMV promoter, or administered at high dose with intravitreal injections of recombinant protein. rAAV2/2 mediated delivery of CMV.GDNF following single intra-vitreous injections achieved a 5 fold increase in expression levels, as compared to basal levels. This was an identical increase to that reported by Wu et al. using a single injection of rAAV2/2 in wild type rats,^{160;308} and likely to be similar to the levels found to mediate rod photoreceptor neuroprotection in the TgN S334ter-4 rat model of RP.² In contrast rAAV2/8 mediated delivery of CMV.GDNF, delivered to the sub-retinal space, resulted in a much larger (over 200 fold) increase in expression levels that is likely to be greater than any reported previously using gene therapy.

Until recently one of the principal challenges with ocular gene replacement techniques has been to achieve levels of expression sufficient to slow

photoreceptor death. For example gene replacement studies in the rds mouse and RCS rat have been effective at improving morphological and functional outcome measures but less successful at halting continued photoreceptor cell death in the longterm.^{130;132} This was probably in part due to inadequate levels of protein being expressed at crucial timepoints. More recent studies using improved vectors and promoters have increased expression levels and proved effective at slowing cell death in even fast models of retinal degeneration.¹³³ It is likely that some gene defects are more readily treated than others with gene replacement therapy, but to a certain extent recent advances have been through maximising expression levels. These advances in viral vector technologies may not necessarily be an improvement for neurotrophic therapies however where bell-shaped dose-response curves may exist.

Although studies in knockout animal models, or those with null mutations, have generally sought to maximise transgene expression it also apparent from other studies that supra-physiological expression can be detrimental. Tan *et al.* bred transgenic mice with rhodopsin overexpression.⁴⁶⁷ Overexpressing rhodopsin by just 23% lead to photoreceptor degeneration, though of note this increased expression was present throughout retinal development. Mao *et al.* evaluated the effect of overexpression in specifically mature photoreceptors with sub-retinal injections of rAAV2/5 and cDNA of the rhodopsin gene with the mouse opsin promoter.⁴²³ Injected wild types had reduced amplitude a and b waves compared to uninjected fellow eyes. Injected eyes were not compared to control vector injected eyes to determine how much of the loss of function was due to the effects of sub-retinal injection. However, the negative effect increased between 1 and 3 months post-injection which would be in keeping with progressively greater, and supra-physiological, levels of rhodopsin expression leading to photoreceptor degeneration.

Persistent and unregulated overexpression of neuroprotective factors could also have detrimental and potentially dangerous consequences. In these experiments the titre of the rAAV2/8 CMV.GDNF (batch#1) was reduced in a step-wise manner with serial dilutions to reduce the number of transduction units delivered to the sub-retinal space. This is however a relatively crude means of titrating

gene therapy as there is likely to be substantial and, more pertinently, largely unpredictable variation in the number of transfection events and transcribed viral genomes when working with viral vectors. The strategies under investigation to enable regulation of gene expression following gene therapy may be broadly categorised into those using exogenous modifiers and those using endogenous modifiers (Figure 9-1).

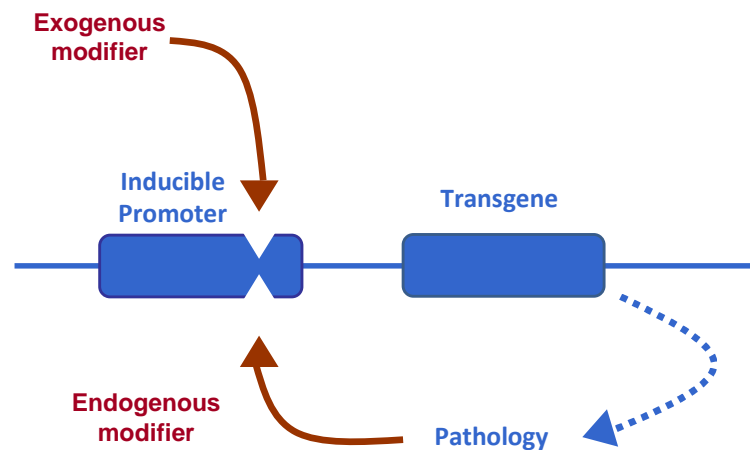


Figure 9-1 Exogenous and endogenous modifiers are used to control gene expression. Endogenous modifiers can be related to the therapeutic target of the transgene and thus constitute an endogenous feedback mechanism

Exogenous stimuli, including physical stimuli such as incident light and ambient temperature, have been used in plant cell technologies to control the activity of inducible promoters.^{468;469} Within the mammalian eye, similar promoters have been used that are sensitive to pharmacological agents, and in particular different tetracycline drugs.^{470;471} Administration of these drugs activates gene expression, and without them the genes are silent, or vice versa. To an extent levels of gene expression are proportional to the dose of exogenous modifier. The drugs however must be administered at doses sufficient to transverse the blood brain barrier, which raises the risks of side-effects and potential drug interactions. In addition the dosing of these regulators would be dependent on changes in the indications for treatment being detectable clinically; this would present a

challenge for both slowly progressive diseases and for pathologies of acute onset such as neovascularisation where the preceding hypoxia is often not apparent clinically. An advantageous approach, where possible, has been to directly couple transgene expression to local tissue changes involved in the pathology to be treated through endogenous modifiers. Bainbridge *et al.* demonstrated *in vivo* that GFP expression could be driven by a promoter sensitive to HIF-1, such that transgene expression was localised to areas of neovascularisation and presumed hypoxia.⁴⁷² This was demonstrated in two murine models in which neovascularisation was induced by exposure of newborn mice to hyperoxia or by laser-induced rupture of Bruch's membrane. Both models entail an acute neovascular response that is limited spatially and diminishes in time. GFP expression, when driven by the hypoxia-responsive element (HRE), was matched to the spatial and temporal patterns of the neovascularisation. This is of relevance to the treatment of patients with neovascular disorders where the hypoxia and neovascular response can be focal and variable in time.

In inherited retinal degenerations the time course of disease is typically slowly progressive, rather than relapsing and remitting. The principal challenge therefore is to achieve therapeutic levels but avoid toxicity. To date this has been best achieved clinically with intra-vitreous implants that slowly release the therapeutic target over many months and can then be removed in the event of toxicity or in the absence of a therapeutic benefit. Expression levels from such implants can be precisely characterised *in vitro*, and these have been used in the clinical trials of CNTF.⁷ Other proteins however are more or only effective if produced close to or within the target cells, necessitating gene therapy. A major challenge for any clinical applications of such proteins, including XIAP and rhodopsin, will be to achieve therapeutic levels and avoid toxicity both in the short-term and potentially for decades after treatment. Furthermore therapeutic levels may vary considerably between patients.

9.4 Efficiency of expression

In the experiments of this thesis up to 1.5×10^{10} rAAV2/8 genomes were delivered to the sub-retinal space of a mouse eye. This is similar to the doses of rAAV2/2

used in the recent clinical trials of retinal gene therapy which used between 1.5×10^{10} vg/eye and 1.0×10^{12} vg/eye.^{3;199;473} In the clinical trials these doses were well tolerated and subsequent trials, aiming to evaluate efficacy rather than safety, are evaluating larger doses still. The requirement for high vector titres is a challenge for vector production, but of greater concern is the increased risk of an immune response. In a clinical trial using AAV2 in patients with haemophilia the long-term transduction of hepatocytes was compromised by immune reactions to the rAAV capsid.⁴⁷⁴ Furthermore, the immune response was dose related. The doses of viral vector used (up to 2.0×10^{12} vg/kg) were however much larger than those employed in ocular gene therapy trials. Of note though, Stieger and colleagues reported that AAV virions persist in the retinae of dogs and primates for up to six years after subretinal injection raising the possibility of immune reactions in the longer-term despite the relative immune privileged status of the subretinal space.⁴⁷⁵ There is therefore a clinical need to optimise the efficiency of gene expression using viral vectors so that minimum doses can be used, and minimise their pathogenic potential.

The experiments here with the rhodopsin construct illustrate how changes to the plasmid may be employed with the aim of maximising transgene expression. As yet the effects of the *in vivo* and therapeutic effects are still to be quantified, but *in vitro* work suggests that Kozak sequence modifications, codon optimisation and promoter sequence optimisation are all likely to improve gene expression.

Another approach is to increase the efficiency of vector transduction. This can be achieved by modifying capsid proteins for example, to remove specific tyrosine residues and reduce proteasome-mediated degradation of the vector.^{476;477} The vectors used in this thesis contained single-stranded DNA. Synthesis of the second strand in transduced cells has been found to be a rate-limiting step for transgene expression. In part this is due to the cellular chaperone protein FKBP52, phosphorylated forms of which interact with the ITRs of the viral genome preventing second-strand DNA synthesis.⁴⁷⁸ Self-complementary (sc) AAV vectors circumvent this step resulting in higher levels of transgene expression and improved kinetics.¹⁹⁴ The principal disadvantage with sc vectors however is that the size of the expression cassette that can be

packaged with in the vector is further reduced. An alternative method has been to co-express enzymes that dephosphorylate FKBP52, which can improve intracellular trafficking of the vector particles to the nucleus as well as facilitate second-strand synthesis.^{479;480}

The rAAV2/8 CMV.GDNF vectors produced for this thesis were found to contain genomes within only about 15% of the capsids. Modifications to vector production methods to reduce the number of empty capsids would be another means of reducing vector-related immune reactions without compromising treatment efficacy. In addition it is the capsid proteins of viral vectors that primarily interact with the host immune system. Modification of these proteins, with knowledge of previous sensitisation in the host, is another approach being used by researchers to improve the efficiency of viral vector mediated gene therapy whilst minimising the potential for immune reactions.^{481;482}

9.5 Future work

The experiments here have demonstrated that a transgenic animal model, with cell-specific reporter gene expression, can be used to repeatedly assess *in vivo* the function and survival of a specific cell-type. Employing such animal models should reduce the numbers required to evaluate potential treatments, and allow the time-scale of treatment effects to be determined in individual animals. The role of *in-vivo* imaging as a research tool and outcome measure is likely to be further advanced by the incorporation of advanced optics technologies. These systems compensate for optical aberrations in order to further improve the resolution of retinal imaging systems. This allows individual cells to be visualised without reporter gene expression,^{483;484} and is likely to aid the assessment of cone neuroprotection in future clinical trials.⁴⁵⁹

It is possible that the greatest value of neuroprotective therapies may lie in an adjunctive role in which they are combined with other therapies. For example whilst the effect of GDNF in the RCS rat is transient its expression can be used to potentiate the effects of gene replacement therapy.¹⁵⁴ Similarly XIAP expression alone was found to confer only structural but not functional protection

of photoreceptors in the rd10 mouse model of retinal degeneration.⁴¹³ It would be interesting to study whether XIAP mediated prolongation of photoreceptor survival increases the time window during which gene replacement therapy is viable. Such a role could be of particular value in the treatment of fast retinal degenerations where high levels of expression can be required at early timepoints. Alternatively neuroprotective factors may be combined with other neuroprotective factors to act synergistically and have an additive effect. GDNF and XIAP have been evaluated together in acute models of neuronal apoptosis. Straten *et al* studied co-expression in the adult rat following optic nerve transection and Eberhardt *et al.* studied co-expression in 1-Methyl-4-phenyl-1,2,3,6-tetrahydropyridine (MPTP) treated mice which have a degeneration of dopaminergic striatal neurons similar to that in patients with Parkinson's disease.^{485;486} In both studies expression was induced with adenovirus, and a treatment effect was seen with expression of either protein alone. When GDNF and XIAP were co-expressed however there was evidence of a synergistic effect. The mechanism for this is not known but could be related to the neuroprotective effects of GDNF being mediated through IAP proteins. Inhibition of XIAP and the neuronal apoptosis inhibitory proteins (NAIP) using anti-sense mRNA, prevents the neuroprotective effects of GDNF.²⁹³ Co-expression of neuroprotective proteins with relatively distinct molecular pathways has also been found to produce synergistic effects, again in the optic nerve transection model of acute neuronal apoptosis.^{298;487} Similar synergistic effects between neurotrophic factors could be of value in inherited retinal degenerations.

The experiments here included modifications to DNA plasmids that can be expected to increase transgene expression on the basis of related *in vitro* experiments. The effects of codon optimisation and intron insertion for example may however vary *in vivo* and with the combination of transgene and promoter used. Further study of the effect of such changes, and quantification of expression levels *in vivo*, could have significant consequences for the efficacy and safety of future gene therapy trials. In the immediate future such trials are likely to be predominantly for recessive monogenic disorders treatable with gene replacement therapies. However the focus for the majority of inherited retinal degeneration patients remains on finding a more widely applicable treatment that

produces a lasting effect on the cone-photoreceptor mediated vision so important for normal functional lives

Chapter 10 Acknowledgements

I would like to thank, and acknowledge, the assistance of the following research group members for help with particular practical components of this body of work:

- Mr Mark Basche and Ms Selina Azam for assistance with viral purification techniques, and purity testing of rAAV2/8.
- Mr Vy Luong for technical assistance with the Heilderberg imaging apparatus used.
- Dr Peter Munro for assistance with electron microscopy.

I am also grateful to the Wellcome Trust who supported the work through a Research Training Fellowship (Grant 086868/Z/08/Z).

Chapter 11 Supplementary Data

11.1 Model characterisation

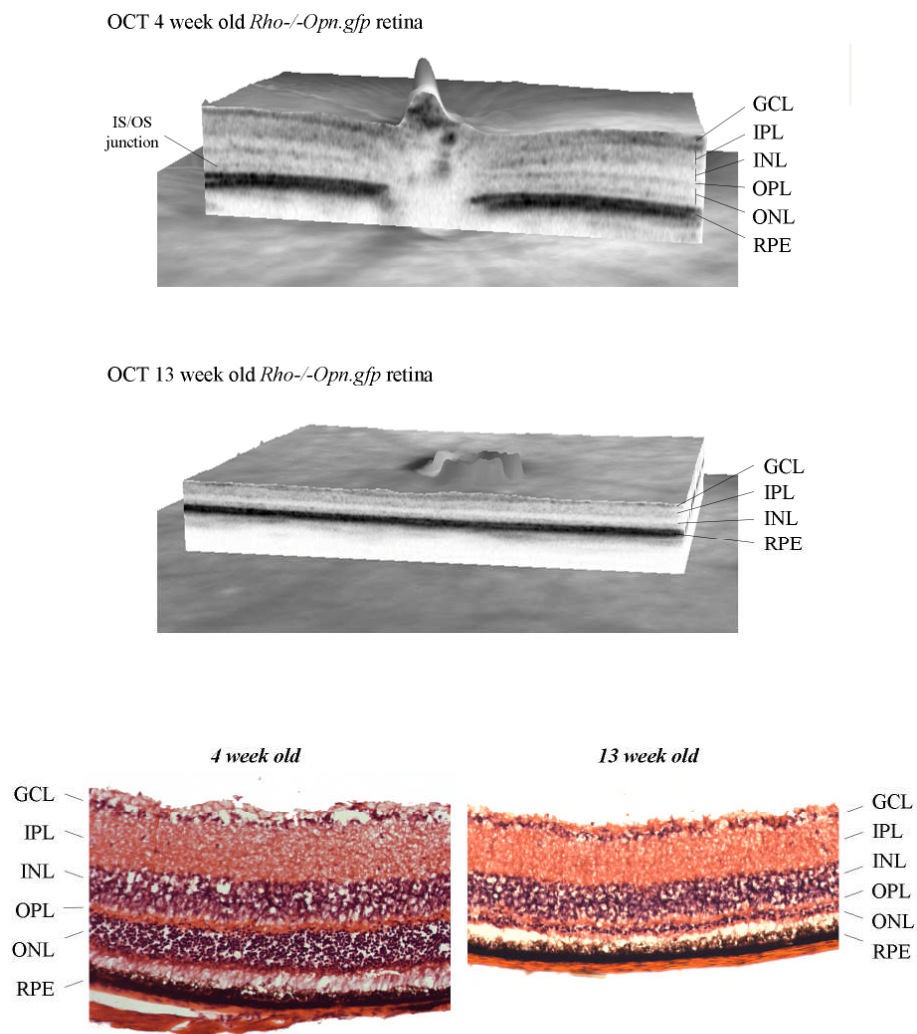


Figure 11-1 Degeneration of the outer retina in the *Rho^{-/-}Opn.gfp* mouse. The retinal thickness of mice with the rhodopsin knockout genotype was examined *in vivo* with ocular coherence tomography (OCT), and histologically (cryo sections were stained with H&E). *In vivo* and histological sections showed loss of the outer retina during the degeneration. The inner retina is relatively preserved.

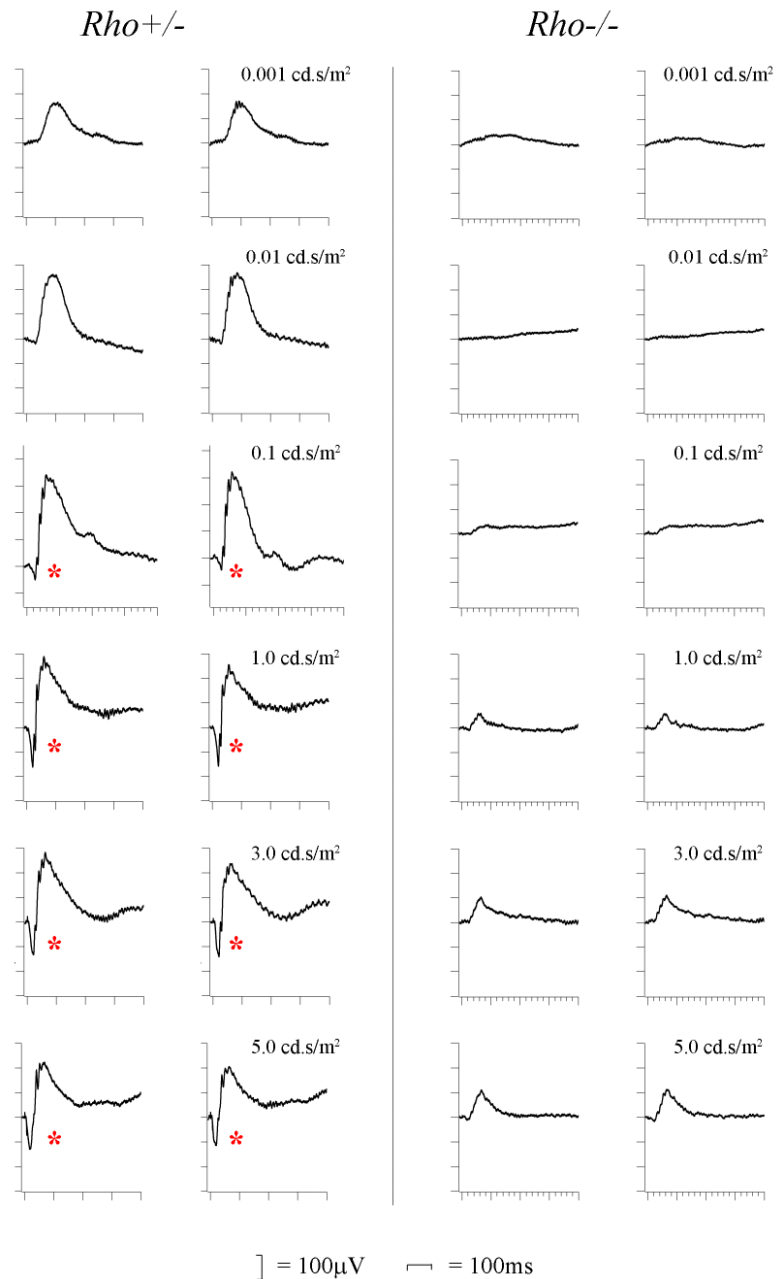


Figure 11-2 The rhodopsin knockout phenotype: rod function as assessed with the scotopic ERG in 6 week old mice. In the rhodopsin knockout heterozygote (*Rho+/-*) there is a significant b wave response to flashes of 0.001 cd.s/m² or brighter. With higher flash intensities an a-wave is also discernable (*). In contrast in the rhodopsin knockout homozygotes there is no consistent response to flash intensities below approximately 0.5 cd.s/m². Even at higher flash intensities there is no discernable a-wave.

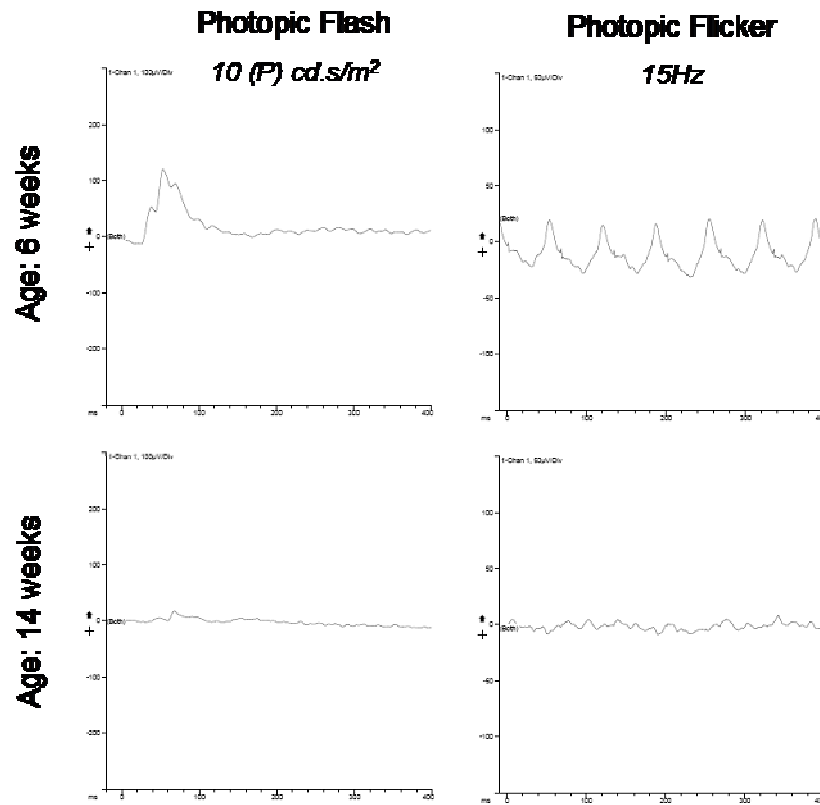
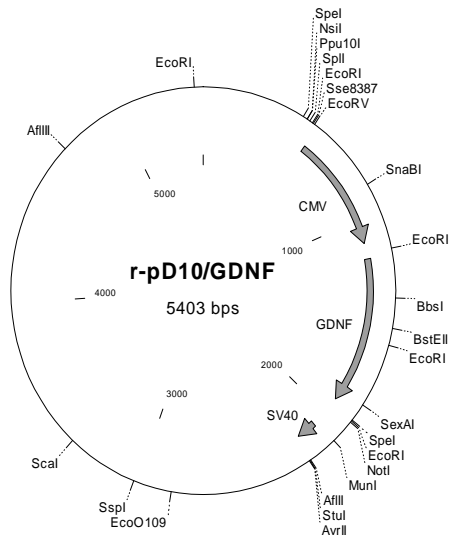


Figure 11-3 The rhodopsin knockout phenotype: cone function as assessed with the photopic and flicker ERG. In the young mouse homozygous for disruption of the rhodopsin gene cone function can be quantified with photopic flash or flicker ERG protocols. This cone function is lost during the course of the retinal degeneration.

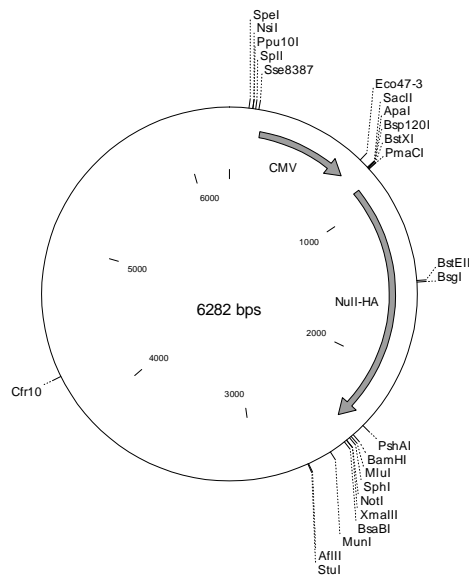
11.2 Plasmid maps

All cloning was carried out with the pd10 plasmid.

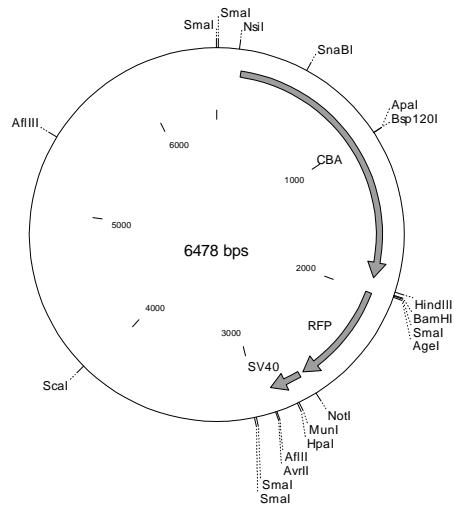
11.2.1 CMV.GDNF plasmid



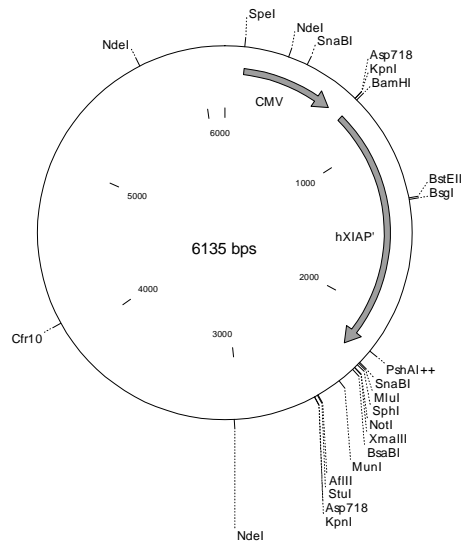
11.2.2 Null plasmid



11.2.3 CBA.RFP

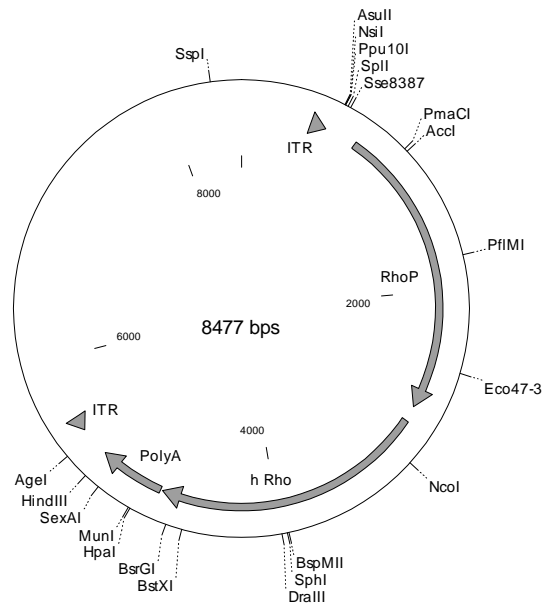


11.2.4 CMV.XIAP



11.2.5 bRHO.hRHO

This plasmid contains the bovine rhodopsin promoter (bRHO or RhoP) and human rhodopsin transgene (hRho).



11.3 rAAV2/8.CMV.Gdnf

11.3.1 Virus titre

The titre of this virus was 5×10^{13} . Standards were prepared in duplicate. Luminance of the 5 μ l and 1 μ l vector samples, and 10^{12} , 10^{11} and 10^{10} samples of both standards was quantified and the titre calculated by comparison of these luminance values.

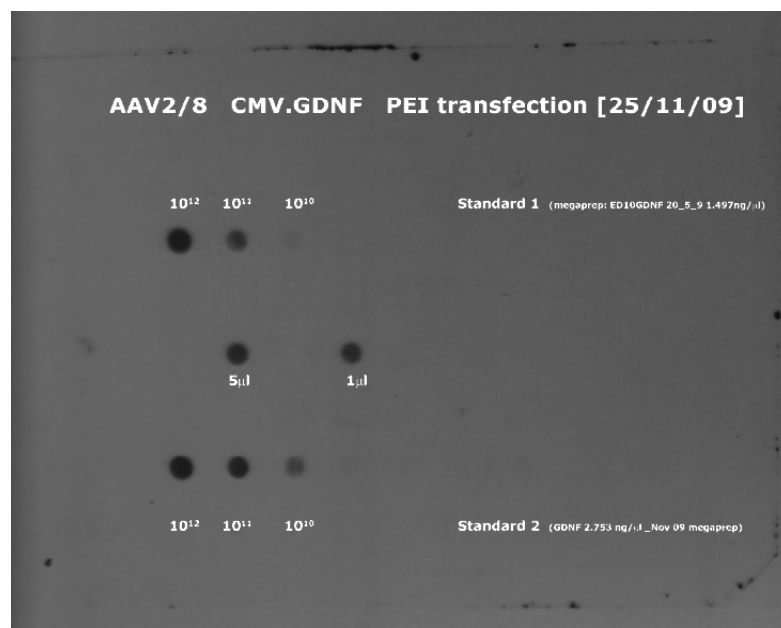


Figure 11-4 Genomic titre of the rAAV2/8.CMV.Gdnf vector.

11.3.2 Protein concentration in samples from rAAV2/8

CMV.GDNF treated eyes

Eyes were enucleated and snap frozen in liquid nitrogen prior to storage at -80°C . On the day of protein assay and GDNF ELISA eyes were removed one by one from the -80°C freezer and crushed in an eppendorf whilst thawing. 120 μl of PBS with protease inhibitor (1/100, Sigma) was added and the samples further homogenised. Centrifugation was performed to separate supernatants that were used for further analysis.

Total protein concentration in the supernatants from each eye was determined using a calorimetric protein assay, and comparison to a standard curve using commercial bovine serum albumin of a known concentration.

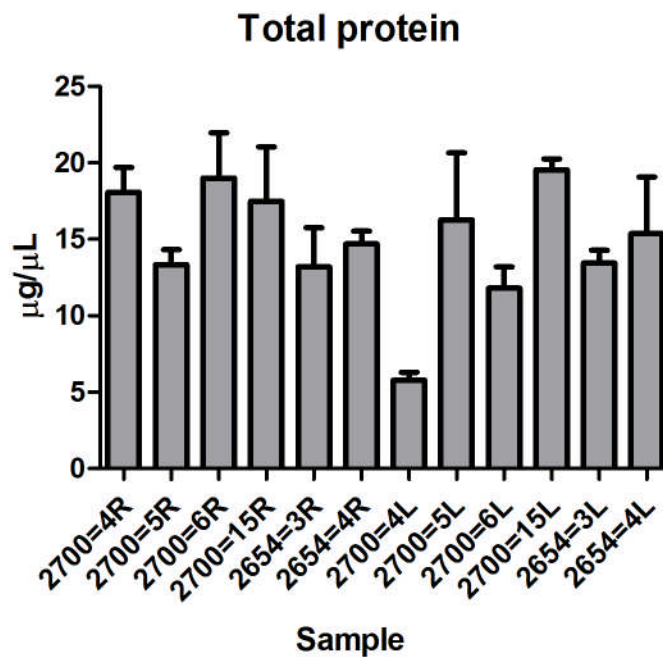


Figure 11-5 Total protein concentration in the eyes of six mice that had been treated with rAAV2/8.CMV.GDNF. Frozen eyes were homogenised. To control for variability in the degree of homogenisation GDNF concentrations were compared relative to total eye protein levels.

11.4 Control Virus

11.4.1 Titre of control virus

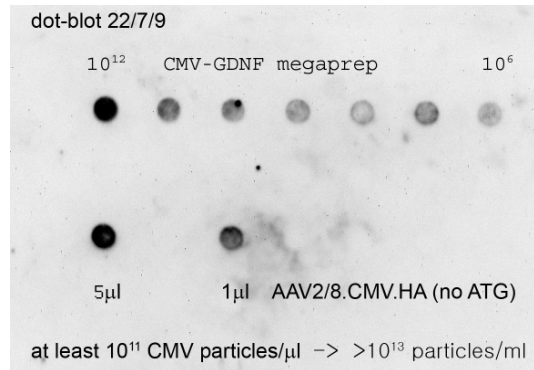


Figure 11-6 Dot-blot titre of rAAV2/8.CMV.HA (no ATG) virus.

11.4.2 Confirmation of absence of transgene expression with control virus

To determine the effects of sub-retinal injection of virus, infection and transcription it was important that the control virus was not producing protein that could independently affect cell function. The plasmid used to generate the control virus contained a CMV promoter and then a haemagglutinin (HA) tag, but without an intervening ATG sequence.

In vitro evaluation transfections

293 T cells (87 500/well) were transfected with the CMV.HA or CMV.GFP plasmids, or left untransfected. Transfections were performed using the lipofectin protocol described in the methods chapter. After 48 hours successful transfection was confirmed by visualisation of GFP expression in the CMV.GFP transfected wells. Lysate was drained and the cells collected and disrupted (by sonification) in RIPA buffer.

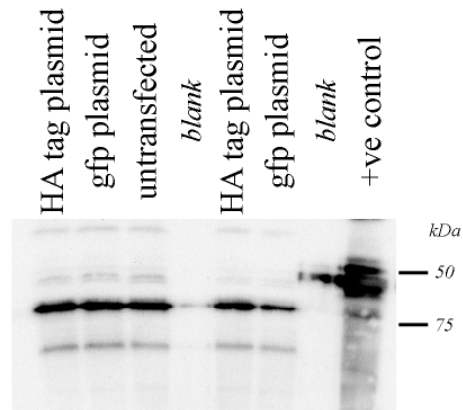
In vivo experiments

AAV2/8 CMV.HA was made and purified using the standard protocols in the methods chapter. This virus had a titre of 1×10^{13} vp/ml (Figure 11-6). 3 mice were injected at P14 of age with superior and inferior injections of 1.5 μ l. Eyes were enucleated after 6 weeks and snap frozen in liquid nitrogen. They were then crushed dry and suspended in RIPA buffer. Following a short-spin the supernatant from each sample was used for further analysis. The treated sample from one animal was compromised during these steps and so the Western blot results are for 2 animals.

Western blot

Protein assays were performed on all samples using a bovine serum albumin (BSA) standard curve. 20 μ g of protein was loaded per well. The primary antibody used was an anti-HA antibody at a concentration of 1/1000. The positive control was 20 μ g of HA-tag peptide with a molecular weight of approximately 55kDa. Both the antibody and HA-tagged protein were supplied by Abcam, Cambridge, U.K. (product codes ab13834 and ab20896 respectively).

in vitro: cell transfections



in vivo: treated & control eyes

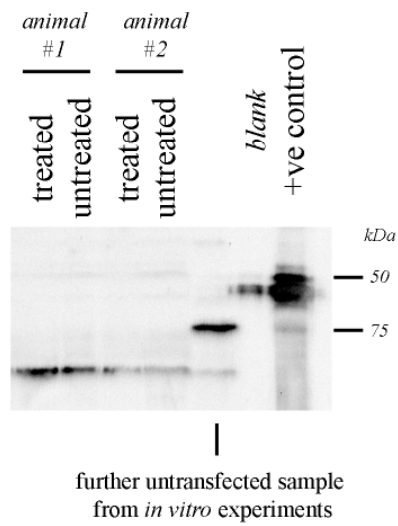


Figure 11-7 Western blots to validate HA plasmid and control virus.

11.5 Rhodopsin constructs

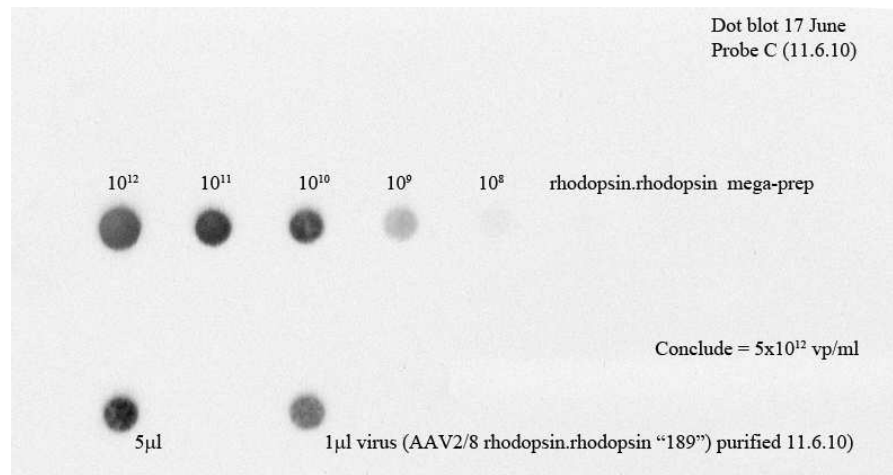


Figure 11-8 The titre of the rhodopsin construct (un-optimised) was determined with a dot blot as 5×10^{12} vg/ml.

11.6 Optimised bRHO.hRHO plasmid

Optimized	758	ATGAACGGAACAGAAAGGACCTAATTCTATGTGCCATTTCAAACGCTACCGGAGTCGTG
Original	758	ATGAATGGCACAGAAAGCCCTAACTTCTACGTGCCCTTCTCCAATGCACGGGTGTGGTA
Optimized	818	CGATCACCAATTCGAATACCCACAGTACTACCTGGCCGAGCCCTGGCAGTTCAGCATGCTG
Original	818	CGCAGCCCCTTCGAGTACCCACAGTACTACCTGGCTGAGCCATGGCAGTTCTCCATGCTG
Optimized	878	GCCGCTTATATGTTTCTGCTGATTGTGCTGGGCTTCCCATCAACTTTCTGACCCTGTAC
Original	878	GCCGCTACATGTTTCTGCTGATCGTGTGGGCTTCCCATCAACTTCTCAGCTCTAC
Optimized	938	GTCACAGTGCAGCACAAAGAACTGCGAACTCCTCTGAACCTATATTCTGTGAACTGCGCC
Original	938	GTCACCGTCCAGCACAAAGAGCTGCGCACGCTCTCAACTACATCCTGCTCAACCTAGCC
Optimized	998	GTGGCTGACCTGTTTCATGTTGCTGGGCGGGTTTACAAGCACTCTGTACACCTCCCTGCAT
Original	998	GTGGCTGACCTTTCATGTTCTAGGTGGCTTACCAGCACCTCTACACCTCTCTGCAT
Optimized	1058	GGATATTTCTGTTTGGGCTACTGGATGCAATCTGGAGGGCTTCTTTGCTACCCTGGGA
Original	1058	GGATACTTCTGTTTGGGCCCCACAGGATGCAATTTGGAGGGCTTCTTTGCCACCTGGGC
Optimized	1118	GGCGAAATTGCCCTGTGGTCCCTGTGGTCTGGCCATCGAGCGGTACGTGCTGTGTC
Original	1118	GGTGAATTTGCCCTGTGGTCCCTGTGGTCTGGCCATCGAGCGGTACGTGGTGGTGT
Optimized	1178	AAGCCAATGTCTAACTTCAGATTTGGCGAAAATCACGCAATCATGGGGTGGCCTTCACA
Original	1178	AAGCCCATGAGCAACTTCCGCTTCGGGGAGAACCATGCCATCATGGCGTTGCCTTCACC
Optimized	1238	TGGGTCATGGCACTGGCATGTGCAACAACCTCTGGCAGGATGGTCTAGATACATTCCT
Original	1238	TGGGTCATGGCGCTGGCCTGCGCCGACCCCCACTCGCCGGCTGGTCCAGGTACATCCCC
Optimized	1298	GAGGGCTGCAGTGCAGTTGTGGAATCGATTACTATACTCTGAAGCCAGAGGTGAACAAT
Original	1298	GAGGGCTGCAGTGCCTGTGTGGAATCGACTACTACACCTCAAGCCGGAGGTCAACAA
Optimized	1358	GAAAGTTTCGTGATCTACATGTTCTGCTGCACTTACCATCCCCATGATCATTATCTTC
Original	1358	GAGTCTTTGTGATCTACATGTTCTGTGGTCCACTTACCATCCCCATGATCATTATCTTT
Optimized	1418	TTTGTCTATGGCAGCTGGTCTTTACAGTGAAGAGGCTGCAGCCAGCAGCAGGAATCC
Original	1418	TTCTGCTATGGCAGCTCGTCTTACCCTCAAGGAGCCGCTGCCAGCAGCAGGAGTCA
Optimized	1478	GCTACCACACAGAAGGCAGAGAAAGAAGTCACCAGGATGGTCATCATGATGTCATTGCC
Original	1478	GCCACCACACAGAAGGCAGAGAAAGAGTCAACCCGATGGTCATCATGATGTCATCGCT
Optimized	1538	TTCCTGATCTGTGGGTGCCTTACGCTTCAGTCGCATTCTATATCTTTACACACCAGGGC
Original	1538	TTCCTGATCTGTGGGTGCCCTACGCCAGCGTGGCATTCTACATCTTACCACCAGGGC
Optimized	1598	AGCAACTTCGGGCCAATCTTCATGACTATCCCCGCTTCTTTGCTAAATCTGCTGCAATC
Original	1598	TCCAACCTCGGTCCCCTTTCATGACCATCCAGCGTCTTTGCCAAGAGCGCCGCTATC
Optimized	1658	TACAATCCCCTGATCTACATCATGATGAACAAGCAGTTTCGCAATTGTATGCTGACTACC
Original	1658	TACAACCTGTCATCTATATCATGATGAACAAGCAGTTCCGGAATGTCATGCTCACCACC
Optimized	1718	ATCTGCTGTGGAAAAACCCCCTGGGCGACGACGAAGCATCCGCTACCCTGAGCAAGACC
Original	1718	ATCTGCTGCGCAAGAACCCTGTTGAGGATGAGGCTCTGCTACCGTGTCCAAGACG
Optimized	1778	GAAACCAGTCAGGTCGACCCCGCATGA
Original	1778	GAGACGAGCCAGGTGGCCCCGGCTAA

Figure 11-9 Nucleotide sequence before and after optimisation. Changes in the optimised plasmid are highlighted in red.

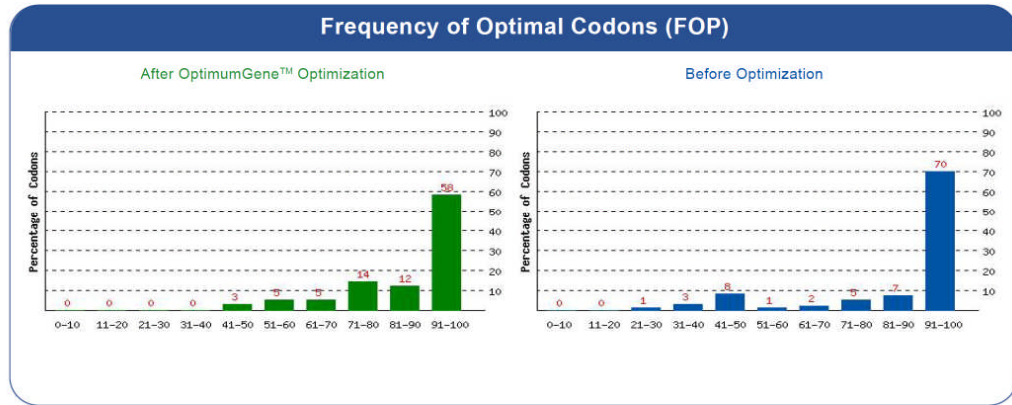


Figure 11-10 Frequency of optimal codons pre and post optimisation. Codon quality groups are shown on the x-axis with a value of 100 for the codon with the highest usage frequency for a given amino acid, and 0 for the least used codon. Percentages of transgene codons within each quality group are shown on the y-axis.

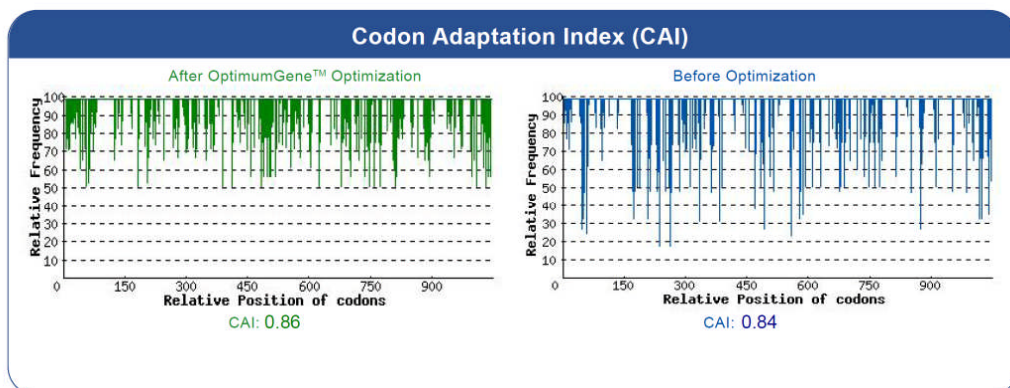


Figure 11-11 The distribution of codon usage frequency along the length of the gene sequence. A CAI of 1.0 is optimal for gene expression.

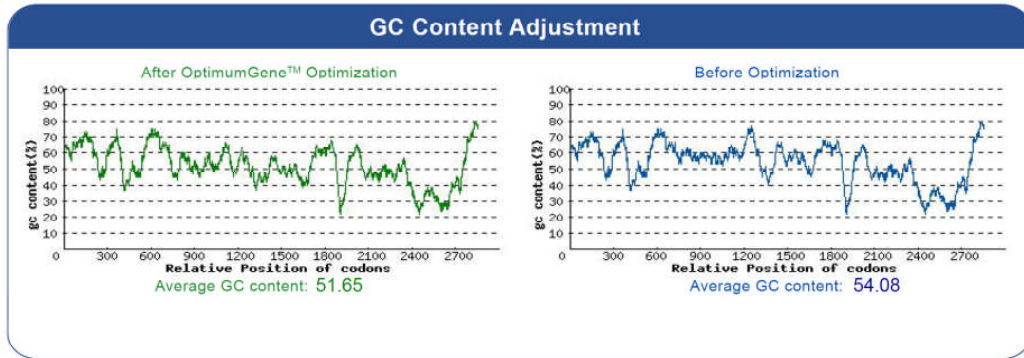


Figure 11-12 Distribution of guanine (G) and cytosine (C) in transgene DNA. G and C content is shown as a percentage of all nucleotides in 60 base pair sequences.

Optimized	1	MNGTEGPNFYVFFSNATGVVRSPPFEYPQYYLAEPWQFSMLAAYMFLLIVLGFPINFLTLY
Original	1	MNGTEGPNFYVFFSNATGVVRSPPFEYPQYYLAEPWQFSMLAAYMFLLIVLGFPINFLTLY
Optimized	61	VTVQHKKLRTPLNYILLNLAVADLFMVLGGFTSTLYTSLHGYFVFGPTGCNLEGGFFATLG
Original	61	VTVQHKKLRTPLNYILLNLAVADLFMVLGGFTSTLYTSLHGYFVFGPTGCNLEGGFFATLG
Optimized	121	GEIALWLSLVLAIERVVVCKPMSNFRFGENHAIMGVAFTWVMALACAAPLAGWSRYIP
Original	121	GEIALWLSLVLAIERVVVCKPMSNFRFGENHAIMGVAFTWVMALACAAPLAGWSRYIP
Optimized	181	EGLQCSCGIDYYTLKPEVNNEFVIYMFVVHFTIPMIIIFFCYQQLVFTVKEAAAQQQES
Original	181	EGLQCSCGIDYYTLKPEVNNEFVIYMFVVHFTIPMIIIFFCYQQLVFTVKEAAAQQQES
Optimized	241	ATTQKAEKEVTRMVIIMVIAFLICWVPYASVAFYIFTHQGSNFGPIFMTIPAFFAKSAAI
Original	241	ATTQKAEKEVTRMVIIMVIAFLICWVPYASVAFYIFTHQGSNFGPIFMTIPAFFAKSAAI
Optimized	301	YNPVIYIMMNKQFRNCMLTTICCGKNPLGDDEASATVSKTETSQVAPA*
Original	301	YNPVIYIMMNKQFRNCMLTTICCGKNPLGDDEASATVSKTETSQVAPA*

Figure 11-13 Protein alignment following optimisation (no change to amino acid sequence)

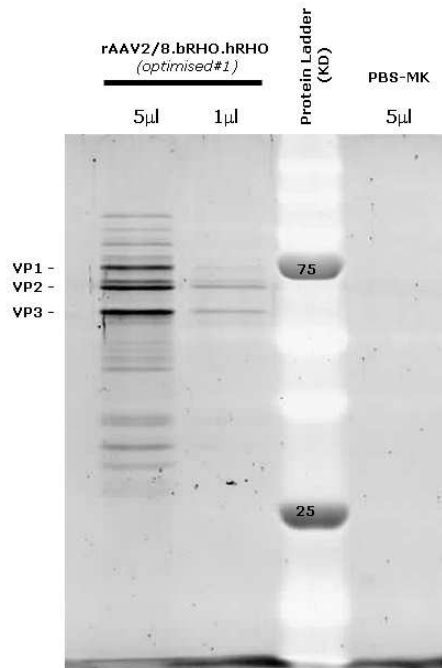


Figure 11-14 Protein stain of the bRHO.hRHO (optimised #1) vector. Proteins were separated by SDS-PAGE and identified with the Spyro Ruby protein stain

11.7 Quantitative real-time PCR

Quantitative real-time PCR reactions for β -actin and XAF1 were performed with the reaction mixes shown below. Example reaction traces are shown for each.

	Gene of interest: β-actin
cDNA	1 μ l of 1/10 and 1/100 dilutions
Mastermix	FastStart TaqMan Probe Mastermix
Probe	#56, Roche. 250 nM
Forward primer	AAG GCC AAC CGT GAA AAG AT; 900 nM
Reverse primer	GTG GTA CGA CCA GAG GCA TAC; 900 nM
Total volume	30 μ l

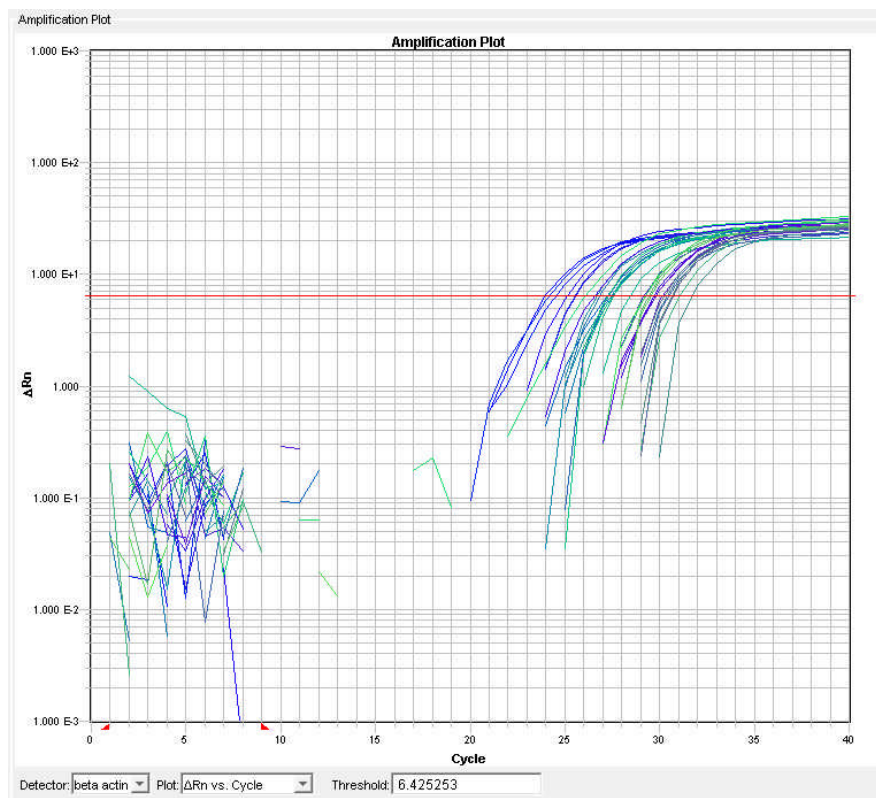


Figure 11-15 Examples of β -actin quantitative real-time PCR reaction traces.

	Gene of interest: XAF1
cDNA	1 μ l of 1/10 and 1/100 dilutions
Mastermix	FastStart TaqMan Probe Mastermix
Probe	#2, Roche. 250 nM
Forward primer	CTT CCC TTG CCC ATT CTA AA; 900 nM
Reverse primer	CCC ACT GGA GTT TCT TTT GG; 900 nM
Total volume	30 μ l

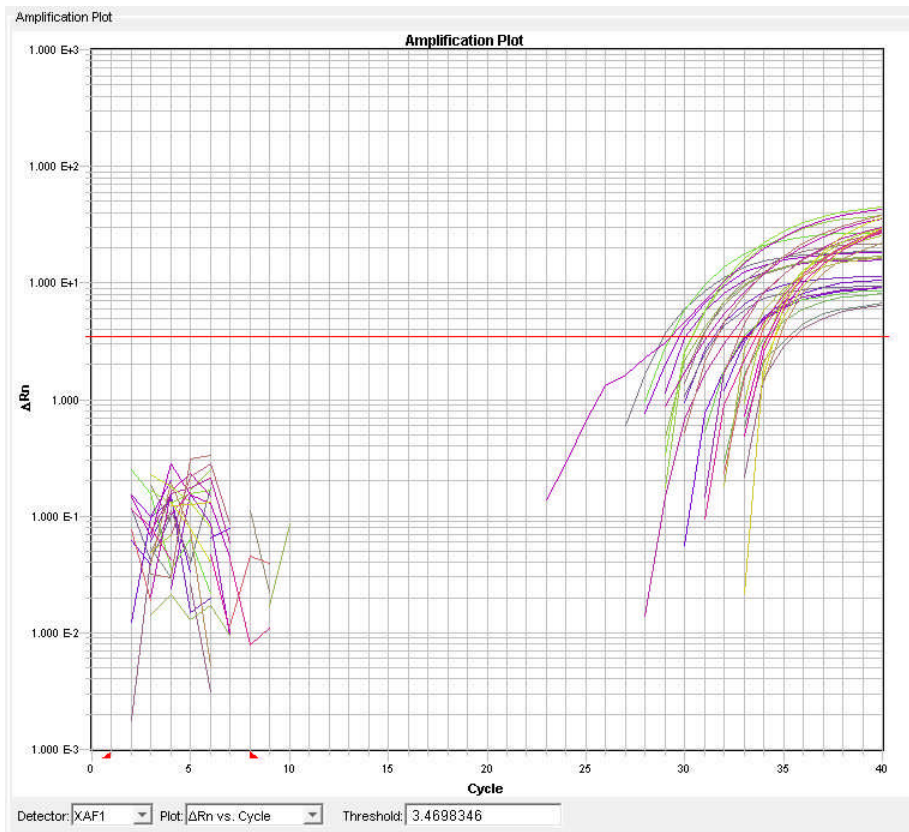


Figure 11-16 Examples of XAF1 quantitative real-time PCR reaction traces.

11.8 Wild Type ERG

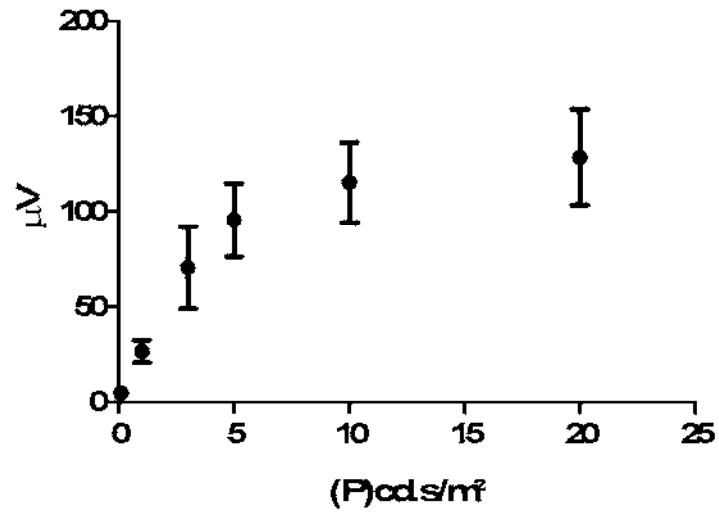


Figure 11-17 Cone function in one year old wild type mice. Three wild type mice were examined with the photopic ERG protocol at one year of age. Mean b wave amplitudes (y axis) are shown with standard deviations at each flash intensity.

Chapter 12 Abbreviations

AAV	adeno-associated virus
Ad	adenovirus
adRP	autosomal dominant retinitis pigmentosa
AMD	age-related macular degeneration
Arr	arrestin
arRP	autosomal recessive retinitis pigmentosa
b	bovine
BDNF	brain-derived neurotrophic factor
bFGF	basic fibroblast growth factor
BHK	baby hamster kidney cells
bp	base pair
cAMP	cyclic AMP
cDNA	complementary DNA
cGMP	cyclic GMP
CMV	cytomegalovirus
CNS	central nervous system
CNTF	ciliary neurotrophic factor
CNV	choroidal neovascularisation
CORD	cone-rod dystrophy
CRALBP	cellular retinaldehyde binding protein
CRBP	cellular retinol-binding protein
CRX	cone-rod otx-like homeobox
DMEM	Dulbecco's Modified Eagle's Medium
DMSO	dimethylsulfoxide
DNA	deoxyribonucleic acid
ds	double stranded
eGFP	enhanced green fluorescent protein

ERG	electroretinogram
ES	embryonic stem cell
FACS	fluorescence-activated cell sorter
FBS	fetal bovine serum
FGF	fibroblast growth factor
GC	ganglion cell
GCAP	guanylate cyclase activator protein
GDNF	glial-cell line derived neurotrophic factor
GMP	guanosine 5'-monophosphate
GTP	guanosine-5'-triphosphate
HEK	human embryonic kidney cells
hrGFP	human recombinised green fluorescent protein
HSV	herpes simplex virus
ILM	inner limiting membrane
INL	inner nuclear layer
IP	intra-peritoneal
IPL	inner plexiform layer
IPM	inter photoreceptor matrix
IRBP	interphotoreceptor retinoid-binding protein
IRD	inherited retinal degeneration
IS	inner segments
ITR	inverted terminal repeats
kb	kilobase
kDa	kilodalton
l	litre
LRAT	lecithin-retinol acyltransferase
LTR	long tandem repeats
m	meter
m-	milli
μ-	micro-
Mertk	mer-receptor tyrosine kinase
min	minute

miRNA	micro RNA
mRNA	messenger RNA
n-	nano-
NF	nerve fibre layer
NRL	neural retina leucine zipper transcription factor
OD	Oculus Dexter (right eye)
OS	Oculus Sinister (left eye)
OLM	outer limiting membrane
ONL	outer nuclear layer
OPL	outer plexiform layer
OS	outer segments
P	postnatal day or photometric units
PCR	polymerase chain reaction
PDE	phosphodiesterase
PEDF	pigment epithelium derived factor
PEG	Polyethylene glycol
Pi	post injection
Prph2	peripherin2
qRT-PCR	quantitative real-time reverse transcription-polymerase chain reaction
rAAV	recombinant AAV
RCS	Royal College of Surgeons
rd	retinal degeneration
rds	retinal degeneration slow
retGC	retinal guanylate cyclase
RFP	red fluorescent protein
RGC	retinal ganglion cells
RGR	retinal G-protein-coupled receptor
Rho	rhodopsin
<i>Rho^{-/-}Opn.gfp</i>	Rhodopsin knockout transgenic mouse with GFP driven by opsin promoter
RISC	RNA induced silencing complex
RK	rhodopsin kinase

RNA	ribonucleic acid
RNAi	RNA interference
ROM-1	retinal outer segment membrane protein-1
RP	retinitis pigmentosa
RPC	retinal progenitor cell
RPE	retinal pigment epithelium
RPGR	retinitis pigmentosa GTPase regulator
RPGRIP	RPGR-interacting protein
rRNA	ribosomal RNA
RT	reverse transcriptase
shRNA	short hairpin RNA
siRNA	short interfering RNA
ss	single strand
TEM	transmission electron microscopy
UTR	untranslated regions
vg	viral genomes
w/v	weight/volume

Chapter 13 References

1. Acland GM, Aguirre GD, Ray J *et al.* Gene therapy restores vision in a canine model of childhood blindness. *Nat.Genet.* 2001;**28**:92-5.
2. Bainbridge JW, Ali RR. Success in sight: The eyes have it! Ocular gene therapy trials for LCA look promising. *Gene Ther.* 2008;**15**:1191-2.
3. Maguire AM, Simonelli F, Pierce EA *et al.* Safety and efficacy of gene transfer for Leber's congenital amaurosis. *N.Engl.J Med.* 2008;**358**:2240-8.
4. Maguire AM, High KA, Auricchio A *et al.* Age-dependent effects of RPE65 gene therapy for Leber's congenital amaurosis: a phase 1 dose-escalation trial. *Lancet* 2009;**374**:1597-605.
5. Cideciyan AV, Hauswirth WW, Aleman TS *et al.* Vision 1 year after gene therapy for Leber's congenital amaurosis. *N.Engl.J Med.* 2009;**361**:725-7.
6. Banin E, Bandah-Rosenfeld D, Obolensky A *et al.* Molecular Anthropology meets Genetic Medicine to Treat Blindness in the North African Jewish Population: Human Gene Therapy Initiated in Israel. *Hum.Gene Ther.* 2010.

7. Sieving PA, Caruso RC, Tao W *et al.* Ciliary neurotrophic factor (CNTF) for human retinal degeneration: phase I trial of CNTF delivered by encapsulated cell intraocular implants. *Proc.Natl.Acad.Sci U.S.A* 2006;**103**:3896-901.
8. McGill TJ, Prusky GT, Douglas RM *et al.* Intraocular CNTF reduces vision in normal rats in a dose-dependent manner. *Invest Ophthalmol Vis Sci* 2007;**48**:5756-66.
9. Wen R, Song Y, Kjellstrom S *et al.* Regulation of rod phototransduction machinery by ciliary neurotrophic factor. *J Neurosci.* 2006;**26**:13523-30.
10. Steinberg RH, Fisher SK, Anderson DH. Disc morphogenesis in vertebrate photoreceptors. *J Comp Neurol.* 1980;**190**:501-8.
11. Nathans J, Thomas D, Hogness DS. Molecular genetics of human color vision: the genes encoding blue, green, and red pigments. *Science* 1986;**232**:193-202.
12. Applebury ML, Antoch MP, Baxter LC *et al.* The murine cone photoreceptor: a single cone type expresses both S and M opsins with retinal spatial patterning. *Neuron* 2000;**27**:513-23.
13. Carter-Dawson LD, Lavail MM. Rods and cones in the mouse retina. I. Structural analysis using light and electron microscopy. *J Comp Neurol.* 1979;**188**:245-62.

14. Carter-Dawson LD, Lavail MM. Rods and cones in the mouse retina. II. Autoradiographic analysis of cell generation using tritiated thymidine. *J Comp Neurol.* 1979;**188**:263-72.
15. Curcio CA, Sloan KR, Kalina RE *et al.* Human photoreceptor topography. *J Comp Neurol.* 1990;**292**:497-523.
16. Masland RH. The fundamental plan of the retina. *Nat. Neurosci.* 2001;**4**:877-86.
17. Bringmann A, Reichenbach A. Role of Muller cells in retinal degenerations. *Front Biosci.* 2001;**6**:E72-E92.
18. Wang JS, Estevez ME, Cornwall MC *et al.* Intra-retinal visual cycle required for rapid and complete cone dark adaptation. *Nat. Neurosci.* 2009;**12**:295-302.
19. Langmann T. Microglia activation in retinal degeneration. *J Leukoc. Biol.* 2007;**81**:1345-51.
20. Murakami A, Yajima T, Sakuma H *et al.* X-arrestin: a new retinal arrestin mapping to the X chromosome. *FEBS Lett.* 1993;**334**:203-9.
21. Polymeropoulos MH, Ide S, Soares MB *et al.* Sequence characterization and genetic mapping of the human VSNL1 gene, a homologue of the rat visinin-like peptide RNVP1. *Genomics* 1995;**29**:273-5.
22. Lamb TD, Pugh EN, Jr. Phototransduction, dark adaptation, and rhodopsin regeneration the proctor lecture. *Invest Ophthalmol Vis Sci* 2006;**47**:5137-52.

23. Mata NL, Radu RA, Clemmons RC *et al.* Isomerization and oxidation of vitamin a in cone-dominant retinas: a novel pathway for visual-pigment regeneration in daylight. *Neuron* 2002;**36**:69-80.
24. Pacione LR, Szego MJ, Ikeda S *et al.* Progress toward understanding the genetic and biochemical mechanisms of inherited photoreceptor degenerations. *Annu.Rev.Neurosci.* 2003;**26**:657-700.
25. Pagon RA. Retinitis pigmentosa. *Surv.Ophthalmol* 1988;**33**:137-77.
26. Daiger SP, Bowne SJ, Sullivan LS. Perspective on genes and mutations causing retinitis pigmentosa. *Arch.Ophthalmol* 2007;**125**:151-8.
27. Haim M. Epidemiology of retinitis pigmentosa in Denmark. *Acta Ophthalmol Scand.Suppl* 2002;1-34.
28. Zanke B, Hawken S, Carter R *et al.* A genetic approach to stratification of risk for age-related macular degeneration. *Can.J Ophthalmol* 2010;**45**:22-7.
29. Ret Net. (www.sph.uth.tmc.edu/Retnet)
30. Maeda A, Maeda T, Golczak M *et al.* Retinopathy in mice induced by disrupted all-trans-retinal clearance. *J Biol.Chem.* 2008;**283**:26684-93.
31. Kim SR, Fishkin N, Kong J *et al.* Rpe65 Leu450Met variant is associated with reduced levels of the retinal pigment epithelium lipofuscin fluorophores A2E and iso-A2E. *Proc.Natl.Acad.Sci U.S.A* 2004;**101**:11668-72.

32. De S, Sakmar TP. Interaction of A2E with model membranes. Implications to the pathogenesis of age-related macular degeneration. *J Gen.Physiol* 2002;**120**:147-57.
33. Radu RA, Mata NL, Bagla A *et al.* Light exposure stimulates formation of A2E oxiranes in a mouse model of Stargardt's macular degeneration. *Proc.Natl.Acad.Sci U.S.A* 2004;**101**:5928-33.
34. Kajiwara K, Berson EL, Dryja TP. Digenic retinitis pigmentosa due to mutations at the unlinked peripherin/RDS and ROM1 loci. *Science* 1994;**264**:1604-8.
35. Dryja TP, Hahn LB, Kajiwara K *et al.* Dominant and digenic mutations in the peripherin/RDS and ROM1 genes in retinitis pigmentosa. *Invest Ophthalmol Vis Sci* 1997;**38**:1972-82.
36. Leroy BP, Kailasanathan A, De Laey JJ *et al.* Intrafamilial phenotypic variability in families with RDS mutations: exclusion of ROM1 as a genetic modifier for those with retinitis pigmentosa. *Br.J Ophthalmol* 2007;**91**:89-93.
37. Stockton RA, Slaughter MM. B-wave of the electroretinogram. A reflection of ON bipolar cell activity. *J Gen.Physiol* 1989;**93**:101-22.
38. Phelan JK, Bok D. A brief review of retinitis pigmentosa and the identified retinitis pigmentosa genes. *Mol.Vis* 2000;**6**:116-24.
39. Kanski JJ, Nischal KK. *Ophthalmology; Clinical signs and Differential Diagnosis*. Harcourt Publishers Limited, U.K., 2000.

40. McGuire RE, Sullivan LS, Blanton SH *et al.* X-linked dominant cone-rod degeneration: linkage mapping of a new locus for retinitis pigmentosa (RP 15) to Xp22.13-p22.11. *Am J Hum. Genet.* 1995;**57**:87-94.
41. Simunovic MP, Moore AT. The cone dystrophies. *Eye (Lond)* 1998;**12** (Pt 3b):553-65.
42. Mazzoni F, Novelli E, Strettoi E. Retinal ganglion cells survive and maintain normal dendritic morphology in a mouse model of inherited photoreceptor degeneration. *J Neurosci.* 2008;**28**:14282-92.
43. Cottet S, Schorderet DF. Mechanisms of apoptosis in retinitis pigmentosa. *Curr.Mol.Med.* 2009;**9**:375-83.
44. Travis GH. Mechanisms of cell death in the inherited retinal degenerations. *Am.J.Hum.Genet.* 1998;**62**:503-8.
45. Stone J, Maslim J, Valter-Kocsi K *et al.* Mechanisms of photoreceptor death and survival in mammalian retina. *Prog.Retin.Eye Res.* 1999;**18**:689-735.
46. Dryja TP, McGee TL, Hahn LB *et al.* Mutations within the rhodopsin gene in patients with autosomal dominant retinitis pigmentosa. *N.Engl.J Med.* 1990;**323**:1302-7.
47. Dryja TP, McGee TL, Reichel E *et al.* A point mutation of the rhodopsin gene in one form of retinitis pigmentosa. *Nature* 1990;**343**:364-6.
48. Sullivan LS, Bowne SJ, Birch DG *et al.* Prevalence of disease-causing mutations in families with autosomal dominant retinitis pigmentosa: a

- screen of known genes in 200 families. *Invest Ophthalmol Vis Sci* 2006;**47**:3052-64.
49. Rosenfeld PJ, Cowley GS, McGee TL *et al.* A null mutation in the rhodopsin gene causes rod photoreceptor dysfunction and autosomal recessive retinitis pigmentosa. *Nat.Genet.* 1992;**1**:209-13.
 50. Kumaramanickavel G, Maw M, Denton MJ *et al.* Missense rhodopsin mutation in a family with recessive RP. *Nat.Genet.* 1994;**8**:10-1.
 51. Reig C, Antich J, Gean E *et al.* Identification of a novel rhodopsin mutation (Met-44-Thr) in a simplex case of retinitis pigmentosa. *Hum.Genet.* 1994;**94**:283-6.
 52. Gal A, Apfelstedt-Sylla E, Janecke AR *et al.* Rhodopsin mutations in inherited retinal dystrophies and dysfunctions. *Progress in Retinal and Eye Research* 1997;**16**:51-79.
 53. Kennan A, Aherne A, Humphries P. Light in retinitis pigmentosa. *Trends Genet.* 2005;**21**:103-10.
 54. Mendes HF, van der SJ, Chapple JP *et al.* Mechanisms of cell death in rhodopsin retinitis pigmentosa: implications for therapy. *Trends Mol.Med.* 2005;**11**:177-85.
 55. Allikmets R, Singh N, Sun H *et al.* A photoreceptor cell-specific ATP-binding transporter gene (ABCR) is mutated in recessive Stargardt macular dystrophy. *Nat.Genet.* 1997;**15**:236-46.

56. Michaelides M, Hardcastle AJ, Hunt DM *et al.* Progressive cone and cone-rod dystrophies: phenotypes and underlying molecular genetic basis. *Surv.Ophthalmol* 2006;**51**:232-58.
57. Cremers FP, van de Pol DJ, van DM *et al.* Autosomal recessive retinitis pigmentosa and cone-rod dystrophy caused by splice site mutations in the Stargardt's disease gene ABCR. *Hum.Mol.Genet.* 1998;**7**:355-62.
58. Martinez-Mir A, Paloma E, Allikmets R *et al.* Retinitis pigmentosa caused by a homozygous mutation in the Stargardt disease gene ABCR. *Nat.Genet.* 1998;**18**:11-2.
59. Lotery A, Trump D. Progress in defining the molecular biology of age related macular degeneration. *Hum.Genet.* 2007;**122**:219-36.
60. Farrar GJ, Kenna P, Jordan SA *et al.* A three-base-pair deletion in the peripherin-RDS gene in one form of retinitis pigmentosa. *Nature* 1991;**354**:478-80.
61. Kajiwara K, Hahn LB, Mukai S *et al.* Mutations in the human retinal degeneration slow gene in autosomal dominant retinitis pigmentosa. *Nature* 1991;**354**:480-3.
62. Clarke G, Goldberg AF, Vidgen D *et al.* Rom-1 is required for rod photoreceptor viability and the regulation of disk morphogenesis. *Nat.Genet.* 2000;**25**:67-73.
63. Bascom RA, Liu L, Heckenlively JR *et al.* Mutation analysis of the ROM1 gene in retinitis pigmentosa. *Hum.Mol.Genet.* 1995;**4**:1895-902.

64. Sakuma H, Inana G, Murakami A *et al.* A heterozygous putative null mutation in ROM1 without a mutation in peripherin/RDS in a family with retinitis pigmentosa. *Genomics* 1995;**27**:384-6.
65. Audo I, Michaelides M, Robson AG *et al.* Phenotypic variation in enhanced S-cone syndrome. *Invest Ophthalmol Vis Sci* 2008;**49**:2082-93.
66. Escher P, Gouras P, Roduit R *et al.* Mutations in NR2E3 can cause dominant or recessive retinal degenerations in the same family. *Hum.Mutat.* 2009;**30**:342-51.
67. Marion V, Stoetzel C, Schlicht D *et al.* Transient ciliogenesis involving Bardet-Biedl syndrome proteins is a fundamental characteristic of adipogenic differentiation. *Proc.Natl.Acad.Sci U.S.A* 2009;**106**:1820-5.
68. Reuber BE, Germain-Lee E, Collins CS *et al.* Mutations in PEX1 are the most common cause of peroxisome biogenesis disorders. *Nat.Genet.* 1997;**17**:445-8.
69. Gibbs D, Azarian SM, Lillo C *et al.* Role of myosin VIIa and Rab27a in the motility and localization of RPE melanosomes. *J Cell Sci* 2004;**117**:6473-83.
70. Annunen S, Korkko J, Czarny M *et al.* Splicing mutations of 54-bp exons in the COL11A1 gene cause Marshall syndrome, but other mutations cause overlapping Marshall/Stickler phenotypes. *Am J Hum.Genet.* 1999;**65**:974-83.

71. Hartong DT, Berson EL, Dryja TP. Retinitis pigmentosa. *Lancet* 2006;**368**:1795-809.
72. McLaughlin ME, Sandberg MA, Berson EL *et al.* Recessive mutations in the gene encoding the beta-subunit of rod phosphodiesterase in patients with retinitis pigmentosa. *Nat.Genet.* 1993;**4**:130-4.
73. Danciger M, Blaney J, Gao YQ *et al.* Mutations in the PDE6B gene in autosomal recessive retinitis pigmentosa. *Genomics* 1995;**30**:1-7.
74. McCall MA, Gregg RG, Merriman K *et al.* Morphological and physiological consequences of the selective elimination of rod photoreceptors in transgenic mice. *Exp.Eye Res.* 1996;**63**:35-50.
75. Punzo C, Kornacker K, Cepko CL. Stimulation of the insulin/mTOR pathway delays cone death in a mouse model of retinitis pigmentosa. *Nat.Neurosci.* 2009;**12**:44-52.
76. Mohand-Said S, Hicks D, Simonutti M *et al.* Photoreceptor transplants increase host cone survival in the retinal degeneration (rd) mouse. *Ophthalmic Res.* 1997;**29**:290-7.
77. Mohand-Said S, udon-Combe A, Hicks D *et al.* Normal retina releases a diffusible factor stimulating cone survival in the retinal degeneration mouse. *Proc.Natl.Acad.Sci U.S.A* 1998;**95**:8357-62.
78. Leveillard T, Mohand-Said S, Lorentz O *et al.* Identification and characterization of rod-derived cone viability factor. *Nat.Genet.* 2004;**36**:755-9.

79. Chalmel F, Leveillard T, Jaillard C *et al.* Rod-derived Cone Viability Factor-2 is a novel bifunctional-thioredoxin-like protein with therapeutic potential. *BMC.Mol.Biol.* 2007;**8**:74.
80. Frasson M, Picaud S, Leveillard T *et al.* Glial cell line-derived neurotrophic factor induces histologic and functional protection of rod photoreceptors in the rd/rd mouse. *Invest Ophthalmol Vis Sci* 1999;**40**:2724-34.
81. Yang Y, Mohand-Said S, Danan A *et al.* Functional cone rescue by RdCVF protein in a dominant model of retinitis pigmentosa. *Mol.Ther.* 2009;**17**:787-95.
82. Lee D, Geller S, Walsh N *et al.* Photoreceptor degeneration in Pro23His and S334ter transgenic rats. *Adv.Exp.Med.Biol.* 2003;**533**:297-302.
83. Milam AH, Li ZY, Fariss RN. Histopathology of the human retina in retinitis pigmentosa. *Prog.Retin.Eye Res.* 1998;**17**:175-205.
84. Gupta N, Brown KE, Milam AH. Activated microglia in human retinitis pigmentosa, late-onset retinal degeneration, and age-related macular degeneration. *Exp.Eye Res.* 2003;**76**:463-71.
85. Kedzierski W, Bok D, Travis GH. Non-cell-autonomous photoreceptor degeneration in rds mutant mice mosaic for expression of a rescue transgene. *J Neurosci.* 1998;**18**:4076-82.
86. Ripps H. Cell death in retinitis pigmentosa: gap junctions and the 'bystander' effect. *Exp.Eye Res.* 2002;**74**:327-36.

87. Fishman GA, Stone EM, Gilbert LD *et al.* Ocular findings associated with a rhodopsin gene codon 106 mutation. Glycine-to-arginine change in autosomal dominant retinitis pigmentosa. *Arch.Ophthalmol* 1992;**110**:646-53.
88. Grover S, Fishman GA, Anderson RJ *et al.* Visual acuity impairment in patients with retinitis pigmentosa at age 45 years or older. *Ophthalmology* 1999;**106**:1780-5.
89. Grover S, Fishman GA, Alexander KR *et al.* Visual acuity impairment in patients with retinitis pigmentosa. *Ophthalmology* 1996;**103**:1593-600.
90. Humphries MM, Rancourt D, Farrar GJ *et al.* Retinopathy induced in mice by targeted disruption of the rhodopsin gene. *Nat.Genet.* 1997;**15**:216-9.
91. Williams DS, Arikawa K, Paallysaho T. Cytoskeletal components of the adherens junctions between the photoreceptors and the supportive Muller cells. *J Comp Neurol.* 1990;**295**:155-64.
92. Steinberg RH, Wood I, Hogan MJ. Pigment epithelial ensheathment and phagocytosis of extrafoveal cones in human retina. *Philos.Trans.R.Soc.Lond B Biol.Sci* 1977;**277**:459-74.
93. Yu DY, Cringle SJ, Su EN *et al.* Intraretinal oxygen levels before and after photoreceptor loss in the RCS rat. *Invest Ophthalmol Vis Sci* 2000;**41**:3999-4006.

94. Yu DY, Cringle S, Valter K *et al.* Photoreceptor death, trophic factor expression, retinal oxygen status, and photoreceptor function in the P23H rat. *Invest Ophthalmol Vis Sci* 2004;**45**:2013-9.
95. Shen J, Yang X, Dong A *et al.* Oxidative damage is a potential cause of cone cell death in retinitis pigmentosa. *J Cell Physiol* 2005;**203**:457-64.
96. Okoye G, Zimmer J, Sung J *et al.* Increased expression of brain-derived neurotrophic factor preserves retinal function and slows cell death from rhodopsin mutation or oxidative damage. *J.Neurosci.* 2003;**23**:4164-72.
97. Yamada H, Yamada E, Ando A *et al.* Fibroblast growth factor-2 decreases hyperoxia-induced photoreceptor cell death in mice. *Am J Pathol.* 2001;**159**:1113-20.
98. Usui S, Komeima K, Lee SY *et al.* Increased expression of catalase and superoxide dismutase 2 reduces cone cell death in retinitis pigmentosa. *Mol.Ther.* 2009;**17**:778-86.
99. Blanks JC, Johnson LV. Specific binding of peanut lectin to a class of retinal photoreceptor cells. A species comparison. *Invest Ophthalmol Vis Sci* 1984;**25**:546-57.
100. Cataldo AM, Hamilton DJ, Barnett JL *et al.* Properties of the endosomal-lysosomal system in the human central nervous system: disturbances mark most neurons in populations at risk to degenerate in Alzheimer's disease. *J Neurosci.* 1996;**16**:186-99.

101. Cardenas-Aguayo MC, Santa-Olalla J, Baizabal JM *et al.* Growth factor deprivation induces an alternative non-apoptotic death mechanism that is inhibited by Bcl2 in cells derived from neural precursor cells. *J Hematother.Stem Cell Res.* 2003;**12**:735-48.
102. Sancho-Pelluz J, rango-Gonzalez B, Kustermann S *et al.* Photoreceptor cell death mechanisms in inherited retinal degeneration. *Mol.Neurobiol.* 2008;**38**:253-69.
103. Lockshin RA, Zakeri Z. Apoptosis, autophagy, and more. *Int.J Biochem.Cell Biol.* 2004;**36**:2405-19.
104. Haas AL, Baboshina O, Williams B *et al.* Coordinated induction of the ubiquitin conjugation pathway accompanies the developmentally programmed death of insect skeletal muscle. *J Biol.Chem.* 1995;**270**:9407-12.
105. Schwartz LM, Kosz L, Kay BK. Gene activation is required for developmentally programmed cell death. *Proc.Natl.Acad.Sci U.S.A* 1990;**87**:6594-8.
106. Salvesen GS. Programmed cell death and the caspases. *APMIS* 1999;**107**:73-9.
107. Blomgren K, Leist M, Groc L. Pathological apoptosis in the developing brain. *Apoptosis.* 2007;**12**:993-1010.
108. Culmsee C, Zhu C, Landshamer S *et al.* Apoptosis-inducing factor triggered by poly(ADP-ribose) polymerase and Bid mediates neuronal

- cell death after oxygen-glucose deprivation and focal cerebral ischemia. *J Neurosci.* 2005;**25**:10262-72.
109. Wenzel A, Grimm C, Samardzija M *et al.* Molecular mechanisms of light-induced photoreceptor apoptosis and neuroprotection for retinal degeneration. *Prog.Retin.Eye Res.* 2005;**24**:275-306.
110. Marigo V. Programmed cell death in retinal degeneration: targeting apoptosis in photoreceptors as potential therapy for retinal degeneration. *Cell Cycle* 2007;**6**:652-5.
111. Xu GZ, Li WW, Tso MO. Apoptosis in human retinal degenerations. *Trans.Am Ophthalmol Soc.* 1996;**94**:411-30.
112. Chang GQ, Hao Y, Wong F. Apoptosis: final common pathway of photoreceptor death in rd, rds, and rhodopsin mutant mice. *Neuron* 1993;**11**:595-605.
113. Portera-Cailliau C, Sung CH, Nathans J *et al.* Apoptotic photoreceptor cell death in mouse models of retinitis pigmentosa. *Proc.Natl.Acad.Sci U.S.A* 1994;**91**:974-8.
114. Liu C, Li Y, Peng M *et al.* Activation of caspase-3 in the retina of transgenic rats with the rhodopsin mutation s334ter during photoreceptor degeneration. *J Neurosci.* 1999;**19**:4778-85.
115. Chen J, Flannery JG, Lavail MM *et al.* bcl-2 overexpression reduces apoptotic photoreceptor cell death in three different retinal degenerations. *Proc.Natl.Acad.Sci U.S.A* 1996;**93**:7042-7.

116. Bennett J, Zeng Y, Bajwa R *et al.* Adenovirus-mediated delivery of rhodopsin-promoted bcl-2 results in a delay in photoreceptor cell death in the rd/rd mouse. *Gene Ther.* 1998;**5**:1156-64.
117. Nir I, Kedzierski W, Chen J *et al.* Expression of Bcl-2 protects against photoreceptor degeneration in retinal degeneration slow (rds) mice. *J Neurosci.* 2000;**20**:2150-4.
118. Tsang SH, Chen J, Kjeldbye H *et al.* Retarding photoreceptor degeneration in Pdegtm1/Pdegtm1 mice by an apoptosis suppressor gene. *Invest Ophthalmol Vis Sci* 1997;**38**:943-50.
119. Leonard KC, Petrin D, Coupland SG *et al.* XIAP protection of photoreceptors in animal models of retinitis pigmentosa. *PLoS. ONE.* 2007;**2**:e314.
120. Rohrer B, Pinto FR, Hulse KE *et al.* Multidestructive pathways triggered in photoreceptor cell death of the rd mouse as determined through gene expression profiling. *J Biol.Chem.* 2004;**279**:41903-10.
121. Lohr HR, Kuntchithapautham K, Sharma AK *et al.* Multiple, parallel cellular suicide mechanisms participate in photoreceptor cell death. *Exp.Eye Res.* 2006;**83**:380-9.
122. Paquet-Durand F, Johnson L, Ekstrom P. Calpain activity in retinal degeneration. *J Neurosci.Res.* 2007;**85**:693-702.

123. Doonan F, Donovan M, Cotter TG. Caspase-independent photoreceptor apoptosis in mouse models of retinal degeneration. *J Neurosci.* 2003;**23**:5723-31.
124. Paquet-Durand F, Silva J, Talukdar T *et al.* Excessive activation of poly(ADP-ribose) polymerase contributes to inherited photoreceptor degeneration in the retinal degeneration 1 mouse. *J Neurosci.* 2007;**27**:10311-9.
125. Ahuja S, huja-Jensen P, Johnson LE *et al.* rd1 Mouse retina shows an imbalance in the activity of cysteine protease cathepsins and their endogenous inhibitor cystatin C. *Invest Ophthalmol Vis Sci* 2008;**49**:1089-96.
126. Ahuja-Jensen, ., Johnsen-Soriano S *et al.* Low glutathione peroxidase in rd1 mouse retina increases oxidative stress and proteases. *Neuroreport* 2007;**18**:797-801.
127. Grasl-Kraupp B, Ruttkay-Nedecky B, Koudelka H *et al.* In situ detection of fragmented DNA (TUNEL assay) fails to discriminate among apoptosis, necrosis, and autolytic cell death: a cautionary note. *Hepatology* 1995;**21**:1465-8.
128. Choi DW. Ischemia-induced neuronal apoptosis. *Curr.Opin.Neurobiol.* 1996;**6**:667-72.
129. Bainbridge JW, Tan MH, Ali RR. Gene therapy progress and prospects: the eye. *Gene Ther.* 2006;**13**:1191-7.

130. Ali RR, Sarra GM, Stephens C *et al.* Restoration of photoreceptor ultrastructure and function in retinal degeneration slow mice by gene therapy. *Nat.Genet.* 2000;**25**:306-10.
131. Pawlyk BS, Smith AJ, Buch PK *et al.* Gene replacement therapy rescues photoreceptor degeneration in a murine model of Leber congenital amaurosis lacking RPGRIP. *Invest Ophthalmol Vis Sci* 2005;**46**:3039-45.
132. Tschernutter M, Schlichtenbrede FC, Howe S *et al.* Long-term preservation of retinal function in the RCS rat model of retinitis pigmentosa following lentivirus-mediated gene therapy. *Gene Ther.* 2005;**12**:694-701.
133. Tan MH, Smith AJ, Pawlyk B *et al.* Gene therapy for retinitis pigmentosa and Leber congenital amaurosis caused by defects in AIPL1: effective rescue of mouse models of partial and complete Aipl1 deficiency using AAV2/2 and AAV2/8 vectors. *Hum.Mol.Genet.* 2009;**18**:2099-114.
134. Lewin AS, Drenser KA, Hauswirth WW *et al.* Ribozyme rescue of photoreceptor cells in a transgenic rat model of autosomal dominant retinitis pigmentosa. *Nat.Med.* 1998;**4**:967-71.
135. Lavail MM, Yasumura D, Matthes MT *et al.* Ribozyme rescue of photoreceptor cells in P23H transgenic rats: long-term survival and late-stage therapy. *Proc.Natl.Acad.Sci U.S.A* 2000;**97**:11488-93.
136. Tolentino M. Interference RNA technology in the treatment of CNV. *Ophthalmol Clin.North Am* 2006;**19**:393-vii.

137. Shen J, Samul R, Silva RL *et al.* Suppression of ocular neovascularization with siRNA targeting VEGF receptor 1. *Gene Ther.* 2006;**13**:225-34.
138. O'Reilly M, Palfi A, Chadderton N *et al.* RNA interference-mediated suppression and replacement of human rhodopsin in vivo. *Am J Hum.Genet.* 2007;**81**:127-35.
139. Geller AM, Sieving PA. Assessment of foveal cone photoreceptors in Stargardt's macular dystrophy using a small dot detection task. *Vision Res.* 1993;**33**:1509-24.
140. Wright AF. A searchlight through the fog. *Nat.Genet.* 1997;**17**:132-4.
141. Delyfer MN, Leveillard T, Mohand-Said S *et al.* Inherited retinal degenerations: therapeutic prospects. *Biol.Cell* 2004;**96**:261-9.
142. Klein R, Klein BE, Linton KL *et al.* The Beaver Dam Eye Study: the relation of age-related maculopathy to smoking. *Am J Epidemiol.* 1993;**137**:190-200.
143. Faktorovich EG, Steinberg RH, Yasumura D *et al.* Photoreceptor degeneration in inherited retinal dystrophy delayed by basic fibroblast growth factor. *Nature* 1990;**347**:83-6.
144. Otto D, Frotscher M, Unsicker K. Basic fibroblast growth factor and nerve growth factor administered in gel foam rescue medial septal neurons after fimbria fornix transection. *J Neurosci.Res.* 1989;**22**:83-91.

145. Sievers J, Hausmann B, Unsicker K *et al.* Fibroblast growth factors promote the survival of adult rat retinal ganglion cells after transection of the optic nerve. *Neurosci.Lett.* 1987;**76**:157-62.
146. Anderson KJ, Dam D, Lee S *et al.* Basic fibroblast growth factor prevents death of lesioned cholinergic neurons in vivo. *Nature* 1988;**332**:360-1.
147. D'Amore PA, Klagsbrun M. Endothelial cell mitogens derived from retina and hypothalamus: biochemical and biological similarities. *J Cell Biol.* 1984;**99**:1545-9.
148. Baird A, Esch F, Gospodarowicz D *et al.* Retina- and eye-derived endothelial cell growth factors: partial molecular characterization and identity with acidic and basic fibroblast growth factors. *Biochemistry* 1985;**24**:7855-60.
149. Lau D, McGee LH, Zhou S *et al.* Retinal degeneration is slowed in transgenic rats by AAV-mediated delivery of FGF-2. *Invest Ophthalmol Vis Sci* 2000;**41**:3622-33.
150. Perry J, Du J, Kjeldbye H *et al.* The effects of bFGF on RCS rat eyes. *Curr.Eye Res.* 1995;**14**:585-92.
151. Tao W, Wen R, Goddard MB *et al.* Encapsulated cell-based delivery of CNTF reduces photoreceptor degeneration in animal models of retinitis pigmentosa. *Invest Ophthalmol Vis Sci* 2002;**43**:3292-8.

152. Liang FQ, Dejneka NS, Cohen DR *et al.* AAV-mediated delivery of ciliary neurotrophic factor prolongs photoreceptor survival in the rhodopsin knockout mouse. *Mol.Ther.* 2001;**3**:241-8.
153. Rhee KD, Ruiz A, Duncan JL *et al.* Molecular and cellular alterations induced by sustained expression of ciliary neurotrophic factor in a mouse model of retinitis pigmentosa. *Invest Ophthalmol Vis Sci* 2007;**48**:1389-400.
154. Buch PK, MacLaren RE, Duran Y *et al.* In contrast to AAV-mediated Cntf expression, AAV-mediated Gdnf expression enhances gene replacement therapy in rodent models of retinal degeneration. *Mol.Ther.* 2006;**14**:700-9.
155. Bok D, Yasumura D, Matthes MT *et al.* Effects of adeno-associated virus-vectored ciliary neurotrophic factor on retinal structure and function in mice with a P216L rds/peripherin mutation. *Exp.Eye Res.* 2002;**74**:719-35.
156. Lawrence JM, Keegan DJ, Muir EM *et al.* Transplantation of Schwann cell line clones secreting GDNF or BDNF into the retinas of dystrophic Royal College of Surgeons rats. *Invest Ophthalmol Vis Sci* 2004;**45**:267-74.
157. Gregory-Evans K, Chang F, Hodges MD *et al.* Ex vivo gene therapy using intravitreal injection of GDNF-secreting mouse embryonic stem cells in a rat model of retinal degeneration. *Mol.Vis* 2009;**15**:962-73.

158. Dong A, Shen J, Krause M *et al.* Increased expression of glial cell line-derived neurotrophic factor protects against oxidative damage-induced retinal degeneration. *J Neurochem.* 2007;**103**:1041-52.
159. Andrieu-Soler C, ubert-Pouessel A, Doat M *et al.* Intravitreal injection of PLGA microspheres encapsulating GDNF promotes the survival of photoreceptors in the rd1/rd1 mouse. *Mol.Vis* 2005;**11**:1002-11.
160. McGee Sanftner LH, Abel H, Hauswirth WW *et al.* Glial cell line derived neurotrophic factor delays photoreceptor degeneration in a transgenic rat model of retinitis pigmentosa. *Mol.Ther.* 2001;**4**:622-9.
161. Patel NK, Bunnage M, Plaha P *et al.* Intraputamenal infusion of glial cell line-derived neurotrophic factor in PD: a two-year outcome study. *Ann.Neurol.* 2005;**57**:298-302.
162. Slevin JT, Gash DM, Smith CD *et al.* Unilateral intraputamenal glial cell line-derived neurotrophic factor in patients with Parkinson disease: response to 1 year of treatment and 1 year of withdrawal. *J.Neurosurg.* 2007;**106**:614-20.
163. Lolley RN, Rong H, Craft CM. Linkage of photoreceptor degeneration by apoptosis with inherited defect in phototransduction. *Invest Ophthalmol Vis Sci* 1994;**35**:358-62.
164. Berson EL, Rosner B, Sandberg MA *et al.* A randomized trial of vitamin A and vitamin E supplementation for retinitis pigmentosa. *Arch.Ophthalmol* 1993;**111**:761-72.

165. Li T, Sandberg MA, Pawlyk BS *et al.* Effect of vitamin A supplementation on rhodopsin mutants threonine-17 --> methionine and proline-347 --> serine in transgenic mice and in cell cultures. *Proc.Natl.Acad.Sci U.S.A* 1998;**95**:11933-8.
166. Radu RA, Yuan Q, Hu J *et al.* Accelerated accumulation of lipofuscin pigments in the RPE of a mouse model for ABCA4-mediated retinal dystrophies following Vitamin A supplementation. *Invest Ophthalmol Vis Sci* 2008;**49**:3821-9.
167. Farber DB, Lolley RN. Cyclic guanosine monophosphate: elevation in degenerating photoreceptor cells of the C3H mouse retina. *Science* 1974;**186**:449-51.
168. Cobbs WH, Pugh EN, Jr. Cyclic GMP can increase rod outer-segment light-sensitive current 10-fold without delay of excitation. *Nature* 1985;**313**:585-7.
169. Fesenko EE, Kolesnikov SS, Lyubarsky AL. Induction by cyclic GMP of cationic conductance in plasma membrane of retinal rod outer segment. *Nature* 1985;**313**:310-3.
170. Lolley RN, Farber DB, Rayborn ME *et al.* Cyclic GMP accumulation causes degeneration of photoreceptor cells: simulation of an inherited disease. *Science* 1977;**196**:664-6.
171. Ulshafer RJ, Garcia CA, Hollyfield JG. Sensitivity of photoreceptors to elevated levels of cGMP in the human retina. *Invest Ophthalmol Vis Sci* 1980;**19**:1236-41.

172. Koch KW, Kaupp UB. Cyclic GMP directly regulates a cation conductance in membranes of bovine rods by a cooperative mechanism. *J Biol.Chem.* 1985;**260**:6788-800.
173. Frasson M, Sahel JA, Fabre M *et al.* Retinitis pigmentosa: rod photoreceptor rescue by a calcium-channel blocker in the rd mouse. *Nat.Med.* 1999;**5**:1183-7.
174. Pawlyk BS, Li T, Scimeca MS *et al.* Absence of photoreceptor rescue with D-cis-diltiazem in the rd mouse. *Invest Ophthalmol Vis Sci* 2002;**43**:1912-5.
175. Pearce-Kelling SE, Aleman TS, Nickle A *et al.* Calcium channel blocker D-cis-diltiazem does not slow retinal degeneration in the PDE6B mutant rcd1 canine model of retinitis pigmentosa. *Mol.Vis* 2001;**7**:42-7.
176. Chen FK, Uppal GS, Rubin GS *et al.* Evidence of retinal function using microperimetry following autologous retinal pigment epithelium-choroid graft in macular dystrophy: outcome in five cases. *Invest Ophthalmol.Vis.Sci.* 2008.
177. Osakada F, Ikeda H, Sasai Y *et al.* Stepwise differentiation of pluripotent stem cells into retinal cells. *Nat.Protoc.* 2009;**4**:811-24.
178. Takahashi K, Yamanaka S. Induction of pluripotent stem cells from mouse embryonic and adult fibroblast cultures by defined factors. *Cell* 2006;**126**:663-76.

179. Takahashi K, Tanabe K, Ohnuki M *et al.* Induction of pluripotent stem cells from adult human fibroblasts by defined factors. *Cell* 2007;**131**:861-72.
180. Hiramani Y, Osakada F, Takahashi K *et al.* Generation of retinal cells from mouse and human induced pluripotent stem cells. *Neurosci.Lett.* 2009;**458**:126-31.
181. Gullapalli VK, Sugino IK, Van PY *et al.* Impaired RPE survival on aged submacular human Bruch's membrane. *Exp.Eye Res.* 2005;**80**:235-48.
182. MacLaren RE, Pearson RA, MacNeil A *et al.* Retinal repair by transplantation of photoreceptor precursors. *Nature* 2006;**444**:203-7.
183. Lamba DA, Gust J, Reh TA. Transplantation of human embryonic stem cell-derived photoreceptors restores some visual function in Crx-deficient mice. *Cell Stem Cell* 2009;**4**:73-9.
184. Benowitz L, Yin Y. Rewiring the injured CNS: lessons from the optic nerve. *Exp.Neurol.* 2008;**209**:389-98.
185. Bull ND, Limb GA, Martin KR. Human Muller stem cell (MIO-M1) transplantation in a rat model of glaucoma: survival, differentiation, and integration. *Invest Ophthalmol Vis Sci* 2008;**49**:3449-56.
186. Bull ND, Irvine KA, Franklin RJ *et al.* Transplanted oligodendrocyte precursor cells reduce neurodegeneration in a model of glaucoma. *Invest Ophthalmol Vis Sci* 2009;**50**:4244-53.

187. Mohand-Said S, Hicks D, Dreyfus H *et al.* Selective transplantation of rods delays cone loss in a retinitis pigmentosa model. *Arch.Ophthalmol.* 2000;**118**:807-11.
188. Fintz AC, Audo I, Hicks D *et al.* Partial characterization of retina-derived cone neuroprotection in two culture models of photoreceptor degeneration. *Invest Ophthalmol Vis Sci* 2003;**44**:818-25.
189. Rosenfeld PJ, Brown DM, Heier JS *et al.* Ranibizumab for neovascular age-related macular degeneration. *N.Engl.J Med.* 2006;**355**:1419-31.
190. Anderson OA, Bainbridge JW, Shima DT. Delivery of anti-angiogenic molecular therapies for retinal disease. *Drug Discov.Today* 2010;**15**:272-82.
191. Campbell M, Ozaki E, Humphries P. Systemic delivery of therapeutics to neuronal tissues: a barrier modulation approach. *Expert.Opin.Drug Deliv.* 2010;**7**:859-69.
192. Chaum E, Hatton MP. Gene therapy for genetic and acquired retinal diseases. *Surv.Ophthalmol* 2002;**47**:449-69.
193. Surace EM, Auricchio A. Versatility of AAV vectors for retinal gene transfer. *Vision Res.* 2008;**48**:353-9.
194. Natkunarajah M, Trittibach P, McIntosh J *et al.* Assessment of ocular transduction using single-stranded and self-complementary recombinant adeno-associated virus serotype 2/8. *Gene Ther.* 2008;**15**:463-7.

195. Rabinowitz JE, Rolling F, Li C *et al.* Cross-packaging of a single adeno-associated virus (AAV) type 2 vector genome into multiple AAV serotypes enables transduction with broad specificity. *J Virol.* 2002;**76**:791-801.
196. Allocca M, Mussolino C, Garcia-Hoyos M *et al.* Novel adeno-associated virus serotypes efficiently transduce murine photoreceptors. *J Virol.* 2007;**81**:11372-80.
197. Bainbridge JW, Mistry A, Schlichtenbrede FC *et al.* Stable rAAV-mediated transduction of rod and cone photoreceptors in the canine retina. *Gene Ther.* 2003;**10**:1336-44.
198. Le Meur G, Weber M, Pereon Y *et al.* Postsurgical assessment and long-term safety of recombinant adeno-associated virus-mediated gene transfer into the retinas of dogs and primates. *Arch.Ophthalmol* 2005;**123**:500-6.
199. Bainbridge JW, Smith AJ, Barker SS *et al.* Effect of gene therapy on visual function in Leber's congenital amaurosis. *N.Engl.J.Med.* 2008;**358**:2231-9.
200. Cai X, Nash Z, Conley SM *et al.* A partial structural and functional rescue of a retinitis pigmentosa model with compacted DNA nanoparticles. *PLoS.ONE.* 2009;**4**:e5290.
201. Bejjani RA, BenEzra D, Cohen H *et al.* Nanoparticles for gene delivery to retinal pigment epithelial cells. *Mol.Vis* 2005;**11**:124-32.

202. Cai X, Conley SM, Nash Z *et al.* Gene delivery to mitotic and postmitotic photoreceptors via compacted DNA nanoparticles results in improved phenotype in a mouse model of retinitis pigmentosa. *FASEB J* 2010;**24**:1178-91.
203. Chang-Lin JE, Attar M, Acheampong AA *et al.* Pharmacokinetics and pharmacodynamics of the sustained-release dexamethasone intravitreal implant. *Invest Ophthalmol Vis Sci* 2010.
204. Schmidt PG, Campbell KM, Hinds KD *et al.* PEGylated bioactive molecules in biodegradable polymer microparticles. *Expert.Opin.Biol.Ther.* 2007;**7**:1427-36.
205. MacDonald IM, Sauve Y, Sieving PA. Preventing blindness in retinal disease: ciliary neurotrophic factor intraocular implants. *Can.J Ophthalmol* 2007;**42**:399-402.
206. Le Meur G, Stieger K, Smith AJ *et al.* Restoration of vision in RPE65-deficient Briard dogs using an AAV serotype 4 vector that specifically targets the retinal pigmented epithelium. *Gene Ther.* 2007;**14**:292-303.
207. Nakagawa T, Zhu H, Morishima N *et al.* Caspase-12 mediates endoplasmic-reticulum-specific apoptosis and cytotoxicity by amyloid-beta. *Nature* 2000;**403**:98-103.
208. Schroder M, Kaufman RJ. The mammalian unfolded protein response. *Annu.Rev.Biochem.* 2005;**74**:739-89.

209. Pittler SJ, Baehr W. Identification of a nonsense mutation in the rod photoreceptor cGMP phosphodiesterase beta-subunit gene of the rd mouse. *Proc.Natl.Acad.Sci U.S.A* 1991;**88**:8322-6.
210. Bowes C, Li T, Danciger M *et al.* Retinal degeneration in the rd mouse is caused by a defect in the beta subunit of rod cGMP-phosphodiesterase. *Nature* 1990;**347**:677-80.
211. Chang B, Hawes NL, Pardue MT *et al.* Two mouse retinal degenerations caused by missense mutations in the beta-subunit of rod cGMP phosphodiesterase gene. *Vision Res.* 2007;**47**:624-33.
212. Jomary C, Thomas M, Grist J *et al.* Expression patterns of neurturin and its receptor components in developing and degenerative mouse retina. *Invest Ophthalmol Vis Sci* 1999;**40**:568-74.
213. Carter-Dawson LD, Lavail MM, Sidman RL. Differential effect of the rd mutation on rods and cones in the mouse retina. *Invest Ophthalmol Vis Sci* 1978;**17**:489-98.
214. Gargini C, Terzibasi E, Mazzoni F *et al.* Retinal organization in the retinal degeneration 10 (rd10) mutant mouse: a morphological and ERG study. *J Comp Neurol.* 2007;**500**:222-38.
215. Travis GH, Sutcliffe JG, Bok D. The retinal degeneration slow (rds) gene product is a photoreceptor disc membrane-associated glycoprotein. *Neuron* 1991;**6**:61-70.

216. Connell G, Bascom R, Molday L *et al.* Photoreceptor peripherin is the normal product of the gene responsible for retinal degeneration in the rds mouse. *Proc.Natl.Acad.Sci U.S.A* 1991;**88**:723-6.
217. Sanyal S, Jansen HG. Absence of receptor outer segments in the retina of rds mutant mice. *Neurosci.Lett.* 1981;**21**:23-6.
218. Sanyal S, De RA, Hawkins RK. Development and degeneration of retina in rds mutant mice: light microscopy. *J Comp Neurol.* 1980;**194**:193-207.
219. McLaughlin ME, Ehrhart TL, Berson EL *et al.* Mutation spectrum of the gene encoding the beta subunit of rod phosphodiesterase among patients with autosomal recessive retinitis pigmentosa. *Proc.Natl.Acad.Sci U.S.A* 1995;**92**:3249-53.
220. Gal A, Orth U, Baehr W *et al.* Heterozygous missense mutation in the rod cGMP phosphodiesterase beta-subunit gene in autosomal dominant stationary night blindness. *Nat.Genet.* 1994;**7**:64-8.
221. Gal A, Orth U, Baehr W *et al.* Heterozygous missense mutation in the rod cGMP phosphodiesterase beta-subunit gene in autosomal dominant stationary night blindness. *Nat.Genet.* 1994;**7**:551.
222. Kajiwara K, Sandberg MA, Berson EL *et al.* A null mutation in the human peripherin/RDS gene in a family with autosomal dominant retinitis punctata albescens. *Nat.Genet.* 1993;**3**:208-12.

223. Gorin MB, Jackson KE, Ferrell RE *et al.* A peripherin/retinal degeneration slow mutation (Pro-210-Arg) associated with macular and peripheral retinal degeneration. *Ophthalmology* 1995;**102**:246-55.
224. Naash MI, Hollyfield JG, al-Ubaidi MR *et al.* Simulation of human autosomal dominant retinitis pigmentosa in transgenic mice expressing a mutated murine opsin gene. *Proc.Natl.Acad.Sci U.S.A* 1993;**90**:5499-503.
225. Machida S, Kondo M, Jamison JA *et al.* P23H rhodopsin transgenic rat: correlation of retinal function with histopathology. *Invest Ophthalmol Vis Sci* 2000;**41**:3200-9.
226. Saliba RS, Munro PM, Luthert PJ *et al.* The cellular fate of mutant rhodopsin: quality control, degradation and aggresome formation. *J Cell Sci* 2002;**115**:2907-18.
227. Illing ME, Rajan RS, Bence NF *et al.* A rhodopsin mutant linked to autosomal dominant retinitis pigmentosa is prone to aggregate and interacts with the ubiquitin proteasome system. *J Biol.Chem.* 2002;**277**:34150-60.
228. Green ES, Menz MD, Lavail MM *et al.* Characterization of rhodopsin mis-sorting and constitutive activation in a transgenic rat model of retinitis pigmentosa. *Invest Ophthalmol Vis Sci* 2000;**41**:1546-53.
229. Sung CH, Makino C, Baylor D *et al.* A rhodopsin gene mutation responsible for autosomal dominant retinitis pigmentosa results in a protein that is defective in localization to the photoreceptor outer segment. *J Neurosci.* 1994;**14**:5818-33.

230. Zhang X, De AM, Hart SL *et al.* High-titer recombinant adeno-associated virus production from replicating amplicons and herpes vectors deleted for glycoprotein H. *Hum. Gene Ther.* 1999;**10**:2527-37.
231. Auricchio A, Hildinger M, O'Connor E *et al.* Isolation of highly infectious and pure adeno-associated virus type 2 vectors with a single-step gravity-flow column. *Hum. Gene Ther.* 2001;**12**:71-6.
232. Grieger JC, Choi VW, Samulski RJ. Production and characterization of adeno-associated viral vectors. *Nat. Protoc.* 2006;**1**:1412-28.
233. Brown KT. The electroretinogram: its components and their origins. *Vision Res.* 1968;**8**:633-77.
234. Penn RD, Hagins WA. Signal transmission along retinal rods and the origin of the electroretinographic a-wave. *Nature* 1969;**223**:201-4.
235. Peachey NS, Goto Y, al-Ubaidi MR *et al.* Properties of the mouse cone-mediated electroretinogram during light adaptation. *Neurosci. Lett.* 1993;**162**:9-11.
236. Krishna VR, Alexander KR, Peachey NS. Temporal properties of the mouse cone electroretinogram. *J Neurophysiol.* 2002;**87**:42-8.
237. Hangai M, Yamamoto M, Sakamoto A *et al.* Ultrahigh-resolution versus speckle noise-reduction in spectral-domain optical coherence tomography. *Opt. Express* 2009;**17**:4221-35.

238. Menke MN, Dabov S, Knecht P *et al.* Reproducibility of retinal thickness measurements in healthy subjects using spectralis optical coherence tomography. *Am J Ophthalmol* 2009;**147**:467-72.
239. Kubista M, Akerman B, Norden B. Characterization of interaction between DNA and 4',6-diamidino-2-phenylindole by optical spectroscopy. *Biochemistry* 1987;**26**:4545-53.
240. Kumar JP, Bowman J, O'Tousa JE *et al.* Rhodopsin replacement rescues photoreceptor structure during a critical developmental window. *Dev.Biol.* 1997;**188**:43-7.
241. Jeon CJ, Strettoi E, Masland RH. The major cell populations of the mouse retina. *J Neurosci.* 1998;**18**:8936-46.
242. Toda K, Bush RA, Humphries P *et al.* The electroretinogram of the rhodopsin knockout mouse. *Vis.Neurosci.* 1999;**16**:391-8.
243. Fei Y, Hughes TE. Transgenic expression of the jellyfish green fluorescent protein in the cone photoreceptors of the mouse. *Vis Neurosci.* 2001;**18**:615-23.
244. Haupts U, Maiti S, Schwille P *et al.* Dynamics of fluorescence fluctuations in green fluorescent protein observed by fluorescence correlation spectroscopy. *Proc.Natl.Acad.Sci U.S.A* 1998;**95**:13573-8.
245. Szel A, von SM, Rohlich P *et al.* Difference in PNA label intensity between short- and middle-wavelength sensitive cones in the ground squirrel retina. *Invest Ophthalmol Vis Sci* 1993;**34**:3641-5.

246. Szel A, Rohlich P, Caffè AR *et al.* Unique topographic separation of two spectral classes of cones in the mouse retina. *J Comp Neurol.* 1992;**325**:327-42.
247. Rex TS, Peet JA, Surace EM *et al.* The distribution, concentration, and toxicity of enhanced green fluorescent protein in retinal cells after genomic or somatic (virus-mediated) gene transfer. *Mol. Vis* 2005;**11**:1236-45.
248. Sokolov M, Lyubarsky AL, Strissel KJ *et al.* Massive light-driven translocation of transducin between the two major compartments of rod cells: a novel mechanism of light adaptation. *Neuron* 2002;**34**:95-106.
249. Elias RV, Sezate SS, Cao W *et al.* Temporal kinetics of the light/dark translocation and compartmentation of arrestin and alpha-transducin in mouse photoreceptor cells. *Mol. Vis* 2004;**10**:672-81.
250. Lobanova ES, Herrmann R, Finkelstein S *et al.* Mechanistic basis for the failure of cone transducin to translocate: why cones are never blinded by light. *J Neurosci.* 2010;**30**:6815-24.
251. Mihelec M, *et al.* Improved visual function following gene therapy in a mouse model of Leber congenital amaurosis (LCA) caused by GC1 deficiency. *under review* 2010.
252. Beck SC, Schaeferhoff K, Michalakis S *et al.* In vivo analysis of cone survival in mice. *Invest Ophthalmol Vis Sci* 2009.

253. Duisit G, Conrath H, Saleun S *et al.* Five recombinant simian immunodeficiency virus pseudotypes lead to exclusive transduction of retinal pigmented epithelium in rat. *Mol.Ther.* 2002;**6**:446-54.
254. Busskamp V, Duebel J, Balya D *et al.* Genetic reactivation of cone photoreceptors restores visual responses in retinitis pigmentosa. *Science* 2010;**329**:413-7.
255. Lin B, Masland RH, Strettoi E. Remodeling of cone photoreceptor cells after rod degeneration in rd mice. *Exp.Eye Res.* 2009;**88**:589-99.
256. Garcia-Fernandez JM, Jimenez AJ, Foster RG. The persistence of cone photoreceptors within the dorsal retina of aged retinally degenerate mice (rd/rd): implications for circadian organization. *Neurosci.Lett.* 1995;**187**:33-6.
257. Jimenez AJ, Garcia-Fernandez JM, Gonzalez B *et al.* The spatio-temporal pattern of photoreceptor degeneration in the aged rd/rd mouse retina. *Cell Tissue Res.* 1996;**284**:193-202.
258. Lavail MM, Matthes MT, Yasumura D *et al.* Variability in rate of cone degeneration in the retinal degeneration (rd/rd) mouse. *Exp.Eye Res.* 1997;**65**:45-50.
259. Milam AH, Li ZY, Cideciyan AV *et al.* Clinicopathologic effects of the Q64ter rhodopsin mutation in retinitis pigmentosa. *Invest Ophthalmol Vis Sci* 1996;**37**:753-65.

260. Coleman JE, Zhang Y, Brown GA *et al.* Cone cell survival and downregulation of GCAP1 protein in the retinas of GC1 knockout mice. *Invest Ophthalmol Vis Sci* 2004;**45**:3397-403.
261. Znoiko SL, Rohrer B, Lu K *et al.* Downregulation of cone-specific gene expression and degeneration of cone photoreceptors in the Rpe65^{-/-} mouse at early ages. *Invest Ophthalmol Vis Sci* 2005;**46**:1473-9.
262. Chen J, Simon MI, Matthes MT *et al.* Increased susceptibility to light damage in an arrestin knockout mouse model of Oguchi disease (stationary night blindness). *Invest Ophthalmol Vis Sci* 1999;**40**:2978-82.
263. Maeda A, Maeda T, Sun W *et al.* Redundant and unique roles of retinol dehydrogenases in the mouse retina. *Proc.Natl.Acad.Sci U.S.A* 2007;**104**:19565-70.
264. Maeda A, Maeda T, Golczak M *et al.* Effects of potent inhibitors of the retinoid cycle on visual function and photoreceptor protection from light damage in mice. *Mol.Pharmacol.* 2006;**70**:1220-9.
265. Naash ML, Peachey NS, Li ZY *et al.* Light-induced acceleration of photoreceptor degeneration in transgenic mice expressing mutant rhodopsin. *Invest Ophthalmol Vis Sci* 1996;**37**:775-82.
266. Paskowitz DM, Lavail MM, Duncan JL. Light and inherited retinal degeneration. *Br.J Ophthalmol* 2006;**90**:1060-6.

267. Krebs MP, White DA, Kaushal S. Biphasic photoreceptor degeneration induced by light in a T17M rhodopsin mouse model of cone bystander damage. *Invest Ophthalmol Vis Sci* 2009;**50**:2956-65.
268. Fishman GA, Stone EM, Gilbert LD *et al.* Ocular findings associated with a rhodopsin gene codon 58 transversion mutation in autosomal dominant retinitis pigmentosa. *Arch.Ophthalmol* 1991;**109**:1387-93.
269. Aleman TS, Cideciyan AV, Sumaroka A *et al.* Retinal laminar architecture in human retinitis pigmentosa caused by Rhodopsin gene mutations. *Invest Ophthalmol Vis Sci* 2008;**49**:1580-90.
270. Cideciyan AV, Hood DC, Huang Y *et al.* Disease sequence from mutant rhodopsin allele to rod and cone photoreceptor degeneration in man. *Proc.Natl.Acad.Sci U.S.A* 1998;**95**:7103-8.
271. Maass A, von Leithner PL, Luong V *et al.* Assessment of rat and mouse RGC apoptosis imaging in vivo with different scanning laser ophthalmoscopes. *Curr.Eye Res.* 2007;**32**:851-61.
272. Crespo D, O'Leary DD, Cowan WM. Changes in the numbers of optic nerve fibers during late prenatal and postnatal development in the albino rat. *Brain Res.* 1985;**351**:129-34.
273. Lin LF, Doherty DH, Lile JD *et al.* GDNF: a glial cell line-derived neurotrophic factor for midbrain dopaminergic neurons. *Science* 1993;**260**:1130-2.

274. Oppenheim RW, Houenou LJ, Johnson JE *et al.* Developing motor neurons rescued from programmed and axotomy-induced cell death by GDNF. *Nature* 1995;**373**:344-6.
275. Clarkson ED, Zawada WM, Freed CR. GDNF improves survival and reduces apoptosis in human embryonic dopaminergic neurons in vitro. *Cell Tissue Res.* 1997;**289**:207-10.
276. Steinkamp M, Geerling I, Seufferlein T *et al.* Glial-derived neurotrophic factor regulates apoptosis in colonic epithelial cells. *Gastroenterology* 2003;**124**:1748-57.
277. Airaksinen MS, Saarma M. The GDNF family: signalling, biological functions and therapeutic value. *Nat.Rev.Neurosci.* 2002;**3**:383-94.
278. Choi-Lundberg DL, Lin Q, Chang YN *et al.* Dopaminergic neurons protected from degeneration by GDNF gene therapy. *Science* 1997;**275**:838-41.
279. Gash DM, Zhang Z, Ovidia A *et al.* Functional recovery in parkinsonian monkeys treated with GDNF. *Nature* 1996;**380**:252-5.
280. Kaddis FG, Zawada WM, Schaack J *et al.* Conditioned medium from aged monkey fibroblasts stably expressing GDNF and BDNF improves survival of embryonic dopamine neurons in vitro. *Cell Tissue Res.* 1996;**286**:241-7.

281. Nosrat CA, Tomac A, Lindqvist E *et al.* Cellular expression of GDNF mRNA suggests multiple functions inside and outside the nervous system. *Cell Tissue Res.* 1996;**286**:191-207.
282. Jing S, Wen D, Yu Y *et al.* GDNF-induced activation of the ret protein tyrosine kinase is mediated by GDNFR-alpha, a novel receptor for GDNF. *Cell* 1996;**85**:1113-24.
283. Carwile ME, Culbert RB, Sturdivant RL *et al.* Rod outer segment maintenance is enhanced in the presence of bFGF, CNTF and GDNF. *Exp. Eye Res.* 1998;**66**:791-805.
284. Treanor JJ, Goodman L, de SF *et al.* Characterization of a multicomponent receptor for GDNF. *Nature* 1996;**382**:80-3.
285. Baloh RH, Enomoto H, Johnson EM, Jr. *et al.* The GDNF family ligands and receptors - implications for neural development. *Curr. Opin. Neurobiol.* 2000;**10**:103-10.
286. Trupp M, Arenas E, Fainzilber M *et al.* Functional receptor for GDNF encoded by the c-ret proto-oncogene. *Nature* 1996;**381**:785-9.
287. Sariola H, Saarma M. Novel functions and signalling pathways for GDNF. *J Cell Sci* 2003;**116**:3855-62.
288. Encinas M, Tansey MG, Tsui-Pierchala BA *et al.* c-Src is required for glial cell line-derived neurotrophic factor (GDNF) family ligand-mediated neuronal survival via a phosphatidylinositol-3 kinase (PI-3K)-dependent pathway. *J Neurosci.* 2001;**21**:1464-72.

289. Koeberle PD, Bahr M. The upregulation of GLAST-1 is an indirect antiapoptotic mechanism of GDNF and neurturin in the adult CNS. *Cell Death.Differ.* 2008;**15**:471-83.
290. Paratcha G, Ledda F, Ibanez CF. The neural cell adhesion molecule NCAM is an alternative signaling receptor for GDNF family ligands. *Cell* 2003;**113**:867-79.
291. Paratcha G, Ledda F. GDNF and GFRalpha: a versatile molecular complex for developing neurons. *Trends Neurosci.* 2008;**31**:384-91.
292. Hauck SM, Kinkl N, Deeg CA *et al.* GDNF family ligands trigger indirect neuroprotective signaling in retinal glial cells. *Mol.Cell Biol.* 2006;**26**:2746-57.
293. Perrelet D, Ferri A, Liston P *et al.* IAPs are essential for GDNF-mediated neuroprotective effects in injured motor neurons in vivo. *Nat.Cell Biol.* 2002;**4**:175-9.
294. Rothermel A, Layer PG. GDNF regulates chicken rod photoreceptor development and survival in reaggregated histotypic retinal spheres. *Invest Ophthalmol Vis Sci* 2003;**44**:2221-8.
295. Jomary C, Darrow RM, Wong P *et al.* Expression of neurturin, glial cell line-derived neurotrophic factor, and their receptor components in light-induced retinal degeneration. *Invest Ophthalmol Vis Sci* 2004;**45**:1240-6.

296. Politi LE, Rotstein NP, Carri NG. Effect of GDNF on neuroblast proliferation and photoreceptor survival: additive protection with docosahexaenoic acid. *Invest Ophthalmol Vis Sci* 2001;**42**:3008-15.
297. Karlsson M, Lindqvist N, Mayordomo R *et al*. Overlapping and specific patterns of GDNF, c-ret and GFR alpha mRNA expression in the developing chicken retina. *Mech.Dev.* 2002;**114**:161-5.
298. Koeberle PD, Ball AK. Neurturin enhances the survival of axotomized retinal ganglion cells in vivo: combined effects with glial cell line-derived neurotrophic factor and brain-derived neurotrophic factor. *Neuroscience* 2002;**110**:555-67.
299. Harada C, Harada T, Quah HM *et al*. Potential role of glial cell line-derived neurotrophic factor receptors in Muller glial cells during light-induced retinal degeneration. *Neuroscience* 2003;**122**:229-35.
300. Harada T, Harada C, Kohsaka S *et al*. Microglia-Muller glia cell interactions control neurotrophic factor production during light-induced retinal degeneration. *J Neurosci.* 2002;**22**:9228-36.
301. Lavail MM, Yasumura D, Matthes MT *et al*. Protection of mouse photoreceptors by survival factors in retinal degenerations. *Invest Ophthalmol.Vis.Sci.* 1998;**39**:592-602.
302. Spencer B, Agarwala S, Gentry L *et al*. HSV-1 vector-delivered FGF2 to the retina is neuroprotective but does not preserve functional responses. *Mol.Ther.* 2001;**3**:746-56.

303. Koeberle PD, Bahr M. Growth and guidance cues for regenerating axons: where have they gone? *J Neurobiol.* 2004;**59**:162-80.
304. Koeberle PD, Ball AK. Effects of GDNF on retinal ganglion cell survival following axotomy. *Vision Res.* 1998;**38**:1505-15.
305. Klocker N, Braunling F, Isenmann S *et al.* In vivo neurotrophic effects of GDNF on axotomized retinal ganglion cells. *Neuroreport* 1997;**8**:3439-42.
306. Yan Q, Wang J, Matheson CR *et al.* Glial cell line-derived neurotrophic factor (GDNF) promotes the survival of axotomized retinal ganglion cells in adult rats: comparison to and combination with brain-derived neurotrophic factor (BDNF). *J Neurobiol.* 1999;**38**:382-90.
307. Hobson AH, Donovan M, Humphries MM *et al.* Apoptotic photoreceptor death in the rhodopsin knockout mouse in the presence and absence of c-fos. *Exp. Eye Res.* 2000;**71**:247-54.
308. Wu WC, Lai CC, Chen SL *et al.* Long-term safety of GDNF gene delivery in the retina. *Curr. Eye Res.* 2005;**30**:715-22.
309. Schlichtenbrede FC, MacNeil A, Bainbridge JW *et al.* Intraocular gene delivery of ciliary neurotrophic factor results in significant loss of retinal function in normal mice and in the Prph2Rd2/Rd2 model of retinal degeneration. *Gene Ther.* 2003;**10**:523-7.
310. Bush RA, Lei B, Tao W *et al.* Encapsulated cell-based intraocular delivery of ciliary neurotrophic factor in normal rabbit: dose-dependent

- effects on ERG and retinal histology. *Invest Ophthalmol Vis Sci* 2004;**45**:2420-30.
311. Gerwins P, Skoldenberg E, Claesson-Welsh L. Function of fibroblast growth factors and vascular endothelial growth factors and their receptors in angiogenesis. *Crit Rev.Oncol.Hematol.* 2000;**34**:185-94.
312. Buch PK, MacLaren RE, Ali RR. Neuroprotective gene therapy for the treatment of inherited retinal degeneration. *Curr.Gene Ther.* 2007;**7**:434-45.
313. Rothermel A, Layer PG. Photoreceptor plasticity in reaggregates of embryonic chick retina: rods depend on proximal cones and on tissue organization. *Eur.J Neurosci.* 2001;**13**:949-58.
314. Layer PG, Rothermel A, Hering H *et al.* Pigmented epithelium sustains cell proliferation and decreases expression of opsins and acetylcholinesterase in reagggregated chicken retinospheroids. *Eur.J Neurosci.* 1997;**9**:1795-803.
315. Komeima K, Rogers BS, Campochiaro PA. Antioxidants slow photoreceptor cell death in mouse models of retinitis pigmentosa. *J Cell Physiol* 2007.
316. Komeima K, Rogers BS, Lu L *et al.* Antioxidants reduce cone cell death in a model of retinitis pigmentosa. *Proc.Natl.Acad.Sci.U.S.A* 2006;**103**:11300-5.

317. Marshall CJ. Specificity of receptor tyrosine kinase signaling: transient versus sustained extracellular signal-regulated kinase activation. *Cell* 1995;**80**:179-85.
318. Kyuno J, Jones EA. GDNF expression during *Xenopus* development. *Gene Expr. Patterns*. 2007;**7**:313-7.
319. Ejstrup R, Kiilgaard J, Tucker B *et al.* Pharmacokinetics of Intravitreal Glial Cell Line-Derived Neurotrophic Factor: Experimental Studies in Pigs. *Invest. Ophthalmol. Vis. Sci.* 2009;**50**.
320. Klieber M. Body size and metabolic rate. *Physiol Rev.* 1947;**27**:511-41.
321. Faktorovich EG, Steinberg RH, Yasumura D *et al.* Basic fibroblast growth factor and local injury protect photoreceptors from light damage in the rat. *J Neurosci.* 1992;**12**:3554-67.
322. Aoi M, Date I, Tomita S *et al.* The effect of intrastriatal single injection of GDNF on the nigrostriatal dopaminergic system in hemiparkinsonian rats: behavioral and histological studies using two different dosages. *Neurosci. Res.* 2000;**36**:319-25.
323. Berkowitz BA, Lukaszew RA, Mullins CM *et al.* Impaired hyaloidal circulation function and uncoordinated ocular growth patterns in experimental retinopathy of prematurity. *Invest Ophthalmol Vis Sci* 1998;**39**:391-6.

324. Lavail MM, Unoki K, Yasumura D *et al.* Multiple growth factors, cytokines, and neurotrophins rescue photoreceptors from the damaging effects of constant light. *Proc.Natl.Acad.Sci U.S.A* 1992;**89**:11249-53.
325. The Royal College of Ophthalmologists. Guidelines for Intravitreal Injections Procedure 2009. *web* 2009.
326. Nutt JG, Burchiel KJ, Comella CL *et al.* Randomized, double-blind trial of glial cell line-derived neurotrophic factor (GDNF) in PD. *Neurology* 2003;**60**:69-73.
327. Kordower JH, Palfi S, Chen EY *et al.* Clinicopathological findings following intraventricular glial-derived neurotrophic factor treatment in a patient with Parkinson's disease. *Ann.Neurol.* 1999;**46**:419-24.
328. Viores SA, Kuchle M, Derevjanik NL *et al.* Blood-retinal barrier breakdown in retinitis pigmentosa: light and electron microscopic immunolocalization. *Histol.Histopathol.* 1995;**10**:913-23.
329. Acland GM, Aguirre GD, Bennett J *et al.* Long-term restoration of rod and cone vision by single dose rAAV-mediated gene transfer to the retina in a canine model of childhood blindness. *Mol.Ther.* 2005;**12**:1072-82.
330. Auricchio A, Kobinger G, Anand V *et al.* Exchange of surface proteins impacts on viral vector cellular specificity and transduction characteristics: the retina as a model. *Hum.Mol.Genet.* 2001;**10**:3075-81.
331. Leberherz C, Maguire A, Tang W *et al.* Novel AAV serotypes for improved ocular gene transfer. *J Gene Med.* 2008;**10**:375-82.

332. Baskar JF, Smith PP, Nilaver G *et al.* The enhancer domain of the human cytomegalovirus major immediate-early promoter determines cell type-specific expression in transgenic mice. *J Virol.* 1996;**70**:3207-14.
333. Prosch S, Stein J, Staak K *et al.* Inactivation of the very strong HCMV immediate early promoter by DNA CpG methylation in vitro. *Biol.Chem.Hoppe Seyler* 1996;**377**:195-201.
334. Wang XS, Qing K, Ponnazhagan S *et al.* Adeno-associated virus type 2 DNA replication in vivo: mutation analyses of the D sequence in viral inverted terminal repeats. *J Virol.* 1997;**71**:3077-82.
335. Silverman MS, Hughes SE. Photoreceptor rescue in the RCS rat without pigment epithelium transplantation. *Curr.Eye Res.* 1990;**9**:183-91.
336. Li L, Turner JE. Optimal conditions for long-term photoreceptor cell rescue in RCS rats: the necessity for healthy RPE transplants. *Exp.Eye Res.* 1991;**52**:669-79.
337. Cao W, Wen R, Li F *et al.* Mechanical injury increases bFGF and CNTF mRNA expression in the mouse retina. *Exp.Eye Res.* 1997;**65**:241-8.
338. Broekman ML, Comer LA, Hyman BT *et al.* Adeno-associated virus vectors serotyped with AAV8 capsid are more efficient than AAV-1 or -2 serotypes for widespread gene delivery to the neonatal mouse brain. *Neuroscience* 2006;**138**:501-10.

339. Inagaki K, Fuess S, Storm TA *et al.* Robust systemic transduction with AAV9 vectors in mice: efficient global cardiac gene transfer superior to that of AAV8. *Mol.Ther.* 2006;**14**:45-53.
340. Wang Z, Zhu T, Rehman KK *et al.* Widespread and stable pancreatic gene transfer by adeno-associated virus vectors via different routes. *Diabetes* 2006;**55**:875-84.
341. Davidoff AM, Gray JT, Ng CY *et al.* Comparison of the ability of adeno-associated viral vectors pseudotyped with serotype 2, 5, and 8 capsid proteins to mediate efficient transduction of the liver in murine and nonhuman primate models. *Mol.Ther.* 2005;**11**:875-88.
342. Yang L, Bula D, Arroyo JG *et al.* Preventing retinal detachment-associated photoreceptor cell loss in Bax-deficient mice. *Invest Ophthalmol Vis Sci* 2004;**45**:648-54.
343. Linberg KA, Sakai T, Lewis GP *et al.* Experimental retinal detachment in the cone-dominant ground squirrel retina: morphology and basic immunocytochemistry. *Vis Neurosci.* 2002;**19**:603-19.
344. Sakai T, Calderone JB, Lewis GP *et al.* Cone photoreceptor recovery after experimental detachment and reattachment: an immunocytochemical, morphological, and electrophysiological study. *Invest Ophthalmol Vis Sci* 2003;**44**:416-25.
345. Sakai T, Lewis GP, Linberg KA *et al.* The ability of hyperoxia to limit the effects of experimental detachment in cone-dominated retina. *Invest Ophthalmol Vis Sci* 2001;**42**:3264-73.

346. Anderson DH, Guerin CJ, Erickson PA *et al.* Morphological recovery in the reattached retina. *Invest Ophthalmol Vis Sci* 1986;**27**:168-83.
347. Anderson R, Macdonald I, Corbett T *et al.* A method for the preparation of highly purified adeno-associated virus using affinity column chromatography, protease digestion and solvent extraction. *J Virol.Methods* 2000;**85**:23-34.
348. Chahal PS, Aucoin MG, Kamen A. Primary recovery and chromatographic purification of adeno-associated virus type 2 produced by baculovirus/insect cell system. *J Virol.Methods* 2007;**139**:61-70.
349. Wu X, Dong X, Wu Z *et al.* A novel method for purification of recombinant adeno-associated virus vectors on a large scale. *Chinese Science Bulletin* 2001;**46**:485-9.
350. Smith RH, Levy JR, Kotin RM. A simplified baculovirus-AAV expression vector system coupled with one-step affinity purification yields high-titer rAAV stocks from insect cells. *Mol.Ther.* 2009;**17**:1888-96.
351. Grimm D, Kern A, Pawlita M *et al.* Titration of AAV-2 particles via a novel capsid ELISA: packaging of genomes can limit production of recombinant AAV-2. *Gene Ther.* 1999;**6**:1322-30.
352. Johnson LV, Hageman GS. Structural and compositional analyses of isolated cone matrix sheaths. *Invest Ophthalmol Vis Sci* 1991;**32**:1951-7.

353. Hageman GS, Marmor MF, Yao XY *et al.* The interphotoreceptor matrix mediates primate retinal adhesion. *Arch.Ophthalmol* 1995;**113**:655-60.
354. Kroll AJ, Machemer R. Experimental retinal detachment in the owl monkey. 3. Electron microscopy of retina and pigment epithelium. *Am J Ophthalmol* 1968;**66**:410-27.
355. Iribarne M, Canto-Soler MV, Torbidoni V *et al.* Controlling retinal pigment epithelium injury after experimental detachment of the retina. *Invest Ophthalmol Vis Sci* 2007;**48**:1348-54.
356. Lewis G, Mervin K, Valter K *et al.* Limiting the proliferation and reactivity of retinal Muller cells during experimental retinal detachment: the value of oxygen supplementation. *Am J Ophthalmol* 1999;**128**:165-72.
357. Mervin K, Valter K, Maslim J *et al.* Limiting photoreceptor death and deconstruction during experimental retinal detachment: the value of oxygen supplementation. *Am J Ophthalmol* 1999;**128**:155-64.
358. Nakazawa T, Takeda M, Lewis GP *et al.* Attenuated glial reactions and photoreceptor degeneration after retinal detachment in mice deficient in glial fibrillary acidic protein and vimentin. *Invest Ophthalmol Vis Sci* 2007;**48**:2760-8.
359. Cook B, Lewis GP, Fisher SK *et al.* Apoptotic photoreceptor degeneration in experimental retinal detachment. *Invest Ophthalmol Vis Sci* 1995;**36**:990-6.

360. Hisatomi T, Sakamoto T, Goto Y *et al.* Critical role of photoreceptor apoptosis in functional damage after retinal detachment. *Curr.Eye Res.* 2002;**24**:161-72.
361. Zacks DN, Hanninen V, Pantcheva M *et al.* Caspase activation in an experimental model of retinal detachment. *Invest Ophthalmol Vis Sci* 2003;**44**:1262-7.
362. Hassan TS, Sarrafizadeh R, Ruby AJ *et al.* The effect of duration of macular detachment on results after the scleral buckle repair of primary, macula-off retinal detachments. *Ophthalmology* 2002;**109**:146-52.
363. Chang CJ, Lai WW, Edward DP *et al.* Apoptotic photoreceptor cell death after traumatic retinal detachment in humans. *Arch.Ophthalmol* 1995;**113**:880-6.
364. Liem AT, Keunen JE, van Meel GJ *et al.* Serial foveal densitometry and visual function after retinal detachment surgery with macular involvement. *Ophthalmology* 1994;**101**:1945-52.
365. Kusaka S, Toshino A, Ohashi Y *et al.* Long-term visual recovery after scleral buckling for macula-off retinal detachments. *Jpn.J Ophthalmol* 1998;**42**:218-22.
366. Rex TS, Fariss RN, Lewis GP *et al.* A survey of molecular expression by photoreceptors after experimental retinal detachment. *Invest Ophthalmol Vis Sci* 2002;**43**:1234-47.

367. COHEN AI. The fine structure of the extrafoveal receptors of the Rhesus monkey. *Exp. Eye Res.* 1961;**1**:128-36.
368. Brown JM, Wilson G. Apoptosis genes and resistance to cancer therapy: what does the experimental and clinical data tell us? *Cancer Biol. Ther.* 2003;**2**:477-90.
369. Srinivasula SM, Ashwell JD. IAPs: what's in a name? *Mol. Cell* 2008;**30**:123-35.
370. Kluck RM, Bossy-Wetzel E, Green DR *et al.* The release of cytochrome c from mitochondria: a primary site for Bcl-2 regulation of apoptosis. *Science* 1997;**275**:1132-6.
371. Yang J, Liu X, Bhalla K *et al.* Prevention of apoptosis by Bcl-2: release of cytochrome c from mitochondria blocked. *Science* 1997;**275**:1129-32.
372. Allsopp TE, Wyatt S, Paterson HF *et al.* The proto-oncogene bcl-2 can selectively rescue neurotrophic factor-dependent neurons from apoptosis. *Cell* 1993;**73**:295-307.
373. Garcia I, Martinou I, Tsujimoto Y *et al.* Prevention of programmed cell death of sympathetic neurons by the bcl-2 proto-oncogene. *Science* 1992;**258**:302-4.
374. Joseph RM, Li T. Overexpression of Bcl-2 or Bcl-XL transgenes and photoreceptor degeneration. *Invest Ophthalmol Vis Sci* 1996;**37**:2434-46.

375. Liston P, Roy N, Tamai K *et al.* Suppression of apoptosis in mammalian cells by NAIP and a related family of IAP genes. *Nature* 1996;**379**:349-53.
376. Deveraux QL, Reed JC. IAP family proteins--suppressors of apoptosis. *Genes Dev.* 1999;**13**:239-52.
377. Deveraux QL, Takahashi R, Salvesen GS *et al.* X-linked IAP is a direct inhibitor of cell-death proteases. *Nature* 1997;**388**:300-4.
378. Holcik M, Gibson H, Korneluk RG. XIAP: apoptotic brake and promising therapeutic target. *Apoptosis.* 2001;**6**:253-61.
379. Kashkar H. XIAP: a chemoresistance factor or a hollow promise. *Clin.Cancer Res.* 2010.
380. Takahashi R, Deveraux Q, Tamm I *et al.* A single BIR domain of XIAP sufficient for inhibiting caspases. *J Biol.Chem.* 1998;**273**:7787-90.
381. Schimmer AD, Dalili S, Batey RA *et al.* Targeting XIAP for the treatment of malignancy. *Cell Death.Differ.* 2006;**13**:179-88.
382. Schimmer AD. Inhibitor of apoptosis proteins: translating basic knowledge into clinical practice. *Cancer Res.* 2004;**64**:7183-90.
383. LaCasse EC, Kandimalla ER, Winocour P *et al.* Application of XIAP antisense to cancer and other proliferative disorders: development of AEG35156/ GEM640. *Ann.N.Y.Acad.Sci* 2005;**1058**:215-34.

384. Schimmer AD, Estey EH, Borthakur G *et al.* Phase I/II trial of AEG35156 X-linked inhibitor of apoptosis protein antisense oligonucleotide combined with idarubicin and cytarabine in patients with relapsed or primary refractory acute myeloid leukemia. *J Clin.Oncol.* 2009;**27**:4741-6.
385. Trapp T, Korhonen L, Besselmann M *et al.* Transgenic mice overexpressing XIAP in neurons show better outcome after transient cerebral ischemia. *Mol.Cell Neurosci.* 2003;**23**:302-13.
386. Wang X, Zhu C, Wang X *et al.* X-linked inhibitor of apoptosis (XIAP) protein protects against caspase activation and tissue loss after neonatal hypoxia-ischemia. *Neurobiol.Dis.* 2004;**16**:179-89.
387. Crocker SJ, Liston P, Anisman H *et al.* Attenuation of MPTP-induced neurotoxicity and behavioural impairment in NSE-XIAP transgenic mice. *Neurobiol.Dis.* 2003;**12**:150-61.
388. Wang J, Menchenton T, Yin S *et al.* Over-expression of X-linked inhibitor of apoptosis protein slows presbycusis in C57BL/6J mice. *Neurobiol.Aging* 2010;**31**:1238-49.
389. Yang Y, Fang S, Jensen JP *et al.* Ubiquitin protein ligase activity of IAPs and their degradation in proteasomes in response to apoptotic stimuli. *Science* 2000;**288**:874-7.
390. Yang YL, Li XM. The IAP family: endogenous caspase inhibitors with multiple biological activities. *Cell Res.* 2000;**10**:169-77.

391. Verhagen AM, Ekert PG, Pakusch M *et al.* Identification of DIABLO, a mammalian protein that promotes apoptosis by binding to and antagonizing IAP proteins. *Cell* 2000;**102**:43-53.
392. Creagh EM, Murphy BM, Duriez PJ *et al.* Smac/Diablo antagonizes ubiquitin ligase activity of inhibitor of apoptosis proteins. *J Biol.Chem.* 2004;**279**:26906-14.
393. Shiozaki EN, Shi Y. Caspases, IAPs and Smac/DIABLO: mechanisms from structural biology. *Trends Biochem.Sci* 2004;**29**:486-94.
394. Du C, Fang M, Li Y *et al.* Smac, a mitochondrial protein that promotes cytochrome c-dependent caspase activation by eliminating IAP inhibition. *Cell* 2000;**102**:33-42.
395. Althaus J, Siegelin MD, Dehghani F *et al.* The serine protease Omi/HtrA2 is involved in XIAP cleavage and in neuronal cell death following focal cerebral ischemia/reperfusion. *Neurochem.Int.* 2007;**50**:172-80.
396. Trencia A, Fiory F, Maitan MA *et al.* Omi/HtrA2 promotes cell death by binding and degrading the anti-apoptotic protein ped/pea-15. *J Biol.Chem.* 2004;**279**:46566-72.
397. Hegde R, Srinivasula SM, Datta P *et al.* The polypeptide chain-releasing factor GSPT1/eRF3 is proteolytically processed into an IAP-binding protein. *J Biol.Chem.* 2003;**278**:38699-706.

398. Liston P, Fong WG, Kelly NL *et al.* Identification of XAF1 as an antagonist of XIAP anti-Caspase activity. *Nat.Cell Biol.* 2001;**3**:128-33.
399. Fong WG, Liston P, Rajcan-Separovic E *et al.* Expression and genetic analysis of XIAP-associated factor 1 (XAF1) in cancer cell lines. *Genomics* 2000;**70**:113-22.
400. Perrelet D, Perrin FE, Liston P *et al.* Motoneuron resistance to apoptotic cell death in vivo correlates with the ratio between X-linked inhibitor of apoptosis proteins (XIAPs) and its inhibitor, XIAP-associated factor 1. *J Neurosci.* 2004;**24**:3777-85.
401. Shibata T, Noguchi T, Takeno S *et al.* Disturbed XIAP and XAF1 expression balance is an independent prognostic factor in gastric adenocarcinomas. *Ann.Surg.Oncol.* 2008;**15**:3579-87.
402. O'Riordan MX, Bauler LD, Scott FL *et al.* Inhibitor of apoptosis proteins in eukaryotic evolution and development: a model of thematic conservation. *Dev.Cell* 2008;**15**:497-508.
403. Li X, Yang Y, Ashwell JD. TNF-RII and c-IAP1 mediate ubiquitination and degradation of TRAF2. *Nature* 2002;**416**:345-7.
404. Silke J, Vaux DL. Two kinds of BIR-containing protein - inhibitors of apoptosis, or required for mitosis. *J Cell Sci* 2001;**114**:1821-7.
405. Rigaud S, Fondaneche MC, Lambert N *et al.* XIAP deficiency in humans causes an X-linked lymphoproliferative syndrome. *Nature* 2006;**444**:110-4.

406. Harlin H, Reffey SB, Duckett CS *et al.* Characterization of XIAP-deficient mice. *Mol. Cell Biol.* 2001;**21**:3604-8.
407. Olayioye MA, Kaufmann H, Pakusch M *et al.* XIAP-deficiency leads to delayed lobuloalveolar development in the mammary gland. *Cell Death. Differ.* 2005;**12**:87-90.
408. Seeger JM, Brinkmann K, Yazdanpanah B *et al.* Elevated XIAP expression alone does not confer chemoresistance. *Br J Cancer* 2010;**102**:1717-23.
409. Kashkar H, Haefs C, Shin H *et al.* XIAP-mediated caspase inhibition in Hodgkin's lymphoma-derived B cells. *J Exp. Med.* 2003;**198**:341-7.
410. Petrin D, Baker A, Brousseau J *et al.* XIAP protects photoreceptors from n-methyl-n-nitrosourea-induced retinal degeneration. *Adv. Exp. Med. Biol.* 2003;**533**:385-93.
411. Petrin D, Baker A, Coupland SG *et al.* Structural and functional protection of photoreceptors from MNU-induced retinal degeneration by the X-linked inhibitor of apoptosis. *Invest Ophthalmol Vis Sci* 2003;**44**:2757-63.
412. Renwick J, Narang MA, Coupland SG *et al.* XIAP-mediated neuroprotection in retinal ischemia. *Gene Ther.* 2006;**13**:339-47.
413. Yao J, Grahek G, Jia L *et al.* XIAP Protection of Photoreceptors in the Retinal Degeneration 10 (rd10) Mutant Mouse. *ARVO abstract* 2010.

414. Xu J, Dodd RL, Makino CL *et al.* Prolonged photoresponses in transgenic mouse rods lacking arrestin. *Nature* 1997;**389**:505-9.
415. Nikonov SS, Brown BM, Davis JA *et al.* Mouse cones require an arrestin for normal inactivation of phototransduction. *Neuron* 2008;**59**:462-74.
416. Craft CM, Whitmore DH, Wiechmann AF. Cone arrestin identified by targeting expression of a functional family. *J Biol.Chem.* 1994;**269**:4613-9.
417. Zadro-Lamoureux LA, Zacks DN, Baker AN *et al.* XIAP effects on retinal detachment-induced photoreceptor apoptosis [corrected]. *Invest Ophthalmol Vis Sci* 2009;**50**:1448-53.
418. Yao J, Kecia Feathers, Hemant Khanna *et al.* XIAP Therapy Increases Survival of Transplanted Rod Precursors in a Degenerating Host Retina. *Invest.Ophthalmol.Vis.Sci.* 2010.
419. Komaromy AM, Alexander JJ, Rowlan JS *et al.* Gene therapy rescues cone function in congenital achromatopsia. *Hum.Mol.Genet.* 2010;**19**:2581-93.
420. Wilson JH, Wensel TG. The nature of dominant mutations of rhodopsin and implications for gene therapy. *Mol.Neurobiol.* 2003;**28**:149-58.
421. Rio FT, Wade NM, Ransijn A *et al.* Premature termination codons in PRPF31 cause retinitis pigmentosa via haploinsufficiency due to nonsense-mediated mRNA decay. *J Clin.Invest* 2008;**118**:1519-31.

422. bu-Safieh L, Vithana EN, Mantel I *et al.* A large deletion in the adRP gene PRPF31: evidence that haploinsufficiency is the cause of disease. *Mol.Vis* 2006;**12**:384-8.
423. Mao H, Thomas JJ, Schwein A *et al.* AAV Delivery of Wild-Type Rhodopsin Preserves Retinal Function in a Mouse Model of Autosomal Dominant Retinitis Pigmentosa. *Hum.Gene Ther.* 2010.
424. Bhisitkul RB, Robinson GS, Moulton RS *et al.* An antisense oligodeoxynucleotide against vascular endothelial growth factor in a nonhuman primate model of iris neovascularization. *Arch.Ophthalmol* 2005;**123**:214-9.
425. Drenser KA, Timmers AM, Hauswirth WW *et al.* Ribozyme-targeted destruction of RNA associated with autosomal-dominant retinitis pigmentosa. *Invest Ophthalmol Vis Sci* 1998;**39**:681-9.
426. Gorbatyuk M, Justilien V, Liu J *et al.* Preservation of photoreceptor morphology and function in P23H rats using an allele independent ribozyme. *Exp.Eye Res.* 2007;**84**:44-52.
427. Fire A, Xu S, Montgomery MK *et al.* Potent and specific genetic interference by double-stranded RNA in *Caenorhabditis elegans*. *Nature* 1998;**391**:806-11.
428. Boutla A, Delidakis C, Livadaras I *et al.* Short 5'-phosphorylated double-stranded RNAs induce RNA interference in *Drosophila*. *Curr.Biol.* 2001;**11**:1776-80.

429. Hammond SM, Caudy AA, Hannon GJ. Post-transcriptional gene silencing by double-stranded RNA. *Nat.Rev.Genet.* 2001;**2**:110-9.
430. Lodowski DT, Angel TE, Palczewski K. Comparative analysis of GPCR crystal structures. *Photochem.Photobiol.* 2009;**85**:425-30.
431. Palczewski K. G protein-coupled receptor rhodopsin. *Annu.Rev.Biochem.* 2006;**75**:743-67.
432. Palfi A, Millington-Ward S, Chadderton N *et al.* Adeno-associated virus-mediated rhodopsin replacement provides therapeutic benefit in mice with a targeted disruption of the rhodopsin gene. *Hum.Gene Ther.* 2010;**21**:311-23.
433. Molday RS, Molday LL. Differences in the protein composition of bovine retinal rod outer segment disk and plasma membranes isolated by a ricin-gold-dextran density perturbation method. *J Cell Biol.* 1987;**105**:2589-601.
434. Mansergh FC, Vawda R, Millington-Ward S *et al.* Loss of photoreceptor potential from retinal progenitor cell cultures, despite improvements in survival. *Exp.Eye Res.* 2010.
435. Swaroop A, Kim D, Forrest D. Transcriptional regulation of photoreceptor development and homeostasis in the mammalian retina. *Nat.Rev.Neurosci.* 2010;**11**:563-76.

436. McNally N, Kenna P, Humphries MM *et al.* Structural and functional rescue of murine rod photoreceptors by human rhodopsin transgene. *Hum.Mol.Genet.* 1999;**8**:1309-12.
437. Young RW. Cell differentiation in the retina of the mouse. *Anat.Rec.* 1985;**212**:199-205.
438. Russell DW. AAV vectors, insertional mutagenesis, and cancer. *Mol.Ther.* 2007;**15**:1740-3.
439. MacLaren RE. An analysis of retinal gene therapy clinical trials. *Curr.Opin.Mol.Ther.* 2009;**11**:540-6.
440. Nott A, Meislin SH, Moore MJ. A quantitative analysis of intron effects on mammalian gene expression. *RNA.* 2003;**9**:607-17.
441. Le HH, Nott A, Moore MJ. How introns influence and enhance eukaryotic gene expression. *Trends Biochem.Sci* 2003;**28**:215-20.
442. Rose AB. Intron-mediated regulation of gene expression. *Curr.Top.Microbiol.Immunol.* 2008;**326**:277-90.
443. Choi T, Huang M, Gorman C *et al.* A generic intron increases gene expression in transgenic mice. *Mol.Cell Biol.* 1991;**11**:3070-4.
444. Bourdon V, Harvey A, Lonsdale DM. Introns and their positions affect the translational activity of mRNA in plant cells. *EMBO Rep.* 2001;**2**:394-8.

445. Khani SC, Pawlyk BS, Bulgakov OV *et al.* AAV-mediated expression targeting of rod and cone photoreceptors with a human rhodopsin kinase promoter. *Invest Ophthalmol Vis Sci* 2007;**48**:3954-61.
446. Kozak M. Initiation of translation in prokaryotes and eukaryotes. *Gene* 1999;**234**:187-208.
447. Kozak M. Point mutations define a sequence flanking the AUG initiator codon that modulates translation by eukaryotic ribosomes. *Cell* 1986;**44**:283-92.
448. Bennicelli J, Wright JF, Komaromy A *et al.* Reversal of blindness in animal models of leber congenital amaurosis using optimized AAV2-mediated gene transfer. *Mol.Ther.* 2008;**16**:458-65.
449. Wegrzyn JL, Drudge TM, Valafar F *et al.* Bioinformatic analyses of mammalian 5'-UTR sequence properties of mRNAs predicts alternative translation initiation sites. *BMC.Bioinformatics.* 2008;**9**:232.
450. Ward NJ, Buckley SM, Waddington SN *et al.* Codon optimisation of human factor VIII cDNAs leads to high level expression. *Blood* 2010.
451. Burgess-Brown NA, Sharma S, Sobott F *et al.* Codon optimization can improve expression of human genes in Escherichia coli: A multi-gene study. *Protein Expr.Purif.* 2008;**59**:94-102.
452. Calderone TL, Stevens RD, Oas TG. High-level misincorporation of lysine for arginine at AGA codons in a fusion protein expressed in Escherichia coli. *J Mol.Biol.* 1996;**262**:407-12.

453. Marin M. Folding at the rhythm of the rare codon beat. *Biotechnol.J* 2008;**3**:1047-57.
454. Tsai CJ, Sauna ZE, Kimchi-Sarfaty C *et al.* Synonymous mutations and ribosome stalling can lead to altered folding pathways and distinct minima. *J Mol.Biol.* 2008;**383**:281-91.
455. Gu W, Zhou T, Wilke CO. A universal trend of reduced mRNA stability near the translation-initiation site in prokaryotes and eukaryotes. *PLoS.Comput.Biol.* 2010;**6**:e1000664.
456. O'Reilly M, Millington-Ward S, Palfi A *et al.* A transgenic mouse model for gene therapy of rhodopsin-linked Retinitis Pigmentosa. *Vision Res.* 2008;**48**:386-91.
457. Osborne NN. Recent clinical findings with memantine should not mean that the idea of neuroprotection in glaucoma is abandoned. *Acta Ophthalmol* 2009;**87**:450-4.
458. Patel NK, Gill SS. GDNF delivery for Parkinson's disease. *Acta Neurochir.Suppl* 2007;**97**:135-54.
459. Talcott KE, Ratnam K, Sundquist SM *et al.* Longitudinal Study of Cone Photoreceptors during Retinal Degeneration and in Response to Ciliary Neurotrophic Factor Treatment. *Invest Ophthalmol Vis Sci* 2010.
460. Galati S, Di GG. Neuroprotection in Parkinson's disease: a realistic goal? *CNS.Neurosci.Ther.* 2010;**16**:327-9.

461. Alexander JJ, Umino Y, Everhart D *et al.* Restoration of cone vision in a mouse model of achromatopsia. *Nat.Med.* 2007;**13**:685-7.
462. Grimm C, Wenzel A, Stanescu D *et al.* Constitutive overexpression of human erythropoietin protects the mouse retina against induced but not inherited retinal degeneration. *J Neurosci.* 2004;**24**:5651-8.
463. Junk AK, Mammis A, Savitz SI *et al.* Erythropoietin administration protects retinal neurons from acute ischemia-reperfusion injury. *Proc.Natl.Acad.Sci U.S.A* 2002;**99**:10659-64.
464. Weishaupt JH, Rohde G, Polking E *et al.* Effect of erythropoietin axotomy-induced apoptosis in rat retinal ganglion cells. *Invest Ophthalmol Vis Sci* 2004;**45**:1514-22.
465. Sharples EJ, Patel N, Brown P *et al.* Erythropoietin protects the kidney against the injury and dysfunction caused by ischemia-reperfusion. *J Am Soc.Nephrol.* 2004;**15**:2115-24.
466. Schmeding M, Neumann UP, Boas-Knoop S *et al.* Erythropoietin reduces ischemia-reperfusion injury in the rat liver. *Eur.Surg.Res.* 2007;**39**:189-97.
467. Tan E, Wang Q, Quiambao AB *et al.* The relationship between opsin overexpression and photoreceptor degeneration. *Invest Ophthalmol Vis Sci* 2001;**42**:589-600.
468. Browning DF, Whitworth DE, Hodgson DA. Light-induced carotenogenesis in *Myxococcus xanthus*: functional characterization of

- the ECF sigma factor CarQ and antisigma factor CarR. *Mol.Microbiol.* 2003;**48**:237-51.
469. Navarre C, Sallets A, Gauthy E *et al.* Isolation of heat shock-induced *Nicotiana tabacum* transcription promoters and their potential as a tool for plant research and biotechnology. *Transgenic Res.* 2010.
470. McGee Sanftner LH, Rendahl KG, Quiroz D *et al.* Recombinant AAV-mediated delivery of a tet-inducible reporter gene to the rat retina. *Mol.Ther.* 2001;**3**:688-96.
471. Auricchio A, Rivera VM, Clackson T *et al.* Pharmacological regulation of protein expression from adeno-associated viral vectors in the eye. *Mol.Ther.* 2002;**6**:238-42.
472. Bainbridge JW, Mistry A, Binley K *et al.* Hypoxia-regulated transgene expression in experimental retinal and choroidal neovascularization. *Gene Ther.* 2003;**10**:1049-54.
473. Hauswirth WW, Aleman TS, Kaushal S *et al.* Treatment of leber congenital amaurosis due to RPE65 mutations by ocular subretinal injection of adeno-associated virus gene vector: short-term results of a phase I trial. *Hum.Gene Ther.* 2008;**19**:979-90.
474. Manno CS, Pierce GF, Arruda VR *et al.* Successful transduction of liver in hemophilia by AAV-Factor IX and limitations imposed by the host immune response. *Nat.Med.* 2006;**12**:342-7.

475. Stieger K, Schroeder J, Provost N *et al.* Detection of intact rAAV particles up to 6 years after successful gene transfer in the retina of dogs and primates. *Mol.Ther.* 2009;**17**:516-23.
476. Petrs-Silva H, Dinculescu A, Li Q *et al.* High-efficiency transduction of the mouse retina by tyrosine-mutant AAV serotype vectors. *Mol.Ther.* 2009;**17**:463-71.
477. Markusic DM, Herzog RW, Aslanidi GV *et al.* High-efficiency Transduction and Correction of Murine Hemophilia B Using AAV2 Vectors Devoid of Multiple Surface-exposed Tyrosines. *Mol.Ther.* 2010;**18**:2048-56.
478. Ponnazhagan S, Mukherjee P, Yoder MC *et al.* Adeno-associated virus 2-mediated gene transfer in vivo: organ-tropism and expression of transduced sequences in mice. *Gene* 1997;**190**:203-10.
479. Jayandharan GR, Zhong L, Li B *et al.* Strategies for improving the transduction efficiency of single-stranded adeno-associated virus vectors in vitro and in vivo. *Gene Ther.* 2008;**15**:1287-93.
480. Zhong L, Zhao W, Wu J *et al.* A dual role of EGFR protein tyrosine kinase signaling in ubiquitination of AAV2 capsids and viral second-strand DNA synthesis. *Mol.Ther.* 2007;**15**:1323-30.
481. Mays LE, Vandenberghe LH, Xiao R *et al.* Adeno-associated virus capsid structure drives CD4-dependent CD8+ T cell response to vector encoded proteins. *J Immunol.* 2009;**182**:6051-60.

482. Vandenberghe LH, Wilson JM, Gao G. Tailoring the AAV vector capsid for gene therapy. *Gene Ther.* 2009;**16**:311-9.
483. Duncan JL, Zhang Y, Gandhi J *et al.* High-resolution imaging with adaptive optics in patients with inherited retinal degeneration. *Invest Ophthalmol Vis Sci* 2007;**48**:3283-91.
484. Wolfing JI, Chung M, Carroll J *et al.* High-resolution retinal imaging of cone-rod dystrophy. *Ophthalmology* 2006;**113**:1019.
485. Eberhardt O, Coelln RV, Kugler S *et al.* Protection by synergistic effects of adenovirus-mediated X-chromosome-linked inhibitor of apoptosis and glial cell line-derived neurotrophic factor gene transfer in the 1-methyl-4-phenyl-1,2,3,6-tetrahydropyridine model of Parkinson's disease. *J Neurosci.* 2000;**20**:9126-34.
486. Straten G, Schmeer C, Kretz A *et al.* Potential synergistic protection of retinal ganglion cells from axotomy-induced apoptosis by adenoviral administration of glial cell line-derived neurotrophic factor and X-chromosome-linked inhibitor of apoptosis. *Neurobiol.Dis.* 2002;**11**:123-33.
487. Logan A, Ahmed Z, Baird A *et al.* Neurotrophic factor synergy is required for neuronal survival and disinhibited axon regeneration after CNS injury. *Brain* 2006;**129**:490-502.

488. Inoue H, Tsukita K, Iwasato T *et al.* The crucial role of caspase-9 in the disease progression of a transgenic ALS mouse model. *EMBO J.* 2003;**15**:6665-74.